CHEMICAL REVIEWS

pubs.acs.org/CR

Review

# Thermodynamic and Molecular Origins of Crack Resistance in Polymer Networks

*Published as part of Chemical Reviews special issue "Tough Gels".*

Zheqi Chen and Zhigang Suo*

Cite This: https://doi.org/10.1021/acs.chemrev.5c00663

Read Online

ACCESS | Metrics & More | Article Recommendations

**ABSTRACT:** A material tears, peels, and breaks by growing a crack. In a zone around the crack front, atoms undergo an irreversible process of breaking—and possibly reforming—bonds. Trailing behind the crack front are two layers of scars. Outside the irreversible zone and scars, atoms undergo the reversible process of elasticity. The irreversible zone is considered localized if it is small relative to the body. The idealization of localized irreversibility leads to a thermodynamic framework centered on the energy release rate. This crack driving force is defined using an ideal body in which a crack is stationary and deformation is elastic, and is applied to a real body in which a crack grows by an irreversible process. The irreversible zone scales with a material length: the fractocohesive length. We review recent advances in the development of crack-resistant elastomers and hydrogels as well as polymer networks reinforced by hard particles, fibers, or fabrics, subject to monotonic, cyclic, and static loading. Emphasis is placed on how molecular features, such as strand length, entanglements, noncovalent bonds, and chemical reactions, govern crack resistance. Design principles are highlighted that reconcile high toughness with low hysteresis through stress deconcentration. This review traces crack resistance to molecular origins, providing a foundation for designing next-generation crack-resistant materials.

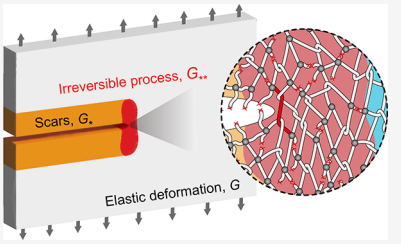


## CONTENTS



**Received:** August 1, 2025
**Revised:** October 12, 2025
**Accepted:** October 24, 2025

Downloaded via PURDUE UNIV on December 21, 2025 at 22:55:44 (UTC).
See https://pubs.acs.org/sharingguidelines for options on how to legitimately share published articles.


© XXXX American Chemical Society

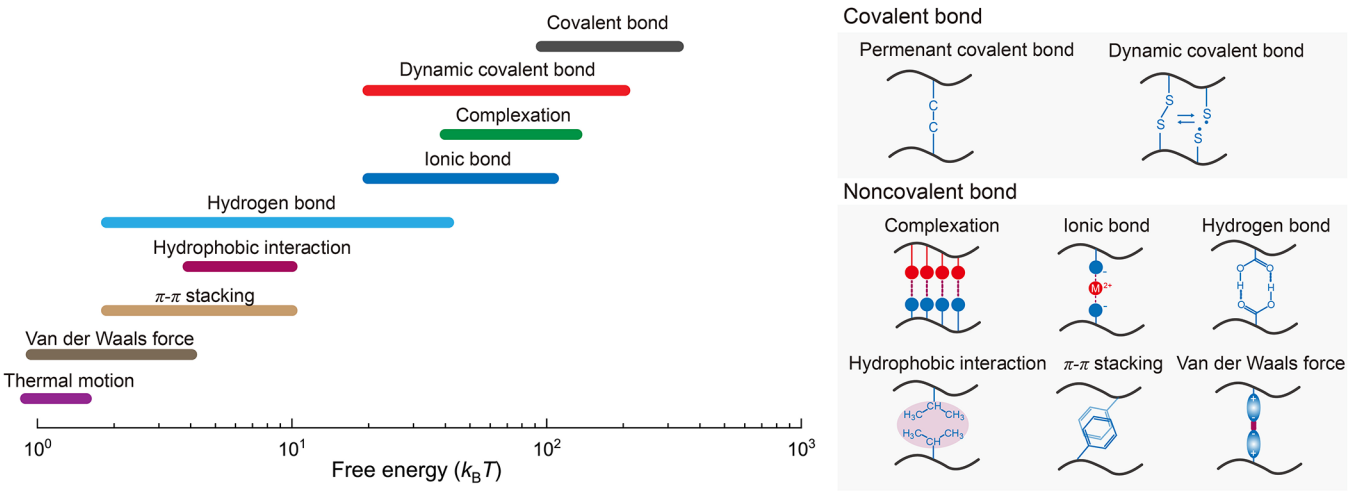


**Figure 1.** Electromagnetic force manifests itself as bonds of various free energies.[4,5]



## 1. INTRODUCTION

This review focuses on thermodynamic and molecular origins of crack resistance in polymer networks, with other materials discussed for comparison. Crack growth provides a powerful lens for examining the thermodynamics of reversible and


https://doi.org/10.1021/acs.chemrev.5c00663
Chem. Rev. XXXX, XXX, XXX−XXX

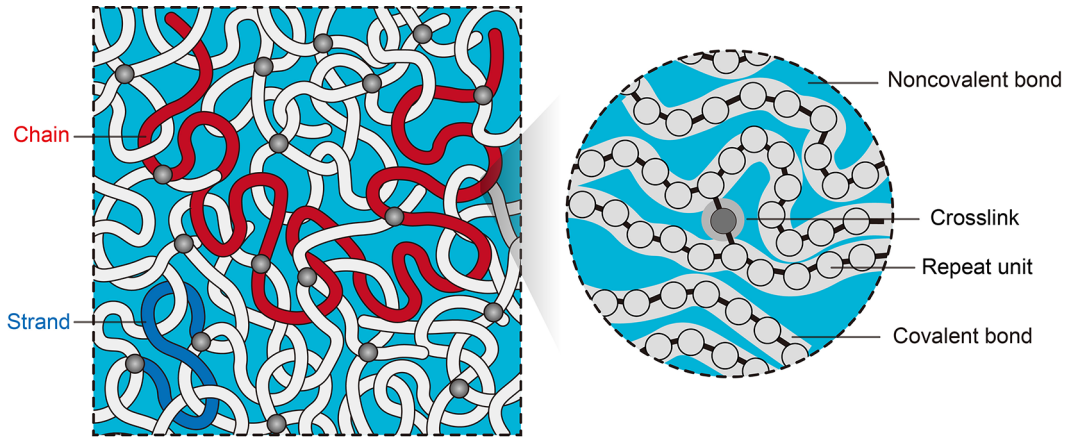


**Figure 2.** A polymer network is an architecture of covalent and noncovalent bonds.

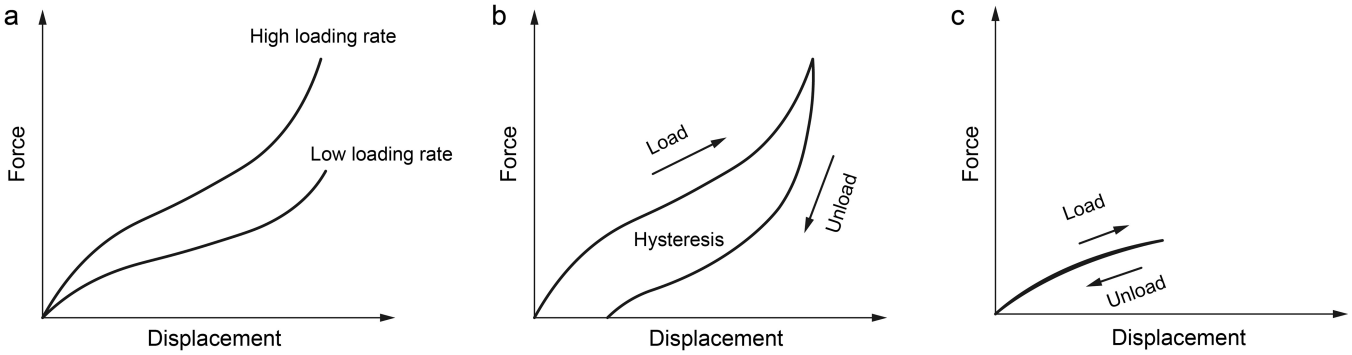


**Figure 3.** Dynamics of noncovalent bond results in rheology. Subject to a force, a polymer network deforms. Such an experiment is recorded as a curve on the plane of force and displacement. (a) The force−displacement curve measured at a high loading rate lies above that measured at a low loading rate. (b) The force−displacement curve during unloading lies below that during loading. (c) In the reversible process of elasticity, the force−displacement curve during unloading coincides with that during loading.

irreversible processes. The commonly used term "elastic crack growth" is a misnomer. Elasticity is a reversible process, whereas crack growth is an irreversible process in every material, even in a material as brittle as silica.

The study of crack growth inevitably draws on the chemistry of bonds. In a material, atoms bind through a fundamental force in nature—the electromagnetic force. This fundamental force manifests in numerous ways, called covalent and noncovalent bonds (Figure 1). Covalent bonds include "permanent" ones such as carbon−carbon bonds (C−C) and "dynamic" ones such as disulfide bonds (S−S).[1,2] Noncovalent bonds include the van der Waals force, $\pi-\pi$ stacking, hydrophobic interaction, hydrogen bonds, ionic bonds, and complexation.[3]

The free energies of the bonds are conveniently reported in units of $k_BT$, where $k_B$ is the Boltzmann constant and $T$ is the absolute temperature. The thermal energy is on the order of $k_BT$. At room temperature (298 K), $k_BT$ = 1/40 eV = 4.11 × $10^{-21}$ J. Representative free energies of permanent covalent bonds include carbon−carbon bonds (∼140 $k_BT$) and silicone−oxygen bonds (∼180 $k_BT$).[4] Representative free energies of dynamic covalent bonds include disulfide bonds (∼100 $k_BT$) and a boronic ester bond (∼40−52 $k_BT$). Covalent bonds are commonly much stronger than noncovalent bonds.

A polymer network is an architecture of covalent and noncovalent bonds (Figure 2). Covalent bonds link repeat units into chains and cross-link the chains into the network. A segment of a chain between two cross-links is called a strand. Strands bind one another by noncovalent bonds. Some noncovalent bonds are sufficiently weak to break and reform by thermal fluctuation. Other noncovalent bonds, of modest strength, can break under external forces and may or may not reform afterward. The covalent bonds within the strands preserve the connectivity of the network, giving the network solid-like attributes. The noncovalent bonds between the strands enable the repeat units in different strands to change neighbors, giving the network liquid-like attributes. The coexistence of covalent and noncovalent bonds makes the polymer network a molecular hybrid of solid and liquid.

A polymer network provides an enduring object for learning mechanochemistry. Subject to a force, a polymer network deforms. For the time being, assume that the force is too small to break covalent bonds. The noncovalent bonds, however, can break and possibly reform. Consequently, the deformation preserves the neighbors of repeat units on each strand but changes neighbors of repeat units on different strands. The intact strands resist deformation by entropic elasticity[6,7] while the noncovalent bonds resist deformation by viscosity.[8] The polymer network undergoes viscoelastic deformation, as studied in rheology, a field that lies outside the scope of this review, but sheds light on crack growth.

In a common experiment in rheology, a network is pulled to record a force−displacement curve (Figure 3a). The breaking and reforming of noncovalent bonds are sensitive to the loading rate so that the force−displacement curve measured at


https://doi.org/10.1021/acs.chemrev.5c00663
Chem. Rev. XXXX, XXX, XXX−XXX

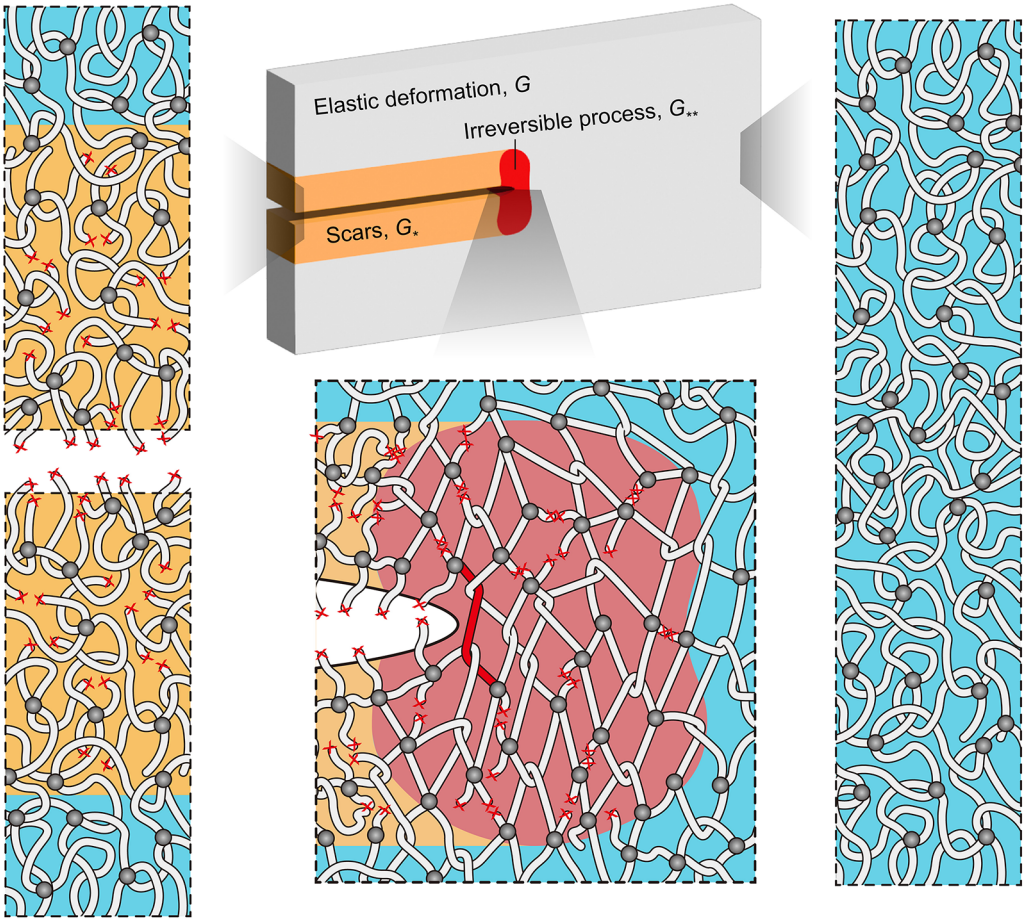


**Figure 4.** A crack grows in a polymer network by the coevolution of three regions: a zone of an irreversible process (red), two layers of scars (yellow), and a background of a reversible process of elastic deformation (gray). This spatial decomposition provides the physical basis for the thermodynamic formulation of crack growth. The formation associates, respectively, the irreversibility with the reduction in free energy, $G_{**}$, the scars with excess free energy, $G_{*}$, and the elasticity with the energy release rate, $G$. The crack grows when the crack driving force equals crack resistance: $G = G_{*} + G_{**}$.

a high loading rate lies above that measured at a low loading rate. When the force is reduced, so is the displacement (Figure 3b). The force–displacement curve of unloading lies below that of loading. This phenomenon, called hysteresis, indicates that the network deforms by an irreversible process in which the noncovalent bonds break and possibly reform. When the force is reduced to zero, the network often does not recover its original shape. The residual displacement results from the reformation of noncovalent bonds, which usually change neighbors of repeat units on different strands. When the loading rate is low enough for the noncovalent bonds to equilibrate, the unloading curve and the loading curve coincide, and the network is said to deform by a reversible process of elasticity (Figure 3c). A reversible process is an idealization. Every actual process is irreversible. The reversible process of elasticity is a useful idealization as long as hysteresis is negligibly small.

A crack grows in a body by coevolving three regions (Figure 4):

1. a zone of an irreversible process around the crack front,
2. two layers of scars trailing behind the crack front, and
3. a background of a reversible process of elastic deformation outside the irreversible zone and scars.

The three regions of coevolution are described separately as follows.

Around the crack front lies an irreversible zone. The irreversibility is mediated by two molecular mechanisms: a small fraction of covalent bonds with strand rupture, and many noncovalent bonds between strands break and possibly reform. The large difference in strength between the covalent and noncovalent bonds sets up the size of the irreversible zone. Before a strand ruptures, noncovalent bonds break and possibly reform so that the strand slips relative to neighbors. The slip enables high tension in the strand to transmit over the entire length of the strand. When one covalent bond ruptures, the strand snaps and the tension of the entire strand relaxes. This snapping is rapid—too fast for noncovalent bonds to remain in equilibrium—resulting in an out-of-equilibrium process. The irreversible zone is usually much larger than the mesh of the polymer network. For the network to tear into two pieces, strands must break to form two crack surfaces. Off the crack surfaces, some other strands may also break. At some distance away from the crack front, noncovalent bonds may still fall out of equilibrium, even though the covalent bonds remain intact.

Trailing behind the crack front are two layers of scars. The broken covalent bonds usually do not reform. Some ends of broken strands are exposed on the surfaces, and others are buried beneath the surfaces. In the scarred network, some broken noncovalent bonds may reform. Even reformed, the


https://doi.org/10.1021/acs.chemrev.5c00663
Chem. Rev. XXXX, XXX, XXX−XXX

repeat units on different strands in general change neighbors so that the scarred network often has residual deformation visible to the naked eye. The thickness of the layers of scars is comparable to the size of the irreversible zone.

Outside the irreversible zone and scars, the body undergoes the reversible process of elastic deformation. The covalent bonds remain intact. The noncovalent bonds, if breaking, reform fast compared to the loading rate. That is, the breaking and reformation of noncovalent bonds equilibrate in the body under elastic deformation, just as in a liquid under a low rate of deformation.

The irreversible zone is considered localized if it is small relative to the body. The idealization of localized irreversibility is not commonly taught in thermodynamics and has led to a particular approach to the study of crack growth, called fracture mechanics. Central to fracture mechanics is the energy release rate—the thermodynamic driving force for crack growth. We frame fracture mechanics as a tale of two bodies. The energy release rate is defined using an ideal body in which a crack is stationary and deformation is elastic, and is applied to a real body in which a crack grows by a localized irreversible process. The idealization of localized irreversibility divides the labor of studying crack growth into two tasks. First, in an ideal body, relate the energy release rate to the geometry and load of the body through a boundary value problem of elasticity. Second, in a real body, use the energy release rate to characterize resistance to crack growth as a material property. The division of labor decouples two sources of complexity: shape and load of the body, and the irreversible process and scars created by the crack. The two sources of complexity take place at two different length scales, which are separated in the idealization of localized irreversibility.

An analogy between rheology and fracture mechanics helps unify their treatment of irreversible processes. Just as stress is the driving force for deformation, the energy release rate is the driving force for crack growth. In rheology, a central question is: given a history of stress, what is the resulting history of deformation? In fracture mechanics, a central question is: given a history of energy release rate, what is the resulting history of crack growth? A monotonically increasing energy release rate is used to measure toughness and the crack resistance curve. A cyclic energy release rate is used to study fatigue crack growth. A static energy release rate is used to study crack growth in materials undergoing viscoelasticity, reaction, or poroelasticity. Viewed in this light, fracture mechanics can be regarded as the rheology of a localized irreversible process, namely, crack growth.

Early development of fracture mechanics has been documented.[9−11] Relevant to this review are milestones that mark the expanding uses of the energy release rate. In 1921, 28-year old British mechanical engineer, Alan Arnold Griffith, initiated fracture mechanics in a paper titled *The Phenomena of Rupture and Flow in Solids*.[12] He introduced the concept of the energy release rate, perhaps not as explicitly as we now wish. His theory (mistakenly) regarded crack growth as a reversible thermodynamic process, but his experiment (correctly) measured what we now call toughness, a quantity resulting from an irreversible thermodynamic process. He studied crack growth in silica, a material so brittle that the difference between reversible and irreversible processes is small. In 1930, Obreimoff studied slow crack growth in mica, which is an irreversible process.[13] In 1944, Orowan traced delayed fracture in silica to another irreversible process: stress-assisted hydrolysis.[14] The energy release rate has been used to measure the toughness of numerous materials, including metals,[15,16] elastomers,[17] plastics,[18] composites,[19] and biological tissues.[20] In each of these materials, toughness is greatly amplified by localized irreversibility. Fatigue crack growth was first studied by Thomas for elastomers[21] and by Paris and colleagues for metals.[22] Crack growth in viscoelastic materials was first studied by Mullins and Greensmith.[23,24] The energy release rate was used to study ozone attack in rubber[25] and stress-assisted hydrolysis in silica.[26] In 1967, Lake and Thomas attributed fatigue resistance to an irreversible process specific to polymer networks: the snapping of a layer of polymer strands.[27] In 1978, Rice reframed crack growth as an isothermal, localized, irreversible process.[28] The study of crack growth in polymer networks—the focus of the present article—has been rejuvenated since the discovery of the double network hydrogel.[29] Advances in crack growth in polymer networks in the last two decades have been reviewed.[30−52]

This review highlights the interplay of thermodynamics and molecular mechanisms. Emphasis is placed on the idealization of localized irreversibility, which leads us to reexamine the concept of the energy release rate within a thermodynamic framework that distinguishes reversible and irreversible processes. Crack resistance comes from two contributions: the excess in free energy due to the scars behind the crack front and the reduction in free energy due to the irreversible process around the crack front. We present the singular elastic field as a scaling relation and characterize the localized irreversibility with a length scale called the fractocohesive length. Also highlighted are the molecular principles used to design crack-resistant materials. Topics are selected with the needs of the experimentalist in mind. But we do not shy away from theoretical concepts and treat them with sufficient rigor for experimental work. It has been a long tradition for many physicists and chemists to study the rheology of polymers. We hope that this review will help people study the fracture of polymers, an area where integrated thermodynamic and molecular understanding is increasingly essential for material innovation.

Sections 2−6 establish the thermodynamic foundation. Section 2 presents the thermodynamics of crack growth as a tale of two bodies: an ideal body and a real body. Section 3 lists the expressions of the energy release rate for several experimental setups. Section 4 presents the singular elastic field and describes the concept of the $G$-annulus and fractocohesive length. Section 5 describes microscopic processes that deconcentrate stresses at crack tips. Section 6 describes crack growth under energy release of several types of histories: monotonic, cyclic, and static. Sections 7−14 describe molecular principles of crack growth in representative polymer networks. Some sections are organized by specific polymers, including polyacrylamide (Section 7), natural rubber (Section 9), and poly(ethylene glycol) (Section 10). Other sections are organized by architectures of networks, including tanglemers (Section 8), networks cross-linked by noncovalent bonds (Section 11), interpenetrating networks (Section 12), polymer networks reinforced by hard particles (Section 13), and polymer networks reinforced by fibers or fabrics (Section 14). Section 15 concludes with outlooks for future development.

This review presents a thermodynamic framework for crack growth in polymer networks and connects it to molecular structure, chemical synthesis, and mechanical testing. While


https://doi.org/10.1021/acs.chemrev.5c00663
Chem. Rev. XXXX, XXX, XXX−XXX

focused on polymer networks, the principles extend to a wide range of soft and tough materials.

## 2. THERMODYNAMICS OF REVERSIBILITY, IRREVERSIBILITY, AND SCARS

Crack growth is a coevolution of a zone of irreversible process, two layers of scars, and a background of the reversible process of elasticity (Figure 4). The coevolution is commonly assumed to take place under the conditions of constant temperature. The thermodynamics of isothermal processes is outlined in this section. Our treatment is consistent with common practice in the experimental study of the mechanical behavior of materials, when the loading rate is low enough for the temperature in the material to homogenize and equilibrate with the temperature in the environment. For such isothermal processes, thermodynamics requires the entropy of the combination of the materials and the environment to be maximized. As we recall below, this requirement is equivalent to the minimization of free energy of the material. It is unfortunate that in the literature of mechanics, the term "free energy" is not often used, giving the erroneous impression that only the internal energy is used. In fact, elastic energy is free energy, and what is being minimized is free energy, not internal energy.

### 2.1. On Being Thermal

The word "thermal" is associated with microscopic interaction. A part of the world is called a system, and the rest of the world is called the surroundings. A thermal system is a part of the world that interacts with the rest of the world in one mode: transferring energy by microscopic interaction. This mode of interaction is called thermal contact. When two thermal systems in thermal contact cease to transfer energy, they are said to be in thermal equilibrium and have the same temperature. A thermal reservoir is a thermal system that keeps its temperature constant when transferring energy with its surroundings.

If a thermal system in thermal equilibrium with a thermal reservoir can still change its state, then we say that the thermal system undergoes an isothermal process (Figure 5). The isothermal process is characterized by the temperature $T$ of the thermal reservoir, as well as by a variable $x$ internal to the thermal system. In later sections, $x$ will represent variables such as the crack length or displacement. The thermal system is characterized by its free energy as a function of temperature and the internal variable, $\Pi(T, x)$.

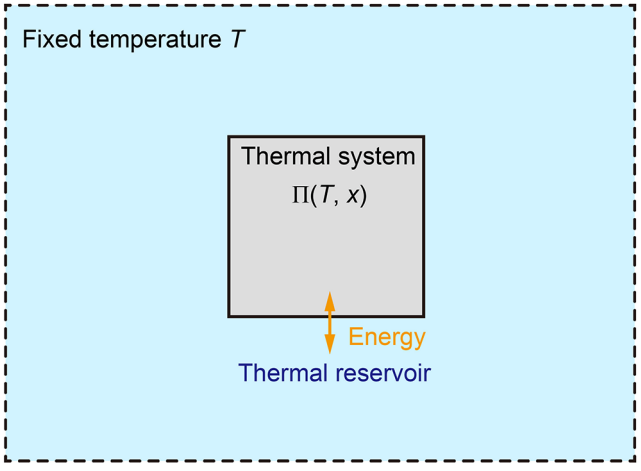


**Figure 5.** A thermal system and a thermal reservoir are in thermal equilibrium and have the same temperature $T$. The thermal system undergoes an isothermal process by exchanging energy with the thermal reservoir and changing an internal variable $x$.

Following a common practice in mechanics of materials, in dealing with an isothermal process we mention neither the thermal reservoir nor temperature. Rather, we assume that a thermal system is in thermal equilibrium with a thermal reservoir and write the free energy of the thermal system, $\Pi(T, x)$, simply as a function of the internal variable, $\Pi(x)$.

In the isothermal process, the thermal system exchanges energy with the thermal reservoir, as well as changes the internal variable $x$. The isothermal process is irreversible when the change in the internal variable reduces the free energy, and is reversible when the change in the internal variable keeps the free energy stationary. The isothermal process equilibrates when the internal variable attains a value that minimizes the free energy.

Incidentally, in an isothermal process, the reduction in free energy is often called "energy dissipation". This phrase is a misnomer. Recall the definition of free energy of a thermal system: $\Pi = U - TS$, where $U$ is the internal energy and $S$ is the entropy. A reduction in free energy does not imply a reduction in internal energy and may instead result from an increase in entropy. Nevertheless, because the phrase "energy dissipation" is widely used in the literature, we adopt it here to mean a "reduction in free energy" under isothermal conditions.

### 2.2. Characterize the Surface of a Liquid by an Excess in Free Energy

We now illustrate the thermodynamics of reversible and irreversible processes using surface tension. The bonding environment of a molecule on the surface of a liquid differs from that of a molecule inside the liquid (Figure 6a). Two drops of the liquid in contact spontaneously merge into a single drop. The merger reduces the number of molecules on the surface. This observation shows that the free energy per molecule at the surface of the liquid is higher than that inside the liquid. Gibbs defined the excess in free energy as the surface free energy.[53] The excess in free energy is localized to the surface within a thickness on the scale of individual molecules. As long as a drop of liquid is composed of many molecules, the surface free energy is proportional to the surface area. We denote the surface free energy per unit surface area by $\gamma$.

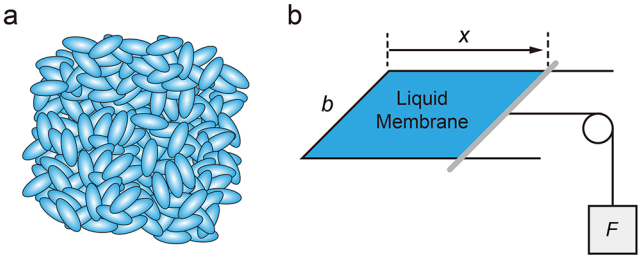


**Figure 6.** Excess in free energy of molecules on the surface relative to that of molecules in the interior. (a) The bonding environment of a molecule at the surface of a liquid differs from that of a molecule inside the liquid. (b) A liquid membrane and a hanging weight constitute a thermal system.

The definition of an excess in free energy leads to its experimental measurement. Consider an experimental setup, in


https://doi.org/10.1021/acs.chemrev.5c00663
Chem. Rev. XXXX, XXX, XXX−XXX

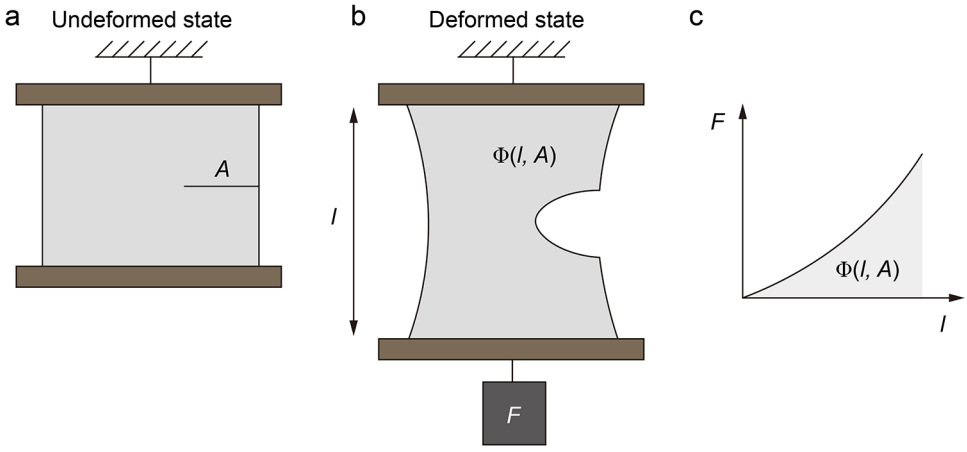


**Figure 7.** In an ideal body subject to a load, deformation is elastic and a crack is stationary. (a) In the undeformed state, the body contains a crack of area $A$. (b) In a deformed state, subject to a force $F$, the body deforms to a length $l$, but the crack does not grow. The body is elastic everywhere and is in thermal equilibrium with a thermal reservoir. (c) The elastic energy of the body is the area under the force−length curve.

which a membrane of liquid is confined by a rigid frame and a slider of length $b$ (Figure 6b). The slider is pulled to a distance $x$ by a fixed force $F$, pictured as a hanging weight. The thickness of the membrane is much larger than the dimension of an individual molecule. The membrane and the hanging weight together constitute a thermal system. The free energy of this thermal system is

$$\Pi = N\varphi + 2\gamma bx - Fx \tag{1}$$

Here, $N$ is the number of molecules in the membrane, $\varphi$ is the free energy per molecule in the bulk of the liquid, $2\gamma bx$ is the excess in free energy, and $-Fx$ is the potential energy of the hanging weight. The factor of 2 comes from the fact that the membrane has two surfaces. The number of molecules in the membrane is constant. When the membrane is stretched, molecules change neighbors, and some molecules migrate from the interior of the membrane to the surfaces of the membrane. The stretch does not affect the free energy per molecule in the bulk of the liquid, $\varphi$, but increases the number of molecules on the surfaces. The concept of the excess in free energy will reappear in our treatment of scars trailing behind the crack front (Section 2.5).

This thermal system has a single internal variable: the distance $x$. The free energy of the thermal system is a function of the distance, $\Pi(x)$. When the slider moves by $dx$, the free energy of the thermal system changes by

$$\Pi(x + dx) - \Pi(x) = (2\gamma b - F)dx \tag{2}$$

When the thermal system equilibrates, the free energy of the thermal system is stationary as the slider moves, $d\Pi = 0$, or

$$(2\gamma b - F)dx = 0 \tag{3}$$

This condition of equilibrium must hold for any small change $dx$ and is equivalent to

$$2\gamma b = F \tag{4}$$

The condition of equilibrium balances the two parts of the thermal system: the hanging weight and the liquid membrane. The slider can equilibrate at any distance $x$. A measurement of the hanging weight in equilibrium gives the excess free energy per unit area, $\gamma$. Equation 4 justifies a common name for $\gamma$: surface tension. An experiment like that described here was used by Griffith to measure the surface energy of silica (Section 5.1)

The excess in free energy scales with the free energy of intermolecular bonds. In silica glass, atoms bind by covalent bonds, $\gamma \approx 1$ J m$^{-2}$. In water, molecules bind by hydrogen bonds, $\gamma \approx 0.07$ J m$^{-2}$. In a polymer liquid in which chains bind by the van der Waals force, $\gamma \approx 0.01$−$0.1$ J m$^{-2}$.

When the thermal system undergoes an irreversible process, as the internal variable $x$ changes, the free energy of the thermal system decreases, $d\Pi < 0$, that is,

$$(2\gamma b - F)dx < 0 \tag{5}$$

This inequality—the condition of irreversibility—holds for any small change in distance, $dx \neq 0$. As an illustration, assume that the membrane is pulled slowly so that the molecules have enough time to change neighbors and equilibrate and that irreversibility results solely from the friction between the slider and frame. When $dx < 0$, the slider moves to the left, and the inequality requires that $F < 2\gamma b$, which means that the friction on the slider points to the right. When $dx > 0$, the slider moves to the right, and the inequality requires that $F > 2\gamma b$, which means that the friction on the slider points to the left. In either case, the inequality requires that the friction points in the direction against the motion of the slider.

### 2.3. Elasticity is a Reversible Thermodynamic Process

As described in the Introduction, a crack grows in a body by coevolving three aspects: a zone of the irreversible process, two layers of scars, and a background of elastic deformation (Figure 4). Under the conditions of localized irreversibility, the thermodynamics of crack growth is studied using two bodies: an ideal body and a real body. This subsection describes elasticity in the ideal body as a reversible thermodynamic process. This assumption of reversibility distinguishes the ideal body from real materials, in which deformation involves irreversible thermodynamic processes. Subsection 2.4 defines energy release rate $G$ using the ideal body. Subsection 2.5 characterizes the scars by the excess in free energy $G_*$ between the ideal body and the real body. Subsection 2.6 characterizes the irreversible process by reduction in free energy $G_{**}$ as the crack grows in the real body. Subsection 2.7 gathers the three coevolving aspects together, arriving at $G = G_* + G_{**}$.

An ideal body has the following characteristics.


https://doi.org/10.1021/acs.chemrev.5c00663
Chem. Rev. XXXX, XXX, XXX−XXX

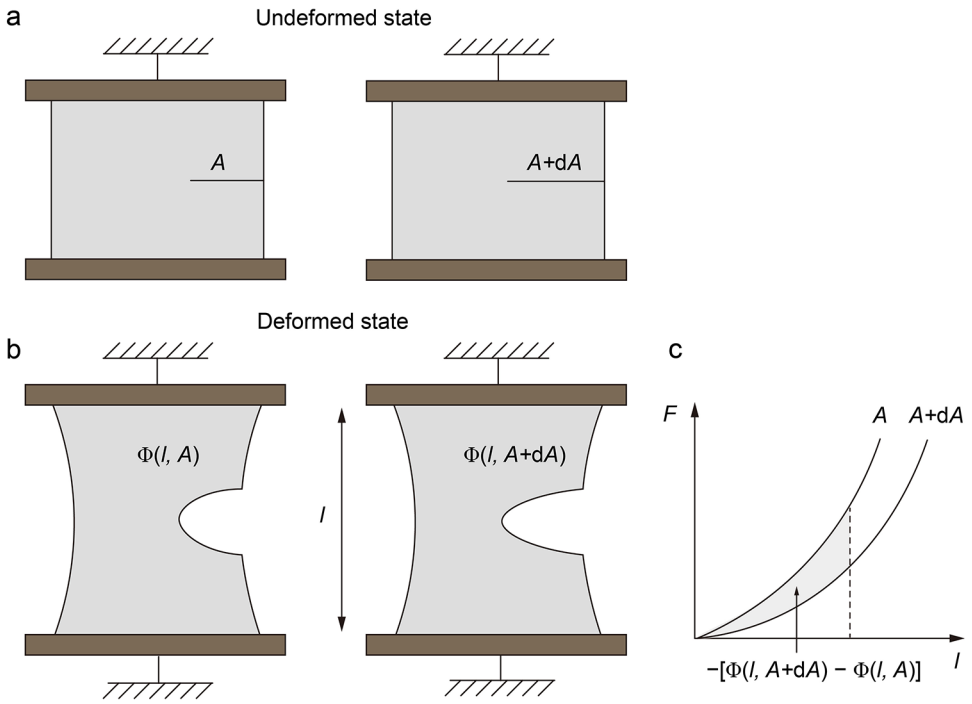


**Figure 8.** Two copies of the ideal body. (a) In the undeformed state, one body has a crack of area $A$, and the other body has a crack of area $A + dA$. In each copy of the ideal body, the crack is stationary; no growth occurs. (b) Each body is pulled to length $l$, but the crack does not grow. (c) The force−length curves of the two bodies.

1. In the undeformed state, the body contains a crack of area $A$ (Figure 7a). The surfaces of the crack are flat planes, and the front of the crack is a straight line. Throughout this article, crack area $A$ is defined in the undeformed state.
2. In a deformed state, subject to a force $F$, the body deforms to length $l$ (Figure 7b). The body is everywhere elastic, in thermal equilibrium with a thermal reservoir. The elasticity deformation changes the shape of the crack surfaces but does not advance the crack front. That is, the crack remains stationary.

When $A$ and $l$ are fixed, the ideal body itself is a thermal system. The free energy of this thermal system, $\Phi$, is called the elastic energy. Consider many copies of the ideal body. Each copy is a thermal system characterized by its own crack area $A$, length $l$, and elastic energy $\Phi$. All copies of the ideal body form a family of thermal systems, characterized by the free energy as a function of the two variables, $\Phi(l, A)$. For two slightly different copies of the ideal body, $(l, A)$ and $(l + dl, A + dA)$, their elastic energies differ by

$$\Phi(l + dl, A + dA) - \Phi(l, A) = \frac{\partial \Phi(l, A)}{\partial l} dl + \frac{\partial \Phi(l, A)}{\partial A} dA \tag{6}$$

We next interpret the two partial derivatives, $\partial\Phi(l, A)/\partial l$ and $\partial\Phi(l, A)/\partial A$.

Consider an ideal body containing a fixed crack area $A$, and subject to a constant force $F$. Represent the constant force by a hanging weight of potential energy, $-Fl$. The body itself is no longer a thermal system because the body interacts with the force. But the body and the hanging weight together constitute a thermal system. The free energy of this thermal system is the sum of two parts, the elastic energy of the body and the potential energy of the hanging weight:

$$\Pi = \Phi(l, A) - Fl \tag{7}$$

The thermal system has two internal variables, $l$ and $A$. For now, let $l$ vary and $A$ be fixed. The ideal body deforms by the reversible process of elasticity, in equilibrium with respect to $l$. This condition of mechanical equilibrium requires $l$ to take a value that minimizes the free energy, so that

$$\left[\frac{\partial \Phi(l, A)}{\partial l} - F\right] dl = 0 \tag{8}$$

The equality holds for any small change in length, $dl$. The condition of equilibrium is equivalent to

$$\frac{\partial \Phi(l, A)}{\partial l} = F \tag{9}$$

This condition of mechanical equilibrium interprets the partial derivative, $\partial\Phi(l, A)/\partial l$. The condition also enables an experimental determination of the free-energy function, $\Phi(l, A)$. Prepare a body with a crack of area $A$. Measure the force−length curve of the body (Figure 7c). As the body is pulled, the crack remains stationary, $dA = 0$. Equation 9 indicates that an integration of the force−displacement curve gives the function of free energy, $\Phi(l, A)$. That is, the elastic energy is the area under the force−displacement curve.

Incidentally, recall the definition of the free energy of a thermal system, $\Phi = U - TS$, where $U$ is the internal energy and $S$ is the entropy of the thermal system. For an elastomer network, the internal energy is a function of temperature $T$ and is nearly independent of length $l$. That is, the internal energy is liquid-like. When the temperature is fixed, the elasticity is entirely due to entropy as a function of length. The elastomer network is said to undergo entropic elasticity.

### 2.4. Define the Energy Release Rate Using an Ideal Body

The ideal body is not a physical system but a reference to define the energy release rate. The definition of the energy release rate does not involve crack growth in a real body.


https://doi.org/10.1021/acs.chemrev.5c00663
Chem. Rev. XXXX, XXX, XXX−XXX

Rather, we consider two copies of the ideal body. In the undeformed state, one copy has a crack of area $A$ and the other copy has a crack of area $A + dA$ (Figure 8a). Let $dA > 0$. When deformed to the same length $l$, the two copies have different amounts of elastic energy, $\Phi(l, A)$ and $\Phi(l, A + dA)$ (Figure 8b). The force−length curve of the body with the large crack lies below the force−length curve of the body with the small crack (Figure 8c). Consequently, deformed to the same length $l$, the copy with a larger crack has lower elastic energy:

$$\Phi(l, A + dA) < \Phi(l, A) \tag{10}$$

This inequality reflects a fact: an ideal elastic body with a longer crack is more compliant and thus stores less elastic energy under the same displacement.

Define the energy release rate by

$$G = -\frac{\Phi(l, A + dA) - \Phi(l, A)}{dA} = -\frac{\partial \Phi(l, A)}{\partial A} \tag{11}$$

Equations 9 and 11 have similar structures. Just as the hanging weight is the thermodynamic driving force for displacement, the energy release rate is the thermodynamic driving force for crack growth. Unlike Equation 9, however, Equation 11 is *not* a condition of equilibrium but merely gives the quantity $-\partial\Phi(l, A)/\partial A$ a name: energy release rate. The definition of the energy release rate comes from Griffith.[12]

The energy release rate is commonly defined as "the reduction in potential energy associated with the growth of a crack by a unit area". This definition reflects Equation 11 but misses many significant facts:

1. The body is an ideal body, not a real body. Thus, $G$ itself is a quantity in reversible thermodynamics, and is not the reduction in free energy associated with an irreversible process.
2. The crack area is measured in the undeformed state.
3. The crack does not grow. Rather, picture copies of the ideal body of different crack areas.
4. The body is in thermal equilibrium with a thermal reservoir.
5. The phrase "potential energy" is the same as "free energy of the thermal system".
6. When the displacement is fixed, the ideal body itself is a thermal system and the free energy is the elastic energy of the ideal body.
7. When the force is fixed, the force is represented by a hanging weight, the ideal body and the hanging weight together constitute a thermal system, and the free energy is the sum of the elastic energy of the ideal body and the potential energy of the hanging weight.

Because in the ideal body the crack is stationary and the deformation is elastic, the energy release rate is a quantity in reversible thermodynamics. How is the energy release rate used to characterize crack growth in a real body, an irreversible process? This question is answered in the following three subsections.

### 2.5. Characterize Scars by the Excess in Free Energy

As recalled before, Gibbs defined the surface energy by the excess in free energy.[50] Here we use the excess in free energy to characterize the scars created by a crack. Consider two bodies: an ideal body and a real body, each being subject to a constant force $F$, represented by a hanging weight (Figure 9). A crack grows in the real body. The real body and the hanging weight together constitute a thermal system, in thermal equilibrium with a thermal reservoir. The free energy of the thermal system is a function of two internal variables, $\Pi(l, A)$. When the hanging weight moves by displacement $dl$ and the crack grows by area $dA$, the free energy of the thermal system changes by

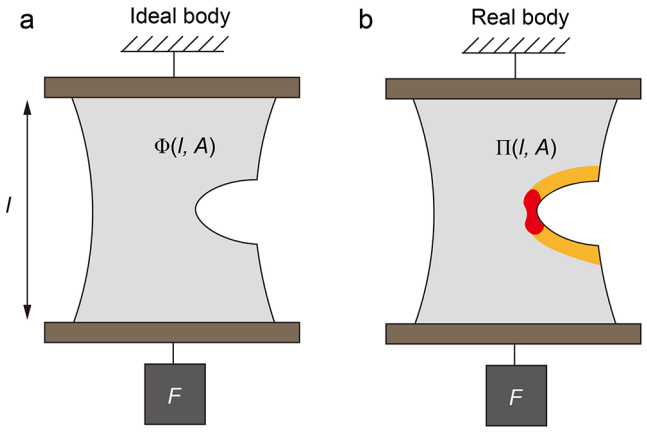


**Figure 9.** A tale of two bodies. (a) In an ideal body, deformation is elastic, and a crack is stationary. (b) In a real body, a crack grows by an irreversible process, leaving behind two layers of scars. Outside the irreversible zone and scars, the real body undergoes the reversible process of elasticity.

$$d\Pi = d\Phi - F\, dl + G_*\, dA \tag{12}$$

Here $\Phi(l, A)$ is the elastic energy of the ideal body, $-Fl$ is the potential energy of the hanging weight, and $G_*$ is the excess in free energy per unit crack area between the real body and the ideal body. For the time being, the crack is taken to grow in a steady state, and the irreversible zone translates in the material so that the free energy stored in the irreversible zone is constant. Thus, in writing the free energy of the real body, we do not add the contribution from the irreversible zone. Note the similarity of Equations 1 and 12. The former defines the excess free energy of a surface, and the latter defines the excess free energy of scars.

The scars represent structural changes that persist after the crack has passed. The form of the scars and magnitude of $G_*$ depend on the materials. When the scars involve only the two fully relaxed surfaces, the excess in free energy coincides with surface energy: $G_* A = 2\gamma A$ (Figure 10a). As mentioned in the Introduction, a polymer network is scarred by broken covalent bonds and noncovalent bonds (Figure 10b). A crack grows in a brittle polymer glass by crazes, in which fibrils are drawn from the bulk of the material (Figure 10c). In a fiber-reinforced composite, fibers may be broken and pulled out of the matrix (Figure 10d). In a brittle metal, scars involve not only the crack surfaces but also dislocations generated by intense deformation (Figure. 10e). In a ductile metal, a crack grows by the nucleation, growth, and coalescence of voids (Figure 10f).

When the hanging weight moves by displacement $dl$ and the crack grows by area $dA$, the free energy of the thermal system changes by

$$\begin{aligned} d\Pi &= \Pi(l + dl, A + dA) - \Pi(l, A) \\ &= \left[\frac{\partial \Phi(l, A)}{\partial l} - F\right] dl + \left[\frac{\partial \Phi(l, A)}{\partial A} + G_*\right] dA \end{aligned} \tag{13}$$

The two internal variables, $l$ and $A$, are treated differently. The thermal system is in equilibrium with respect to


https://doi.org/10.1021/acs.chemrev.5c00663
Chem. Rev. XXXX, XXX, XXX−XXX

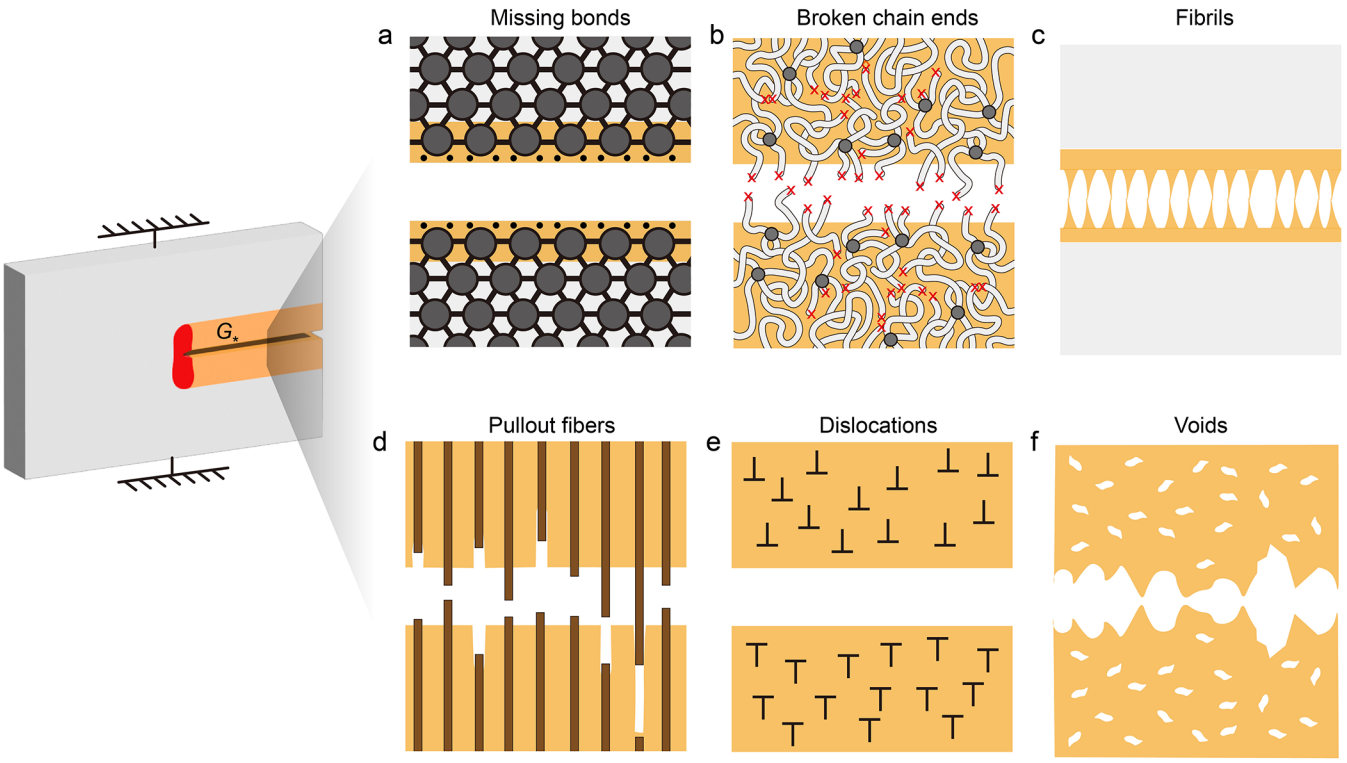


**Figure 10.** Mechanisms of scars depend on materials. (a) Broken bonds on surfaces. (b) Broken polymer strands and noncovalent bonds in an elastomer. (c) Fibrils in a polymer glass. (d) Pullout fibers in a composite. (e) Dislocations in a metal. (f) Voids in a metal. Like surface energy, scars are characterized by an excess in free energy, $G_*$. Scars in the wake of the crack provide forensic evidence for the irreversible process around the front of the crack.

displacement, d$l$, so that the first bracket vanishes, which recovers the condition of mechanical equilibrium: $F = \partial\Phi(l, A)/\partial l$

The thermal system, however, is out of equilibrium with respect to crack growth, d$A$, so that the second bracket does not vanish. Recall the definition of the energy release rate, $G = -\partial\Phi(l, A)/\partial A$. Equation 13 becomes

$$d\Pi = (-G + G_*)dA \tag{14}$$

When the crack grows by d$A$, the ideal body changes its elastic energy by $-G$ d$A$ and the scars change the excess free energy by $+G_*$ d$A$. Together, they change the free energy of the real body by dΠ. An equation like equation 14 was derived by Rice.[28]

## 2.6. Characterize the Irreversible Process by the Reduction in Free Energy

A crack grows in a real body by an irreversible process, which reduces the free energy. Specifically, crack growth in a polymer network is an irreversible process mediated by two molecular mechanisms: strand scission and strand slip (Figure 4).

When the crack grows by d$A$, denote the change in free changes by

$$d\Pi = -G_{**}\, dA \tag{15}$$

Here, $G_{**} > 0$ is the reduction in free energy associated with crack growth per unit area. The reduction in free energy, $G_{**}$, differs from the excess in free energy, $G_*$. The former, $G_{**}$, characterizes the irreversible process—the free energy lost as the crack grows. The latter, $G_*$, characterizes the scars—the free energy stored in the wake of the crack. Figure 10 illustrates scars in several types of materials. Pictured in each case is the microscopic mechanism of scars. One can imagine the irreversible process that leads to the scars. For example, in ductile metals, the scars are voids in the metals, and the irreversible process is the plastic deformation that causes the voids to grow (Figure 10f).

## 2.7. Irreversible Process, Scars, and Elasticity

A comparison of Equations 14 and 15 gives

$$G = G_* + G_{**} \tag{16}$$

The three terms come from the three coevolving aspects of crack growth (Figure 4). The crack driving force, the energy release rate $G$, comes from the reversible process of elasticity. The crack resistance results from two contributions: the free energy reduction due to the irreversible process around the front of the crack, $G_{**}$, and the excess in free energy due to the scars in the wake of the crack, $G_*$.

Equation 16 is the condition for crack growth: a crack grows when the crack driving force, $G$, equals the crack resistance, $G_* + G_{**}$. This equation dates back to Irwin[15] and Orowan.[16] This condition holds regardless of material class and loading mode; it is a general thermodynamic principle of crack growth. In experiments, the driving force $G$ is set by the applied load (Section 3). As a crack grows, an experimental determination of crack driving force $G$ gives crack resistance $G_* + G_{**}$. Never in practice are the two contributions to crack resistance, $G_*$ and $G_{**}$, measured separately. But the two contributions are distinct, as illustrated in the following example.

Consider a crack in a material under monotonically increasing driving force $G$. The crack grows in a steady state when $G$ reaches a certain value, $G_c$, called toughness. Toughness results from the two contributions: $G_c = G_* +$


https://doi.org/10.1021/acs.chemrev.5c00663
Chem. Rev. XXXX, XXX, XXX−XXX

$G_{**}$. We have considered crack growth in a polymer network (Figure 4). Behind the crack front, the scars include the ends of broken strands as well as broken and possibly reformed noncovalent bonds. Even reformed noncovalent bonds may scar the material by leaving residual deformation. Each strand consists of many repeat units. Consequently, in the scarred zone, the repeat units greatly outnumber the broken ends of strands, and $G_*$ is expected to be on the order of the surface energy of a polymer melt. The surface energy of a polymer melt scales with the energy of noncovalent bonds, so that excess in free energy $G_*$ is on the order of $10^{-2}$ J m$^{-2}$. Around the crack front, the irreversible process is mediated by the slip and scission of strands. Just before a strand breaks, the tension in the strand is near the covalent bond strength and is transmitted over the entire length of the strand. The high tension in the strand also causes many strands to slip by breaking and reforming noncovalent bonds. When the strand breaks at a single covalent bond, the entire strand snaps, leading to a large reduction in free energy, so that $G_* \ll G_{**}$. The measured toughness $G_c$ of a polymer network often exceeds $10^3$ J m$^{-2}$. That is, scars contribute negligibly to toughness. Scars, however, are observable and have led to the discipline of fractography. Scars provide forensic evidence for the irreversible process (Figure 10).

### 2.8. Stress, Stretch, and Elastic Energy Density

In general, an elastic body deforms by an inhomogeneous field, governed by the differential equations of the continuum theory of elasticity. Imagine that the body consists of many small pieces. Each small piece is large compared to the microstructure of the material so that the piece can be represented as a continuum and is small compared to the size of the body so that the deformation in the piece is regarded as being homogeneous. Associated with the inhomogeneous deformation of the body are many small pieces, each undergoing a homogeneous deformation. This review does not describe the differential equations of elasticity but invokes quantities like stress, stretch, and elastic energy density.

As an illustration, consider a rod undergoing a homogeneous elastic deformation. In the undeformed state, the rod has cross-sectional area $A$ and length $L$ (Figure. 11a). In a deformed state, the rod is subject to a force $F$, and has cross-sectional area $a$ and length $l$ (Figure. 11b). The thermodynamic analysis of the rod is similar to that in Section 2.4. Specifically, the elastic energy of the rod is a function of length $\Phi(l)$, and equilibrium with respect to $l$ requires that $F = \mathrm{d}\Phi(l)/\mathrm{d}l$. Thus, the elastic energy $\Phi(l)$ is the area under the force–length curve (Figure 11c).

Assume that the rod undergoes a homogeneous deformation. Define stress by the force in the deformed state divided by the cross-sectional area in the undeformed state, $s = F/A$. Define stretch by the length in the deformed state divided by the length in the undeformed state, $\lambda = l/L$. Define elastic energy density by the elastic energy in the deformed state divided by the volume in the undeformed state, $W = \Phi/LA$. The elastic energy density is a function of stretch, $W(\lambda)$. The condition of equilibrium $F = \mathrm{d}\Phi(l)/\mathrm{d}l$ becomes $s = \mathrm{d}W(\lambda)/\mathrm{d}\lambda$. Thus, the elastic energy density is the area under the stress–stretch curve (Figure 11d).

### 2.9. Work of Fracture

A rod can be stretched to rupture (Figure 12). Here, $\lambda_c$ is the stretchability and $s_c$ is the strength. The area underneath the stress–stretch curve is the work of fracture, $W_c$. A polymer network fractures by breaking covalent bonds, but the strength of a polymer network is typically orders of magnitude lower than that of covalent bonds.[54−56] The origin of this enormous discrepancy is still under active investigation.[57−59]

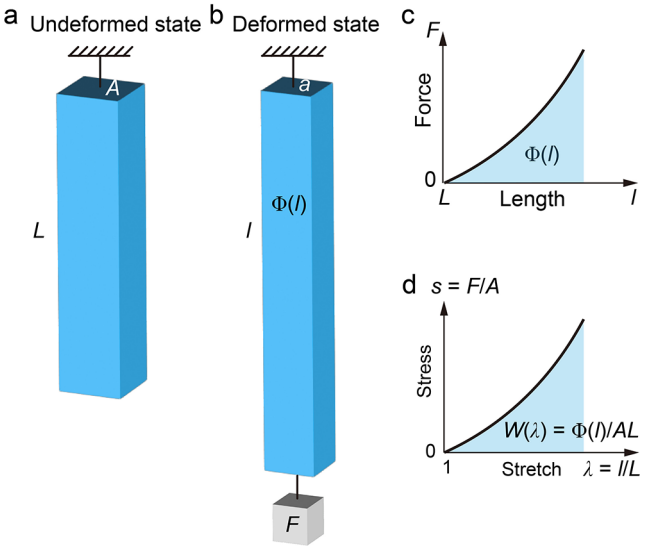


**Figure 11.** A rod undergoing a homogeneous, elastic deformation. (a) Undeformed state. (b) Deformed state. (c) Force–length curve. (d) Stress–stretch curve.

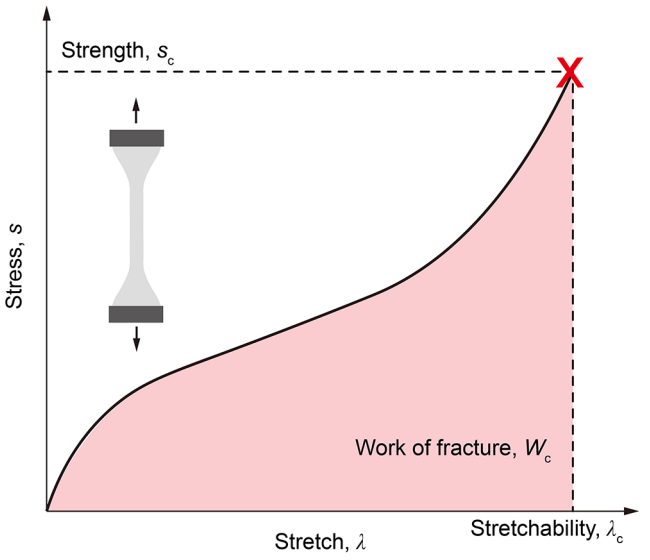


**Figure 12.** A sample without a precut crack is stretched until fracture. The area under the stress–stretch curve gives the work of fracture.

## 3. ENERGY RELEASE RATES FOR SPECIMENS COMMONLY USED TO STUDY CRACK GROWTH

The concept of the energy release rate divides the study of crack growth into two tasks. This section mainly deals with the first task: relate the energy release rate to the geometry and load of an ideal body in which the crack is stationary and deformation is elastic. Of particular interest are specimens commonly used in studying crack growth. In the second task, the energy release rate is used as a driving force for crack growth in a real body. This task is illustrated here by the experimental measurement of toughness and will be described in considerable depth in later sections.


https://doi.org/10.1021/acs.chemrev.5c00663
Chem. Rev. XXXX, XXX, XXX−XXX

### 3.1. Specimen with a Center Crack or Single Edge Crack in Linearly Elastic Materials

Consider two geometries: a sheet of width $2b$ and with a center crack of length $2c$ (Figure 13a) and a sheet of width $b$ with a single edge crack of length $c$ (Figure 13b). The material is linearly elastic and has Young's modulus $E$. The sheet is thin and has a thickness of $t$. The specimen is subject to remote stress $s$. Relative to the sheet without a crack, the sheet with a crack lowers the free energy by $\Delta\Phi \sim -s^2c^2t/E$. Here, the free energy density scales as $s^2/E$ and the relevant volume associated with the crack scales as $c^2t$. By definition, the energy release rate is the reduction in free energy associated with the crack increase by a unit area. Consequently, the energy release rate takes the form

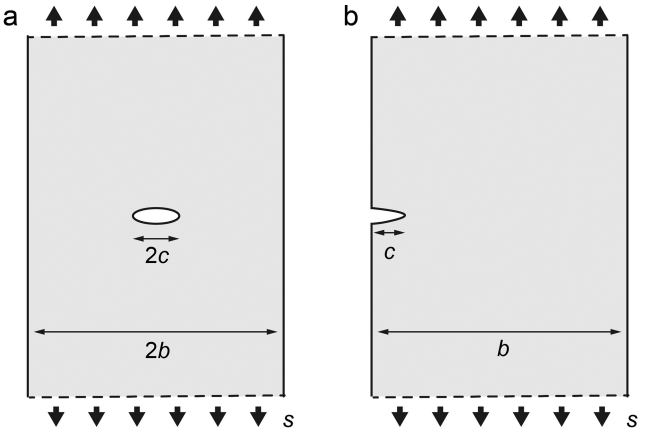


**Figure 13.** Two specimens used to study crack growth in linearly elastic materials. (a) A center crack. (b) An edge crack.

$$G = \beta\frac{s^2c}{E} \tag{17}$$

The coefficient $\beta$ is a dimensionless function of $c/b$, which is determined by solving the boundary value problems of elasticity.[60] In particular, $\beta = \pi$ for a center crack in an infinite sheet and $\beta = 3.9$ for an edge crack in an infinite sheet.

The above equation expresses the energy release rate in terms of measurable quantities, and is used in the experimental determination of toughness as follows. Prepare a strip of a material, cut a crack in the strip, pull the strip using a monotonically increasing stress $s$, and record the critical stress when the crack grows, $s_c$. By inserting $s_c$ into the above equation, one obtains the toughness of the material, $G_c$.

### 3.2. Specimen with an Edge Crack for Soft Materials

Next, consider a soft material of width $b$ and an edge crack of length $c$ (Figure 14a), $c \ll b$, and the height of the specimen is much larger than the width. The specimen is subjected to a stretch $\lambda$. The energy release rate takes the form[17]

$$G = 2k(\lambda)\, W(\lambda)c \tag{18}$$

The elastic energy density $W(\lambda)$ is measured by a specimen without a crack (Figure 14b). The dimensionless function $k(\lambda)$ is determined by solving the boundary value problem of elasticity using the finite element method.[61]

When measuring toughness, the precracked specimen is monotonically stretched to determine the critical stretch at fracture, $\lambda_c$. The critical stretch is inserted into the above equation to obtain the toughness of the material, $G_c$.

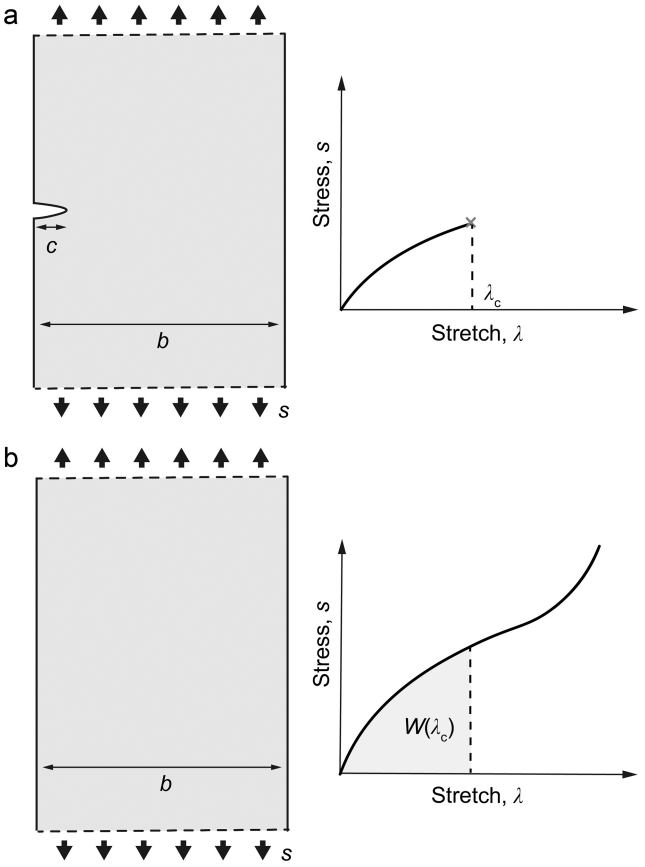


**Figure 14.** Single edge crack in soft materials. (a) A precracked specimen is stretched until fracture to get the critical stretch, $\lambda_c$. (b) The specimen without a precrack is stretched to get the stress–stretch curve and obtain the elastic energy density as a function of stretch, $W(\lambda)$.

### 3.3. Rectangular Sheet Pulled on Long Edges

In the undeformed state, a rectangular sheet of a material is clamped by a rigid material on the two long edges (Figure 15a). The specimen has a width $b$, a height $H$, and a crack of length $c$, where $b \gg c \gg H$. When the sheet is stretched by $\lambda$, the energy release rate is[17]

$$G = W(\lambda)H \tag{19}$$

The elastic energy density $W(\lambda)$ is measured by a specimen without a crack (Figure 15b).

This setup is widely used to study crack growth in soft materials because the energy release rate $G$ is independent of the crack length $c$. Furthermore, the energy release rate is determined by measuring the stress–stretch curve, and no boundary value problem needs to be solved. When measuring toughness, the precracked specimen is monotonically stretched until fracture to determine the critical stretch at fracture, $\lambda_c$. By inserting the critical stretch into the above equation, one obtains toughness $G_c$.

### 3.4. Peel

In a peel test, a layer of a soft material is often attached with two inextensible backing layers (Figure 16a). Let $b$ be the width of the specimen. The backing layers suppress the deformation of the soft material far away from the crack front. The two legs of the specimen are pulled apart by a tensile tester with a force $F$. When the crosshead of the tensile tester


https://doi.org/10.1021/acs.chemrev.5c00663
Chem. Rev. XXXX, XXX, XXX−XXX

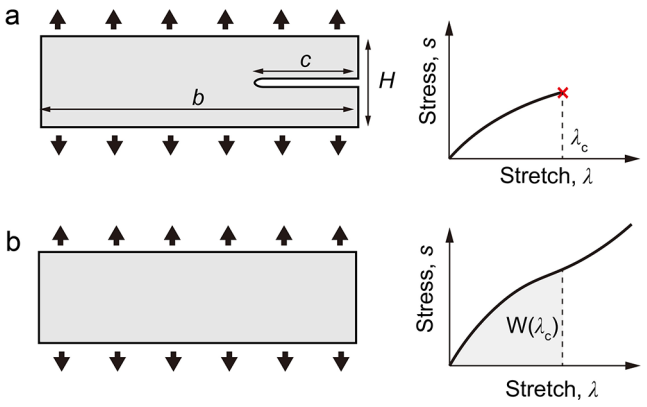


**Figure 15.** A rectangular sample pulled on long edges. (a) A precracked specimen is stretched until fracture to get the critical stretch, $\lambda_c$. (b) The specimen without crack is stretched to get the stress–stretch curve and obtain the elastic energy density as a function of stretch, $W(\lambda)$.

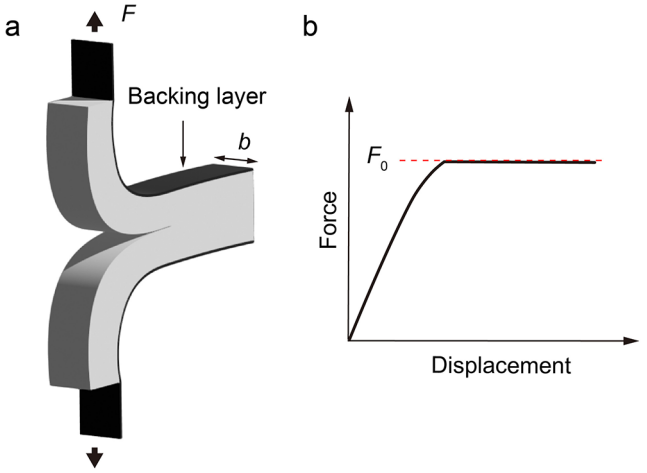


**Figure 16.** Peel test. (a) Specimen geometry. (b) Force–displacement curve.

moves by a displacement $d$, the crack length grows by $d/2$ and the crack area grows by $bd/2$. The elastic energy of the specimen changes negligibly, so that the change in free energy is entirely due to the reduction in the potential energy of the force, $Fd$. The energy release rate is

$$G = 2F/b \tag{20}$$

The energy release rate in the peel is unaffected by the model of elasticity of the polymer network.

As the crosshead moves, the force is recorded as a function of the displacement (Figure 16b). When the force is small, the crack does not extend but blunts. As the force increases, the crack blunts further. At some level of the force, the crack extends. Upon further loading, the crack may grow into a steady state and the force may reach a plateau $F_0$. By substituting the plateau force into the above equation, one obtains the toughness $G_c$. The peel test is desirable because the energy release rate is calculated without requiring knowledge of the crack length and the elasticity of the material.

### 3.5. Tear

In the tear test, the specimen is also often attached with two inextensible backing layers (Figure 17a). Let $t$ be the thickness of the soft material. The backing layers suppress the

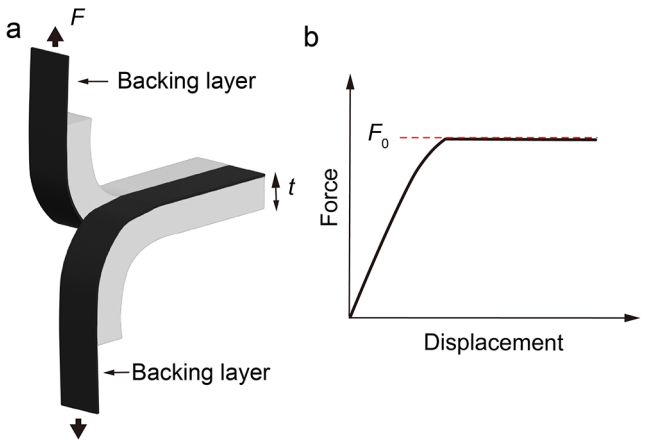


**Figure 17.** Tear test. (a) Specimen geometry. (b) Force–displacement curve.

deformation of the soft material far away from the crack front. The two legs of the specimen are pulled apart by a tensile tester with a force $F$. When the crosshead of the tensile tester moves by a displacement $d$, the crack length grows by $d/2$, and the crack area grows by $td/2$. The elastic energy of the specimen changes negligibly, so that the change in free energy is entirely due to the reduction in the potential energy of the force, $Fd$. The energy release rate is

$$G = 2F/t \tag{21}$$

The energy release rate depends on the width of the material in the peel test and on the thickness of the material in the tear test. The energy release rate in the tear is unaffected by the model of elasticity of the polymer network.

As the crosshead moves, the force is recorded as a function of the displacement (Figure 17b). When the force is small, the crack does not extend but blunts. As the force increases, the crack blunts further. At some level of force, the crack grows. Upon further loading, the crack may grow into a steady state, and the force may reach a plateau $F_0$. By substituting the plateau force into the above equation, one obtains the toughness, $G_c$.

## 4. WHEN A CRACK GROWS BY A LOCALIZED IRREVERSIBLE PROCESS

A scaling analysis leads to a singular field for a crack in an ideal body. This singular field establishes the existence of an annulus, called the $G$-annulus, for a crack growing in a real body by a localized irreversible process. The annulus separates the two types of complexity: the shape of the body and the irreversibility at the crack tip. The size of the irreversible zone is characterized by a material length scale called the fractocohesive length.

### 4.1. Singular Elastic Field in an Ideal Body

Consider an ideal body in which deformation is elastic and a crack is stationary (Figure 18a). Furthermore, the body is infinite, and the crack is semi-infinite. The body is composed of many material particles. In the undeformed state, label a material particle by its polar coordinates centered at the crack tip, $(R, \Theta)$.

In a deformed state, the same material particle moves to a different place in space (Figure 18b). The body is made of a homogeneous material but undergoes an inhomogeneous deformation. The elastic energy density varies from particle


https://doi.org/10.1021/acs.chemrev.5c00663
Chem. Rev. XXXX, XXX, XXX−XXX

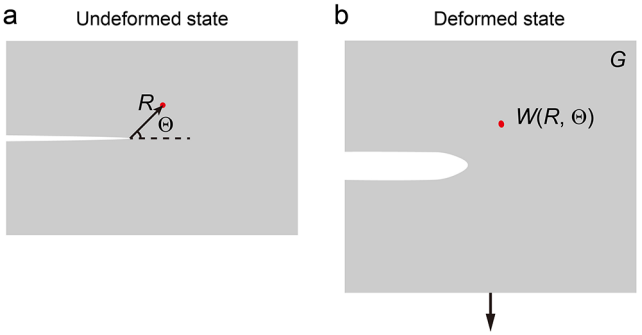


**Figure 18.** A semi-infinite crack in an infinite ideal body, in which the crack is stationary and deformation is elastic. (a) In the undeformed state, a material particle is labeled by polar coordinates $(R, \Theta)$. (b) In the deformed state, the applied load is represented by energy release rate $G$, and the elastic energy density varies with the material particle, represented by function $W(R, \Theta)$.

to particle, represented by a function $W(R, \Theta)$. Represent the applied load by energy release rate $G$. The elastic energy of the body is the elastic energy density integrated over the volume of the body. The energy release rate is the change in the elastic energy of the body associated with the change in the crack per unit area. Both operations are linear. Consequently, the field of elastic energy density scales with the energy release rate, $W(R, \Theta) \sim G$.

Energy density, $W$, has the dimensions of energy per unit volume. The energy release rate, $G$, has the dimensions of energy per unit area. The governing equations of elasticity have no length scale. For the semi-infinite crack in the infinite body, the boundary conditions also provide no length scale. For each material particle, the only length scale is the radial distance $R$ of the material particle from the crack tip. Consequently, the field of energy density takes the form

$$W(R, \Theta) = \frac{G}{R} f(\Theta) \tag{22}$$

Here, $f$ is a dimensionless function of the polar angle $\Theta$ and is independent of the radial distance $R$. Also, $f$ may depend on dimensionless constants of elasticity. The explicit form of the function $f(\Theta)$ is determined by solving the boundary value problem of elasticity.[62] But function $f(\Theta)$ will not be used in this article. The $1/R$ scaling emerges from the absence of intrinsic length scales in the governing equations, and holds for any linear and nonlinear models of elasticity.

### 4.2. G-Annulus

A crack grows in a real body by an irreversible process, and the real body has a finite size. Consider a real body in a commonly used experimental setup: a crack grows in a long rectangular sheet, which is gripped on the long edges and pulled to stretch $\lambda$. The length of the crack is large compared to the height of the sheet. Following a common practice, we label material particles by their coordinates in the undeformed state (Figure 19a). Denote the size of the irreversible process zone by $R_p$ and the height of the sheet by $H$. When $R_p \ll H$, the irreversible process is localized.

We sketch the strain energy density directly ahead of the crack tip as a function of the radial distance $R$ (Figure 19b). In the irreversible zone, the material is inelastic, the $1/R$ elastic field is invalid, and the strain energy density is comparable to the work of fracture, $W \approx W_c$. On a scale comparable to the size of the body, the field is determined by the external boundary conditions, and the $1/R$ elastic field is invalid also. In particular, far ahead of the crack tip, $R \gg H$, the field of strain energy density is homogeneous, as given by the applied value $W(\lambda)$. As long as the irreversible process is localized, $R_p \ll H$, an annulus exists in which the $1/R$ elastic field prevails, $W \sim G/R$. The internal radius of the annulus is larger than the size of the inelastic zone, $R_p$, and the external radius of the annulus is smaller than the size of the sample, $H$. We call this elastic region the $G$-annulus because it is where the energy release rate $G$ governs the local stress and energy field. Unlike the irreversible zone, the $G$-annulus lies entirely in the elastic region.

Imagine crack growth in two real bodies of the same material. The two real bodies have different loads, shapes, sizes, and crack lengths. Regardless of all these differences, the field in the $G$-annulus depends on the boundary conditions through a single parameter: the energy release rate $G$. That is, as long as the irreversible zone is small compared to each body, $G$ is the sole messenger between the boundary conditions and the irreversible process. The doctrine of fracture mechanics has been summarized as follows: given a material, the same history of the energy release rate, $G(t)$, causes the same history of

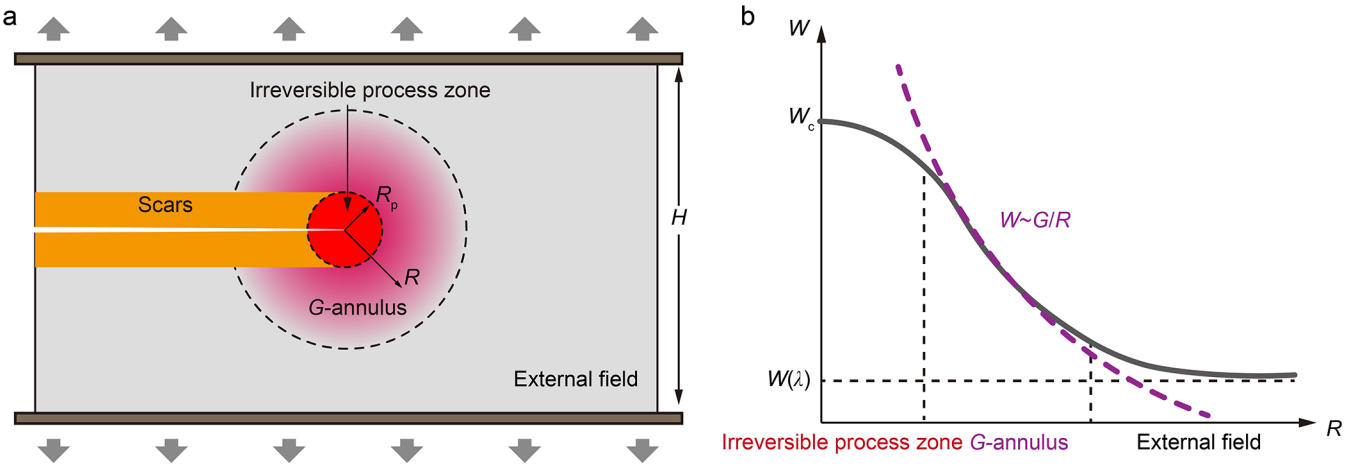


**Figure 19.** $G$-annulus. (a) When the irreversible process is localized, $R_p \ll H$, an annulus exists, called the $G$-annulus, in which the elastic field $W \sim G/R$ is valid. (b) Elastic energy density, $W$, as a function of $R$ when a crack grows in a real body by a localized irreversible process.


https://doi.org/10.1021/acs.chemrev.5c00663
Chem. Rev. XXXX, XXX, XXX−XXX

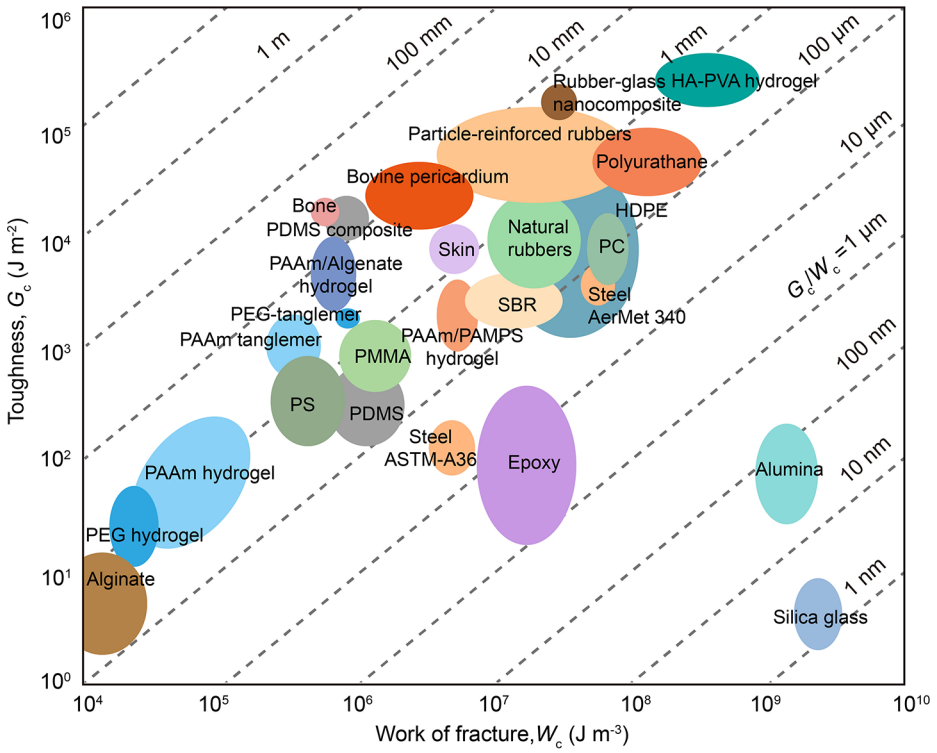


**Figure 20.** Various materials are plotted on the plane of two axes: work of fracture $W_c$ and toughness $G_c$, both on the logarithmic scale. Also marked are the lines of constant fractocohesive length $G_c/W_c$. Data are collected from the following papers: alginate hydrogel;[64−66] poly(ethylene glycol) (PEG) hydrogel;[67,68] polyacrylamide (PAAm) hydrogel;[69,70] PAAm tanglemer;[69] polystyrene (PS), poly(methyl methacrylate) (PMMA), styrene−butadiene rubber (SBR), polycarbonate (PC), and expoxy;[63,71] alginate/PAAm hydrogel;[64,72] PEG tanglemer;[68] polydimethylsiloxane (PDMS) and PDMS composite;[73] bone;[74] bovine pericardium;[75] poly(2-acylamido-2-methylpropanesulfonic acid) (PAMPS)/PAAm hydrogel;[29] natural rubber;[17,76] particle-reinforced rubber;[71,77,78] high-density polyethylene (HDPE);[71,79,80] rubber−glass nanocomposite;[81] polyurethane;[82] hierarchical poly(vinyl alcohol) (PVA) hydrogel;[83] and steel, alumina, and glass.[63]

crack growth, $A(t)$. The relation between the energy release rate and crack growth is specific to materials, and is independent of the shapes and sizes of bodies.

The idealization of localized irreversibility divides the labor of studying crack growth into two tasks. First, in an ideal body, relate the energy release rate to the geometry and load of the body through a boundary value problem of elasticity. Second, in a real body, use the energy release rate to characterize crack resistance as a material property. The division of labor hits a sweet spot. In load-bearing applications, materials are subject to repeated loading and unloading, and are often designed to be elastic below some amplitude of load. Cracks are inevitably generated in a body during fabrication and operation. At the fronts of the cracks, stress is concentrated and the material is inelastic. The division of labor isolates the two types of complexity: the shape of the body and the irreversibility at the crack tip.

### 4.3. Fractocohesive Length

Given a material, the toughness $G_c$ is measured using a sample containing a precut crack, and the work of fracture $W_c$ is measured using a sample without a precut crack. The two material properties have different dimensions: $G_c$ has dimensions of energy per unit area, and $W_c$ has dimensions of energy per unit volume. The toughness divided by the work of fracture, $G_c/W_c$, has a dimension of length. This length, called the fractocohesive length, is also a material property.[63]

Various materials are plotted on the plane of two axes: work of fracture, $W_c$, and toughness, $G_c$ (Figure 20). The dashed lines are the lines of constant fractocohesive length, $G_c/W_c$. Silica glass has a fractocohesive length of ∼1 nm. Polymers and metals typically have a fractocohesive length over micrometers.

### 4.4. Size of Irreversible Zone

For a crack growing in a real body by a localized irreversible process, the irreversible zone is small compared to the body, and the size of the irreversible zone is also a material property. Under the conditions of localized irreversibility, the size of the irreversible zone is comparable to the fractocohesive length:

$$R_p \sim G_c/W_c \tag{23}$$

The fractocohesive length quantifies the localization of an irreversible process.

Note that $G_c/W_c$ is a material-specific length scale. The length scales with the size of the irreversible process zone $R_p$, but the numerical prefactor depends on materials. The same is true for the length for flaw sensitivity discussed below. Furthermore, the work of fracture $W_c$ depends on the type of stress state. For example, the value measured under uniaxial tension differs from that measured under biaxial tension.

The fractocohesive length $G_c/W_c$ characterizes the length scale over which stress deconcentrates at a crack tip in a material under a monotonic load. To gain intuition, we compare two model materials—a silica glass and a polymer network. As idealization, the crack is taken to break a single layer of atomic bonds in silica glass and a single layer of strands in the polymer network while other parts of the materials deform elastically. In this idealization, the fractocohesive length is on the atomic scale (∼1 nm) for silica glass and on the scale of the end-to-end length of a strand (∼10−100 nm) for the


https://doi.org/10.1021/acs.chemrev.5c00663
Chem. Rev. XXXX, XXX, XXX−XXX

polymer network. For silica glass, this idealization closely approximates reality. However, for polymer networks, the fractocohesive length often exceeds 100 $\mu$m. This enormous amplification of fractocohesive length results from two factors. First, the work of fracture of polymer networks, $W_c$, is commonly orders of magnitude lower than the covalent energy density. This reduction in the work of fracture results from the sequential breaking of a small fraction of high-tension paths.[58,59] Second, before a strand ahead of the crack tip breaks, high tension prevails in a zone around the crack tip, in which many strands break and many noncovalent bonds disassociate so that the toughness, $G_c$, is orders of magnitude larger than the covalent energy in a single layer of strands. These two factors together amplify the fractocohesive length $G_c/W_c$. This synergy between crack bridging and background dissipation will be discussed in Section 5.5.

### 4.5. Flaw Sensitivity

Here, by a flaw we mean a pre-existing notch or defect that can serve as a site for crack nucleation. We consider flaw sensitivity under the idealization of localized irreversibility. The fractocohesive length also quantifies flaw sensitivity (Figure 21). When the flaw is small compared to the fractocohesive length, $c \ll G_c/W_c$, nearly the entire sample reaches the state of $W_c$, and the strength is insensitive to the flaw. When a flaw is large compared to the fractocohesive length, $c \gg G_c/W_c$, only a small zone around the front of the cut reaches the state of $W_c$, and the strength is sensitive to the flaw.

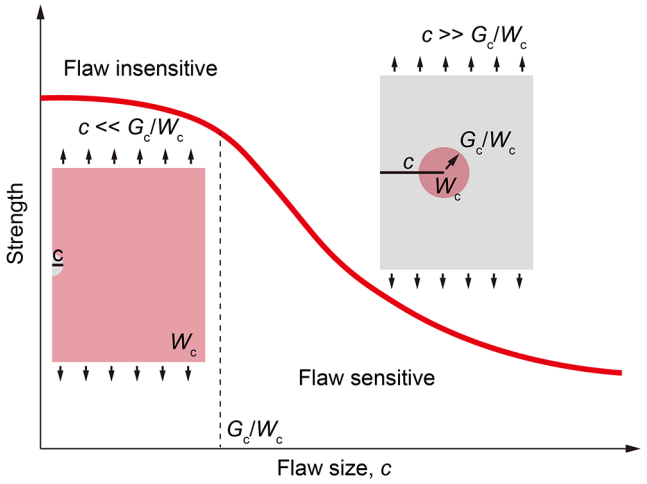


**Figure 21.** Flaw sensitivity of a material. The strength is insensitive to a flaw when the flaw is small compared to the fractocohesive length, $c \ll G_c/W_c$, but is sensitive to a flaw when the flaw is large compared to the fractocohesive length, $c \gg G_c/W_c$.

In a material, flaws commonly exist over a range of sizes, say between atomic dimensions to 0.1 mm. Silica has a fractocohesive length of ~1 nm, and the strength of silica is sensitive to flaws and hence scatters a lot. For a material with a fractocohesive length of ~1 mm, such as a ductile polymer or metal, the strength is insensitive to the flaws.

If one wishes to measure the strength of a material independently of flaws, then one should ensure that a sample has flaws small compared to the fractocohesive length. If one wishes to measure the toughness of a material, then one should ensure that the crack grows in a body by localized irreversibility; that is, the size of the body and the length of the crack should be large compared to the fractocohesive length.

### 4.6. Material Length Scales in Fracture Mechanics

We next compare the fractocohesive length, $G_c/W_c$, to the other material length scales commonly used in fracture mechanics.

A length, $G_c/(\sigma_0^2/E)$, appears in the crack bridging model, where $\sigma_0$ is the peak traction in the traction−separation curve.[84,85] In the crack bridging model, the material outside the bridging zone is linearly elastic, with Young's modulus $E$. The work of fracture near the crack tip is given by $\sigma_0^2/E$. For highly stretchable materials, however, the material outside the bridging zone is nonlinearly elastic. The fractocohesive length $G_c/W_c$ generalizes $G_c/(\sigma_0^2/E)$ when linear elasticity does not apply.

Another length, $G_c/E$, is frequently discussed.[35] Recall the crack tip field in a nonlinear elastic material, $W \sim G/R$. For example, take the neo-Hookean elastic energy density $W = \frac{E}{3}(\lambda_1^2 + \lambda_2^2 + \lambda_3^2 - 3)$. The deformation is said to be large when $\lambda_1^2 + \lambda_2^2 + \lambda_3^2 - 3$ exceeds the order of unity. Consequently, $G_c/E$ characterizes the size of the zone of large elastic deformation. Outside this zone, the strain is small. This zone of large deformation is distinct from the zone of inelasticity. For a polymer network capable of large and elastic deformation, the length $G_c/E$ greatly overestimates the size of the irreversible zone and the length of flaw sensitivity. For such a polymer network, $W_c \gg E$ so that $G_c/W_c \ll G_c/E$.

In Section 6.1, we will introduce a length in the crack resistance curve—the crack growth needed to reach the steady state, $L_{ss}$. Because $L_{ss}$ characterizes the size of the irreversible zone in the steady state, the length $L_{ss}$ is comparable to the fractocohesive length $L_{ss} \sim G_c/W_c$.

The idea of fractocohesive length also extends to cyclic loading conditions. When a sample with a precrack is cyclically stretched, an amplitude of energy release rate exists, called the fatigue threshold, $G_{th}$, below which the crack does not grow in a steady state. When a sample without a precrack is cyclically stretched, a strain energy density exists, called the endurance work of fracture, $W_e$, below which the material can be stretched for an infinite number of cycles. The ratio $G_{th}/W_e$ defines the endurance fractocohesive length, which represents the flaw insensitivity of a material under cyclic load.[50,86]

## 5. MICROSCOPIC ORIGINS OF STRESS DECONCENTRATION AND CRACK RESISTANCE

This section describes how the localization of irreversibility results from microscopic processes concurrent with crack growth. The description here will be general. Further details will be described in later sections for various materials.

### 5.1. Silica

To set the background for crack growth in polymer networks, we begin with crack growth in silica (Figure 22). In silica, silicon and oxygen atoms form covalent Si−O bonds. A crack grows in silica by breaking a plane of Si−O bonds. Griffith tacitly made two theoretical assumptions.[12] First, the excess in free energy of the crack surfaces is the same as the surface energy, $G_* = 2\gamma$. Second, the crack grows by a reversible process so that the free energy remains stationary, $G_{**} = 0$. The two theoretical assumptions lead to the Griffith criterion: toughness equals twice the surface energy, $G_c = 2\gamma$.


https://doi.org/10.1021/acs.chemrev.5c00663
Chem. Rev. XXXX, XXX, XXX−XXX

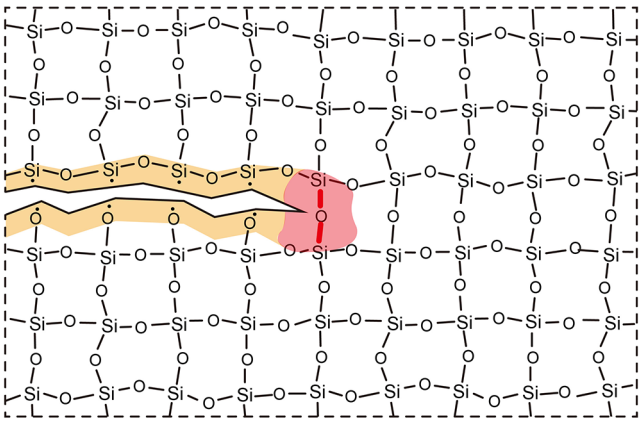

**Figure 22.** A crack grows in silica, an amorphous material assembled by Si−O bonds. Each silicon atom is bonded to four oxygen atoms, and each oxygen atom is bonded to two silicon atoms. When a crack grows in silica, stress is concentrated to the length scale of the individual bond.

Griffith tested his theory by conducting two independent experiments. His experiment 1 measured toughness by the procedure familiar to us today. He prepared a sheet of silica, cut a crack in the sheet, and loaded the sheet until the crack grew. His experiment 1 gave a value of toughness $G_c$ = 3.5 J $m^{-2}$. His experiment 2 measured surface energy. He prepared a fiber of silica, and hung a weight on the fiber. At an elevated temperature, silica behaves like a highly viscous liquid. Atoms change neighbors, and the fiber creeps. The hanging weight tends to elongate the fiber, but the surface energy tends to shorten the fiber. In equilibrium, the two effects balance, and the hanging weight measures the surface energy. Griffith repeated the experiment at several elevated temperatures at which the fiber crept fast enough to be observable. He then extrapolated the measured surface energy from the elevated temperature to room temperature. His experiment 2 gave $2\gamma$ = 1.08 J $m^{-2}$. Thus, the toughness $G_c$ and twice the surface energy $2\gamma$ differ by a factor of about 3.

We now know that his two theoretical assumptions are both wrong. First, a surface created by crack growth differs from a surface created by creep. In the former, atoms near the crack surfaces may not reach local equilibrium, the crack surfaces may not be flat to the atomic scale, and there may be broken bonds beneath the surface. Consequently, the excess in free energy exceeds twice the surface energy $G_* > 2\gamma$. Second, crack growth is an irreversible process: breaking a covalent bond is a dynamic event, and free energy is reduced by thermal conduction and sound generation. This reduction in free energy requires that $G_{**} > 0$.

Grifith's two experiments have withstood the test of time, but his two theoretical assumptions have not. For silica, the errors in his theoretical assumptions lead to modest disagreement with experiments. But the disagreement for most other materials is enormous. For most materials, crack growth creates scars much more extensive than two relaxed surfaces of atomistic flatness, so that $G_* \gg 2\gamma$ (Figure 10). Furthermore, free energy reduction by the irreversible zone around the crack tip often far exceeds the excess free energy of the scars, $G_{**} \gg G_*$. Fracture mechanics has been made applicable for numerous materials by adopting his experiment 1 and by giving up both of his theoretical assumptions.

### 5.2. Lake−Thomas Model

In a polymer network, the noncovalent bonds between strands are much weaker than the covalent bonds that link repeat units and cross-link chains. The Lake−Thomas model neglects the noncovalent bonds and focuses on the covalent bonds (Figure 23).[27] When a crack impinges on a strand, once the noncovalent bonds are neglected, the strand slips without friction relative to the neighboring strands. Consequently, the high tension in the strand transmits over the entire length of the strand. The strand meets several other strands at a cross-link so that the high tension in the strand is shared by several strands. Just before the strand ruptures, the free energy stored in the strand predominantly results from the stretching of covalent bonds and far exceeds the free energy due to entropic elasticity. When the strand breaks at a single covalent bond, the free energy associated with the high tension in the entire strand dissipates. The Lake−Thomas model further assumes that the crack grows by breaking a single layer of strands, so that the strands off the crack surfaces remain intact. Consequently, the free energy reduction associated with the irreversible process of crack growth per unit area scales as

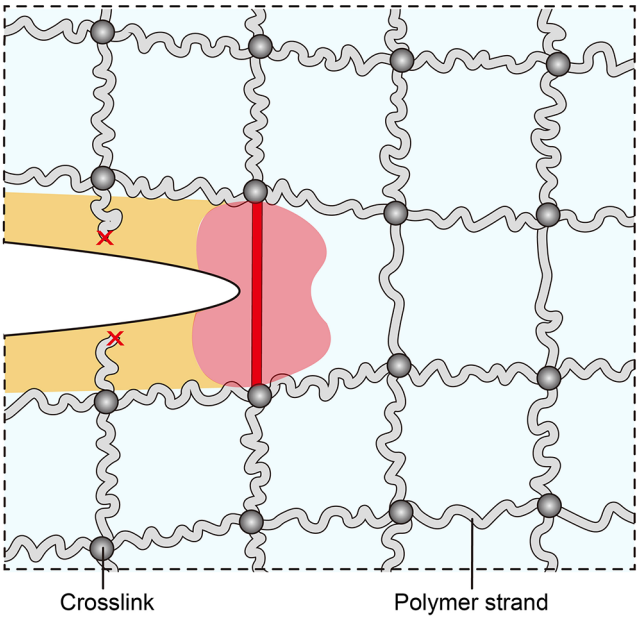


**Figure 23.** When a crack impinges upon a strand in a polymer network, the high tension in the strand is transmitted over the entire strand. When the strand breaks at a single covalent bond, the free energy due to the stretch of the entire strand is dissipated.

$$G_{**} = eL \tag{24}$$

where $e$ is the free energy per unit volume stored in strands just before rupture and $L$ is the end-to-end distance of a strand in the undeformed network.

The free energy reduction per unit volume is

$$e = J/v \tag{25}$$

where $J$ is the free energy stored in a repeat unit just before rupture and $v$ is the volume per repeat unit.

In the undeformed network, a strand is assumed to take a conformation of a random walk so that its end-to-end distance is[7,87]


https://doi.org/10.1021/acs.chemrev.5c00663
Chem. Rev. XXXX, XXX, XXX−XXX

$$L = \sqrt{b_k bn} \tag{26}$$

where $n$ is the number of repeat units in the strand, $b$ is the length of a repeat unit, and $b_k$ is the Kuhn length of the polymer. The values of $b_k$ for many polymers have been tabulated.[88] For example, the ratio $b_k/b$ is 1.7 for natural rubber, 3.3 for polyacrylamide, and about 20 for cellulose.

We note several further considerations of the Lake−Thomas model. First, Equation 24 is a scaling relation. There is no reason that free energy dissipates in only one layer of strands. The discrepancy between the experimental data and the Lake−Thomas model is accounted for by introducing a coefficient $\alpha$, and we write $G_{**} = \alpha eL$.[67,89−91]

Second, toughness $G_c$ measures the resistance of a material to the growth of a crack and results from two contributions: the free energy reduction by the irreversible process around the crack tip, $G_{**}$, and the excess in free energy due to the scars in the wake of the crack, $G_*$. The Lake−Thomas model estimates $G_{**}$ but neglects $G_*$. For a crack growing in a polymer network, $G_{**}$ scales with the energy of covalent bonds. In a polymer network, each strand consists of many repeat units. Consequently, in the scar, the repeat units greatly outnumber the broken ends, and $G_*$ is expected to be on the order of the surface energy of a polymer melt. The surface energy of a polymer melt scales with the energy of noncovalent bonds so that the excess in free energy $G_*$ is on the order of $10^{-2}$ J m$^{-2}$. By comparison, the measured toughness $G_c$ often exceeds $10^3$ J m$^{-2}$. Consequently, scars contribute negligibly to toughness: $G_* \ll G_{**}$.

Third, off the crack surfaces, some polymer strands may also break. Off-crack scission takes place in all polymer networks and is made pronounced in interpenetrating networks.[92,93]

Forth, when a crack grows in a network at a finite velocity, the rate of deformation near the crack tip is high so that the breaking and reforming of noncovalent bonds are out of equilibrium. As the crack grows, two layers of materials undergo hysteresis, namely, an irreversible process contributes to $G_{**}$. The thickness of the dissipative layers can be much larger than the length of a strand. This effect of background dissipation is not included in the Lake−Thomas model. In practice, the Lake−Thomas model is compared to the fatigue threshold rather than toughness.[27,35,39,94,95]

Fifth, even though the noncovalent bonds between strands are much weaker than the covalent bonds along a strand, the accumulative effect of many noncovalent bonds can be large. In particular, for a network of long strands, the noncovalent bonds may resist the slip of a strand and thereby limit the length over which high tension transmits.[96] This effect is even more pronounced in thermoplastics than in rubbery networks.[97]

### 5.3. Modulus−Threshold Conflict

As noted above, the Lake−Thomas model is often compared with the fatigue threshold. A combination of Equations 24−26 predicts that the fatigue threshold scales as $G_{th} \sim n^{1/2}$. The more the repeat units per strand, the larger the fatigue threshold. On the other hand, the modulus scales as $E \sim n^{-1}$.[6,7,87] The more the repeat units per strand, the lower the modulus. The two scaling relations predict a modulus−threshold conflict:

$$G_{th} \sim E^{-1/2} \tag{27}$$

This conflict has been observed in elastomers (Figure 24).

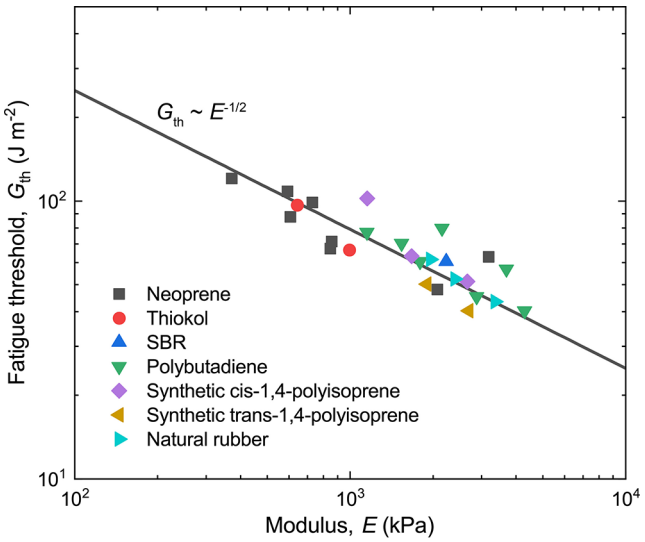


**Figure 24.** Modulus−threshold conflict. The figure is reproduced with permission from ref 98. Copyright 1988 Taylor and Francis.

The inverse relationship implies that increasing fatigue resistance by lengthening strands inherently softens the material, limiting its utility in load-bearing applications. The apparent trade-off motivates the search for network architectures that decouple the modulus from the threshold. Examples include tanglemers (Section 8), interpenetrating networks (Section 12), and composites (Sections 13 and 14).

### 5.4. Deconcentrate Stress over Various Length Scales

Compare a crack growing in silica and a crack growing in a polymer network. We may as well regard silica as a network in which every strand has only two Si−O bonds (Figure 23). When the crack impinges on an oxygen bridge, the high tension in the oxygen bridge is shared by multiple oxygen bridges off the crack plane. Thus, the stress is concentrated to the scale of a few atoms. When the oxygen bridge at the crack tip breaks, the energy dissipation is localized to the atom scale. By contrast, in a polymer network, each strand consists of many repeat units (Figure 24). At a cross-link, the high tension in the strand is shared by several other strands. Thus, the stress is deconcentrated over the length of the strand. When the crack impinges on a strand, the high tension is deconcentrated over the entire length of the strand.

One may design architectures of materials to deconcentrate stress over various length scales (Figure 25). As we noted above, a polymer network deconcentrates stress over the length of a strand.[27] This deconcentration results from architectural features of the polymer network: the covalent bonds between repeat units along a strand are much stronger than the noncovalent bonds between repeat units in different strands. Beyond the molecular scale of individual strands, materials can be designed to deconcentrate stress at mesoscopic and macroscopic scales, including particle clusters, semicrystalline domains, and reinforcing fibers.

In a particle-reinforced polymer network, when a crack impinges on a cluster of particles, the high tension transmits over multiple gaps between particles.[99] The stress is deconcentrated over the length scale of a particle cluster, which can be on the order of micrometers.

In a semicrystalline polymer network, when a crack impinges on a crystalline domain, the high tension can be transmitted


https://doi.org/10.1021/acs.chemrev.5c00663
Chem. Rev. XXXX, XXX, XXX−XXX

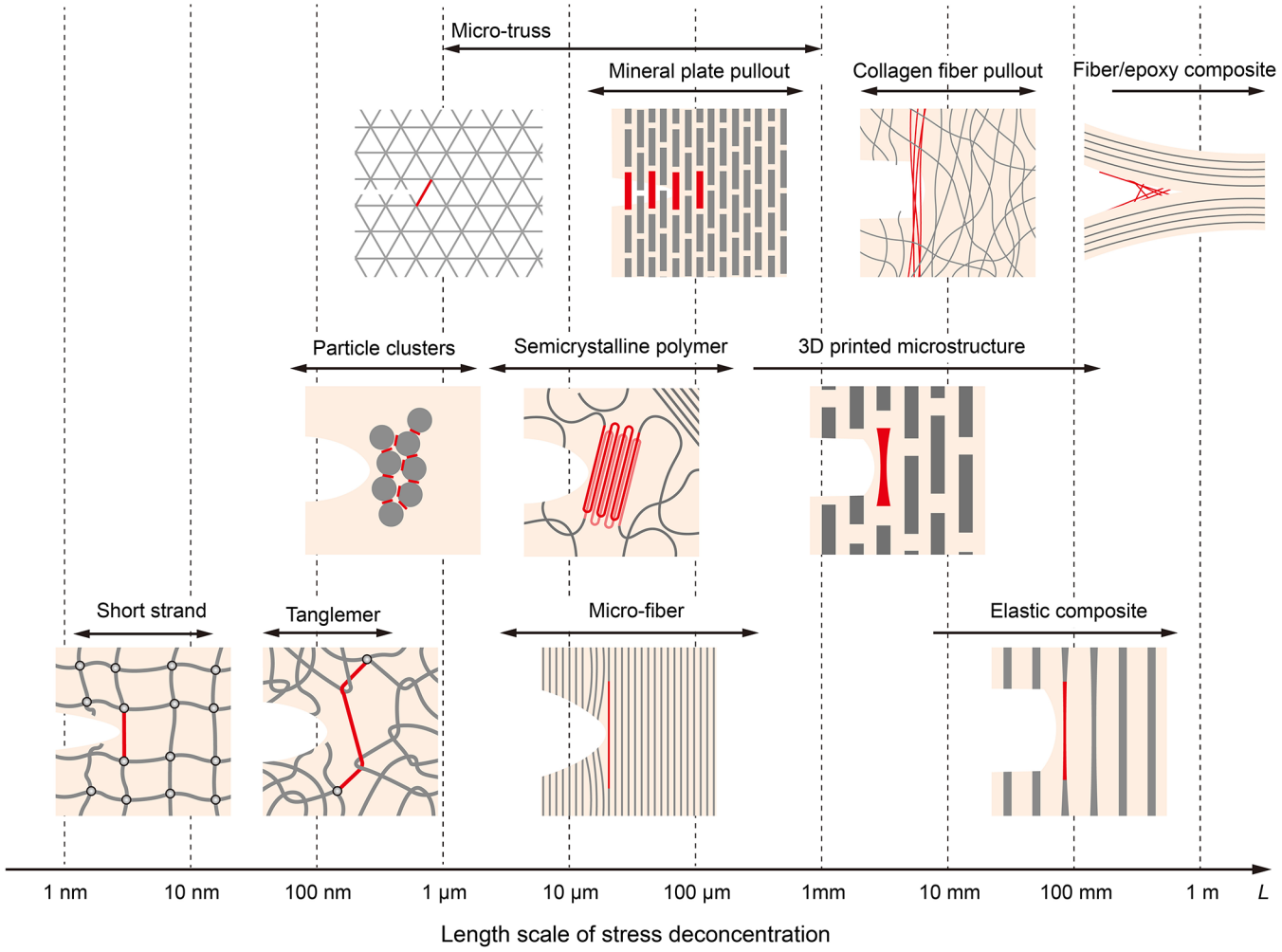


**Figure 25.** Design materials to deconcentrate stress at various length scales.

over a fiber-like structure of crystalline domains and amorphous gaps.[100] The stress is concentrated over a fiber-like structure, which can be on the order of several micrometers.

In a fiber-reinforced polymer network in which rigid fibers and soft matrix strongly adhere, when a crack impinges on a fiber, the high tension transmits over a long segment of fiber by the shear of the soft matrix.[73,101] The stress is deconcentrated over the length scale of a fiber, which can be on the order of millimeters.

In a fiber-reinforced polymer in which fibers and polymer matrix form weak interfaces, when a crack impinges on a fiber, the fiber slips relative to the matrix and pulls out. The high tension transmits over a long segment of pullout fiber.[19,84] The stress is deconcentrated over the length scale of the pullout fiber, which can be on the order of centimeters.

By designing materials to deconcentrate stress over increasingly larger length scales, one can systematically increase the fracture toughness and raise the fatigue threshold, even in stiff materials. This strategy enables designers to escape the modulus−threshold conflict identified in Section 5.3.

### 5.5. Synergy of Crack Bridging and Background Hysteresis

When a crack grows in a polymer network, a layer of polymer strands must break. The stress needed to break a strand is set by the strength of covalent bonds. Such a high stress will affect a large volume of the network, in which the stress is much lower than then the strength of covalent bonds but is high enough to break noncovalent bonds. When the crack grows at a finite velocity, the breaking and possibly reforming for the noncovalent bonds are not in equilibrium. Thus, the reduction in free energy, $G_{**}$, results from two contributions: the covalent bonds that bridge the crack and the noncovalent bonds that exist in a large volume around the crack (Figure 26).

The two contributions work synergistically. The polymer strand bridges the crack tip and sets up high tension in a region around the crack tip, where irreversible processes extensively happen. The irreversible processes around the crack tip also shield the polymer strand at the crack tip from the load applied remote from the crack tip. The synergy between crack bridging and background hysteresis has been modeled in metals,[102] ceramics,[103] ceramic matrix composites,[103] and polymer networks.[104] It is likely that such models will be developed to represent polymeric materials of various architectures.

As noted before, when a sample of a polymer network without a precut crack is pulled in tension, the strength of the network is typically orders of magnitude lower than the strength of covalent bonds.[54−56] The large difference is under active investigation.[57−59] This enormous reduction in strength results from a sequential breaking of a small fraction of high-tension paths. At a given stretch of the polymer network, only a small fraction of paths approach the strength of a covalent bond, while most strands in the network have low tension and


https://doi.org/10.1021/acs.chemrev.5c00663
Chem. Rev. XXXX, XXX, XXX−XXX

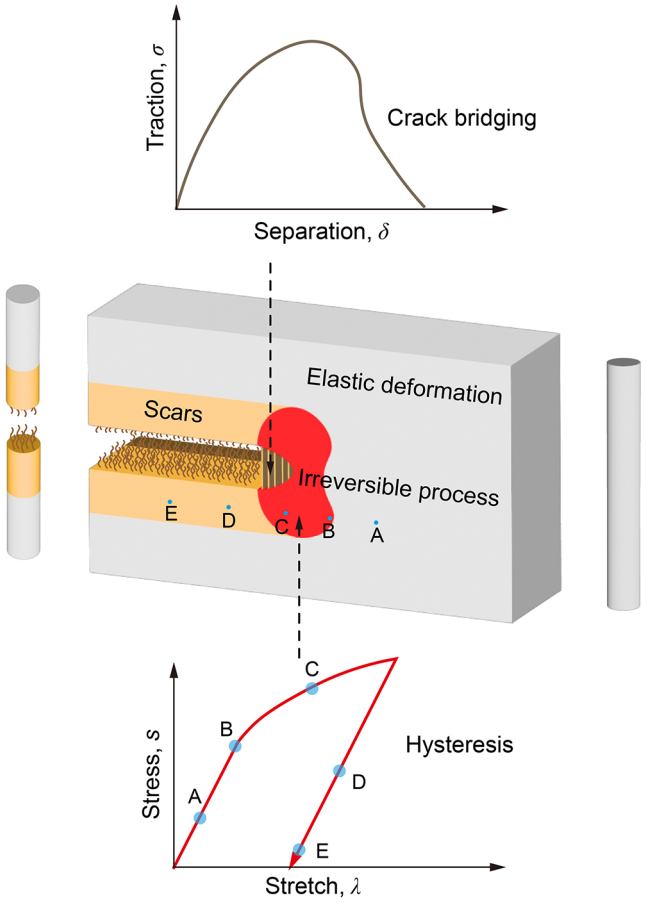


**Figure 26.** Resist crack growth by a synergy of crack bridging and background hysteresis. At the crack tip, a structure bridges the crack. As the crack grows, the structure breaks, and two layers of the material deform with hysteresis. Crack bridging is characterized by a traction-separation curve, and background hysteresis is characterized by a stress–stretch loop. The five points A, B, C, D, and E on the stress–stretch loop correspond to the five states in the material. Outside the layers of hysteresis, the material is elastic.

deform by entropic elasticity. How to account for this large difference in a numerical simulation of crack growth in a polymer network has not been explored.

### 5.6. Materials with Small Hysteresis and Large Toughness

Many applications require stretchable materials to have low hysteresis during loading and unloading, but high toughness to resist crack growth. Although both toughness and hysteresis arise from irreversible processes, their spatial localization differs. Toughness can be enhanced by highly localized dissipation at the crack tip, while hysteresis reflects distributed energy loss throughout the material.

We quantify hysteresis by a dimensionless number: the area between the loading and unloading stress–stretch curves divided by the area under the loading stress–stretch curve (Figure 3b). This measure of hysteresis depends on the amplitude of stretch. For example, a metal has a negligible hysteresis when stressed below the yield condition but has a large hysteresis when stressed above the yield condition. In this discussion, we focus on stretchable materials and measure hysteresis for a stretch amplitude of 2.

Compare various materials in the plane of toughness and hysteresis (Figure 27). For many materials, hysteresis and toughness correlate. For example, a polyacrylamide hydrogel

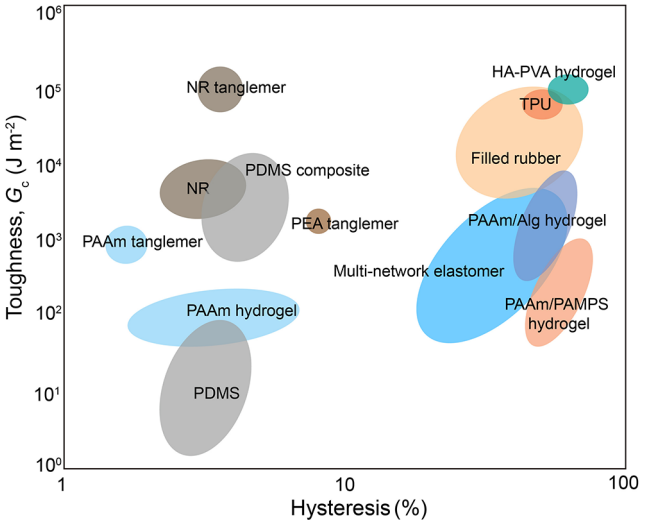


**Figure 27.** Various materials are plotted on the plane of hysteresis and toughness. Data are collected from the following papers: PEG hydrogel;[67,68] PAAm hydrogel;[69,70] PDMS;[73] PAAm tanglemer;[69] PEG tanglemer;[68] PDMS composite;[73] poly(ethyl acrylate) (PEA) tanglemer;[69] natural rubber and natural rubber tanglemer;[76] alginate/PAAm hydrogel;[64,72] PAMPS/PAAm hydrogel;[29] particle-reinforced rubber;[71,77,78] and hierarchical PVA hydrogel.[83]

has low hysteresis and low toughness (Section 7). As another example, an alginate/polyacrylamide hydrogel has high hysteresis and high toughness (Section 12.3).

But the hysteresis–toughness correlation does not hold for all materials. Natural rubber has a low hysteresis and a high toughness (Section 9). At small stretches, the noncovalent bonds between strands of natural rubber are weak and give low hysteresis. Beyond a stretch of about 4, the strands align and crystallize. Upon unloading, the crystals melt. This stretch-induced crystallization and subsequent melting give natural rubber appreciable hysteresis at large stretches. At a crack tip, the stretch is large so that the large hysteresis contributes to toughness. Later we will also describe another material of low hysteresis and high toughness: a composite of soft and hard polymethylsiloxane (Section 14.1).

## 6. CRACK GROWTH UNDER A MONOTONIC, CYCLIC, OR STATIC ENERGY RELEASE RATE

The resistance of a material to crack growth is characterized by prescribing the energy release rate as a function of time $t$. An analogy to rheology helps. The central question in rheology is this: given a history of force, $F(t)$, what is the history of displacement, $l(t)$? By analogy, the central question in fracture mechanics is this: given a history of energy release rate, $G(t)$, what is the history of crack area, $A(t)$?

It is difficult to answer this question in general. In experiments, the energy release rate is commonly prescribed as a function of time of three types: monotonic, cyclic, and static (Figure 28). The monotonic energy release rate is prescribed to measure the toughness and crack resistance curve. The cyclic energy release rate is prescribed to study fatigue crack growth. The static energy release rate is prescribed to study crack growth in viscoelastic, hydrolytic, or poroelastic materials. We next describe them in turn.


https://doi.org/10.1021/acs.chemrev.5c00663
Chem. Rev. XXXX, XXX, XXX–XXX

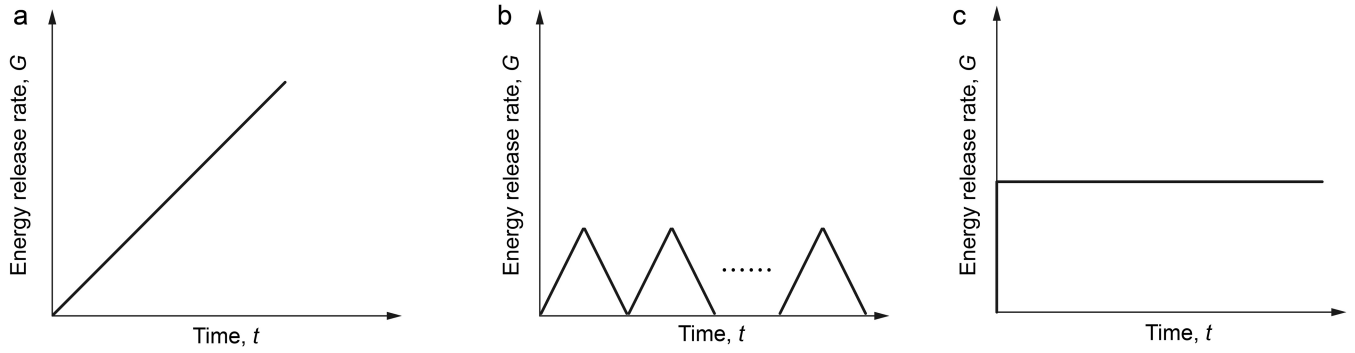


**Figure 28.** Energy release rate is commonly prescribed as a function of time of three types: (a) monotonic, (b) cyclic, and (c) static.

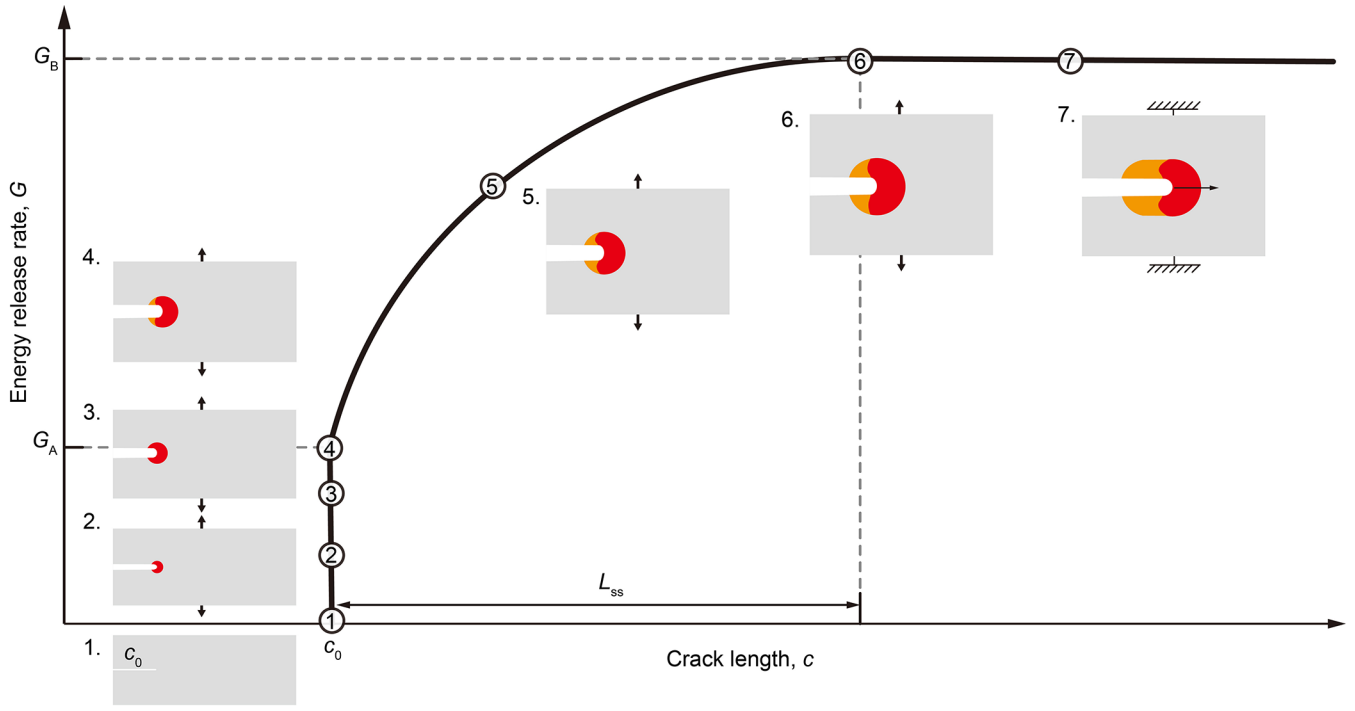


**Figure 29.** Crack resistance curve. Before any loading, a sample is precut with a crack of length $c_0$. The crack resistance curve represents the energy release rate, $G$, as a function of crack growth, $\Delta c$. The crack growth is initiated at an energy release rate of $G_A$. After a growth of $L_{ss}$, the energy release rate plateaus at $G_B$.

### 6.1. Monotonic Energy Release Rate

A crack is introduced in a sample using a blade, a laser cutter, or a pair of scissors. The sample is then loaded monotonically, and the crack growth is observed with a microscope. The energy release rate, $G$, is plotted as a function of crack growth, $\Delta c$ (Figure 29). This curve characterizes the resistance to crack growth in the material under monotonic loading and is called the crack resistance curve or the $R$-curve.

The $R$-curve characterizes the evolution of the irreversible process. Before any loading, a sample is precut with a crack of length $c_0$ (snapshot 1). At a small $G$, the crack does not grow, but a small region of the material around the crack tip deforms inelastically (snapshot 2). After increasing $G$ slightly, the crack still does not grow, but the inelastic zone enlarges (snapshot 3). At a critical energy release rate $G_A$, the crack starts to grow (snapshot 4). As $G$ is increased further, the higher the level of $G$, the longer the crack and the larger the inelastic zone (snapshot 5). The crack growth is stable in that the crack arrests whenever $G$ is held constant. When the energy release rate plateaus at $G_B$, the crack grows in steady state and generates two layers of scars of constant thickness (snapshots 6 and 7).

For the time being, consider a material in which the irreversible process is rate-insensitive. Consequently, as long as $G(t)$ is a monotonically increasing function, the shape of the function does not affect the $R$-curve. Furthermore, if the irreversible zone is small compared to the sample, then the $R$-curve is characteristic of the material, and is independent of the geometry of the sample. Under these conditions, the $R$-curve defines three material properties: the energy release rate for the onset of crack growth, $G_A$, the energy release rate for steady-state crack growth, $G_B$, and the crack growth needed to attain steady state, $L_{ss}$. Because $L_{ss}$ characterizes the size of the irreversible zone in the steady state, the irreversible process is localized if $L_{ss}$ is small compared to the specimen size and the total crack length. The length $L_{ss}$ is comparable to the fractocohesive length:

$$L_{ss} \sim G_c/W_c \tag{28}$$


https://doi.org/10.1021/acs.chemrev.5c00663
Chem. Rev. XXXX, XXX, XXX−XXX

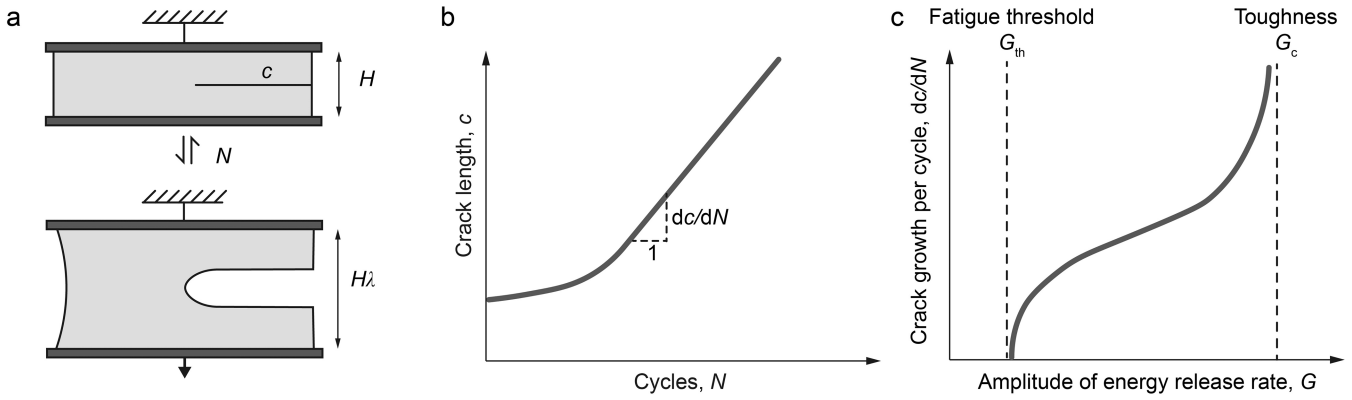


**Figure 30.** Crack growth in a material under cyclic load. (a) Prepare a sample with a precut crack, and subject the sample to cyclic load. (b) The crack growth is recorded as a function of the number of cycles. (c) The steady-state crack growth per cycle, d$c$/d$N$, is plotted as a function of the amplitude of the energy release rate.

The experimental measurement of the $R$-curve was introduced by Thomas.[21] He prepared a sample of natural rubber with a precut crack formed by a razor blade. The sample was placed in a tensometer, and the tip of the cut was observed through a microscope. For natural rubber, he reported $L_{ss} \approx 20-30$ $\mu$m, $G_A \approx 1.5$ kJ m$^{-2}$, and $G_B \approx 7$ kJ m$^{-2}$. Thomas measured the crack growth by painting the surfaces of the precut crack with an ink. The freshly torn surface appeared to be in the form of a shallow arrowhead. More recently, crack growth has been measured by digital image correlation.[75,105]

For silica, the $R$-curve is never reported. For such an extremely brittle material, we expect that $L_{ss} \sim 1$ nm and $G_A \approx G_B$. Namely, the resistance curve of silica takes the form of a step function. $R$-curves have been commonly measured for tough and stiff materials such as metals,[106] composites,[19,20,107] bones,[108] and adhesive joints.[109] For soft materials, such as elastomers and hydrogels, the $R$-curve is rarely reported, possibly because the crack growth $L_{ss}$ needed to attain steady state is small for most soft materials. Recent studies show that some tough soft materials can have $L_{ss} \sim 1$ mm.[76]

### 6.2. Cyclic Energy Release Rate

Fatigue crack growth was also first characterized using the energy release rate by Thomas.[21] A sample is precut with a crack and is subject to cyclic load (Figure 30a). The load is represented by the energy release rate. As the energy release rate cycles with a fixed amplitude, the crack length $c$ increases with the number of cycles $N$. After a period of transient growth, the crack attains steady-state growth per cycle, d$c$/d$N$ (Figure 30b). When the experiment is repeated for many amplitudes $G$, the data points are connected as a curve on the plane of d$c$/d$N$ and $G$ (Figure 30c).

An amplitude of the energy release rate exists, called the fatigue threshold, $G_{th}$, below which the crack does not grow. When the amplitude of the energy release rate exceeds the threshold $G > G_{th}$, the steady-state growth per cycle increases with $G$. The crack growth per cycle becomes too large to attain steady state when $G$ reaches a critical value $G_c$, corresponding to the toughness measured under monotonic load.

Recent work on fatigue crack growth in polymers, with an emphasis on the fatigue threshold, is reviewed elsewhere.[39,50] Accurate measurement of the fatigue threshold is challenging. The steady-state crack growth rate, d$c$/d$N$, is estimated as the total crack growth divided by the total number of cycles. The resolution of total crack growth is limited by the resolution of the microscope, whereas the total number of cycles is limited by the duration of the test. For instance, if the minimum detectable crack growth is 10 $\mu$m and the number of cycles is 50,000, then the resolution of d$c$/d$N$ is 0.2 nm/cycle. A coarse resolution may overestimate fatigue threshold. In the literature, the reported resolution of d$c$/d$N$ commonly ranges from 0.1 nm/cycle to 1 $\mu$m/cycle. Fatigue thresholds in different papers should be compared with caution.

### 6.3. Static Energy Release Rate: A Crack Growing in a Viscoelastic Material

To use the energy release rate to study a crack growing in a viscoelastic body, one must ensure that elasticity prevails in a large part of the body and that viscoelasticity is localized in a zone small compared to the body. This idea is described here using a long crack growing in a long rectangular sheet.

Prepare a long rectangular sheet without crack, clamped along the two long edges (Figure 31a). The height of the sheet is $H$ in the undeformed state and is $\lambda H$ in a deformed state. For a viscoelastic material, the stress−stretch curve depends on the stretch rate. At a sufficiently low stretch rate, the network is relaxed, and the experiment records a stress−stretch curve in a reversible process of relaxed elasticity. The area under the relaxed stress−stretch curve gives the free energy density, $W(\lambda)$.

Next consider a sheet held at a constant stretch $\lambda$ for a long time, and a crack grows slowly (Figure 31b). In a zone around the crack tip, the material undergoes the irreversible process of two mechanisms: viscoelasticity and scission. The irreversible zone is localized if it is small compared to the height of the sheet, $H$. Outside the irreversible zone, the sheet deforms by relaxed elasticity. Far ahead of the crack tip, the sheet is in the state of relaxed elasticity with free energy density $W(\lambda)$. Far behind the crack tip, the sheet relaxes to zero stress. The energy release rate is $G = W(\lambda)H$. Given a constant stretch $\lambda$, the energy release rate $G$ is constant. The crack length $c$ is recorded as a function of time, and the slope gives the crack velocity. After some time of transient growth, the crack attains a steady state of constant velocity. As usual for crack growth in a material accompanied by large deformation, the crack length is defined in the undeformed state.

Repeat this test at various values of constant stretch, and record the steady-state crack velocity as a function of the energy release rate (Figure 31c). An energy release rate exists,


https://doi.org/10.1021/acs.chemrev.5c00663
Chem. Rev. XXXX, XXX, XXX−XXX

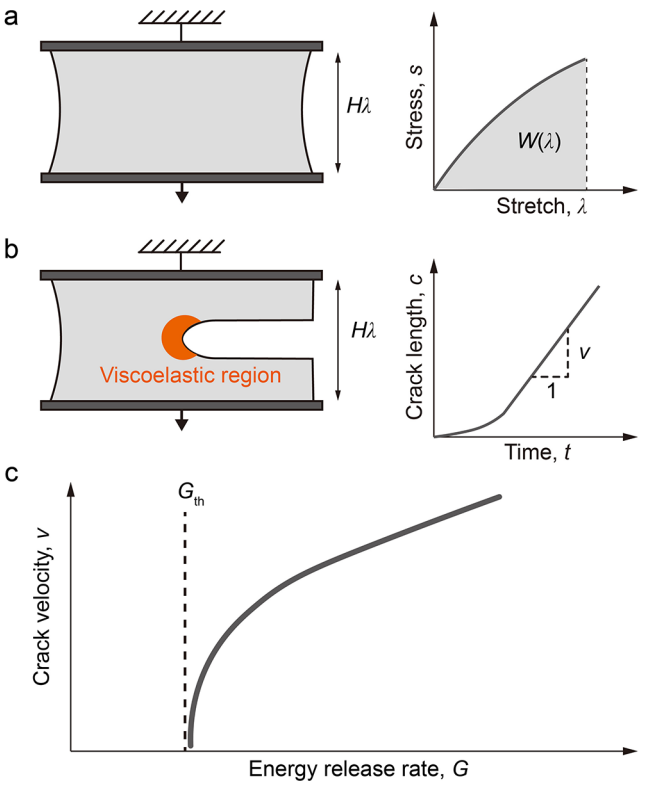


**Figure 31.** Crack growth in a viscoelastic material under static load. (a) A long rectangular sample of height $H$ in the undeformed state is pulled at a low rate to a stretch $\lambda$. The experiment records a relaxed stress–stretch curve, the area under which gives the free-energy density, $W(\lambda)$. (b) A precracked sample of height $H$ in the undeformed state is held at a stretch $\lambda$. The crack length $c$ is recorded as a function of time, and the slope gives the crack velocity. As the crack grows, the material deforms by viscoelasticity in a localized zone around the crack tip. After some time of transient growth, the crack attains a steady state of constant velocity, $v$. (c) The steady-state crack velocity, $v$, as a function of the energy release rate, $G$.

called the slow crack threshold, $G_{th}$, below which the crack remains stationary.

The crack velocity in viscoelastic materials as a function of the energy release rate was first reported by Mullins in 1959 and Greensmith in 1960.[23,24] More extensive data are collected in ref 110. The crack velocity may not be a monotonically increasing function of the energy release rate, and the nonmonotonic function may lead to stick–slip crack growth.[24,111] Theoretical studies of viscoelastic crack growth have been reviewed.[112−114] Given a polymer network, the slow crack threshold is commonly larger than the fatigue threshold.[115]

### 6.4. Static Energy Release Rate: Hydrolytic Crack Growth

Subject to a static load, silica may survive for a long time (days, weeks, or years) and then, without warning, break suddenly. In 1944, Orowan pointed out that this delayed fracture in silica originates not from viscoelasticity but from hydrolysis.[14] A $H_2O$ molecule may migrate from the environment to the crack tip, and hydrolyze a siloxane bond (Si−O−Si) into two silanol groups (SiOH) (Figure 32a). Silica has long been used to make water containers. The hydrolysis of silica, if it goes forward at all, must be extraordinarily slow. In fact, two silanol groups often condense into a siloxane bond and release a $H_2O$ molecule. That is, silica is stable in water. At the crack tip, however, a siloxane bond is strained, which assists a water molecule in attacking a siloxane bond to form two silanol groups.

Once grown in silica, a crack is hard to heal, even though the free energy of reaction favors the condensation of silanol groups. This observation is attributed to the fact that the crack surfaces are not atomistically flat and silica is a hard material, so that most silanol groups are too far apart to condense. Incidentally, two smooth surfaces of silica can form strong bonds, as demonstrated in the technology of wafer bonding.[117] The toughness of silica surfaces so bonded is comparable to that of silica itself.

The stress-assisted hydrolysis results in the delayed fracture of silica. A crack inevitably exists on the surface of silica. When silica is under a static load, the crack tip concentrates stress. Assume that the load is too low to break the siloxane bonds at the crack tip. But the intense stress at the crack tip strains the siloxane bonds, making them vulnerable to stress-assisted hydrolysis. In an environment where $H_2O$ molecules exist as either liquid or gas, a crack opens a path to transport $H_2O$

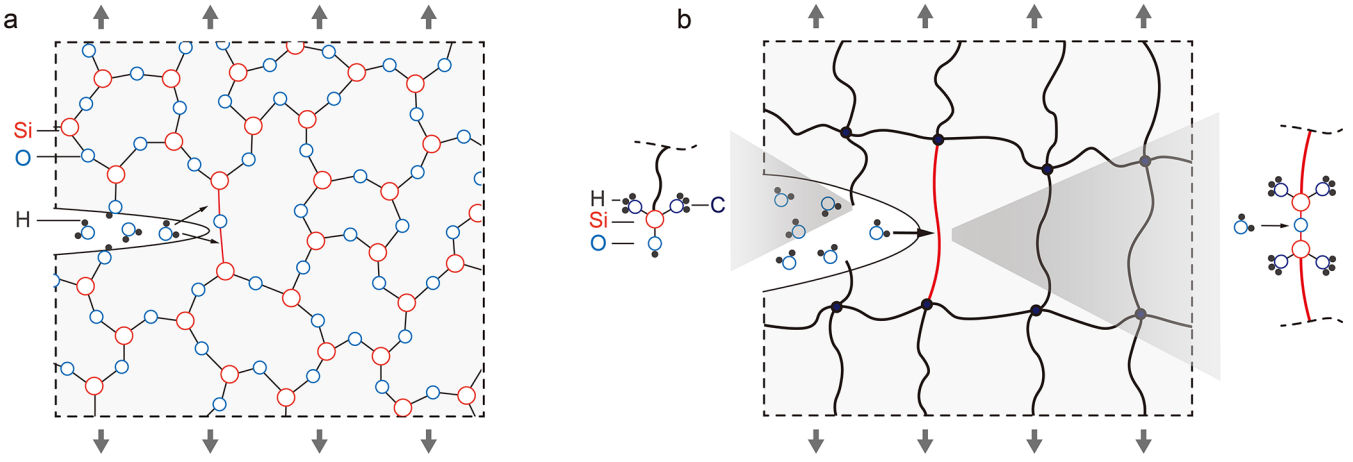


**Figure 32.** Stress-assisted hydrolysis. When a siloxane-bonded material is subject to a tensile force, the tip of a crack concentrates stress, which assists hydrolysis. The reaction converts siloxane bonds to silanol groups, advancing the crack. (a) Silica ($SiO_2$) is a network of siloxane bonds. (b) Polydimethylsiloxane (PDMS) is also a network of siloxane bonds. The figure is reproduced with permission from ref 116. Copyright 2019 Elsevier.


https://doi.org/10.1021/acs.chemrev.5c00663
Chem. Rev. XXXX, XXX, XXX−XXX

molecules from the environment to the crack tip. The stress-assisted hydrolysis grows the crack by converting a layer of siloxane bonds into two surfaces of silanol groups. When the crack is long enough, the static load will be high enough for the crack to grow without further assistance of hydrolysis.

Hydrolytic crack growth in silica is a phenomenon of mechanochemistry. The irreversible process of stress-assisted hydrolysis takes place at the crack tip, in a zone of atomic dimensions. Outside this localized irreversible zone, silica deforms by a reversible process of elasticity. Consequently, the applied load can be represented by the energy release rate.[26] In such an experiment, a sample of glass is precut with a crack, and is loaded in an environment of fixed temperature and humidity. The crack velocity is measured as a function of the energy release rate. A value of the energy release rate exists, called the threshold, below which the crack does not grow. Hydrolytic crack growth in silica has been reviewed.[118]

Recently, hydrolytic crack growth has been observed in polydimethylsiloxane (PDMS) (Figure 32b).[116] The backbone is a chain of siloxane bonds, whereas the methyl side groups make the material hydrophobic. When a sample is stretched, a crack provides a path for $H_2O$ molecules to migrate from the environment to the crack tip. When the crack impinges upon a PDMS strand, the high tension transmits over the entire length of the stand. When a $H_2O$ molecule hydrolyzes a siloxane bond in the strand into two silanol groups, the strand snaps and releases the tension of the entire strand. Consequently, at the same energy release rate, a crack grows in PDMS much slower than in silica. Hydrolytic crack growth has also been studied in other polymers in which backbones are susceptible to hydrolysis. Examples include poly(lactic acid),[119] poly(ethylene terephthalate),[120] and poly(glycerol sebacate).[121] The resistance to hydrolytic crack growth is enhanced in a composite of soft and hard PDMS.[122]

Beside hydrolysis, other chemical reactions may break polymer strands. Perhaps the best known example is elastomers with backbones containing carbon−carbon double bonds, which are susceptible to oxidation.[123] As another example, epoxy is susceptible to oxidation, which may cause crack growth in semiconductor devices and composites.[124]

### 6.5. Static Energy Release Rate: A Crack Growing in a Poroelastic Material

In a hydrogel, a polymer network is swollen with water. For the hydrogel to deform, the network must deform and the water molecules must change neighbors (Figure 33). In one mode of deformation, water molecules rearrange locally. This mode of deformation, called viscoelasticity, occurs over a time scale that is independent of the size of the sample. In another mode of deformation, water molecules migrate over long distances. This mode of deformation, called poroelasticity, occurs on a time scale that becomes long when the sample is large. Water itself has low viscosity. If water molecules screen the noncovalent bonds between polymer strands, then the hydrogel is negligibly viscoelastic but is poroelastic.

Cracks in poroelastic materials have been studied theoretically[126−128] and experimentally.[129−131] Here we will describe several general considerations. Like viscoelasticity, poroelasticity is an irreversible process. To apply the energy release rate to a crack in a poroelastic body, experiments need to be devised such that a large part of the body undergoes a reversible process of elasticity and poroelasticity occurs in a zone small compared to the body. A poroelastic material

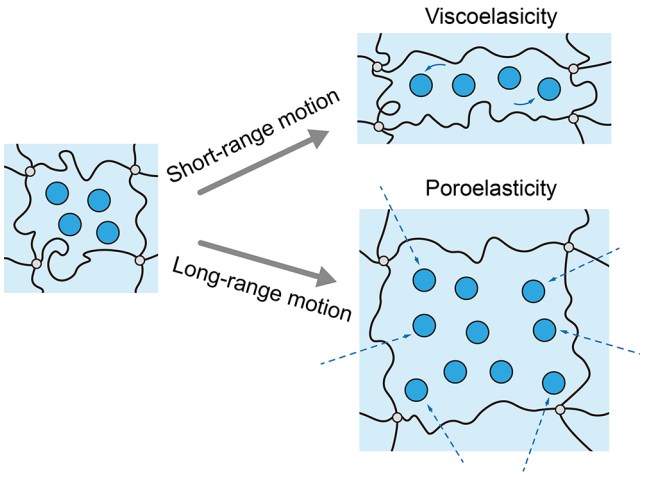


**Figure 33.** Viscoelasticity vs poroelasticity in a hydrogel. Reproduced with permission from ref 125. Copyright 2008 Elsevier.

undergoes elastic deformation under two conditions: when the time is either so long that water migrates to equilibrium or so short that water does not migrate appreciably.

As an illustration, consider a sheet of hydrogel of a long rectangular shape in the undeformed state (Figure 34a). The hydrogel is clamped along the two long edges, submerged in pure water, and pulled at such a low rate that water molecules have enough time to migrate into the hydrogel. At each stretch $\lambda$, the water molecules in the hydrogel equilibrate with those outside the hydrogel. Such a slow loading stress−stretch curve is an example of elasticity of the first type. Subsequently, the hydrogel is unloaded so rapidly that water molecules in the hydrogel have no time to migrate and do not equilibrate with water molecules outside the hydrogel. Such a fast unloading stress−stretch curve is an example of elasticity of the second type. The two curves are distinct.

As an illustration of using elasticity of the first type, consider a precut crack in a hydrogel submerged in pure water (Figure 34b). The hydrogel is held at a constant stretch independent of time. After a long time, water molecules in the hydrogel equilibrate with those outside the hydrogel while the crack remains stationary. At equilibrium, the concentration of water in the hydrogel is inhomogeneous. Far ahead of the crack tip, the hydrogel follows the elasticity of the first type. Far behind the crack tip, the hydrogel relaxes to another state of equilibrium, in which the concentration of water is lower than that far ahead of the crack tip. Around the crack tip, a high concentration of water exists in a zone small compared to the sample. The energy release rate is $HW_1$, where $W_1$ is the elastic energy density associated with the slow loading curve. By repeating the experiment at various stretches, one can determine the threshold energy release rate, above which the crack grows.

As an illustration of using elasticity of the second type, consider the fast growth of a postcut crack in a hydrogel submerged in water (Figure 34c). The hydrogel without a crack is pulled to a constant stretch, and water molecules in the hydrogel equilibrate with those outside the hydrogel. A crack is cut in the gel, and the crack grows so rapidly in the hydrogel that water molecules have no time to migrate in the main part of the hydrogel. In a zone small compared to the body, water molecules can migrate. The energy release rate is given by $HW_2$, where $W_2$ is the elastic energy density associated with


https://doi.org/10.1021/acs.chemrev.5c00663
Chem. Rev. XXXX, XXX, XXX−XXX

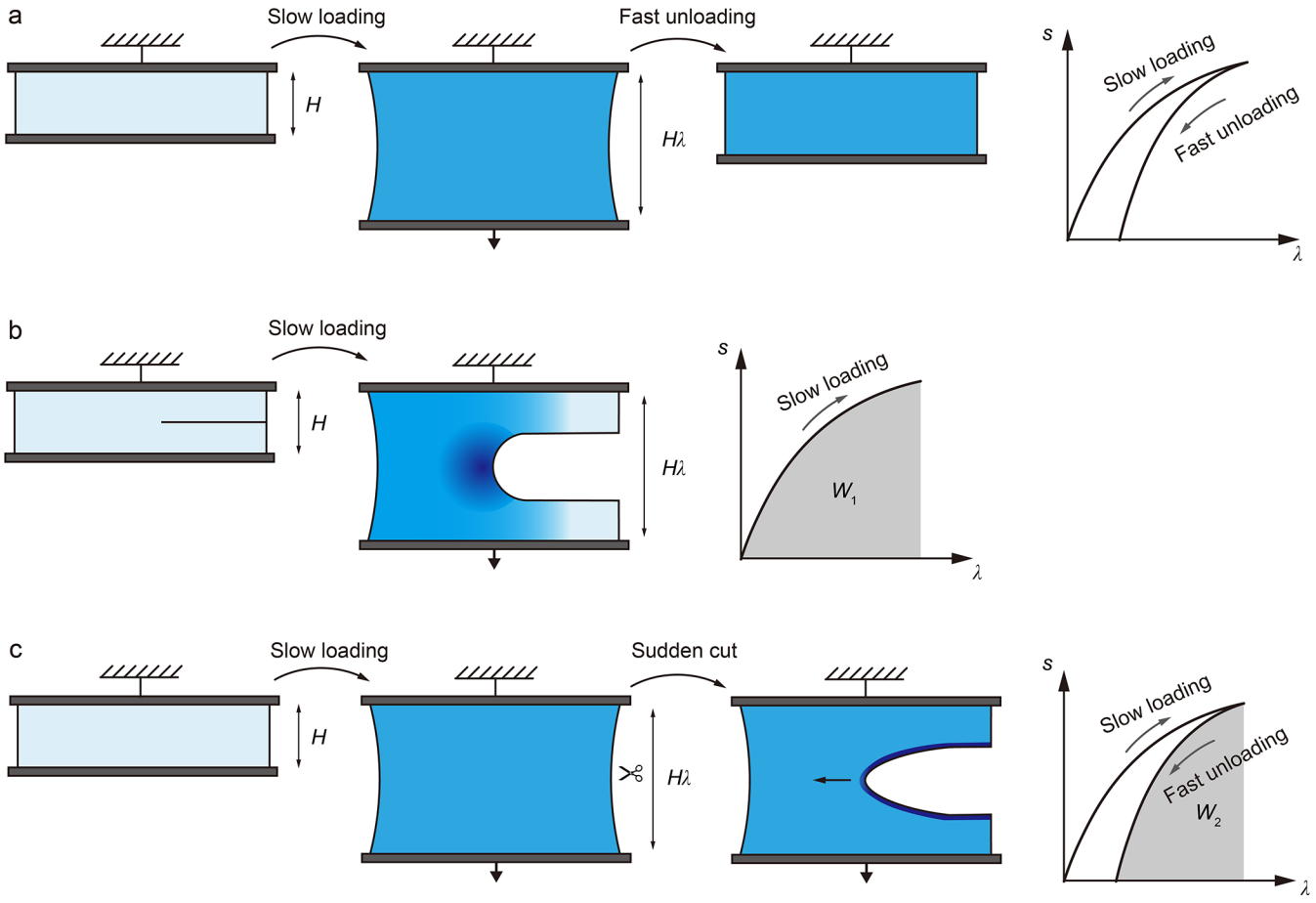


**Figure 34.** Crack growth in a poroelastic material under static load. (a) A hydrogel of a long rectangular shape is clamped on the two long edges, submerged in pure water, loaded slowly, and unloaded rapidly. (b) For a stationary crack, the hydrogel equilibrates with pure water, and the concentration of water in the hydrogel is inhomogeneous. (c) A crack grows so fast that the concentration of water remains unchanged and uniform in a large part of the hydrogel. In a small zone around the crack tip, water migrates.

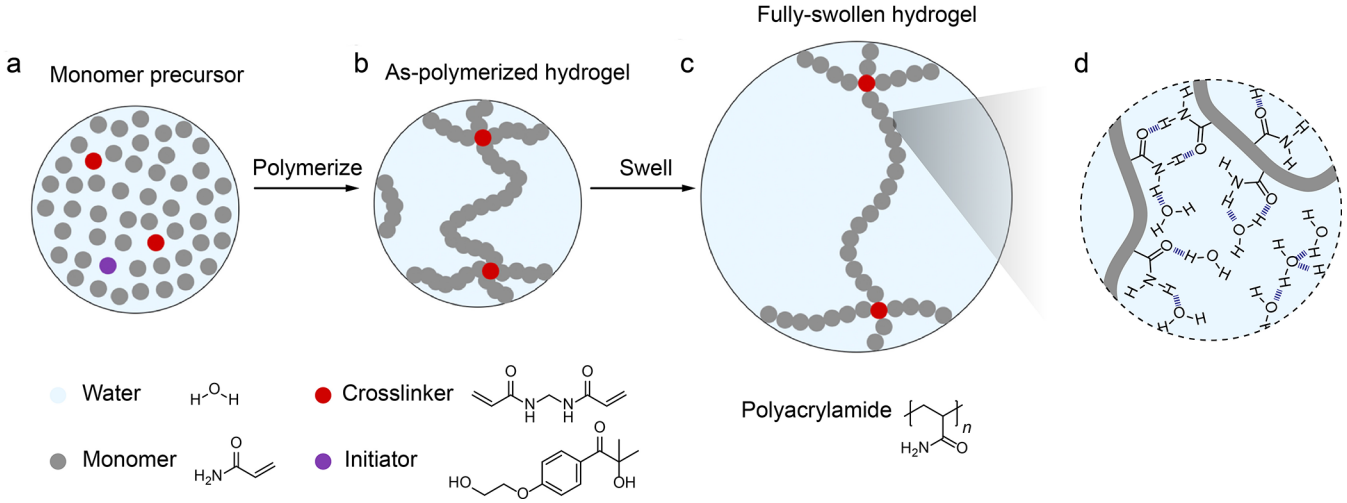


**Figure 35.** A polyacrylamide hydrogel synthesized by photoinitiated radical polymerization. (a) A solution of four components: monomer (acrylamide), cross-linker (*N*,*N*′-methylenebis(acrylamide)), photoinitiator (2-hydroxy-4′-(2-hydroxyethoxy)-2-methylpropiophenone), and water. (b) As-polymerized hydrogel. (c) Fully swollen hydrogel. (a–c) Reproduced with permission from ref 70. Copyright 2023 Elsevier. (d) Hydrogen bonds between water molecules, between water molecules and carbamoyl groups, and between carbamoyl groups.

the fast unloading curve. By repeating this experiment by holding the hydrogel at various stretches, one can measure the crack velocity as a function of the energy release rate.

In a study of crack growth in the body of hydrogel, it is commonly assumed that the experiment is performed in a short enough time that poroelasticity is localized in a zone small compared with the body. The main part of the body is



https://doi.org/10.1021/acs.chemrev.5c00663
Chem. Rev. XXXX, XXX, XXX−XXX

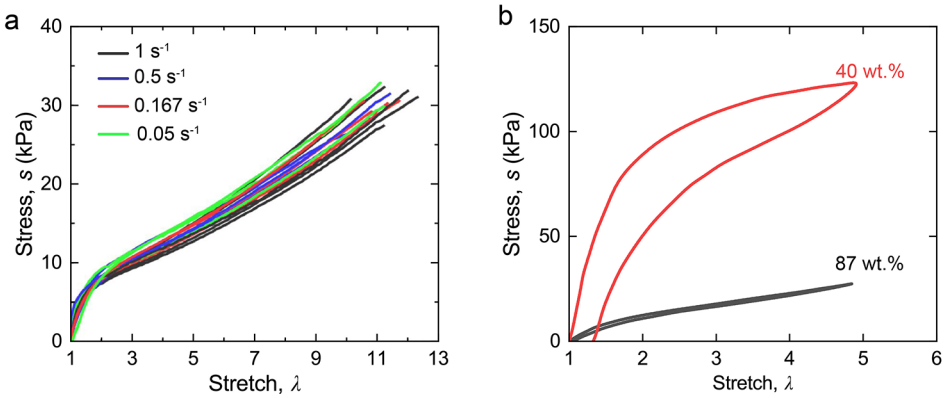


**Figure 36.** Stress−stretch curves of polyacrylamide hydrogels. (a) The stress−stretch curve of a polyacrylamide hydrogel of a water fraction of 87 wt % is insensitive to stretch rate. Reproduced with permission from ref 56. Copyright 2019 Elsevier. (b) The hysteresis increases as the water fraction decreases. Loading and unloading curves are measured at a stretch rate of 0.1 $s^{-1}$. Reproduced with permission from ref 140. Copyright 2024 Springer Nature OA license agreement (CC BY 4.0).

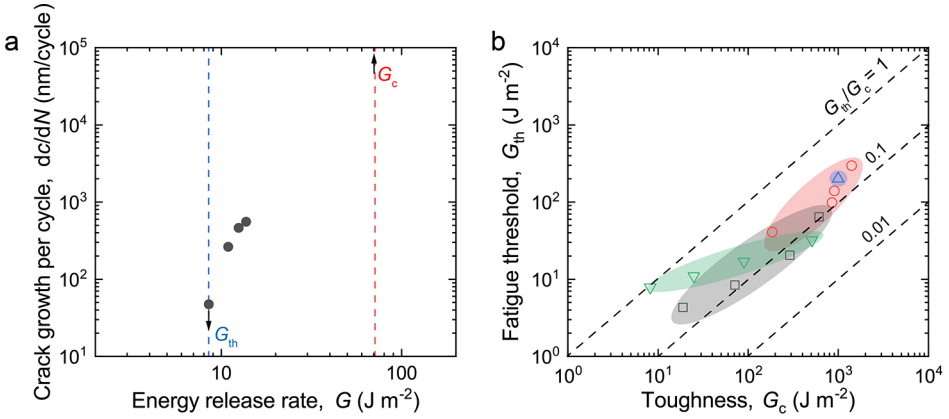


**Figure 37.** Toughness and fatigue threshold of PAAm hydrogels. (a) For an as-polymerized PAAm hydrogel with 87 wt % water under cyclic stretch, the crack growth per cycle is recorded as a function of the amplitude of the energy release rate. Reproduced with permission from ref 139. Copyright 2018 The Royal Society of Chemistry. (b) Collected on the plane of fatigue threshold and toughness are data from four papers for PAAm hydrogels prepared under various conditions.[69,89,139,144]

taken to undergo elasticity of the second type, and the energy release rate is calculated using the theory of elasticity.

## 7. POLYACRYLAMIDE HYDROGEL

The remainder of this article describes molecular principles of crack growth in representative polymer networks. We begin with polyacrylamide hydrogels, which have broad and well-established applications in biology, agriculture, and medicine and mechanical, chemical, and biological properties that have been extensively characterized.[39,132,133] Just as silica is a model hard material, so is polyacrylamide hydrogel a model soft material.

### 7.1. Synthesis

A polyacrylamide hydrogel is commonly prepared by radical polymerization. For example, photoinitiated polymerization starts with a solution of four components: monomer, cross-linker, photoinitiator, and water (Figure 35a). Often, the solution has a high mass fraction of water of ∼80%. Each monomer molecule consists of a vinyl group ($-CH{=}CH_2$) and a carbamoyl group ($-CONH_2$). Each cross-linker molecule consists of two vinyl groups and two hydrophilic groups. When the solution is exposed to ultraviolet light, a photoinitiator molecule decomposes into two radicals. Each radical initiates a chain reaction, in which monomer molecules open their carbon−carbon double bonds and link into a chain of carbon−carbon single bonds. Each cross-linker opens both carbon−carbon double bonds, which link into two chains. The polymerization turns the solution into a hydrogel, in which covalent bonds link repeat units into polymer chains and cross-link the chains into a polymer network (Figure 35b). The as-polymerized hydrogel evaporates water when exposed to dry air, and imbibes water when submerged in pure water. Because hydrogels are commonly used in contact with water, attention here is focused on fully swollen hydrogels in equilibrium with pure water (Figure 35c). The mass fraction of water in a fully swollen hydrogel varies between ∼80% to nearly 100%.

### 7.2. PAAm Hydrogel with a High Water Fraction Has Nearly Perfect Elasticity

A mixture of polyacrylamide and water has three types of hydrogen bonds (Figure 35d). The hydrogen bond between a carbamoyl group and a water molecule is stronger than the hydrogen bond between two carbamoyl groups, which is stronger than the hydrogen bond between two water molecules.[134,135] The water molecules bonded to polyacrylamide chains are called bound water, and the water molecules surrounded by other water molecules are called free water.[135,136]


https://doi.org/10.1021/acs.chemrev.5c00663
Chem. Rev. XXXX, XXX, XXX−XXX

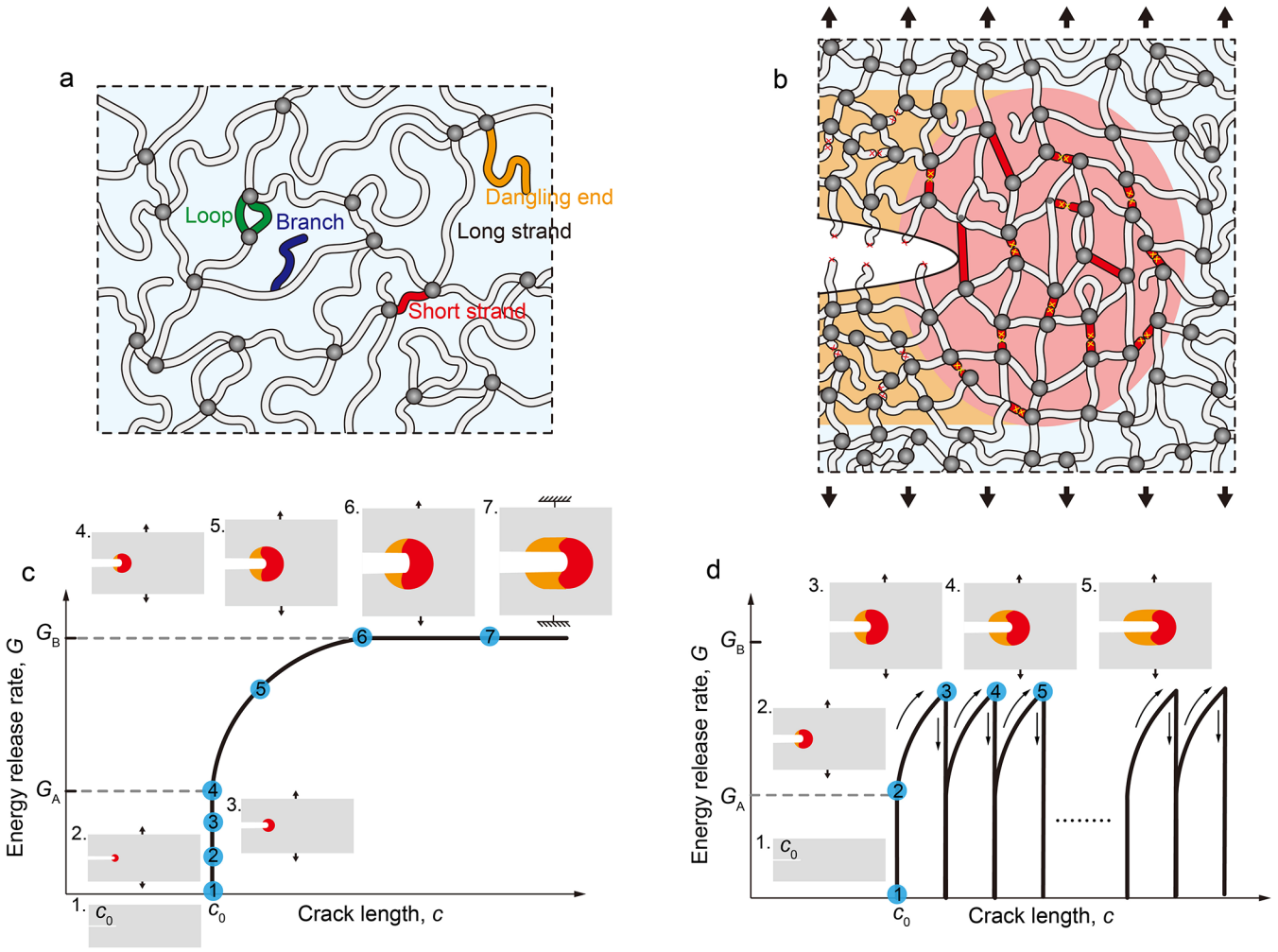


**Figure 38.** A crack grows in a PAAm hydrogel. (a) The polymer network is imperfect. Coexistent in the network are dangling ends, branches, loops, and strands of various lengths. (b) A crack grows by breaking strands on and off the crack plane. (c) Crack resistance curve under a monotonic load. In snapshots, a red zone represents the part of the network in which some strands are breaking, and a yellow zone represents the scarred network. (d) Crack resistance curve under cyclic load.

The dissimilar hydrogen bonds result in rich macroscopic behavior. The hydrogen bonds between water molecules break and reform by thermal fluctuation rapidly on a time scale of $\sim 10^{-6}$ s, leading to a low viscosity of $\sim 10^{-3}$ Pa·s.[137] Dry polyacrylamide is a polymer glass in which carbamoyl side groups form hydrogen bonds.[133−135,138] Uncrosslinked polyacrylamide chains dissolve in water. The viscosity of the polyacrylamide−water mixture increases as the water fraction decreases.[133] For a low mass fraction, water molecules plasticize polyacrylamide.

For a hydrogel of high water fraction, the free water is abundant, which lubricates polyacrylamide chains so that the hydrogel exhibits nearly perfect elasticity. For example, the stress−stretch curve of a polyacrylamide hydrogel of a water fraction of 87 wt % is rate-insensitive (Figure 36a) and has small hysteresis (Figure 36b).[56,70,96,139] When the water fraction drops to 40 wt %, the hysteresis increases markedly (Figure 36b).[140,141] When the water fraction drops to about 20 wt %, a gel-to-glass transition takes place.[141,142]

A similar gel-to-glass phenomenon is observed in an ionogel, where a glassy polymer network of poly(acrylic acid) (PAAc) is mixed with an ionic liquid.[143] The small molecules of ionic liquid break the dense hydrogen bonds between PAAc strands, and solvate the strands. A moderate amount of ionic liquid (~45 wt %) leads to a stiff, ductile, and tough ionogel.[143]

### 7.3. Toughness and Fatigue Threshold

A sample of polyacrylamide hydrogel is precut with a crack and cyclically stretched. The crack growth per cycle is recorded as a function of the amplitude of the energy release rate (Figure 37a). The hydrogel has a toughness of 71.2 J $m^{-2}$ and a fatigue threshold of 8.5 J $m^{-2}$. Data of polyacrylamide hydrogels prepared under various conditions are collected on the plane of the toughness and fatigue threshold (Figure 37b). For most samples, the toughness is much higher than the fatigue threshold. This experimental finding is interpreted as follows.

In a highly swollen hydrogel, polyacrylamide strands are fully solvated by water molecules. The polyacrylamide strands interact indirectly, mediated through free water. The hydrogen bonds between water molecules break and reform rapidly so that the highly swollen PAAm hydrogel has a low hysteresis upon loading and unloading, even when the stretch is large. It is likely that the weak hydrogel bonds play a small role in resisting crack growth. As an idealization, this discussion excludes the role of the hydrogen bonds, and focuses on the role of covalent bonds of the polyacrylamide network. The network is imperfect, containing dangling ends, branches,


https://doi.org/10.1021/acs.chemrev.5c00663
Chem. Rev. XXXX, XXX, XXX−XXX

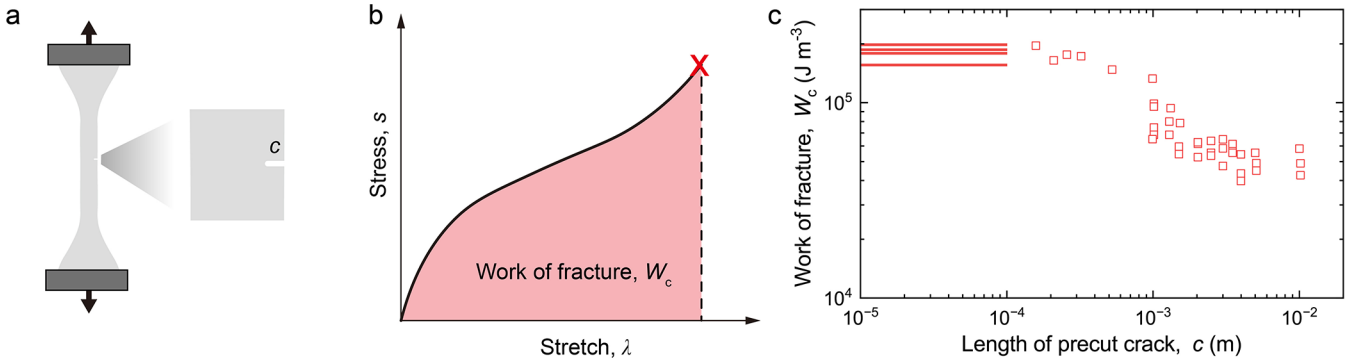


**Figure 39.** Flaw sensitivity. (a) A sample containing a precut crack of length $c$ is stretched to rupture. (b) The stress−stretch curve. The area under the curve is the work of fracture. (c) Work of fracture as a function of crack length for a PAAm hydrogel with a water fraction of 87 wt %. Solid lines represent the value measured using samples without cut. The data points are measured using samples with cut. Reproduced with permission from ref 56. Copyright 2019 Elsevier.

loops, and strands of various lengths (Figure 38a). Subject to monotonic load, the hydrogel grows a crack by breaking covalent bonds (Figure 38b). In the network, off the crack plane, some strands break, while other strands remain intact. Before a strand breaks, because the hydrogen bonds are negligibly weak, high tension is transmitted over the entire length of the strand. When the strand breaks at a single covalent bond, the energy stored in the entire strand dissipates. Consequently, toughness results from energy dissipated in breaking not only the strands on the crack plane but also some strands off the crack plane.[56]

The scission of strands off the crack plane has been observed using light-emitting mechanophores for a crack growing in poly(methyl acrylate), in which scission is detected as far as 100 $\mu$m away from the crack plane.[145] This finding is consistent with a fact mentioned before. A polymer network fractures by breaking covalent bonds, but the strength of a polymer network is typically orders of magnitude lower than that of covalent bonds.[56] The energy density of breaking covalent bonds is $\sim 10^9$ J m$^{-3}$, and that of breaking a polymer network is $\sim 10^5$−$10^7$ J m$^{-3}$. Recall that the crack tip field scales as $W \sim G/R$. The strand length of the network is $R_1 \approx$ 10 nm. At a distance of $R_2 \approx 100$ $\mu$m, the energy density decreases by a factor of $R_2/R_1 \approx 10^4$. This estimate is consistent with the experimental finding of scission far away from the crack plane.

In principle, the distributed scissions lead to a crack resistance curve, although such a curve has never been reported for a PAAm hydrogel. Imagine the crack resistance curve of a PAAm hydrogel (Figure 38c). At a low energy release rate, the network deforms elastically, and no strand breaks. As the energy release rate increases, some strands break, but the scissions are isolated around the crack tip and the crack does not grow. A threshold of the energy release rate exists, $G_A$, above which the crack grows by breaking strands on the crack plane, and some strands off the crack plane may have already broken. The crack growth is stable in that the energy release rate must increase to grow the crack further and to enlarge the zone in which some strands break. Ahead of the crack, the scission of a strand, on or off the crack plane, is a dynamic event that dissipates energy. Behind the crack, the network is scarred with broken strands. At a certain energy release rate, $G_B$, the crack grows in a steady state, breaking strands ahead of the crack and leaving scars behind the crack, while the thickness of the scarred zone remains invariant. When a single value of toughness $G_c$ is reported, we take it to be $G_B$.

Now consider a network subject to a cyclic load with an amplitude of the energy release rate, $G$, within the range $G_A < G < G_B$ (Figure 38d). During the first loading, the strands off and on the crack plane break as described for the sample under monotonic loading. Upon unloading, the broken strands do not heal, and the crack length remains unchanged. Upon reloading, the broken strands no longer resist crack growth. Consequently, the crack must grow to access a fresh network, breaking additional strands on and off the crack plane. This need to access the fresh network explains why the crack under the cyclic load grows under an amplitude of energy release rate lower than $G_B$.

In the above discussion, we tacitly assume that the fatigue threshold measured under cyclic loading is the same as the threshold of the onset of crack growth measured under monotonic loading. This assumption has not been examined experimentally. For natural rubber, it has been reported that the fatigue threshold measured under cyclic loading is much lower than the threshold measured under monotonic stretch. The difference is probably due to the large difference in resolution between the two types of experiments. Under cyclic stretch, the experiment resolves crack growth with resolution $\sim 10^{-4}$ $\mu$m/cycle, whereas under monotonic stretch, the experiment resolves a crack growth of $\sim 10$ $\mu$m. This said, existing evidence does not exclude the possibility that the two types of thresholds are different.

### 7.4. Flaw Sensitivity and Fractocohesive Length

Prepare a sample in which a precut crack is small compared to the dimensions of the sample (Figure 39a). Stretch the sample to rupture and record the stress−stretch curve (Figure 39b). The area under the curve is the work of fracture, $W_c$. The work of fracture is insensitive to the crack when the crack is short, but is sensitive to the crack when the crack is long (Figure 39c).[56] The work of fracture measured using samples with short precut cracks coincides with that measured using samples containing no precut cracks. This work of fracture $W_c$ is a material property with the dimensions of energy per unit volume. Recall that toughness $G_c$ is measured using a sample containing a long precut crack and is a material property with dimensions of energy per unit area. The ratio $G_c/W_c$ is also a material property, with a dimension of length, called the fractocohesive length.[63] Samples containing precut cracks are insensitive to the cracks when the cracks are shorter than a


https://doi.org/10.1021/acs.chemrev.5c00663
Chem. Rev. XXXX, XXX, XXX−XXX

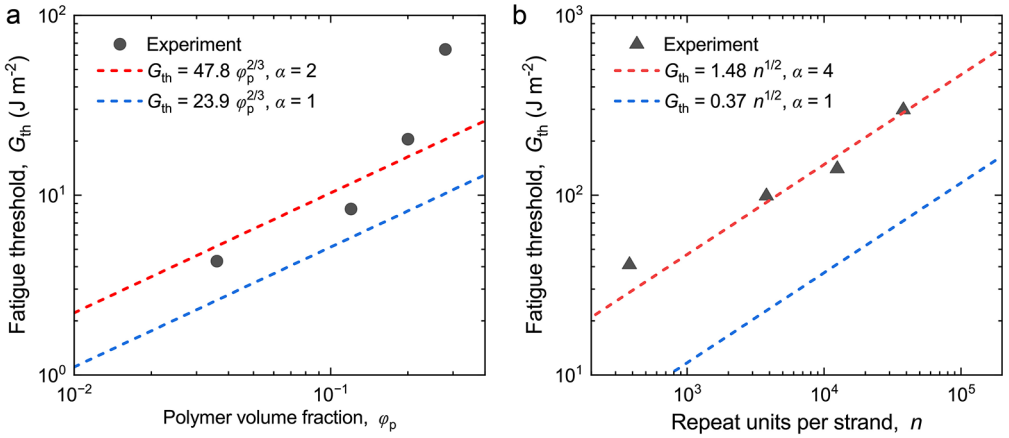


**Figure 40.** A hydrogel resists fatigue crack growth by dense and long polymer strands. (a) Fatigue threshold as a function of polymer content, when the strand length is fixed. The figure is reproduced with permission from ref 139. Copyright 2018 The Royal Society of Chemistry. (b) Fatigue threshold as a function of the number of repeat units per strand, when the polymer volume fraction is fixed. The figure is reproduced with permission from ref 89. Copyright 2020 Elsevier.

certain length, which is estimated by the fractocohesive length. Representative values are $W_c = 2 \times 10^5$ J m$^{-3}$, $G_c = 500$ J m$^{-2}$, and $G_c/W_c = 250$ $\mu$m. The fractocohesive length gives a fairly accurate estimate of the crack length around which the flaw sensitivity takes place.

### 7.5. Lake–Thomas Model Predicts the Fatigue Threshold

The hydrogel is taken to contain enough water to solvate all polymer strands such that the noncovalent bonds between strands are negligible. When a crack impinges upon a strand, the high tension transmits along the entire strand. Assume that a crack grows in the hydrogel by breaking a layer of strands so that the fatigue threshold is $G_{th} = eL$.

In the hydrogel, water is not load-bearing, and the free energy in the backbone per unit volume is

$$e = \varphi_p J/v \tag{29}$$

where $\varphi_p$ is the volume fraction of polymer, $J$ is the energy stored in a repeat unit just before a strand ruptures, and $v$ is the volume of a repeat unit.

The hydrogel is prepared by radical polymerization. In the as-polymerized state, each polymer strand is taken to be relaxed so that the end-to-end distance is $(nb_k b)^{1/2}$, where $b_k$ is the Khun length, $b$ is the length of a repeat unit, and $n$ is the number of repeat units per strand. Let $\varphi_{p,0}$ be the volume fraction of polymer in the as-polymerized hydrogel. The hydrogel then swells or deswells to reach a volume fraction of polymer $\varphi_p$. In the state after swelling or deswelling, the end-to-end distance of a strand is

$$L = (\varphi_{p,0}/\varphi_p)^{1/3}(nb_k b)^{1/2} \tag{30}$$

Just before the strand breaks, the free energy in each carbon–carbon single bond on the backbone is $\sim 1.06 \times 10^{-19}$ J.[146,147] Each repeat unit has two carbon–carbon single bonds on the backbone, so the energy stored per repeat unit is $J \approx 2.12 \times 10^{-19}$ J. The density is $\rho = 1.13 \times 10^6$ g m$^{-3}$. The chemical formula of the repeat unit is $CH_2CHCONH_2$, so the mass per repeat unit is $m = 1.18 \times 10^{-22}$ g. Thus, the volume per repeat unit is $v = m/\rho = 1.04 \times 10^{-28}$ m$^3$. For a representative value of $\varphi_p = 13$ vol %, the energy stored per unit volume just before the strand breaks is $e = \varphi_p J/v \approx 2.65 \times 10^8$ J m$^{-3}$. The Khun length is $b_k = 1.58 \times 10^{-9}$ m.[148] The length per repeat unit is estimated by $b \approx v^{1/3} = 4.71 \times 10^{-10}$ m. Take a representative value of the number of repeat units per strand $n = 720$. The strand length is $L = (nb_k b)^{1/2} = 2.31 \times 10^{-8}$ m (23.1 nm). The fatigue threshold is $G_{th} = eL \approx 6.12$ J m$^{-2}$.

This estimate by the Lake–Thomas model is close to the experimental value. In the experiment, a hydrogel is prepared from a precursor with 87 wt % water, and the cross-linker-to-monomer molar ratio is $C = 7 \times 10^{-4}$.[139] The number of repeat units per strand is estimated by $n \approx 1/(2C) \approx 714$. The measured fatigue threshold of this as-polymerized hydrogel is 8.4 J m$^{-2}$.

### 7.6. Long Polymer Strands Amplify the Fatigue Threshold

A combination of eqs 29 and 30 gives

$$G_{th} = \varphi_{p,0}^{1/3}\varphi_p^{2/3}(nb_k b)^{1/2} J/v \tag{31}$$

Given a species of polymer, $b_k$, $b$, $J$, and $v$ are constant. However, $\varphi_{p,0}$, $\varphi_p$, and $n$ can be varied during fabrication.

In the as-polymerized hydrogel, $\varphi_{p,0}$ can vary from approximately 0 to 100%. The as-polymerized hydrogel is commonly submerged in pure water for some time, after which the hydrogel is taken out of the pure water and homogenized to reach a polymer fraction of $\varphi_p$, which is not necessarily the polymer fraction of the fully swollen hydrogel in equilibrium with pure water. For a hydrogel prepared this way, $\varphi_p$ ranges between $\varphi_{p,0}$ and the polymer fraction of a fully swollen hydrogel. The latter depends on $\varphi_{p,0}$ and $n$. As we note later, for a polymer network in which entanglements greatly outnumber cross-links, the polymer fraction of a fully swollen gel is set by the number of repeat units between neighboring entanglements, $n_e$, and is independent of the number of repeat units between neighboring cross-links, $n$.

The as-polymerized hydrogel can also be left in the open air for some time and then homogenized to a polymer fraction of $\varphi_p$. In this case, $\varphi_p$ ranges from 0 to $\varphi_{p,0}$. Recall the Lake–Thomas model applies only to a polymer network in which the noncovalent bonds between strands are negligible. Thus, when applying the model, $\varphi_p$ needs to be low enough for all strands to be fully solvated.

Equation 31 also indicates several scaling relations. First, for a hydrogel polymerized with a given $n$ and $\varphi_{p,0}$ and then swollen or dehydrated to polymer volume fraction $\varphi_p$, the


https://doi.org/10.1021/acs.chemrev.5c00663
Chem. Rev. XXXX, XXX, XXX–XXX

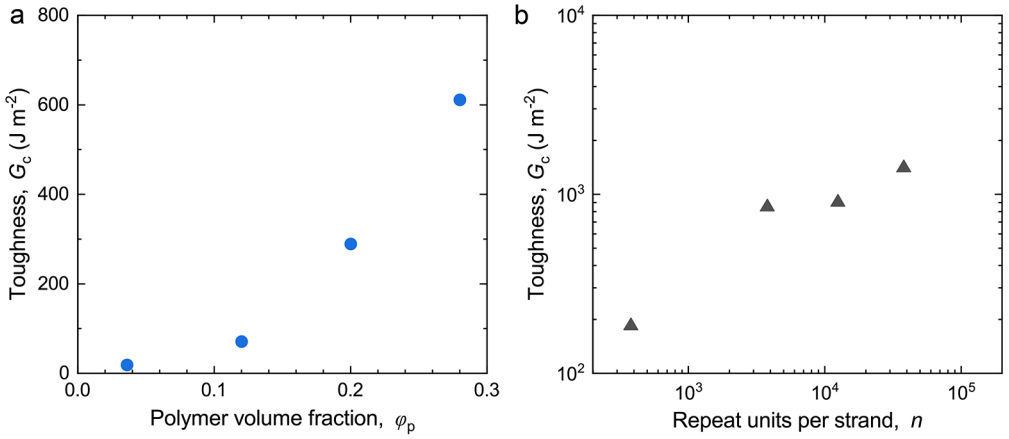


**Figure 41.** Hydrogel toughness can be amplified by the dense and long polymer strand. (a) Toughness as a function of polymer volume fraction, when the strand length is fixed. The figure is reproduced with permission from ref 139. Copyright 2018 The Royal Society of Chemistry. (b) Toughness as a function of the number of repeat units per strand, when the polymer content is fixed. The figure is reproduced with permission from ref 89. Copyright 2020 Elsevier.

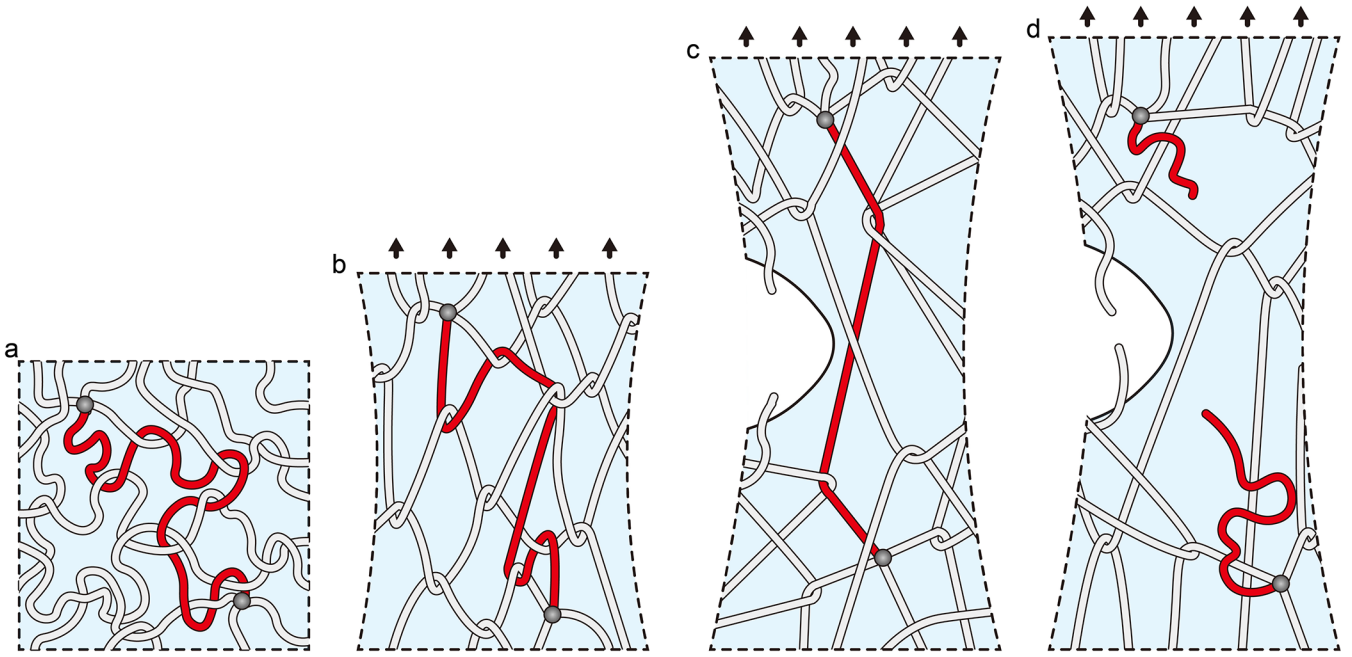


**Figure 42.** Entanglements stiffen but do not embrittle the polymer network. (a) A tanglemer is a polymer network in which entanglements greatly outnumber cross-links. (b) When the network is stretched, both entanglements and cross-links stiffen the polymer network. (c) When a crack impinges on a strand, entanglements readily slip and allow high tension to transmit over the entire length of the strand. By contrast, when the strand meets a cross-link, the high tension in the strand is shared by several other strands. (d) When the strand ruptures at a single covalent bond, the free energy stored in the entire strand dissipates. Reproduced with permission from ref 69. Copyright 2021 The American Association for the Advancement of Science.

threshold scales as $G_{th} \sim \varphi_p^{2/3}$. Second, for a hydrogel polymerized with a given $\varphi_{p,0}$ and then swollen or dehydrated to a given $\varphi_p$, the threshold scales with the number of repeat units per strand as $G_{th} \sim n^{1/2}$. Third, for a hydrogel polymerized with a given $n$ and then swollen or dehydrated to a given $\varphi_p$, the threshold scales with the polymer volume fractions in the as-polymerized state as $G_{th} \sim \varphi_{p,0}^{1/3}$. Some of these scalings are illustrated by the experimental data as follows.

Experiment 1 keeps $n$ = 720 and $\varphi_{p,0}$ = 13 vol % and then varies $\varphi_p$ by dehydrating an as-polymerized hydrogel (Figure 40a).[139] In a cyclic test, the $G_{th}-\varphi_p$ plot roughly follows the scaling relation of $G_{th} \sim \varphi_p^{2/3}$ at low $\varphi_p$. The data differs from the Lake−Thomas model by a prefactor $\alpha$, $G_{th} = \alpha eL$. Fitting the data of this set of the experiment, we obtain $\alpha$ = 2. The experimental data deviates with the model at $\varphi_p$ = 28 vol %; the origin of this deviation is not understood. Despite this deviation, both the experimental data and the Lake−Thomas prediction show that for a hydrogel a higher polymer fraction enhances the fatigue threshold. In this experiment, $\varphi_p$ is not a material property. Many approaches, such as introducing hydrophobic components and increasing entanglements, can control $\varphi_p$ as a material property in a fully swollen state. These approaches enhance the fatigue threshold.[69,149,150]

Experiment 2 keeps $\varphi_{p,0} = \varphi_p$ = 21 vol % and varies $n$ by changing the cross-link density (Figure 40b).[89] In a cyclic peel


https://doi.org/10.1021/acs.chemrev.5c00663
Chem. Rev. XXXX, XXX, XXX−XXX

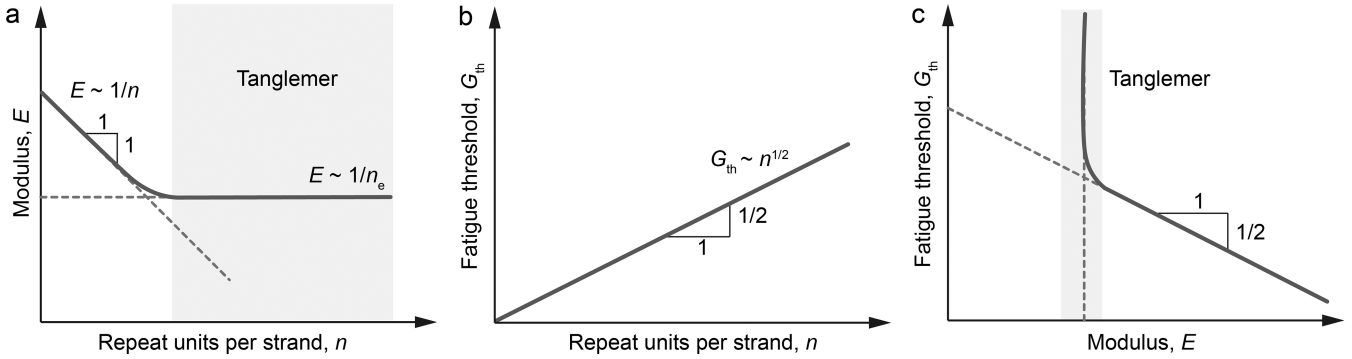


**Figure 43.** Tanglemer resolves the modulus−threshold conflict. (a) The modulus is sketched as a function of repeat units per strand. (b) The fatigue threshold is sketched as a function of repeat units per strand. (c) The fatigue threshold is sketched as a function of the modulus.

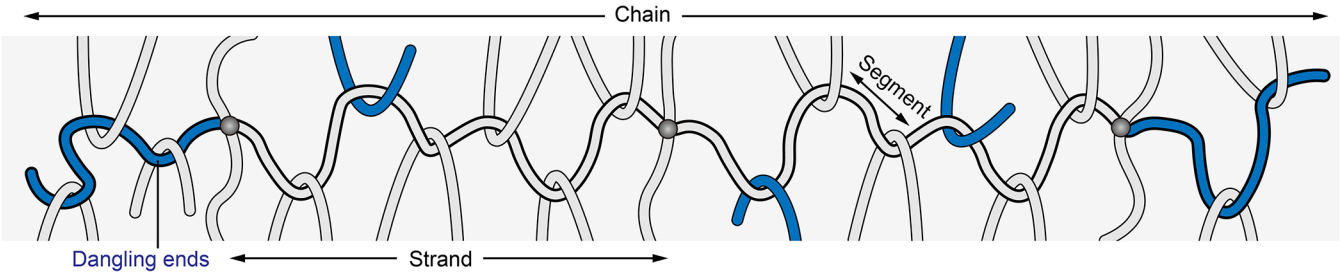


**Figure 44.** Topology of a tanglemer. Cross-links divide a chain into multiple strands (gray) and two dangling ends (blue). Entanglements divide a strand into multiple segments.

test, the $G_{th}-n$ plot follows a scaling relation of $G_{th} \sim n^{1/2}$, consistent with the Lake−Thomas model. In this case, coefficient $\alpha$ is 4. This result is consistent with an important principle that a long polymer strand enhances the resistance to fatigue crack growth.

The dense and long polymer strands can also amplify toughness (Figure 41). The dense and long poly strands bridge the crack, and allow the dissipative processes such as sequential strand scission to happen in a volume around the crack tip. Toughness is contributed by the two processes synergistically, and is amplified by both the polymer volume fraction (Figure 41a) and strand length (Figure 41b).

## 8. TANGLEMER

A tanglemer is a polymer network in which entanglements greatly outnumber cross-links (Figure 42a). Sparse cross-links trap the dense entanglements, allowing entanglements to slip on the long strand between neighboring cross-links while preventing flow.

The effects of entanglements on the rheology of polymer melts, solutions, and networks have been extensively studied.[6,87,151−154] These studies have been commonly restricted to deformation and flow without scission. The effects of entanglements on crack growth in polymer networks have received attention in recent years.[68,69,76,99,155−159]

Uncrosslinked long polymer chains entangle by thermal motion. When a melt of long chains reaches equilibrium, the entanglement density is set by the chemical structure of the chains. In a common test in rheology, the modulus is measured as a function of frequency. The rubbery plateau of the modulus determines the entanglement molecular weight.[160] The data have been tabulated for many species of polymers.[88] In a polymer solution at equilibrium, the entanglement density depends on not only the chemical structure of the polymer but also the chemical structure and fraction of the solvent.[161]

### 8.1. Entanglements Stiffen but Do Not Embrittle the Polymer Network

When a polymer network deforms, both cross-links and entanglements contribute to the modulus (Figure 42b).[6,7] At the crack tip, however, cross-links and entanglements behave differently.[69] Assume that the noncovalent bonds between strands are negligibly weak compared to the covalent bonds along a strand. When the crack impinges on a strand, entanglements readily slip, so the high tension in the strand transmits over the entire length of the strand (Figure 42c). By contrast, where the strand meets a cross-link, the tension of the strand transmits through the cross-link to several other strands. Consequently, the single strand bears higher tension than the other strands. That is, cross-links concentrate stress, but entanglements deconcentrate stress. When the strand ruptures at a single covalent bond, the strand snaps, and the free energy stored along the entire strand dissipates (Figure 42d).

In a tanglemer, the number of repeat units between neighboring entanglements, $n_e$, sets the modulus (Figure 43a):

$$E \sim 1/n_e \tag{32}$$

Because the entanglements do not impede the transmission of high tension along a strand, it is the number of repeat units between cross-links, $n$, that sets the fatigue threshold (Figure 43b):

$$G_{th} \sim 1/n \tag{33}$$

The tanglemer resolves the modulus−threshold conflict (Figure 43c). Whereas the modulus is kept constant by the number of units between entanglements, $n_e$, the fatigue threshold increases with the number of repeat units per strand, $n$.


https://doi.org/10.1021/acs.chemrev.5c00663
Chem. Rev. XXXX, XXX, XXX−XXX

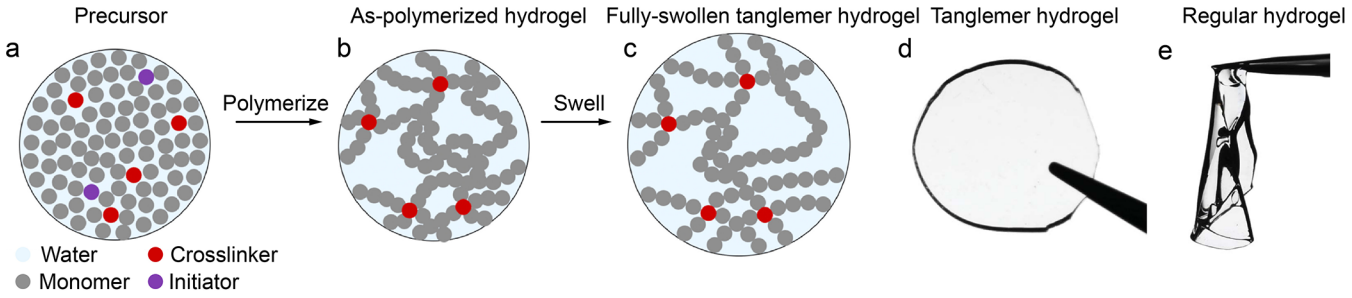


**Figure 45.** Preparing a tanglemer hydrogel by radical polymerization. (a) The precursor contains monomer and unusually low amounts of initiator, water, and cross-linker. (b) As-polymerized hydrogel. (c) Fully swollen hydrogel. (a–c) Reproduced with permission from ref 70. Copyright 2023 Elsevier. (d) Photograph of a tanglemer hydrogel. (e) Photograph of a regular hydrogel. (d, e) Reproduced with permission from ref 69. Copyright 2021 The American Association for the Advancement of Science.

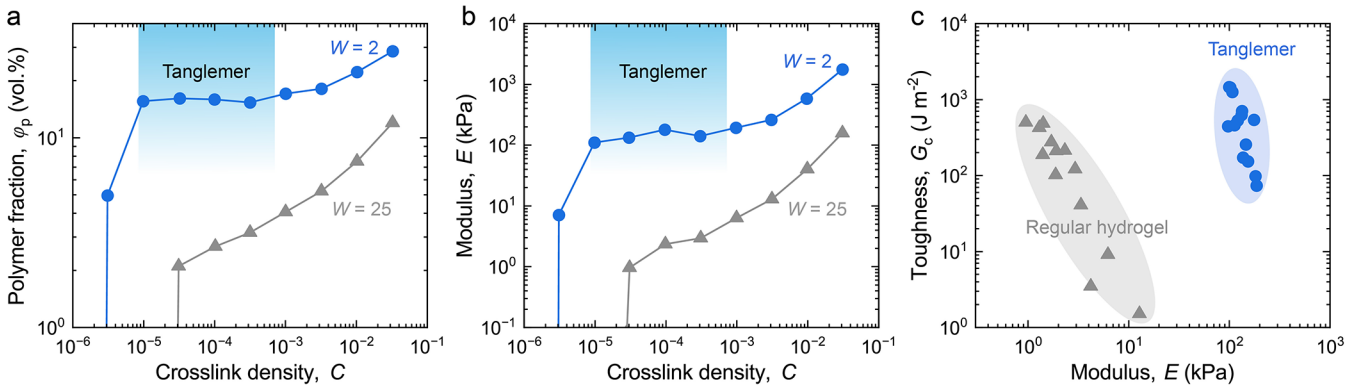


**Figure 46.** PAAm tanglemer hydrogel versus PAAm regular hydrogel. (a) Polymer volume fraction as a function cross-link density when $W = 2$ and 25. (b) Modulus as a function of cross-link density, when $W = 2$ and 25. A tanglemer is a family of materials in the $\varphi_p - C$ plot where $\varphi_p$ plateaus and in the $E - C$ plot where $E$ plateaus. (c) Two families of hydrogels plotted in the modulus–toughness plane. The figure is reproduced with permission from ref 69. Copyright 2021 The American Association for the Advancement of Science.

The tanglemer has become a strategy to fabricate crack-resistant polymer networks.[68,69,76,81,99,150,155−158,162−164] Tanglemers can be made by polymerizing monomers[69,99] and by cross-linking existing polymers.[68,76,156] Tanglemers can be mixed with nanoparticles[81,99] and nanoplates[165] to further enhance crack resistance. Tanglemers can be applied in an interpenetrating network structure.[150,162,164] Additionally, biopolymers can be made into tanglemers to enhance its properties and sustainability.[68,76,158]

## 8.2. A Tanglemer Requires Dense Entanglements, Sparse Cross-Links, and Long Chains

In a polymer network, cross-links divide a chain into multiple strands and two dangling ends, and entanglements divide a strand into multiple segments (Figure 44). The entanglements between strands are trapped and cannot disentangle unless the strands break. By contrast, any entanglement between strands and a dangling end, or between two dangling ends, is not trapped.

Let $n_{total}$ be the number of repeat units per chain, $n$ be the number of repeat units per strand, and $n_e$ be the number of repeat units per segment between neighboring trapped entanglements. A tanglemer requires dense entanglements, sparse cross-links, and long chains:

$$n_e \ll n \ll n_{total} \tag{34}$$

The three requirements are discussed as follows.

1. Dense entanglements—a small $n_e$—enable a high modulus. In a polymer melt in equilibrium, $n_e$ is a thermodynamic property of the polymer.[88] In a polymer solution at equilibrium, $n_e$ is determined by the species and fraction of solvent. To densify entanglements in a gel, one should minimize the solvent fraction and let the chains entangle to equilibrium before cross-linking the chains.[69] Efforts have been made to further densify entanglements by methods such as a supramolecular template.[159,166] It is also conceivable that entanglements can be densified beyond the equilibrium density by nonequilibrium processes, but we are unaware of any experimental report.

2. Sparse cross-links—a large $n$—deconcentrate stress. Sparse cross-links are achieved by using a small amount of cross-linker to form a polymer network. However, when cross-links are too sparse, the polymer chains no longer form a proper network, modulus drops, and viscoelastic behavior dominates.

3. Long chains—a large $n_{total}$—enable an elastic network of sparse cross-links. Dangling ends do not bear loads. Because cross-links are random, each dangling end has a similar number of repeat units as a strand. Thus, the fraction of repeat units belonging to load-bearing strands is $1 - \frac{2n}{n_{total}}$.[87] A chain needs to be much longer than a strand, $n_{total} \gg n$, to achieve a high fraction of load-bearing strands.[156] In other words, only long chains can be sparsely cross-linked into a proper network.

For polymers synthesized via radical polymerization, forming long chains requires a low radical concentration, which can be achieved by a small amount of initiator and slow decomposition kinetics of the initiator. For pre-existing long polymer


https://doi.org/10.1021/acs.chemrev.5c00663
Chem. Rev. XXXX, XXX, XXX−XXX

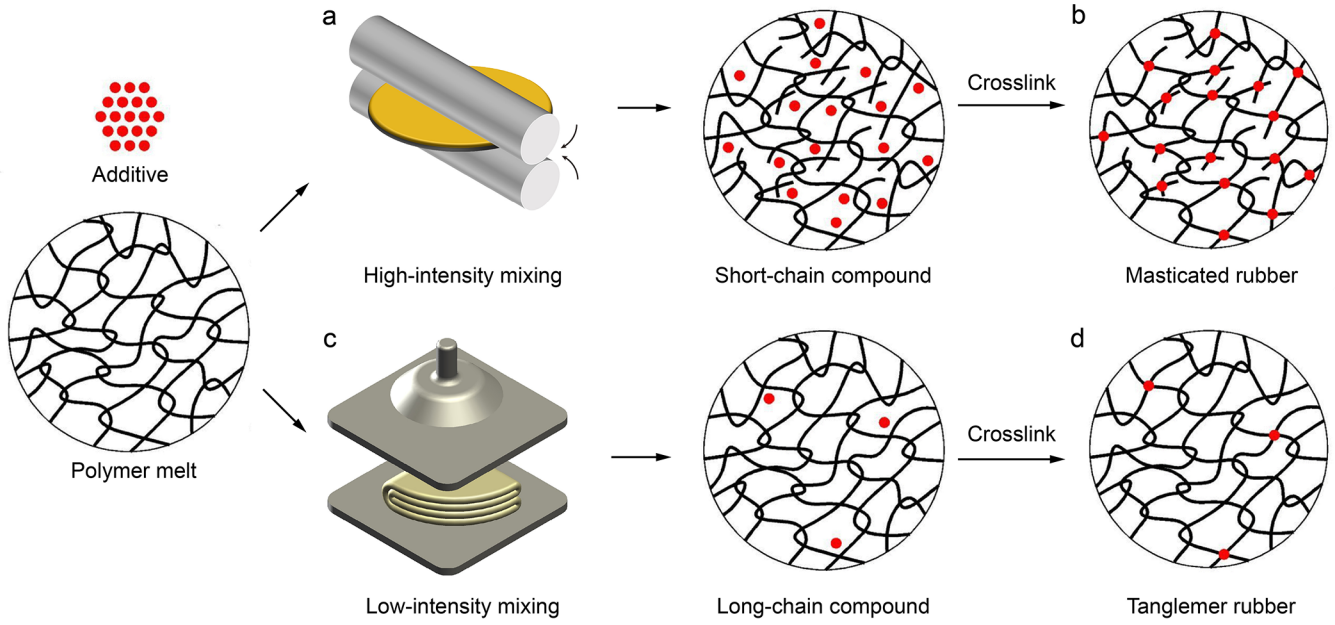


**Figure 47.** Tanglemer rubber versus masticated rubber. (a) A high-intensity process cuts chains short. (b) The short-chain compound necessitates dense cross-links to form a network of masticated rubber. (c) A low-intensity process keeps chains long. (d) The long-chain compound allows sparse cross-links to form a network of rubber tanglemer. The figure is reproduced with permission from ref 156. Copyright 2023 The Royal Society of Chemistry.

chains, subsequent processing must be gentle to avoid breaking the chains.[156]

### 8.3. Tanglemer Hydrogel

A tanglemer hydrogel can be prepared by polymerizing a precursor containing monomer and unusually low amounts of initiator, water, and cross-linker (Figure 45a). Denote the molar ratio of water-to-momonor by $W$, cross-linker-to-monomer by $C$, and initiator-to-monomer by $I$. These three parameters address three principles: a low $W$ to achieve dense entanglements, a low $C$ to achieve sparse cross-links, and a low $I$ to achieve long chains. Upon polymerization, a network forms in which entanglements between strands are trapped (Figure 45b). When the as-polymerized hydrogel is immersed in water, the hydrogel swells into equilibrium. Cross-links prevent entanglements from disentangling, and dense entanglements resist swelling (Figure 45c).

Consider PAAm to be a representative example.[69,155] Prepared by using $I = 1.3 \times 10^{-5}$, $C = 3.2 \times 10^{-5}$, and $W = 2$, a fully swollen PAAm tanglemer is turgid (Figure 45d), achieving a polymer fraction of about 18 vol % and a modulus of about 100 kPa.[69] In comparison, prepared by using the same $I$ and $C$ but $W = 25$, the fully swollen PAAm regular hydrogel is flaccid (Figure 45e), having a polymer fraction of 2 vol % and a modulus of about 1 kPa.

When $W = 2$, monomers in the precursor are crowded and polymerize into a network of dense entanglements. Submerged in pure water, the network swells to equilibrium. The equilibrium polymer fraction $\varphi_p$ plateaus when the cross-link density is in the range of $10^{-5} < C < 10^{-3}$ (Figure 46a). In this range, entanglements greatly outnumber cross-links, and the dense entanglements control the swelling ratio. When $C > 10^{-3}$, $\varphi_p$ increases with $C$, indicating that cross-links are dense enough to prevail over entanglements. When $W = 25$, monomers are dilute in the precursor and polymerize into a network of sparse entanglements. There is no plateau of $\varphi_p$, as the cross-links control the swelling ratio. The modulus as a function of cross-link density for the two families of hydrogels is also plotted (Figure 46b). The modulus of a hydrogel is

$$E = \frac{3}{2v}\varphi_p^{1/3} k_B T\left(\frac{1}{n} + \frac{1}{n_e}\right) \tag{35}$$

where $v$ is the volume of a repeat unit. The dense entanglements contribute to two terms—$\varphi_p$ and $1/n_e$.

We define a tanglemer as a family of materials in the $\varphi_p$−C plane where $\varphi_p$ plateaus and in the $E$−$C$ plane where $E$ plateaus.

The PAAm tanglemer exhibits nearly perfect elasticity: the stress−stretch curve is rate-independent in a wide range of stretch rates and has negligible hysteresis.[96] When the tanglemer is stretched, the short polymer segment between neighboring entanglements sets the modulus. At a crack tip, the long polymer strand between neighboring cross-links deconcentrates stress, and sets the fatigue threshold and toughness. The PAAm tanglemer enhances toughness while maintaining a high modulus, whereas the regular PAAm hydrogel faces a conflict between toughness and modulus (Figure 46c).

Consider a PAAm tanglemer prepared by using $W = 2$, $\varphi_{p,0} = 67\%$, and $\varphi_p = 18\%$. The number of repeat units per strand is estimated by $n = 1/(2C)$. When $C = 10^{-5}$, $n = 50{,}000$. The Kuhn length is $b_k = 1.58 \times 10^{-9}$ m. The repeat unit length is $b = 4.71 \times 10^{-10}$ m. Equation 30 gives $L = 2.98 \times 10^{-7}$ m (298 nm). The sparse cross-links make the strand in the PAAm tanglemer hydrogel much longer than that in a PAAm regular hydrogel (~20 nm) so that the stress can be deconcentrated over a larger length scale. The stress deconcentration by the sparse cross-links, along with antiswelling by the dense entanglement, leads to a high toughness of ~1,000 J m$^{-2}$ and a high fatigue threshold of ~250 J m$^{-2}$.[69] This result is compared with the Lake−Thomas model. Note that the energy stored per unit volume just before the strand breaks is $e = \varphi_p J/v \approx 3.67 \times 10^8$ J m$^{-3}$. The fatigue threshold is predicted by $G_{th}$


https://doi.org/10.1021/acs.chemrev.5c00663
Chem. Rev. XXXX, XXX, XXX−XXX

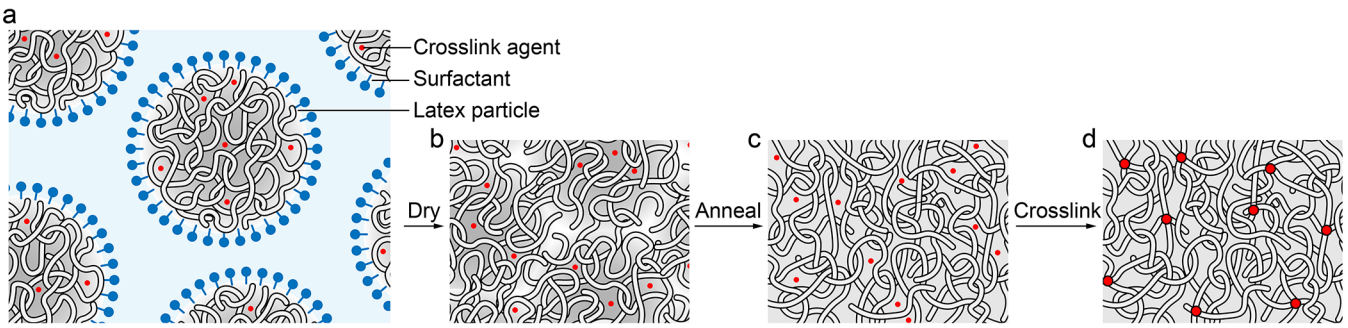


**Figure 48.** Latex process. (a) Polymer latex. (b) As-dried polymer sheet. (c) Fully entangled polymer sheet. (d) Cross-linked polymer network.

$= eL = 109$ J m$^{-2}$, which differs from the experimental value by a factor of ~2.

A tanglemer hydrogel has also been prepared by 3D printing.[157] The work resolves a dilemma: printing requires fast polymerization, but the formation of a tanglemer requires slow polymerization. This dilemma is resolved by using two types of initiators. During printing, a photoinitiator enables fast polymerization of a small fraction of monomers to form a scaffold hydrogel. The scaffold hydrogel itself does not have good mechanical properties but retains the printed shape. The scaffold is then transferred to a dark environment, where a thermal initiator enables slow polymerization of the remaining monomers to form a tanglemer. Submerged in water, the printed tanglemer swells to equilibrium. A tanglemer elastomer is also printed by a similar method, which does not involve swelling. A tanglemer hydrogel can also be prepared from pre-existing polymers. Examples include PEG and cellulose.[68] The PEG tanglemer hydrogel will be discussed in Section 10.4.[68]

### 8.4. Tanglemer Elastomer

Some elastomers can be easily prepared from monomers in the laboratory. Examples include polyacrylate elastomers. A tanglemer elastomer can be prepared by polymerizing a monomer precursor containing no solvents and unusually low amounts of initiator and cross-linker. During polymerization, chains readily move and entangle. For example, a tanglemer elastomer of poly(ethyl acrylate) (PEA) achieves a modulus of 700 kPa, a toughness of 2300 J m$^{-2}$, and a fatigue threshold of 200 J m$^{-2}$.[69]

Most commercial rubber products are made by cross-linking pre-existing polymers. The polymer chains are mixed with additives, such as cross-linkers, accelerators, antioxidants, and reinforcement particles, forming a compound.[77] The mixing is commonly conducted by a high-intensity process using an internal mixer or roll mill, which lowers the viscosity yet cuts chains short (Figure 47a).[167,168] Forming a proper network from short chains necessitates dense cross-links (Figure 47b). Alternatively, if the mixing could be conducted in a mild way, such as kneading, the long chains could be preserved (Figure 47c).[156] The preserved long chains allow sparse cross-links to form a tanglemer (Figure 47d). Taking polybutadiene rubber (BR) as a specific example, a BR tanglemer is prepared by kneading the polybutadiene chains of high molecular weight ($6 \times 10^5$ g mol$^{-1}$), annealing, and sparsely cross-linking.[156] Kneading homogenizes the compound while keeping the polymer chains long. Annealing allows the long chains to densely entangle. At an elevated temperature, the small amount of cross-link agent sparsely cross-links the entangled long chains into a tanglemer. The tanglemer BR achieves a modulus of 1.3 MPa, a fatigue threshold of 440 J m$^{-2}$, and a toughness of 4700 J m$^{-2}$. In comparison, a masticated BR requires denser cross-links to achieve a modulus comparable to that of the tanglemer BR. As a result, the masticated BR has a lower fatigue threshold of 130 J m$^{-2}$ and a toughness of 1600 J m$^{-2}$.

### 8.5. Resolving the Conflict between Chain Length and Viscosity by a Latex Process

The viscosity of an entangled polymer melt increases with chain length, scaling with the total number of repeat units as $\eta \sim n_{\text{total}}^{3.4}$.[169] High viscosity makes the melt hard to process. This conflict between chain length and viscosity is resolved by a latex process (Figure 48).[76,81] A polymer latex is a suspension of polymer particles in water.[170] The polymer particles have diameters of 0.1−1 $\mu$m. The individual polymer chains are hydrophobic, but the polymer particles are stabilized in water by a surfactant (Figure 48a). In a particle of long polymer chains, chains are densely entangled. Between particles, there is a sufficient amount of water. Consequently, the viscosity of a latex is independent of the chain length. The latex of long polymers has low viscosity and readily flows.

Latex can be biosynthesized, such as the latex from rubber trees, guayules, and dandelions.[171] Latex can also be synthesized by emulsion polymerization, such as polyacrylate latex, styrene−butadiene rubber latex, and nitrile butadiene rubber latex.[172] To form a tanglemer, the latex is mixed or copolymerized with a cross-link agent and then dried. During drying, particles undergo a sintering process of several stages.[173,174] As water evaporates, the latex particles come into contact. The capillary force lets the particles deform and coalesce into a continuous polymer sheet.[175,176] At this stage, some polymer chains begin to diffuse across particle boundaries. In the as-dried polymer sheet, entanglement density at these interparticle junctions may differ from that within individual particles (Figure 48b).[173] The as-dried sheet is then annealed. The annealing conditions must differ from the cross-linking conditions. For example, if a thermal cross-linking agent is used, then annealing should be performed at a temperature below the decomposition temperature of the cross-linking agent. The annealing allows the uncrosslinked chains to entangle further by thermal motion, and the individual particle loses its identity (Figure 48c).[177] Subsequently, the polymer chains cross-link into a polymer network, which traps entanglements (Figure 48d). The latex process avoids high-intensity mixing, preserves long chains, and enables dense entanglements. The latexes, once produced, are free of volatile organic compounds and are stable for long-distance distribution and long-time storage. The process is environmentally friendly, compatible with various open-air manufacturing processes such as coating, casting, spraying, printing, and brushing.[178]


https://doi.org/10.1021/acs.chemrev.5c00663
Chem. Rev. XXXX, XXX, XXX−XXX

## 9. NATURAL RUBBER

The literature on natural rubber is extensive. This section focuses on one aspect: preserving long chains without mastication. Natural rubber latex, a milky white fluid in many plants, is a suspension of particles in water (Figure 49a).

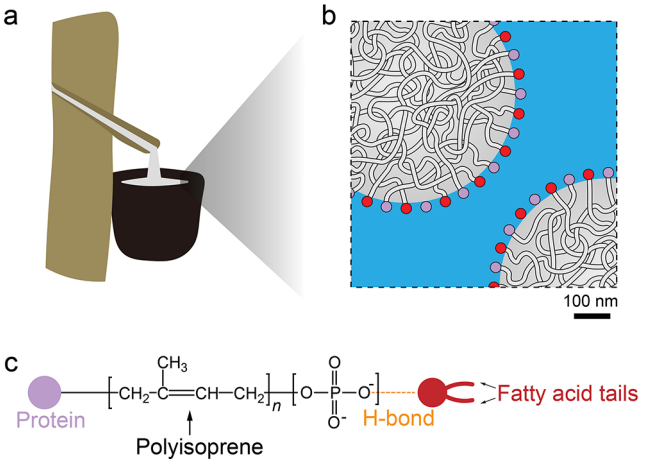


**Figure 49.** Natural rubber latex. (a) Collecting natural rubber latex from a tree. (b) Latex is a suspension of particles in water. Each particle is made of long, highly entangled polyisoprene chains. (c) A polyisoprene chain is terminated with nonpolyisoprene components.

Each particle is made of polyisoprene chains of a high molecular weight of up to ~1,000,000 g $mol^{-1}$ and nearly perfect stereoregularity of the *cis*-configuration.[171] The polyisoprene chains are flexible, with a low entanglement molecular weight of ~3,000 g $mol^{-1}$, so that the chains are highly entangled in the particle (Figure 49b).[179] Each polyisoprene chain is hydrophobic but is ended with hydrophilic nonpolyisoprene components such as proteins and phospholipids (Figure 49c).[180,181] These hydrophilic ends act as surfactants to stabilize the particles in water. When a plant is wounded, the latex is exuded, water evaporates, and the polyisoprene particles sinter into a solid, sealing the wound. That is, the plant has evolved the biosynthesis of latex as well as the colloidal process to defend itself. The aqueous suspension of long chains is a wisdom of nature to resolve a conflict between processability and performance. To seal a wound, the polyisoprene chains need to be long. To be exuded, the long polymer chains need to be in the form of particles suspended in water. Neither a polymer solution nor a polymer melt could be deployed because the viscosity is too high.

The processing of natural rubber by humans dates back to at least 1600 B.C., when Mesoamericans made rubber products by mixing latex from trees and the juice of vines to enhance mechanical behavior.[182] Modern developments of rubber technology are extensively documented (e.g., ref 183). In 1770, an English chemist, Joseph Priestley, observed that the material could rub out pencil marks and coined the word "rubber". The process of mastication was developed by Hancock in the 1820s.[184] A breakthrough took place in 1844, when an American inventor, Charles Goodyear, discovered vulcanization—a process of heating rubber with sulfur to cross-link the polymer chains into a network.[185] This discovery laid the foundation for the modern rubber industry. Natural rubber was among the initial substances used by Hermann Staudinger in testing the polymer hypothesis.[186] The phenomenon of strain-induced crystallization was first observed in 1925.[187]

### 9.1. Latex Process of Natural Rubber

The latex process of natural rubber is widely used to make various products, such as gloves, condoms, balloons, catheter, baby soothers, etc.[188] Common colloid processes include dipping, foaming, and extrusion.

Dipping is the most widely used process. Take the manufacturing of gloves as a specific example. Before dipping, the latex is mixed with additives such as the cross-linking agent, antioxidant, and stabilizer, forming a compounded latex. The mold, generally made of a ceramic or a metal, is cleaned, coated with a coagulant and dried. The mold is immersed in the compounded latex and pulled out, during which a thin layer of latex deposits on the mold. The coagulant screens the noncovalent bonds between the nonpolyisoprene components, causing the latex to fuse into a membrane and some water to be exuded. The membrane at this stage is called a "wet gel", in which polymer chains in neighboring latex particles interdiffuse and entangle. The wet gel has sufficient strength to maintain its shape on the mold and is washed.[189] The wet gel is placed in an oven at an elevated temperature for water to evaporate and for the polymer chains to further interdiffuse and entangle. The

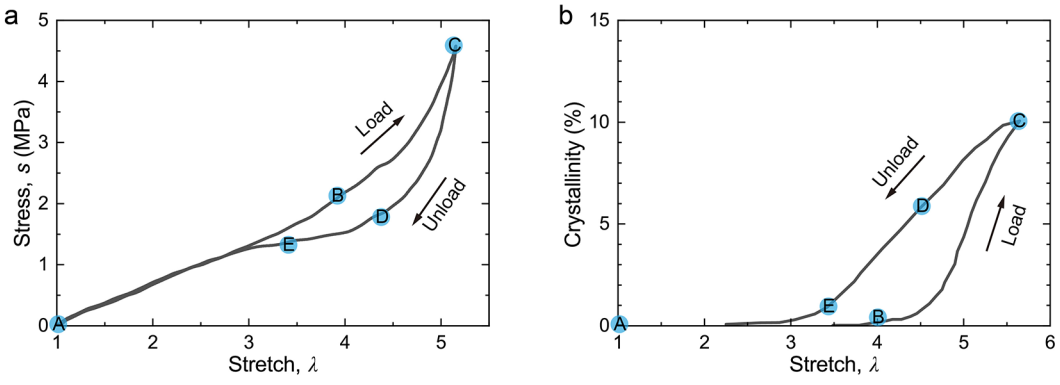


**Figure 50.** Stress−stretch curve and strain-induced crystallization of regular natural rubber. (a) Load the sample to a stretch of ~5 and unload. (b) Crystallinity as a function of stretch during loading and unloading. Define crystallinity by the volume of crystals divided by the volume of the sample. The test is conducted at a stretch rate of 0.0005 $s^{-1}$. The figure is reproduced with permission from ref 198. Copyright 2003 American Chemical Society.


https://doi.org/10.1021/acs.chemrev.5c00663
Chem. Rev. XXXX, XXX, XXX−XXX

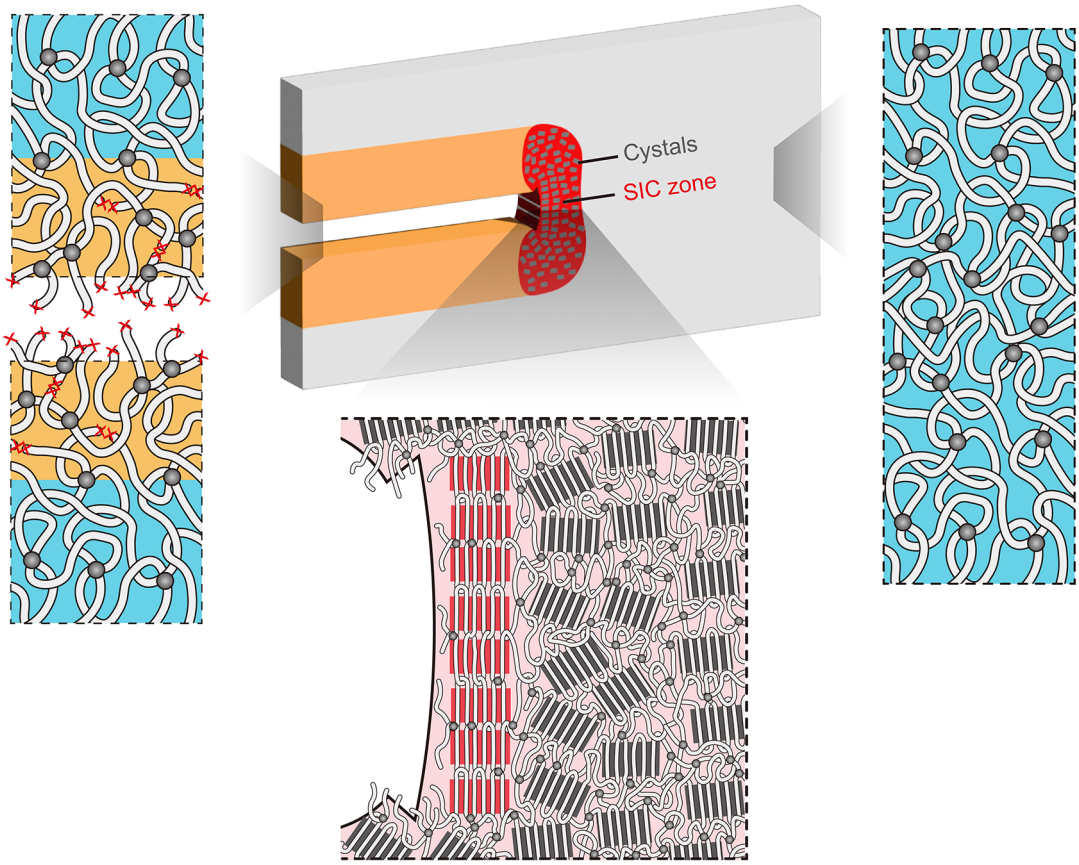


**Figure 51.** When a crack grows in a natural rubber, strain-induced crystalline domains form ahead of the crack tip and melt behind the crack tip.

individual latex particles completely lose their identities, and the polymer chains cross-link into a single network.

The extrusion of latex is a process used to fabricate a rubber thread.[190] A compounded latex is continuously extruded through a nozzle into a bath of coagulant, where the latex particles coalesce into a thread. The extruded threads are washed, dried, and cured.

The latex process does not involve intense mixing and can preserve the long polymer chains in the final products. We will later review the importance of preserving the long chains in the mechanical properties of products, especially in resisting crack growth.

### 9.2. Mastication

Mastication is a process used to make rubber compounds for various rubber products, such as tires and belts.[191] The latex is coagulated and dried to form blocks of polymer. The polymer block of long chains has a high viscosity. The polymer block is mixed with additives in machines like internal mixers, extruders, and roll mills. Such a mixing process is of high intensity, where the shear force cuts chains short.[167,192,193] The high-intensity mixing homogenizes the mixture and masticates polymer chains to lower the viscosity for shaping the final products. As the time of mastication is prolonged, the molecular weight can decrease by up to one order of magnitude.[194] Consider a long polymer of natural rubber with a molecular weight of $M_n \approx 300$ kg mol$^{-1}$, corresponding to ~4,400 repeat units per chain. Mastication reduces the repeat units per chain to ~440. These short chains require a molar ratio of cross-links to repeat units of $C \approx 10^{-2}$ to form a network. We call such a highly cross-linked network a regular natural rubber.

### 9.3. Regular Natural Rubber

Subject to a small to moderate stretch $\lambda < 4$, the regular natural rubber exhibits small hysteresis during cyclic loading, indicating that the noncovalent bonds between strands are weak.[76,195] Beyond a critical stretch $\lambda > 4$, the natural rubber exhibits evident hysteresis (Figure 50a). This hysteresis is ascribed to strain-induced crystallization (SIC).[195−200] The crystals nucleate and grow when the strands are stretched to alignment, and melt when the strands are relaxed. As in many crystallization−melting processes, the crystallization of natural rubber exhibits a delay whereas melting does not.[201] Consequently, the crystallinity−stretch curve does not overlap during loading and unloading (Figure 50b), which is an irreversible process.[196−199,201] The irreversible process recurs during cyclic loading: when natural rubber is relaxed to zero stress and then reloaded, the crystallinity−stretch curve does not overlap during subsequent loading and unloading.[200,202] In the stress−stretch curves, this irreversible process contributes to the hysteresis. The larger the stretch, the higher the crystallinity, and the larger the hysteresis.[76,198] This dissipation mechanism does not break the covalent bonds along the strands, such that the residual stretch of the natural rubber after unloading is small. SIC is a dissipation mechanism at a large stretch, making natural rubber elastic at small to moderate stretches and tough to resist crack growth.

Under a monotonic load, at the crack tip, strands crystallize to form crystallites, and many crystallites align to form a fiber-like structure that bridges the crack (Figure 51). The high


https://doi.org/10.1021/acs.chemrev.5c00663
Chem. Rev. XXXX, XXX, XXX−XXX

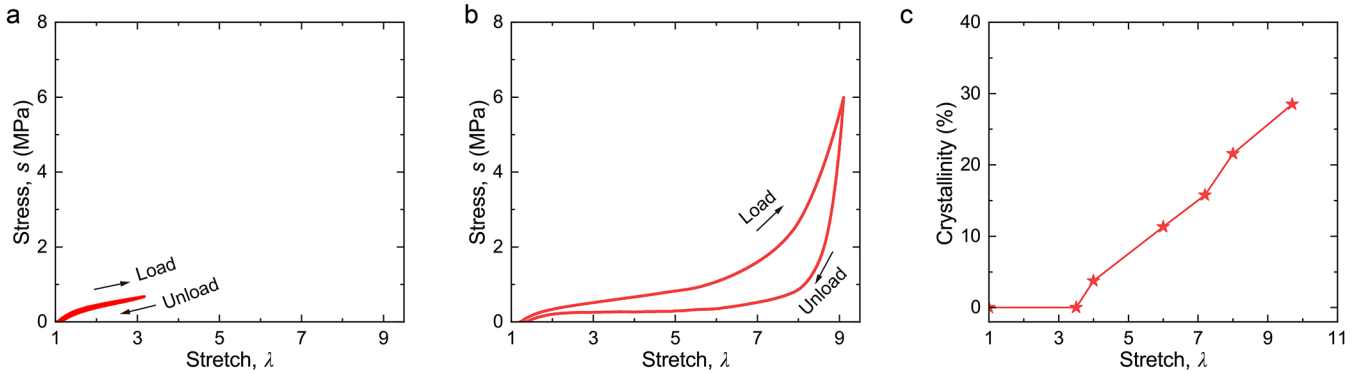


**Figure 52.** Stress−stretch curve and strain-induced crystallization of natural rubber tanglemer. (a) Load the sample to a stretch of three and unload. (b) Load the sample to a stretch of nine and unload. (c) Crystallinity as a function of stretch. The figure is reproduced with permission from ref 76. Copyright 2025 Springer Nature.

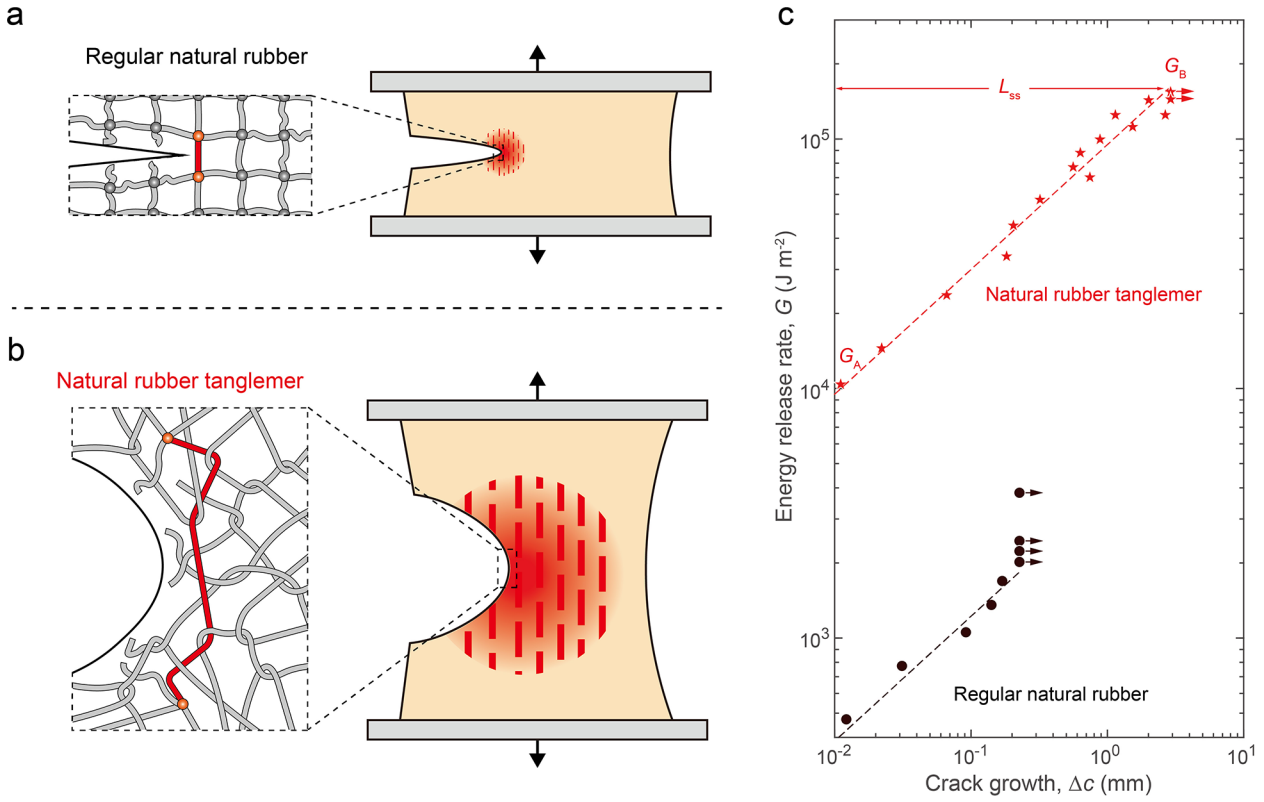


**Figure 53.** Natural rubber tanglemer outperforms regular natural rubber. (a) In regular natural rubber, a short polymer strand at a crack tip deconcentrates stress over a short distance, while SIC extends to a small volume. (b) In a natural rubber tanglemer, a long polymer strand at a crack tip deconcentrates stress over a long distance, while SIC extends to a large volume. (c) Crack resistance curve. The figure is reproduced with permission from ref 76. Copyright 2025 Springer Nature.

tension at the crack tip transmits over the long fiber-like structure, which is much longer than individual strands. The stress deconcentration by the long fiber-like structure causes the SIC to occur in a region around the crack tip. Behind the crack tip, the crack leaves two layers of scars in which the strand relaxes and the crystallites melt, while only very few covalent bonds break. Crystallization and melting in a large volume dissipate large amounts of energy.

The toughness of the natural rubber results from two processes. First, ahead of the crack tip, the fiber-like structure bridges the crack and deconcentrates stress. Once the fiber breaks at a point, the high energy stored in the long segment of the fiber dissipates. Second, in a zone around the crack tip, the network undergoes crystallization and melting.[203−205] The two processes synergize. The fiber-like structure transmits high stress over a large volume, in which the network undergoes SIC. In its turn, SIC changes the stress field, which shields the crack tip from the load from the far field. This shielding effect is analogous to plasticity deformation in metal,[102] and phase transformation in some ceramics.[206] Both the fiber-like structure and SIC dissipate energy, and their synergy leads to a high toughness on the order of 10,000 J m$^{-2}$, even though the strands in a regular natural rubber are relatively short. By comparison, a synthetic rubber commonly does not undergo SIC, and its toughness is on the order of 1,000 J m$^{-2}$.


https://doi.org/10.1021/acs.chemrev.5c00663
Chem. Rev. XXXX, XXX, XXX−XXX

SIC, however, does not significantly enhance fatigue threshold.[27] This statement is consistent with the following experimental observations. Synthetic rubbers commonly do not undergo SIC but have a fatigue threshold comparable to that of natural rubber.[27] The fatigue threshold of natural rubber is estimated by the Lake−Thomas model as follows. Just before the strand ahead of the crack tip breaks, the energy stored in each carbon−carbon bond on the backbone is ∼1.06× $10^{-19}$ J.[146] Each repeat unit of polyisoprene has four carbon−carbon bonds on the backbone, so the energy stored per repeat unit is $J \approx 4.24 \times 10^{-19}$ J. The density is $\rho = 9.2 \times 10^5$ g $m^{-3}$. The mass per repeat unit is $1.13 \times 10^{-22}$ g. The volume per repeat unit is $v = m/\rho = 1.23 \times 10^{-28}$ $m^3$. The energy stored per unit volume just before the strand breaks is $e = J/v \approx 3.46 \times 10^9$ J $m^{-3}$. The length per repeat unit is estimated by $b \approx v^{1/3} = 4.97 \times 10^{-10}$ m. The Kuhn length is $b_k = 8.2 \times 10^{-10}$ m. Take a representative value of the number of repeat units per strand $n = 50$. The strand length is $L = (nb_k b)^{1/2} = 4.52 \times 10^{-9}$ m.[88] Assume that a crack grows in a natural rubber by breaking a layer of strands, and the fatigue threshold is $G_{th} = eL \approx 15.6$ J $m^{-2}$. This value differs from the experimental observation of ∼40−50 J $m^{-2}$ by a factor of 3.[27,76]

In a test in which the load is not reduced to zero during unloading, the fatigue threshold is greatly enhanced.[207] Some of the crystals do not melt because the material is always subject to tension during cyclic loading, and because the stress is high at the crack tip. This superior fatigue resistance can be attributed to the aligned crystallites ahead of the crack tip. The energy dissipation of breaking the aligned crystallites is much higher than that of breaking a layer of strand.

### 9.4. Natural Rubber Tanglemer

Both the fatigue threshold and toughness can be greatly amplified for natural rubber made by a latex process without mastication.[76] The preserved long polymer chains form a tanglemer. The repeat units per chain is $n_{total} \approx 4{,}400$, and the number of repeat units between neighboring entanglements is $n_e \approx 50$. Consider a network with a low cross-link density of $C \approx 10^{-3}$; that is, the number of repeat units per strand is $n \approx 500$. This network design fulfills the requirement of forming a tanglemer: long chains, sparse cross-links, dense entanglements, and $n_{total} \gg n \gg n_e$.

Subject to a small to moderate stretch, the natural rubber tanglemer also exhibits small hysteresis, similar to that of the regular natural rubber (Figure 52a). However, the natural rubber tanglemer is much more stretchable than regular natural rubber. When the tanglemer is loaded to a large stretch $\lambda = 9$ and unloaded, the hysteresis is large, yet the residual stretch remains small (Figure 52b). This large hysteresis is ascribed to SIC, which is amplified by long strands (Figure 52c).[76,198] SIC occurs when network strands are stretched to alignment. At each entanglement or cross-link, SIC cannot occur. Entanglements can slide somewhat but cross-links cannot, so the natural rubber tanglemer has a higher crystallinity than the regular natural rubber.[76,198,208]

The synergy between long strands and SIC enables the natural rubber tanglemer to have toughness more than an order of magnitude greater than that of regular natural rubber. The precise molecular picture for this toughening has not been studied. Some qualitative remarks may be offered. At the crack tip, the long strands in the tanglemer deconcentrate stress to a larger extent than the regular network (Figure 53a,b). These long strands crystallize ahead of the crack tip, forming a fiber-like structure. The fiber has higher crystallinity in the tanglemer than in a regular network. The longer and more crystallized fiber-like structure, in turn, transmits high stress to a larger volume, in which the network undergoes SIC. Within this SIC zone, the enhanced crystallinity in the tanglemer leads to a higher energy dissipation per unit volume. The stress deconcentration by the long fiber, along with the energy dissipation in a large volume, leads to a high toughness of ∼100,000 J $m^{-2}$.

The natural rubber tanglemer exhibits a crack-resistance curve: the energy release rate as a function of crack growth (Figure 53c). The curve identifies two values of the energy release rate, $G_A$ and $G_B$, as well as a length $L_{ss}$. The crack does not grow when $G < G_A$, grows stably when $G_A < G < G_B$, and grows unstably across the entire sample when $G = G_B$. The unstable growth takes place when the crack length increases by $L_{ss}$.

Under a cyclic load, the natural rubber tanglemer amplifies the fatigue threshold by the stress deconcentration of long strands. The fatigue threshold as a function of repeat units per strand follows the Lake−Thomas scaling, $G_{th} \sim n^{1/2}$. In the natural rubber tanglemer of $C = 10^{-3}$, $n \approx 500$, which corresponds to a strand length of $L = 1.43 \times 10^{-8}$ m. The energy stored per unit volume just before the strand breaks is $e \approx 3.46 \times 10^9$ J $m^{-3}$. The Lake−Thomas model gives the prediction of fatigue threshold $G_{th} = eL \approx 49.4$ J $m^{-2}$, which differs from the experimental observation of 200 J $m^{-2}$ by a factor of 4. In the natural rubber tanglemer, the modulus is ∼1 MPa, set by the number of repeat units between neighboring entanglements, $E \sim 1/n_e$.

## 10. POLY(ETHYLENE GLYCOL) (PEG)

Section 7 describes polyacrylamide hydrogels, which are commonly made by the radical polymerization of monomers. Many other hydrogels, however, are made from preexisting polymers for two reasons. First, some synthetic polymers, such as poly(ethylene glycol) (PEG)[209] and poly(vinyl alcohol) (PVA),[210] are polymerized under specialized conditions. Second, many sustainable polymers under development are derived from natural polymers, such as cellulose, alginate, chitosan, hyaluronic acid, collagen, and gelatin.[211] Here, we take PEG as a representative example.

PEG is a polymer composed of repeat units of ethylene oxide, $-CH_2-CH_2-O-$. Depending on its molecular weight, the same polymer may be called PEG, poly(ethylene oxide) (PEO), or polyoxyethylene (POE). In this review, regardless of the molecular weight, we call this polymer PEG. At room temperature, PEG of low molecular weight is a liquid, whereas the PEG of high molecular weight is a semicrystalline solid with a glass -transition temperature of ∼−55 °C and a melting temperature of ∼60 °C.[212] Without cross-links, PEG dissolves in water. With cross-links, a PEG network imbibing water becomes a hydrogel. PEG and PEG hydrogels have found wide applications, including drug delivery,[213] biomedical engineering,[214] and solid polymer electrolytes.[215]

### 10.1. Linear PEG

The basic form of a linear PEG chain consists of PEG with two hydroxyl end groups (−OH), available in a broad spectrum of molecular weights ranging from ∼200 to 8,000,000 g $mol^{-1}$ (Figure 54a). A linear PEG can be cross-linked into a network


https://doi.org/10.1021/acs.chemrev.5c00663
Chem. Rev. XXXX, XXX, XXX−XXX

by using a cross-link agent such as benzophenone (Figure 54b).[68]

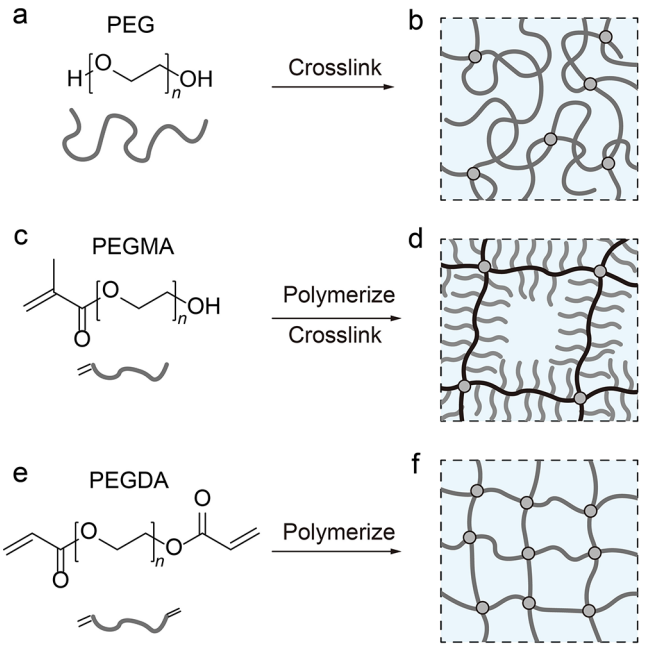


**Figure 54.** Polymer network prepared from linear PEG. (a) PEG consists of a chain with two ends of hydroxyl groups. (b) A network prepared by cross-linking PEG. (c) PEGMA consists of a chain with one end of a hydroxyl group and the other end of a carbon−carbon double bond. (d) A bottlebrush network prepared by polymerizing and cross-linking PEGMA. (e) PEGDA consists of a chain with two ends of carbon−carbon double bonds. (f) A network prepared by polymerizing PEGDA.

One reason for PEG's versatility is that a large variety of derivatives have been developed. As the first example, the linear PEG chain can be modified with a carbon−carbon double bond on one end. A specific example is poly(ethylene glycol) methacrylate (PEGMA), with available molecular weights ranging from hundreds to thousands (Figure 54c). PEGMA, mixed with a cross-linker, can be polymerized into a bottlebrush network of very low modulus, where the PEG side chains reduce the entanglement density and the load-bearing strand density (Figure 54d).[216]

As the second example, the linear PEG chain can be modified with two carbon−carbon double bonds on two ends. A specific example is poly(ethylene glycol) diacrylate (PEGDA), with available molecular weights ranging from hundreds to thousands (Figure 54e). PEGDA can polymerize itself to become a network (Figure 54f). Due to this convenience, PEGDA is widely applied in biomedical fields,[217] microfluidics,[218] and 3D printing.[219] Because PEGDA is of low molecular weight, the network prepared from PEGDA is of short strands and brittle (toughness ≈ 10 J $m^{-2}$).[68]

### 10.2. Tetra-Arm PEG Hydrogel

Beyond linear chains, multiarm PEG has been prepared to serve as multifunctional cross-linkers or network building blocks. A representative example is tetra-arm PEG, consisting of four PEG chains linked at a central core to form a four-armed star polymer.

A polymer network made through two tetra-arm PEGs of complementary reactive end groups can reduce topological defects.[220,221] Consider one tetra-arm PEG with four end groups of *N*-hydroxysuccinimide ester (−NHS) and the other tetra-arm PEG with four end groups of amide ($-NH_2$), where each arm is of equal length (Figure 55a). Mix the aqueous solutions of the two tetra-arm PEGs in stoichiometric portions, such that a pair of −NHS and $-NH_2$ groups react. The reaction is conducted at a polymer concentration around the overlap concentration, such that the entanglements do not form. The reaction results in a nearly ideal network in which cross-links are homogeneous and each strand is of equal length (Figure 55b).[222,223] However, small concentrations of topological defects, such as dangling ends and loops, still exist in the network.[224,225]

The network of tetra-arm PEG, swollen in water until equilibrium, is a hydrogel. The water lubricates strands such that the noncovalent bonds between strands are negligible. Due to the existence of water and the nearly ideal network structure, the hydrogel is highly elastic, with a rate-independent stress−stretch curve and a low mechanical tan$\delta$ of ~$10^{-4}$.[221,226] The tetra-arm PEG hydrogel serves as a model system in which many mechanical properties can be predicted by models in polymer physics.[221,224,226,227]

For a tetra-arm PEG hydrogel, the toughness and fatigue threshold coincide.[226] This finding is interpreted as follows. The hydrogel is highly elastic so that the noncovalent bonds

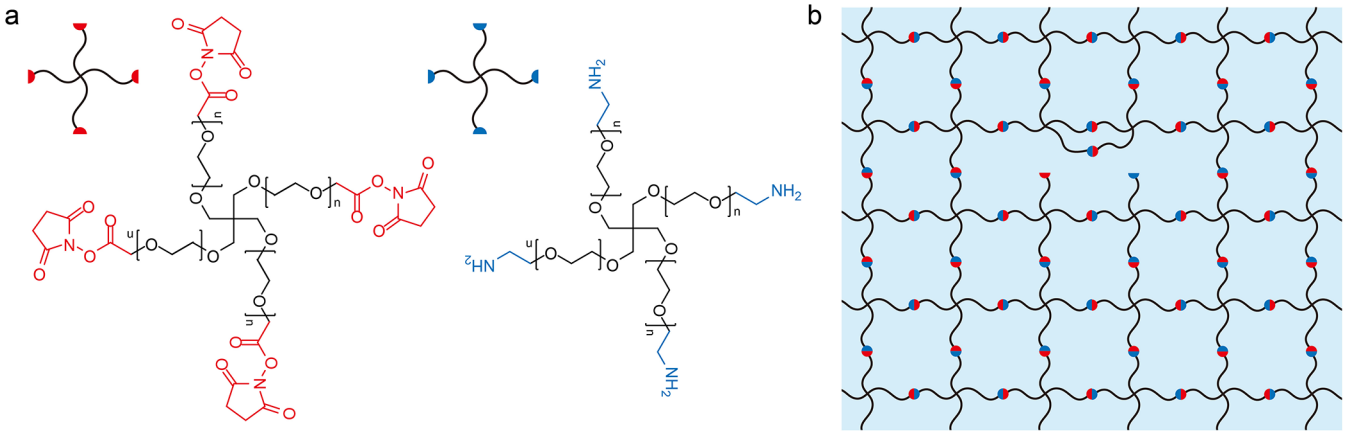


**Figure 55.** Polymer network prepared from two kinds of tetra-arm PEG. (a) One tetra-arm PEG with four end groups of *N*-hydroxysuccinimide ester (−NHS) and the other tetra-arm PEG with four end groups ($-NH_2$). (b) The polymer network prepared from the tetra-arm PEG.


https://doi.org/10.1021/acs.chemrev.5c00663
Chem. Rev. XXXX, XXX, XXX−XXX

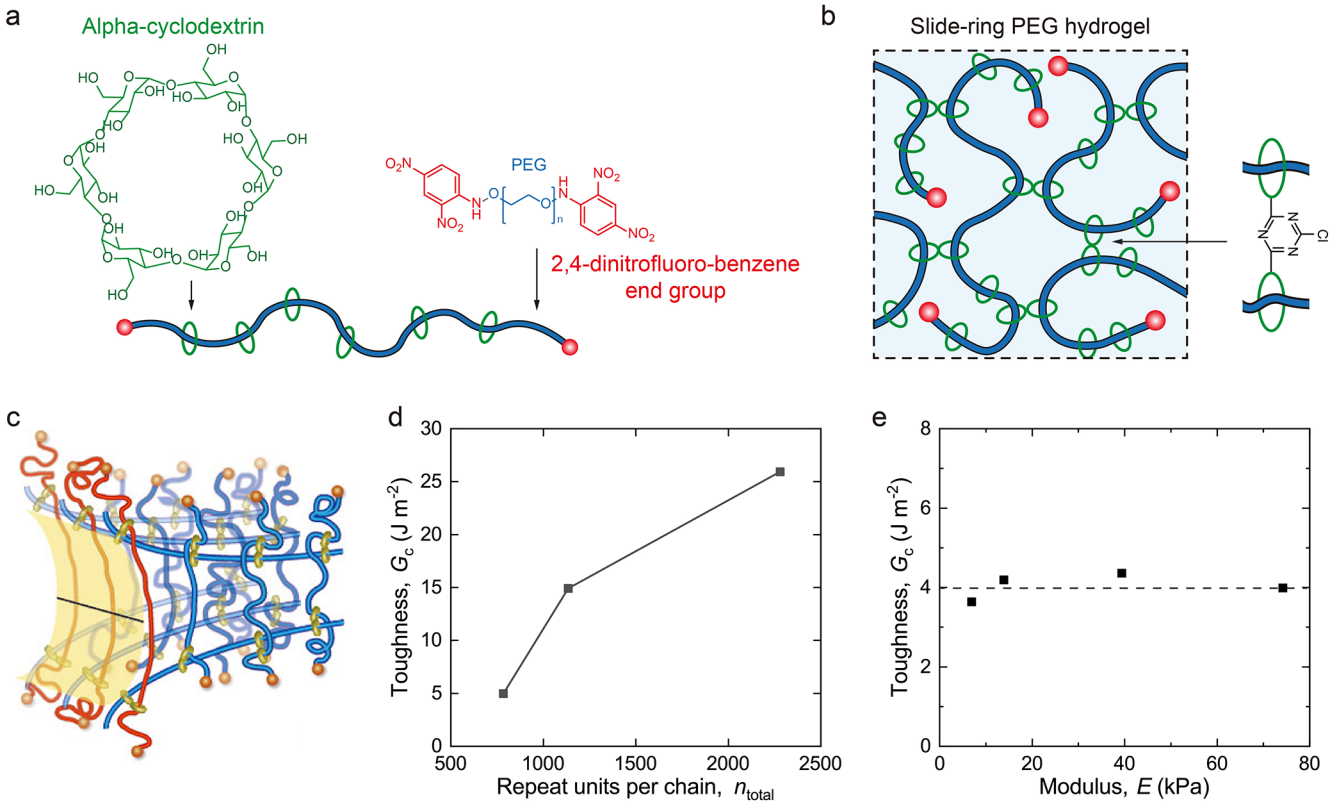


**Figure 56.** Slide-ring hydrogel. (a) Chemical structure of the ring, $\alpha$-cyclodextrin, and the polymer chain, PEG. Each PEG chain threads though multiple rings and is terminated on both ends with bulky groups. (b) A bifunctional molecule links a pair of rings into a figure-of-eight junction. The figure-of-eight junctions contribute to the modulus. (a, b) Reproduced with permission from ref 44. Copyright 2021 MDPI under an open access Creative Commons CC BY 4.0 license. (c) At a crack tip, the rings slide along the polymer chain ahead of the crack tip, which deconcentrates stress. (d) Toughness as a function of repeat units per chain. (e) Toughness as a function of modulus. (c–e) Reproduced with the permission from ref 230. Copyright 2017 American Chemical Society.

between strands are too weak to contribute to toughness. Furthermore, the strands in the network have equal lengths so that a crack is likely to grow by breaking a layer of strands, leaving the strands off the crack plane intact. These two considerations eliminate the difference between toughness and fatigue threshold.

As such, the tetra-arm PEG hydrogel is a model system to compare with the Lake–Thomas model. Consider a hydrogel prepared by using a tetra-arm PEG with the molecular weight of each arm of ~5,000 g mol$^{-1}$ such that each strand has repeat units of $n = 227$. The network is prepared by using the polymer fraction in the as-polymerized state $\varphi_{p,0} = \varphi_p = 3.4\%$. Just before the strand breaks, the energy stored in each bond on the backbone is $\sim 1.06 \times 10^{-19}$ J.[146,147] Each repeat unit of PEG has three bonds on the backbone, so the energy stored per repeat unit is $J \approx 3.18 \times 10^{-19}$ J. The density is $\rho = 1.13 \times 10^6$ g m$^{-3}$. The mass per repeat unit is $7.3 \times 10^{-23}$ g. Thus, the volume per repeat unit is $v = m/\rho = 6.47 \times 10^{-29}$ m$^3$. The energy stored per unit volume just before the strand breaks is $e = \varphi_p J/v \approx 1.68 \times 10^8$ J m$^{-3}$. The length per repeat unit is estimated by $b \approx v^{1/3} = 4.01 \times 10^{-10}$ m. The Kuhn length is $b_k = 7 \times 10^{-10}$ m.[228] The end-to-end distance of a strand is $L = (nb_k b)^{1/2} = 8.0 \times 10^{-9}$ m. The model predicts a fatigue threshold of $G_{th} = eL = 1.34$ J m$^{-2}$. The toughness of the tetra-arm PEG hydrogel is ~5–40 J m$^{-2}$, depending on the strand length and polymer volume fraction.[67] For a hydrogel comparable to that used in the above theoretical estimate, the experimental measured toughness is ~10 J m$^{-2}$.[67] This experimental value differs from the theoretical estimate by a factor of ~7. We have discussed possible origins of this difference in the section on polyacrylamide hydrogels. Despite this factor, the toughness as a function of the repeat units per strand nearly follows the scaling relation given by the Lake–Thomas model, $G_c \sim n^{1/2}$.[67]

### 10.3. Slide-Ring PEG Hydrogel

In a slide-ring hydrogel, each PEG chain threads through multiple rings of $\alpha$-cyclodextrin and terminates on both ends with bulky groups of 2,4-dinitrofluoro-benzene (Figure 56a).[229] The rings slide along a chain, while the bulky end groups prevent the chain from pulling out. A bifunctional molecule, hexamethylene diisocyanate, links a pair of rings into a figure-of-eight junction (Figure 56b). These junctions, together with the bulky end groups, turn the PEG chains into a polymer network. The network, submerged in water, becomes a hydrogel, called a slide-ring hydrogel.[44,230]

The slide-ring hydrogel resolves the conflict between the modulus and crack resistance. When the hydrogel is subject to low to moderate stretch, the network remains intact and the slide-ring junctions behave like cross-links and set the modulus. When a crack impinges upon a PEG chain, the tension in the chain is high, and the rings slide along the chain, which deconcentrates the high tension over the entire chain (Figure 56c). The modulus is set by the number of repeat units of the segment between neighboring slide rings, whereas the toughness is set by the number of repeat units of the entire chain (Figure 56d). Consequently, the toughness of the slide-


https://doi.org/10.1021/acs.chemrev.5c00663
Chem. Rev. XXXX, XXX, XXX–XXX

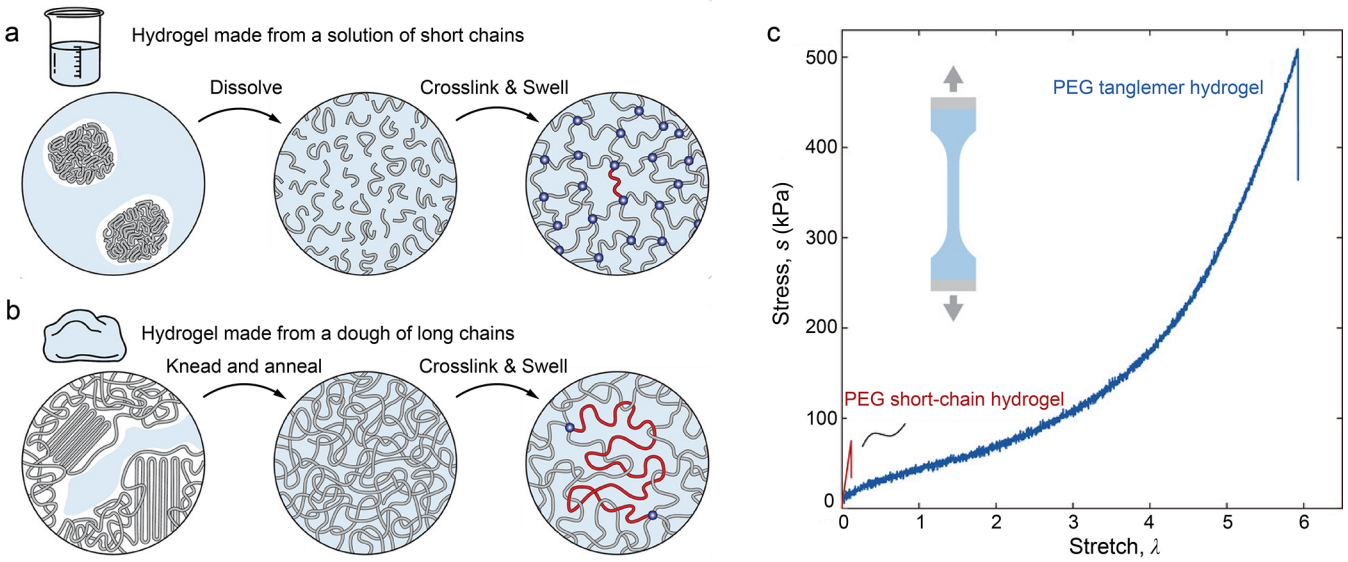


**Figure 57.** PEG tanglemer hydrogel versus PEG short-chain hydrogel. (a) A PEG short-chain hydrogel is made from polymerizing a solution of short chains. (b) A PEG tanglemer hydrogel is made from kneading, annealing, and sparsely cross-linking a dough of long chains. (c) Stress–stretch curves. The figure is reproduced with permission from ref 68. Copyright 2021 John Wiley and Sons.

ring hydrogel is decoupled from the modulus (Figure 56e).[230] In contrast, the regular hydrogel of covalently cross-linked PEG hydrogel suffers from the modulus–toughness conflict, roughly following $G_c \sim E^{-1/2}$.[230]

Incidentally, in the slide-ring hydrogel, each PEG chain interacts with the $\alpha$-cyclodextrin rings by noncovalent bonds. The strength of the noncovalent bonds has not been characterized. To enable the high tension to deconcentrate over the entire chain, the noncovalent bonds should be as low as possible. It has been reported that the toughness of the slide-ring hydrogel is low when the density of the rings is too high.[231] This observation may indicate that the noncovalent bonds between a ring and a chain are appreciable. Further investigation will shed light.

The slide-ring hydrogel has inspired several similar network topologies. For example, a network of slide-ring polydimethylsiloxane (PDMS) has been reported in which PDMS chains are entangled with PDMS rings.[232] For another example, the slide rings are replaced by covalent organic frameworks or molecular sieves.[233]

### 10.4. Tanglemer PEG Hydrogel

To prevent dissolution or excessive swelling, PEG is often densely cross-linked into a network of short strands by using cross-linkable PEG derivatives such as PEGDA and tetra-arm PEG (Figure 57a). Consequently, a PEG hydrogel is usually brittle. A tanglemer PEG hydrogel is prepared by mixing a PEG of high molecular weight ($\sim 8 \times 10^6$ g mol$^{-1}$) with a small amount of water and photoinitiator (Figure 57b).[68] The mixture is inhomogeneous initially and is homogenized to form a dough by kneading gently without breaking the chains. The dough is then annealed at an elevated temperature, during which long chains densely entangle by thermal motion. Subsequently, ultraviolet light activates the photoinitiator, which sparsely cross-links the long polymer chains into a network. The network is submerged in water to swell to equilibrium. The stress–stretch curve of a PEG tanglemer hydrogel differs greatly from that of a PEG short-chain hydrogel (Figure 57c). The fully swollen PEG tanglemer hydrogel achieves a toughness of 1600 J m$^{-2}$ and fatigue threshold of 100 J m$^{-2}$.[68] In comparison, the fully swollen PEG short-chain hydrogel prepared from PEGDA has a toughness of <8 J m$^{-2}$.

### 10.5. Strain-Induced Crystallization

Strain-induced crystallization (SIC) occurs in a PEG hydrogel of sufficiently low water fraction.[234] SIC of a hydrogel is observed in a slide-ring PEG hydrogel under the following conditions: low fraction of slide-ring junctions, low water fractions, and long PEG chains.[235] When the side-ring PEG hydrogel is loaded, the rings slide along the chains, allowing the chains to align in the direction of stretch. The aligned PEG segments then crystallize. When the hydrogel is unloaded, the crystallites melt. The crystallization and melting are rapid so that SIC has a small hysteresis under cyclic loading of low and modest stretch rates.[234,236,237]

At a crack tip, SIC introduces a fiber-like structure of crystallites and aligned rubbery strands, analogous to natural rubber. The fiber-like structure deconcentrates stress to an extent much larger than a layer of strands. Consequently, the slide-ring PEG hydrogel with a water fraction of 62% achieves a high toughness of ~3,000 J m$^{-2}$. SIC happens only in the slide-ring hydrogel of a moderate to low fraction of water (<82%) and does not happen in a PEG hydrogel in equilibrium with water.[234] For instance, a slide-ring PEG hydrogel with a water fraction of 87% cannot crystallize under tension, having a low toughness of ~50 J m$^{-2}$.

SIC is also observed in tetra-arm PEG networks of a moderate to low water fraction (<60%) and long strands ($n$ > 227).[236,237] SIC is observed in an ionic gel, in which a slide-ring PEG network is mixed with a lithium salt.[238] For a tanglemer PEG hydrogel in equilibrium with pure water, with a water fraction of 93%, SIC is not observed.[68]

## 11. NETWORK CROSS-LINKED BY NONCOVALENT BONDS

In a polymer network cross-linked by covalent bonds, three types of bonds commonly serve distinct functions. The covalent bonds along an individual polymer strand are strong


https://doi.org/10.1021/acs.chemrev.5c00663
Chem. Rev. XXXX, XXX, XXX–XXX

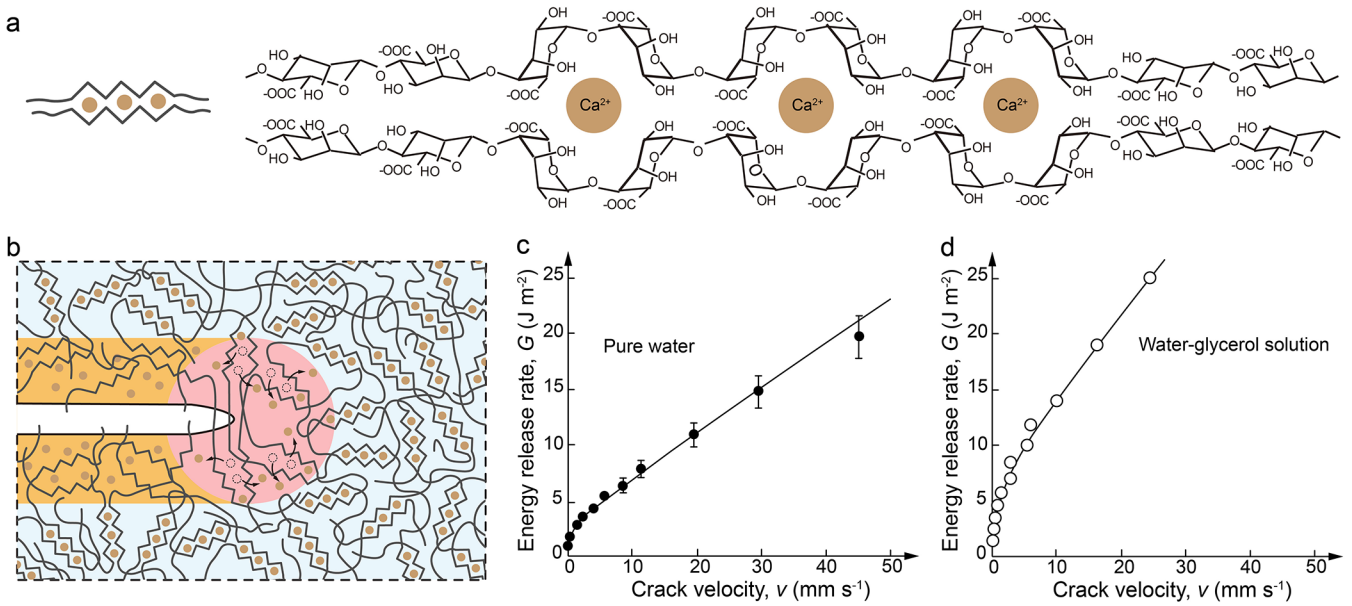


**Figure 58.** Crack growth in alginate hydrogel. (a) Chemical structure of alginate. (b) In an alginate hydrogel, a crack advances by unzipping noncovalent bonds and pulling out chains. (c) Rate-dependent toughness of an alginate hydrogel in (c) pure water and (d) water−glycerol solution. (c, d) Reproduced with permission from ref 66. Copyright 2009 AIP Publishing.

to maintain chains. The covalent bonds that cross-link chains are also strong to maintain the network. The noncovalent bonds between strands are weak, so strands are flexible and deform with low hysteresis. This section modifies this picture and describes a class of polymer networks in which polymer chains are cross-linked by noncovalent bonds. The function of various noncolvant bonds in hydrogels has been summarized in a recent review.[51] Here we focus on the recent understanding of crack growth in polymer networks cross-linked by noncovalent bonds.

### 11.1. Alginate Hydrogel

Alginate hydrogels, derived from brown seaweed, are widely applied in biomedical applications such as drug delivery and tissue engineering.[239] An alginate chain consists of two kinds of segments: $\alpha$-L-guluronate and $\beta$-D-mannuronate (Figure 58a). Dry alginate is a polymer glass. Submerged in an aqueous solution containing calcium ions ($Ca^{2+}$), the $\alpha$-L-guluronate segments form coordination complexes and the $\beta$-D-mannuronate segments are flexible. The coordination complexes cross-link the alginate chains into a network, which is stable in water and forms a hydrogel.

The free energy of the coordination complex in the alginate hydrogel is $\sim 12 k_B T$,[66] which is much weaker than that of a covalent bond ($\sim 200\ k_B T$) along the chain. The noncovalent bonds break at a moderate tension. Subject to a constant compressive strain, the alginate hydrogel relaxes to nearly zero stress.[240]

At a crack tip, the coordination complex unzips and releases free chains. The crack grows by pulling out the free chains rather than breaking chains (Figure 58b).[66] The unzipping of the complex and pullout of chains happens in a localized zone around the crack tip (<100 nm).[241]

A crack grows in an alginate hydrogel by the irreversible processes of complex unzipping and chain pullout. Both processes are rate-dependent. The crack resistance is characterized by measuring the energy release rate as a function of crack velocity (Figure 58c).[66] When the crack velocity approaches zero, the energy release rate approaches a threshold of ~1 J $m^{-2}$. When the crack velocity is high (~50 mm $s^{-1}$), the energy release rate is ~20 J $m^{-2}$.

The chain pullout is resisted by viscous drag against the solvent. Consequently, the energy release rate at a finite crack velocity is amplified by replacing water with a water−glycerol solution, which has a higher viscosity than water (Figure 58d).[66,241] However, the threshold toughness at nearly zero crack velocity is unaffected by the viscosity of the solvent. This behavior is also observed in similar polymer networks cross-linked by noncovalent bonds, such as gelation hydrogels.[241]

### 11.2. Thermoplastic Elastomers

A thermoplastic elastomer (TPE) is commonly made from a block copolymer of dissimilar segments.[242−246] For example, a triblock copolymer, poly(styrene-butadiene-styrene) (SBS), consists of a middle polybutadiene segment and two end polystyrene segments. When many such copolymer chains aggregate, the middle polybutadiene segments form a rubbery matrix, and the end polystyrene segments form glassy domains (Figure 59a). At a low volume fraction (<20%), the glassy domains are separated by the rubbery matrix.[247] The rubbery matrix enables large and repeated deformation. At room

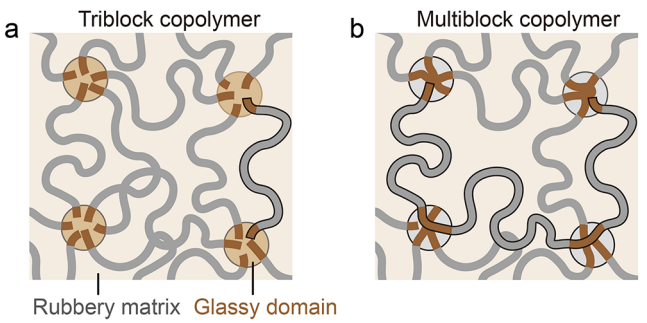


**Figure 59.** Thermoplastic elastomer made of (a) triblock copolymer and (b) multiblock copolymer.


https://doi.org/10.1021/acs.chemrev.5c00663
Chem. Rev. XXXX, XXX, XXX−XXX

temperature, the glassy domains function as cross-links and maintain the network. At elevated temperatures, these domains become rubbery, flow, and allow the material to be shaped.

At room temperature, the noncovalent bonds between the segments in the glassy domains are of intermediate strength, much stronger than the noncovalent bonds between the segments in the rubbery matrix, but much weaker than the covalent bonds along the polymer chains. When a triblock copolymer elastomer is subject to a small to moderate stretch, the glassy domains remain intact, and the material deforms elastically. When the elastomer is subject to a large stretch, the segments in the glassy domains may slip and even be pulled out from the domains, resulting in large hysteresis.[244,248,249] Large hysteresis is undesirable in many applications but also contributes to toughness. For example, SBS achieves a high toughness of ~20 kJ $m^{-2}$.[250] We are unable to identify any systematic study of the fatigue threshold of triblock copolymer elastomers. We expect that if the glassy segments are pulled out under the high tension at the crack tip, the crack grows by pullout rather than scission, resulting in a low fatigue threshold.

In a thermoplastic elastomer of a multiblock copolymer, each long polymer chain threads through multiple glassy domains (Figure 59b). The multiblock copolymer may allow the glassy segments to slip under high tension while resisting pullout. Multiblock copolymers show a higher strength than their counterparts of triblock copolymers.[244,251−255] We expect such a multiblock copolymer to have a high fatigue threshold, but we have not found any study of the effect.

### 11.3. Thermoplastic Urethane

A thermoplastic urethane (TPU) is a multiblock copolymer often prepared from three components: a long-chain diol HO−R−OH ($M_n$ ≈ 400−6000 g $mol^{-1}$), a diisocyanate (OCN−R′−NCO), and a small-molecule diol HO−R″−OH (Figure 60a).[256,257] The two ends of the long-chain diol react with diisocyanate to form a prepolymer chain with cyanate end groups (−NCO). The ends of the prepolymer chain then react with the small-molecule diol to form a multiblock copolymer of two alternating segments. The long-chain diol contributes to soft segments, and diisocyanate and small-molecule diol contribute to hard segments. The multiblock structure separates into nanophases. The hard segments, driven by the hydrogen bonds between urethane groups (−NH−COO−), form hard domains of size ~5−30 nm (Figure 60b).[82] The hard domains can be amorphous or crystalline, depending on the chemical structure of the diisocyanate.[257] The soft segments form a soft matrix. Because each chain has multiple hard segments, a chain threads through multiple hard domains. The soft matrix can be either rubbery or semicrystalline, depending on the chemical structure of the long-chain diol. For instance, a TPU prepared from the long-chain diol of a polyether is rubbery, and a TPU prepared from the long-chain diol of a polyester is semicrystalline. When a TPU is subject to large stretches, the soft matrix often undergoes strain-induced crystallization (SIC).[82,258−260]

TPU has a wide design space for tuning its properties.[82,261−268] For example, the family of TPUs covers a wide range of modulus from ~1 to 1000 MPa.

Soft TPUs are used as rubbers, which have a modulus on the order of 1−10 MPa and can sustain large stretches over 6−10. A TPU is elastic at a small stretch ($\lambda$ < 1.1), softens at a moderate stretch, and stiffens at a large stretch.[269] Under a

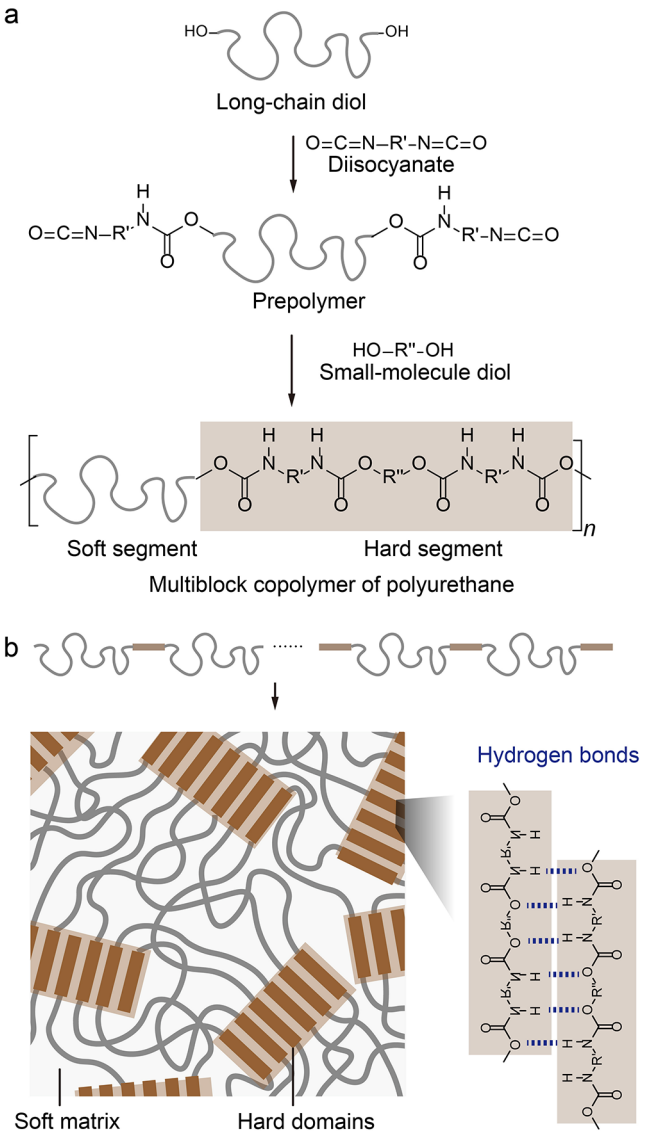


**Figure 60.** Chemical structure of a thermoplastic polyurethane. (a) Preparation of a thermoplastic polyurethane. (b) The multiblock copolymer of thermoplastic polyurethane separates into two phases.

cyclic load of moderate to large stretch, a TPU shows hysteresis and the Mullins effect.[269] These behaviors are ascribed to the strain-induced crystallization of the soft matrix, as well as the fragmentation and rearrangement of hard domains.[259,269,270] The rearrangement of the microstructure is permanent, and the material does not recover its original state.[258,269] A commercial TPU achieves a toughness of over 20 kJ $m^{-2}$.[82] A recently reported TPU has a high toughness of 215 kJ $m^{-2}$.[267]

One of the most striking advantages of TPUs is their resistance to crack growth under cyclic loading. At a crack growth resolution of ~1 nm per cycle, a commercial TPU is reported as having a high fatigue threshold of over 3,000 J $m^{-2}$.[82] This high fatigue threshold is ascribed to self-strengthening. The repeated stretch causes rearrangement and even fragmentation of large hard domains into smaller ones (Figure 61a). The microstructural rearrangement strengthens the material ahead of the crack tip and deconcentrates stress over a large volume (Figure 61b). Upon unloading, some segments in the soft matrix cannot

AQ

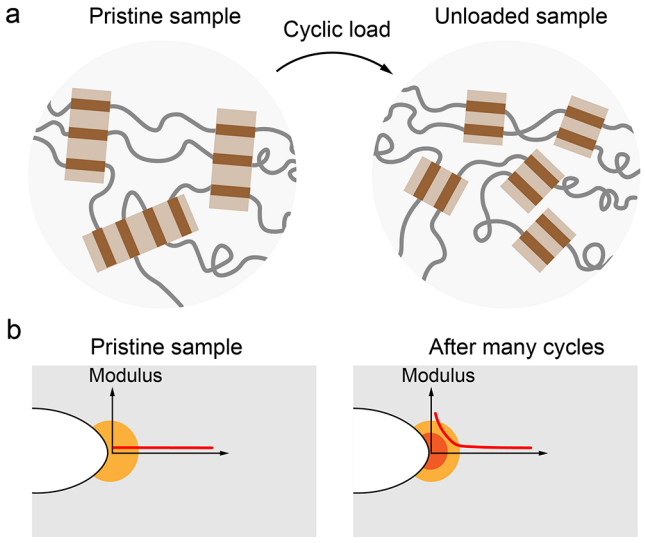


**Figure 61.** Self-strengthening of thermoplastic polyurethane (TPU). (a) Rearrangement of hard domains after cyclic loading. Reproduced with permission from ref 271. (b) After many cycles, the microstructural rearrangement at the crack tip generates a hard core with a higher local modulus than the bulk, which strengthens the crack tip. Reproduced with permission from ref 82. Copyright 2021 American Chemical Society.

recover their original configurations, thus remaining partially stretched in the unloaded sample. Consequently, if the TPU crystallizes upon loading, the strain-induced crystallites partially remain in the unloaded sample, which further enhances the fatigue threshold.

### 11.4. Poly(vinyl alcohol)

A poly(vinyl alcohol) (PVA) chain consists of a carbon−carbon backbone and hydroxyl side groups (−OH) (Figure 62a). The dense −OH groups form hydrogen bonds between polymer chains, promoting chain alignment into crystallites (Figure 62b). The dense hydrogen bonds stabilize the crystals in cold water. At an elevated temperature of ∼90 °C, the crystallites melt, and the powder of PVA dissolves in water. A cyclic freeze−thaw process of PVA solutions induces crystallites (Figure 62c).[272] During freezing, the polymers and water separate into two phases. In the polymer-rich phase, polymers pack and crystallize. Upon thawing, the crystallites are stable in water, yielding a network cross-linked by crystalline domains. The network, swollen in water, becomes a hydrogel.[273]

The crystallinity of the PVA hydrogel is not a material property. Rather, the crystallinity is process-dependent, an interplay of chain mobility, chain alignment, and crystallization. The interplay makes the PVA hydrogel a material of rich space to tailor the property.[83,100,274−282]

A PVA hydrogel of high fatigue threshold is prepared by combining cyclic prestretch and free-thawing.[278] The process enhances crystallinity and changes the crystalline domains into long and oriented nanofibrils (Figure 63a). As the crack grows

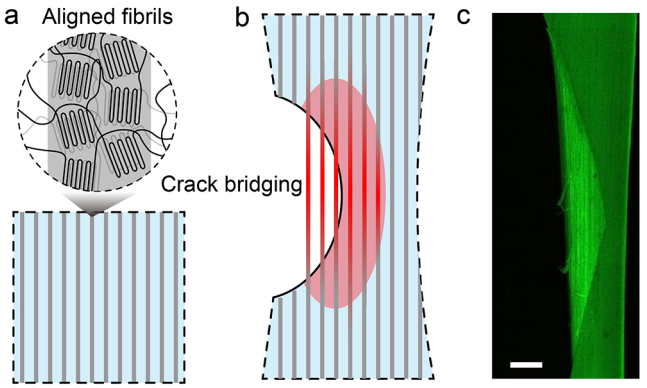


**Figure 63.** Crack growth in a PVA hydrogel of aligned crystalline fibrils. (a) A PVA hydrogel of an aligned crystalline fibril is prepared by combining cyclic prestretch and free thawing.[278] (b) As the crack grows in this PVA hydrogel, the fibrils are pulled out, bridging the crack and deconcentrating stress. (c) Confocal microscopic image of the precracked hydrogel subject to a stretch of 2.7. The scale bar represents 250 $\mu$m. Reproduced with permission from ref 278. Copyright 2019 National Academy of Sciences under CC BY-NC-ND 4.0 license.

in the hydrogel, the nanofibrils are pulled out. The pullout fibers bridge the crack, and high tension transmits along a long segment of the fibril (Figure 63b,c). Once the long nanofibril breaks at a point, the high energy stored in the entire fibril is dissipated. This energy dissipation is much higher than that of breaking a layer of strands. The mechanism leads to a high fatigue threshold of over 1,000 J $m^{-2}$.[278]

An even more fatigue-resistant PVA hydrogel is prepared by combining freeze-casting and salting out.[83] PVA solution is first directionally frozen, where a honeycomb-like micro-network with aligned pore walls forms by the ice template. In the walls, PVA chains form close packing. The material is then immersed in a solution of sodium citrate. The salt solution

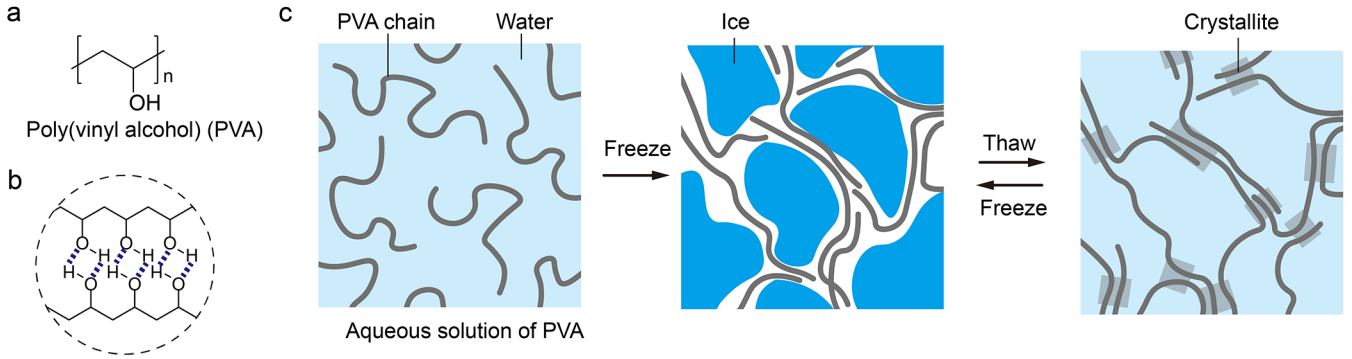


**Figure 62.** Poly(vinyl alcohol) (PVA) hydrogel. (a) Chemical formula of PVA. (b) PVA forms hydrogen bonds between chains. (c) Preparing a PVA hydrogel by a cyclic freeze−thaw process.


https://doi.org/10.1021/acs.chemrev.5c00663
Chem. Rev. XXXX, XXX, XXX−XXX

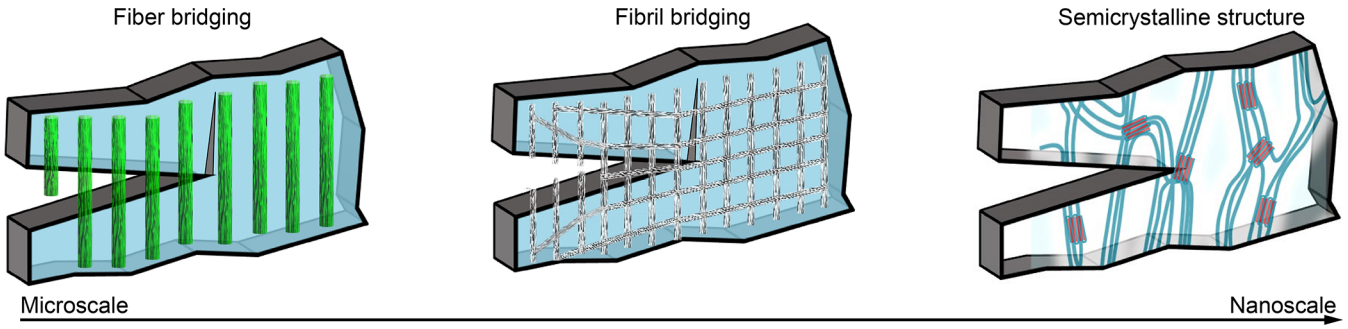


**Figure 64.** Multiscale stress deconcentration in a PVA hydrogel prepared by combining freeze-casting and salting out. Reproduced with permission from ref 83. Copyright 2021 Springer Nature.

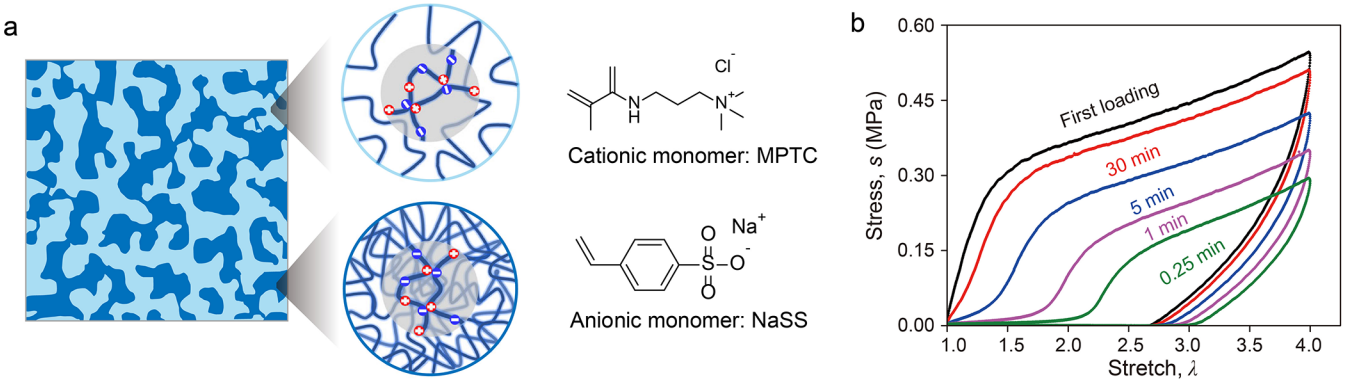


**Figure 65.** Polyampholyte network. (a) Structure of the polyampholyte hydrogel. Reproduced with permission from ref 287. Copyright 2018 American Physical Society. (b) First loading and unloading curve and second loading and loading curves after storing the unloaded hydrogel for various periods. The curves are measured at a stretch rate of 0.14 $s^{-1}$. Reproduced with permission from ref 283. Copyright 2013 Springer Nature.

amplifies the phase separation between water and PVA chains, resulting in PVA nanofibrils of high crystallinity. The multiscale structures of this PVA hydrogel bridge the crack and deconcentrate stress (Figure 64). The crack blunts and bifurcates. During cyclic load, even at an amplitude of the energy release rate of ~10,000 J $m^{-2}$, the crack still nearly does not grow.

### 11.5. Polyampholyte Network

A polyampholyte hydrogel is synthesized by random copolymerization or sequential homopolymerization of two species of oppositely charged monomers.[283−289] Consider a polyampholyte hydrogel prepared from an aqueous solution of a cationic monomer, 3-(methacryloylamino)propyl-trimethylammonium chloride (MPTC), and an anionic monomer, sodium p-styrenesulfonate (NaSS) (Figure 65a).[283] The two monomers copolymerize to form polymer chains. After dialyzing the small molecular counterions ($Na^+$, $Cl^-$), the oppositely charged side groups form ionic bonds. Each ionic bond is weak in water, with a free energy of ~$k_BT$.[290] However, a sequence of ionic bonds constitute a complex, which shows a wide spectrum of strength.[283] Some strong complexes of ionic bonds have strength comparable to that of covalent bonds.[283] Since the backbone of the polymer chain is hydrophobic, once the hydrophilic side groups from a complex, the hydrophobic interactions drive phase separation.[287,288] Consequently, the hydrogel shrinks during dialysis. The polyampholyte hydrogel has a bicontinuous phase structure in which the hard phase of densely packed polymer and the soft phase of loosely packed polymer interpenetrate.[287,288]

When loaded to a moderate stretch and unloaded, the polyampholyte hydrogel shows a large hysteresis (Figure 65b). The noncovalent bonds between chains break during loading and reform during unloading. Over time, these noncovalent bonds return to equilibrium, and the stress−stretch curve recovers to its original loading curve after ~2 h.

Under a monotonic load, the polyampholyte hydrogel resists crack growth by breaking noncovalent bonds between chains and breaking the bicontinuous structure.[287] The hydrogel achieves a toughness of ~4,000 J $m^{-2}$. However, the viscoelasticity does not contribute to the fatigue threshold, and the polyampholyte hydrogel has a fatigue threshold of ~50 J $m^{-2}$.[291,292]

A similar structure can be realized by hydrogen bonds between amide groups ($-NH_2$) and carboxyl groups ($-COOH$), and several tough hydrogels are developed.[293−295] A similar principle can be applied to achieve instant, tough, noncovalent adhesion.[296,297]

### 11.6. Network of Unusually Long Polymers Cross-Linked by Domains of Noncovalent Bonds

A network cross-linked by noncovalent bonds usually has large hysteresis, even under a moderate stretch. The large hysteresis leads to high toughness but does not enhance the fatigue threshold. The energy dissipation associated with hysteresis is undesired in many applications. Furthermore, the unzipping of noncovalent bonds lowers the modulus over the cyclic stretch.

A polymer network, in which unusually long polymers are cross-linked by domains of noncovalent bonds, can simultaneously achieve low hysteresis, a high modulus, and a high fatigue threshold (Figure 66a).[163] The chains outside the


https://doi.org/10.1021/acs.chemrev.5c00663
Chem. Rev. XXXX, XXX, XXX−XXX

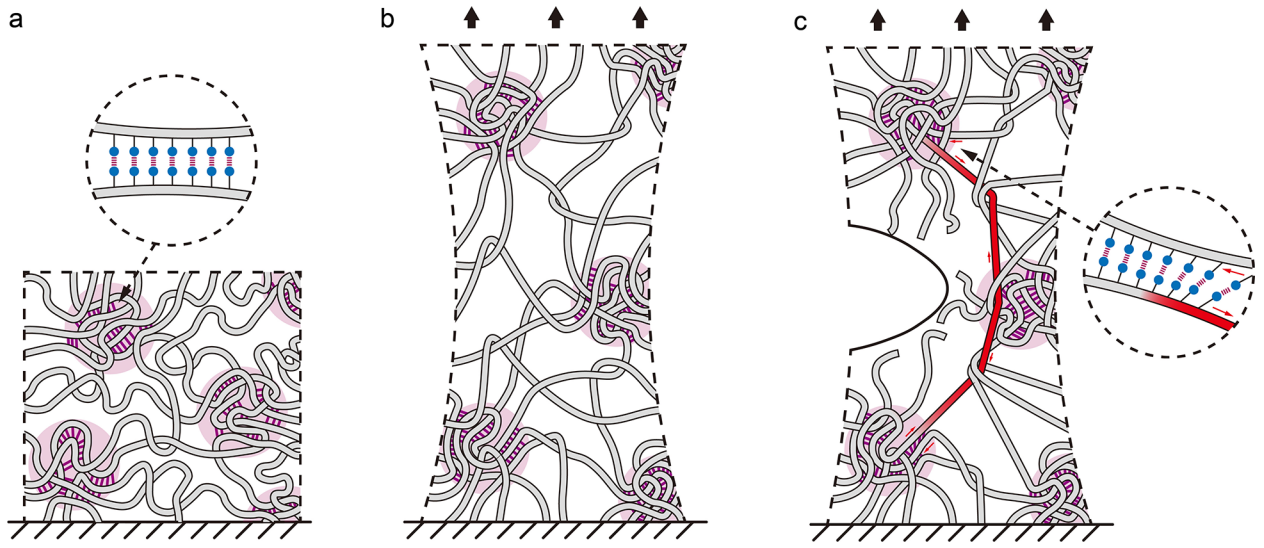


**Figure 66.** A network of unusually long chains cross-linked by domains of noncovalent bonds. (a) Undeformed network. (b) When the network without a precut crack is subject to a moderate stress, the chains in the domains slip negligibly, and domains function like hard particles. (c) When the network with a precut crack is stretched, at the crack tip, the chains in the domains slip, transmitting high tension over a long distance. Reproduced with permission from ref 163. Copyright 2015 Springer Nature OA license agreement (CC BY 4.0).

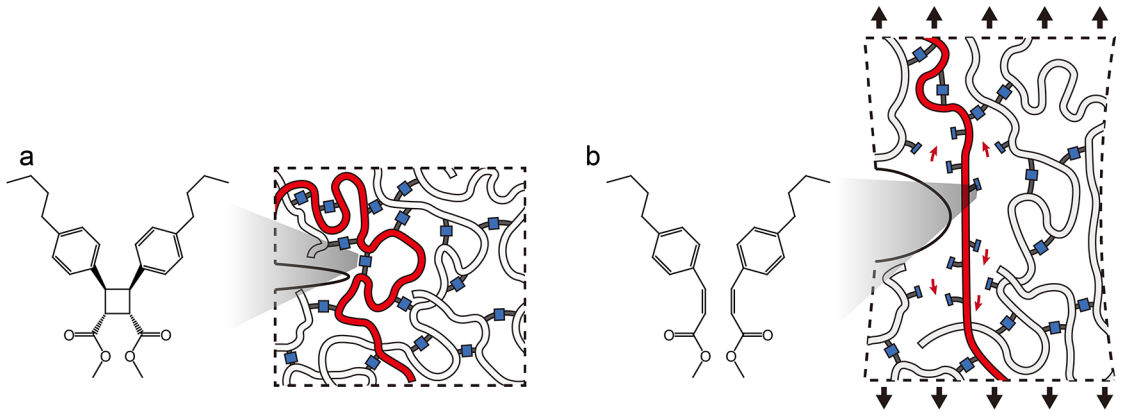


**Figure 67.** A polymer network cross-linked by covalent bonds of intermediate strength. (a) Each cross-link is five times weaker than a carbon−carbon bond along the polymer chain. (b) At a crack tip, the cross-links break, which deconcentrates stress to a length scale greater than a layer of strand. The noncovalent bonds between the polymer chains are much weaker than the covalent bonds of the cross-links. Reproduced with permission from ref 298. Copyright 2023 The American Association for the Advancement of Science.

domains are flexible and densely entangled and have low interchain friction. In a domain, each noncovalent bond is weak, but a domain of many noncovalent bonds is strong enough to function like hard particles under moderate stress (Figure 66b). Consequently, the network without a precut crack has a high modulus and low hysteresis.

The noncovalent bonds between chains are much weaker than the covalent bonds along individual chains so that at a crack tip the chains in the domains slip without scission. Each chain is so long that it is cross-linked through multiple domains to other chains, ensuring that the chain can slip but not be pulled out of the domains (Figure 66c). Consequently, at the crack tip, the high tension can be transmitted to a segment of the chain longer than the segment between neighboring domains, leading to a high fatigue threshold.

This design is demonstrated by a hydrogel of two species of polymers. A powder of unusually long PEG is mixed with liquid monomers of acrylic acid (AAc) and an unusually small amount of photoinitiator. After kneading and annealing, the mixture becomes a homogeneous dough. Upon exposure to ultraviolet light, the photoinitiator decomposes and polymerizes AAc into unusually long PAAc chains. The ether groups of PEG and carboxyl groups of PAAc can form hydrogen bonds. A sequence of the ether−carbonyl hydrogen bonds constitutes a complex. The PEG−PAAc mixture separates into two phases: domains of complexes and regions that do not form complexes. Analogous to a semicrystalline polymer, a polymer of such a two-phase structure may be called a "semicomplex" polymer. The semicomplex polymer has a high strength of 55 MPa and can be stretched to 5.5 times its original length.

The PEG−PAAc mixture has high hysteresis because the noncovalent bonds between chains in the uncomplexed regions are strong. The noncovalent interactions are greatly reduced when the mixture is submerged in water and swells. Both polymers are hydrophilic. Once a complex forms, the backbones of the two polymers are hydrophobic. The hydrophobic interactions stabilize the complex in water. Outside the domains, the polymers of uncomplexed regions form hydrogen bonds with water and are flexible and highly entangled and have low interchain friction. The PEG−PAAc−


https://doi.org/10.1021/acs.chemrev.5c00663
Chem. Rev. XXXX, XXX, XXX−XXX

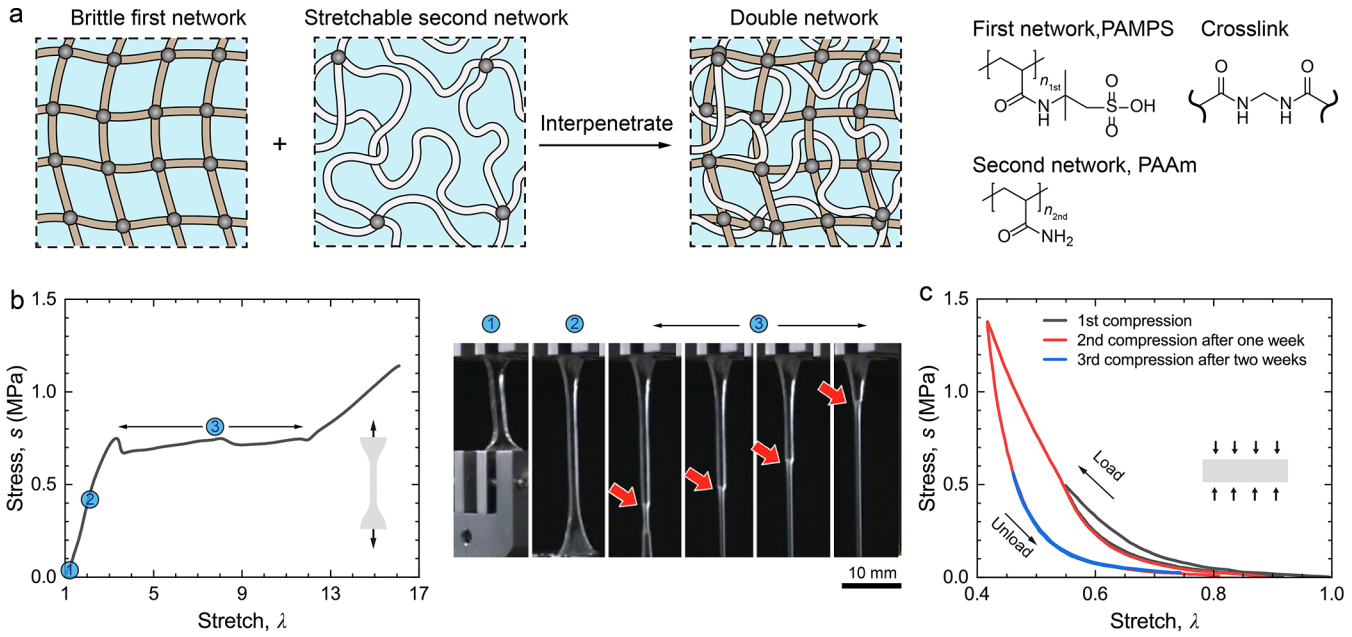


**Figure 68.** Double network hydrogel and its stress–stretch curve. (a) A double network hydrogel is composed of a brittle network and a stretchable network. Two networks interpenetrate together. (b) Stress–stretch curve and photographs. Reproduced with permission from ref 31. Copyright 2003 Royal Society of Chemistry. (c) Cyclic compression stress–stretch curves. Reproduced with permission from ref 301. Copyright 2007 American Chemical Society.

water mixture is a hydrogel. The PEG–PAAc hydrogel archives a high modulus (510 kPa), low hysteresis (13%), high toughness (4100 J $m^{-2}$), and a high fatigue threshold (180 J $m^{-2}$).

### 11.7. Network Cross-Linked by Covalent Bonds of Intermediate Strength

This design uses covalent cross-links of intermediate strength.[298] Polymer chains are cross-linked into a network by a *cis*-diaryl-substituted cyclobutane-based mechanophore, which divides each chain into multiple strands (Figure 67a). The cross-link has an intermediate strength of ~0.8 nN, weaker than that of a carbon–carbon single bond along the strands, ~4 nN, yet much stronger than the noncovalent bonds between the strands. Even though the chains are cross-linked by covalent bonds, we describe this material here because its behavior is similar to that of networks cross-linked by noncovalent bonds.

This design leads to an elastomer of high toughness and high fatigue threshold but low hysteresis. When the elastomer without a precut crack is subject to a small to moderate stretch, neither cross-links nor strands break, and the elastomer exhibits nearly perfect elasticity. The modulus is determined by both cross-links and entanglements. When the elastomer with a precut crack is stretched, at the crack tip, the cross-links of intermediate strength break such that the high tension transmits beyond one strand (Figure 67b). Compared to a network cross-linked by covalent bonds of high strength and with a similar cross-link density, the network cross-linked by covalent bonds of intermediate strength has the same modulus yet amplifies toughness from 10 to 110 J $m^{-2}$ and amplifies the fatigue threshold from 8.2 to 52 J $m^{-2}$.

## 12. INTERPENETRATING POLYMER NETWORKS

An interpenetrating polymer network (IPN) is composed of two or more polymer networks that interlace but do not interlink with each other.[299] IPNs have been widely explored for designing tough, soft materials since the pioneering work of double network hydrogels.[29]

### 12.1. Double Network Hydrogel

A typical double network hydrogel consists of two covalent polymer networks with markedly different stretchability (Figure 68a). The first network is stiff and brittle, such as the densely cross-linked polyelectrolyte network poly(2-acylamido-2-methylpropanesulfonic acid) (PAMPS). The second network is soft and stretchable, such as sparsely cross-linked PAAm. The double network is fabricated by polymerizing the monomer of the second network within the preformed first network. The mass fraction of the second network is much higher than that of the first network.[31]

Denote the number of repeat units per strand of the PAMPS network by $n_{first}$ and that of the PAAm network by $n_{second}$. In the hydrogel, $n_{first} \ll n_{second}$. Subject to small deformations, the hydrogel behaves elastically, and the PAMPS network provides a high modulus. The modulus of the PAMPS/PAAm hydrogel reaches 400 kPa, much higher than that of a regular PAAm hydrogel (10 kPa). Under moderate stretches, the hydrogel yields (Figure 68b). Necking is observed, and the neck propagates through the entire sample. The necking behavior is ascribed to the fracture of PAMPS,[300] while the stretchable second network maintains structural integrity and sustains further elongation. The fracture of the PAMPS network does not heal. As a result, at a moderate amplitude of stretch, the stress–stretch curve has pronounced hysteresis in the first cycle of loading but almost no hysteresis in the following loading cycles (Figure 68c).[301] The damaged hydrogel never recovers its mechanical properties.

A crack grows in the double network hydrogel by breaking both networks. The two networks differ in stretchability and resist crack growth by synergy. The second network deconcentrates stress over long strands and transmits stress


https://doi.org/10.1021/acs.chemrev.5c00663
Chem. Rev. XXXX, XXX, XXX–XXX

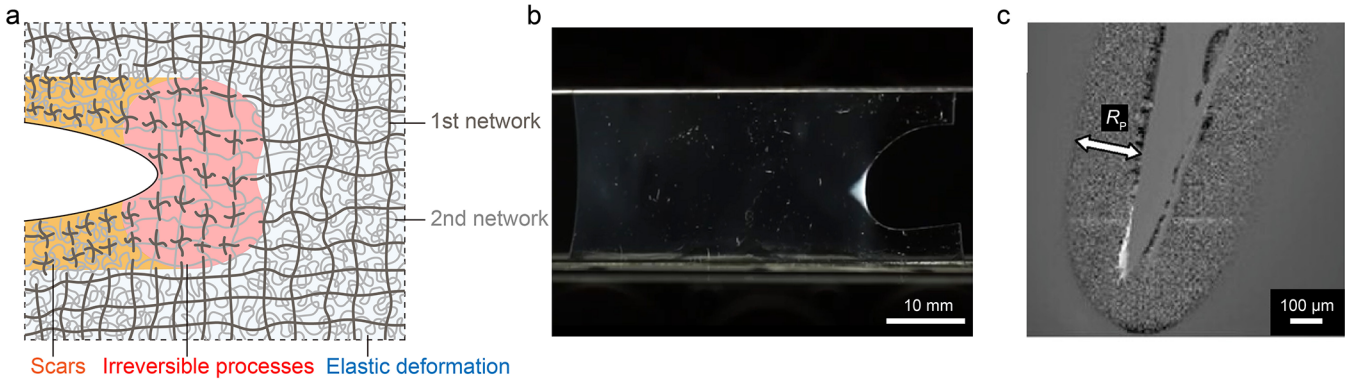


**Figure 69.** Crack growth in a double network hydrogel. (a) As the crack grows in a double network hydrogel, the long polymer strand of the second network bridges cracks, setting up high stress in a zone, in which short strands of the first network break. (b) Birefringence image of a precracked double network hydrogel when loaded. Reproduced with permission from ref 302. National Academy of Sciences under a CC BY-NC-ND 4.0 license. (c) Scarred layers observed under a confocal microscope. Reproduced with permission from ref 92. Copyright 2009 American Chemical Society.

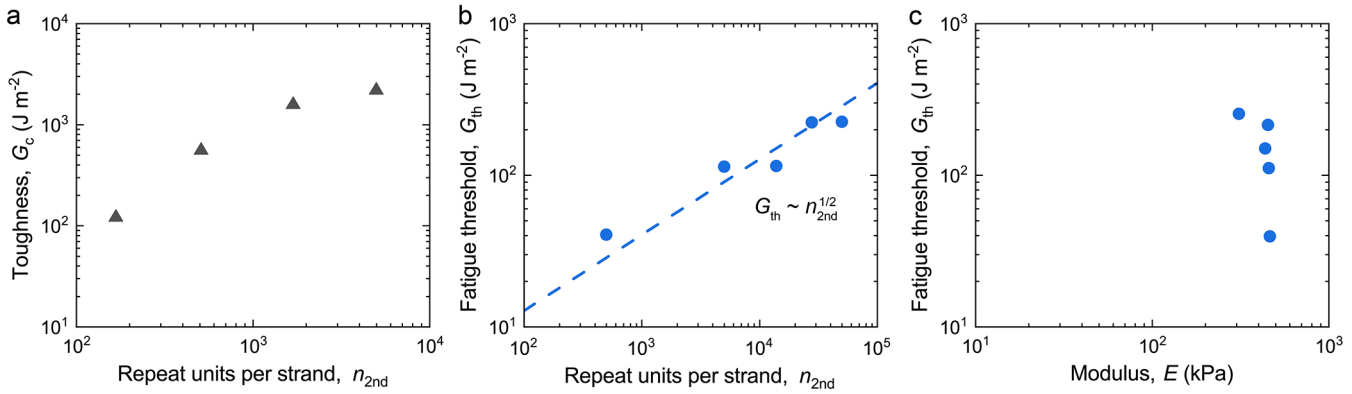


**Figure 70.** Toughness and fatigue threshold. (a) Toughness $G_c$ as a function of the repeat units per strand in the second network, $n_{2nd}$. Reproduced with permission from ref 303. Copyright 2009 American Chemical Society. (b) Fatigue threshold $G_{th}$ as a function of the repeat units per strand in the second network, $n_{2nd}$. (c) Double network hydrogel resolves the modulus−threshold conflict. (b, c) Reproduced with permission from ref 304. Copyright 2020 ASME International.

to a large zone, in which the first network breaks (Figure 69a). The high tension around the crack tip can be observed under polarized light (Figure 69b).[302] In this zone, many strands of the first network break but most strands of the second network remain intact. The crack growth dissipates energy much more than breaking a single layer of strands of either network. The hydrogel achieves a toughness of over 1000 J m$^{-2}$.

The crack creates two layers of scars, which can be observed with a confocal microscope (Figure 69c).[92] The thickness of a scarred layer is ∼100 $\mu$m, much thicker than a layer of strands. The number of broken chain ends in the double network hydrogel is expected to be much more than that in a single network hydrogel. The excess in free energy, $G_*$, of the double network hydrogel is expected to be larger than that of a single network hydrogel but should still be on the order of the surface energy of the polymer melt. The high toughness mainly comes from the reduction in free energy, $G_{**}$, associated with the irreversible process of snapping many strands.

Both the toughness and fatigue threshold increase as the strand length of the second network increases. A longer strand can deconcentrate stress to a larger extent and set up a dissipative region of a larger volume. These two processes synergize to amplify the toughness (Figure 70a).[303] The dissipative region does not amplify the fatigue threshold, so the fatigue threshold of the double network hydrogel is one order of magnitude lower than the toughness. The fatigue threshold of the double network hydrogel follows the scaling relation indicated by the Lake−Thomas model, $G_{th} \sim eL \sim n_{2nd}^{1/2}$ (Figure 70b).[304]

Double network hydrogels resolve the modulus−threshold conflict (Figure 70c). In a double network hydrogel, the short strands of the first network set the high modulus, $E \sim 1/n_{1st}$, while the long strands of the second network set the high fatigue threshold, $G_{th} \sim n_{2nd}^{1/2}$.

Besides the PAMPS/PAAm system, various other polymers have been investigated in the double network topology and have achieved high toughness.[31,305−308] Double network hydrogels have found applications in biomedical fields.[32,309]

Mechanical forces can result in the scission of covalent bonds, and a broken bond becomes two radicals. The radicals are reactive. If there are monomers inside the network, then the radical will initiate polymerization.[310] In the double network hydrogel, force can trigger extensive bond breaking of the first network.[311] The efficiency of the radical generation can further increase by using weak cross-linkers in the first network, such as the azoalkane bond (−C−N═N−C−).[312] This mechanochemistry is capable of strengthening the hydrogel during cyclic loading,[311] fabricating microstructures,[313] and resisting crack growth.[314]


https://doi.org/10.1021/acs.chemrev.5c00663
Chem. Rev. XXXX, XXX, XXX−XXX

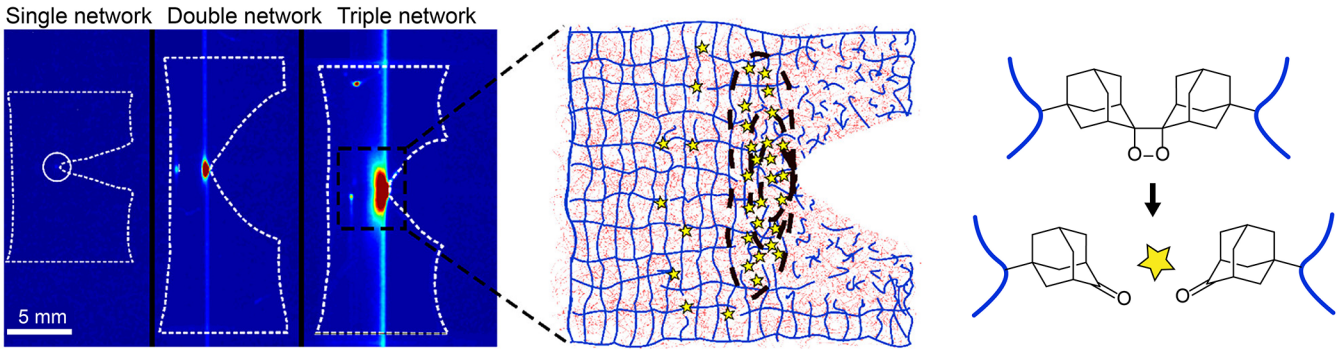


**Figure 71.** Visualization of scission in a multinetwork elastomer. Under high tension, the dioxetane group breaks and emits light. Reproduced with permission from ref 93. Copyright 2014 The American Association for the Advancement of Science.

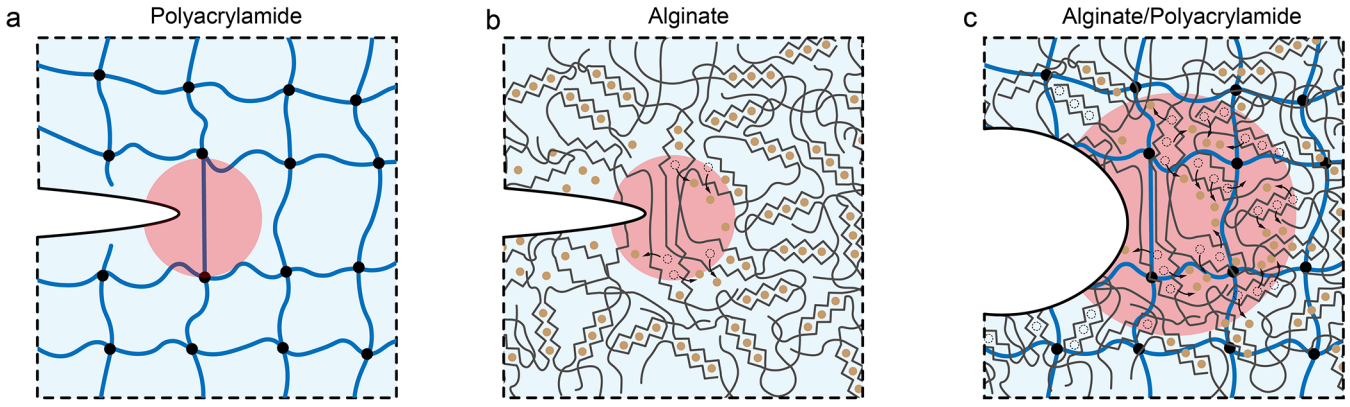


**Figure 72.** Alginate/PAAm hydrogel. (a) PAAm hydrogel. (b) Alginate hydrogel. (c) Alginate/PAAm hydrogel.[64] Copyright 2012 Springer Nature.

### 12.2. Interpenetrating Network Elastomers

An interpenetrating network elastomer is prepared by sequential swelling and polymerization of monomers.[93,315,316] The networks have different stretchabilities. Under small stretches, all networks remain intact and the elastomer behaves elastically. Under moderate stretches, the first network breaks, which dissipates energy and contributes to hysteresis, while the rest of networks remain intact and sustain the load. Yielding behavior, similar to that observed in double network hydrogels, is also reported in multinetwork poly(ethyl acrylate) elastomers.[315] Around a crack tip, the first network breaks and dissipates energy, which enhances toughness. For instance, a triple network elastomer achieves a toughness of 5000 J $m^{-2}$, whereas the toughness of the single network elastomer is 50 J $m^{-2}$.[93]

The fracture of the first network is visualized by using a mechanophore. A representative mechanophore is a chemiluminescent cross-linker, bis(adamantyl)-1,2-dioxetane bisacrylate (BADOBA) (Figure 71).[93] The dioxetane group in BADOBA has a dissociation energy of about $60k_BT$, which is weaker than the carbon−carbon single bond (about 140 $k_BT$) along a polymer strand. Under high tension, the dioxetane group breaks and emits light, serving as a molecular marker of bond scission. Under a cyclic load, the total emitted light scales with the hysteresis, confirming that the covalent bond breaking underlies the hysteresis. Around a crack tip, the multinetwork elastomer shows a much larger region of light emission compared to a single network elastomer (Figure 71). For a single network elastomer, the light emission around the crack tip is due to the sequential strand scission, whereas for the multinetwork elastomer, the light emission is due to the extensive scission of the first network.

### 12.3. Alginate/Polyacrylamide Hydrogel

Concurrent crack growth and plastic deformation take place in a hydrogel of two polymer networks: polyacrylamide and alginate (Figure 72).[64] Polyacrylamide by itself is a network of covalent cross-links (Figure 72a), and alginate by itself is a network of ionic cross-links (Figure 72b). Each network by itself has a low toughness, ∼100 J $m^{-2}$ for polyacrylamide and ∼10 J $m^{-2}$ for alginate. Their hybrid, an interpenetrating polymer network, has a high toughness, ∼8000 J $m^{-2}$. At a crack tip, before a polyacrylamide chain snaps, many alginate chains unzip their ionic cross-links (Figure 72c). The alginate off the plane of the crack undergoes deformation similar to plastic deformation in steel.

In the PAMPS/PAAm double network hydrogel, both networks are cross-linked by covalent bonds. By contrast, in the alginate/PAAm hydrogel, the alginate network is cross-linked by ionic bonds, and the polyacrylamide network is cross-linked by covalent bonds. Unlike the PAMPS/PAAm hydrogel, the alginate/PAAm hydrogel can heal after first loading.

Adhesion between a hydrogel and an inorganic or biological substrate is commonly weak (1−10 J $m^{-2}$) because water contributes negligibly to adhesion and because the noncovalent bonds between the hydrogel and the substrate are commonly weak.[40,317] The alignate/PAAm hydrogel has been used to develop tough adhesives.[318,319] The PAAm network is interlinked to the substrate through covalent bonds. When a crack grows on the interface, the strong interlinks sustain a high stress, which unzips ionic cross-links in alginate in a large


https://doi.org/10.1021/acs.chemrev.5c00663
Chem. Rev. XXXX, XXX, XXX−XXX

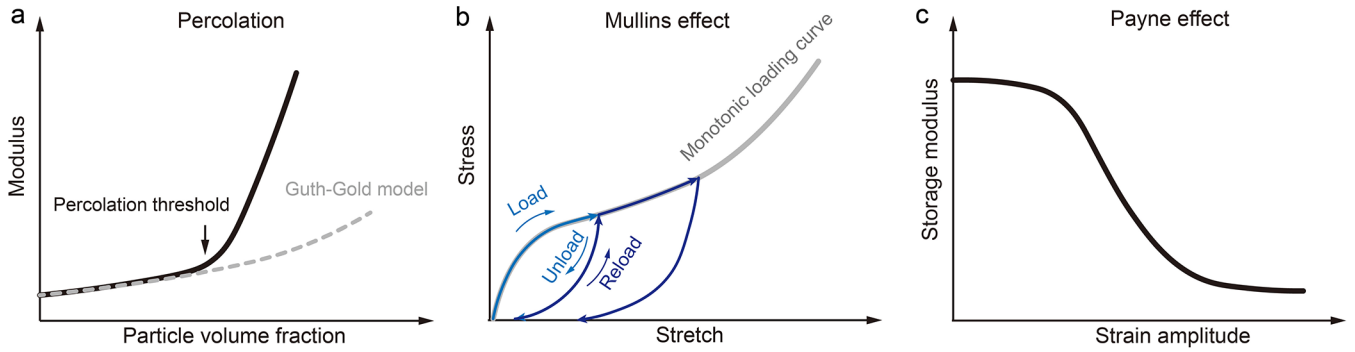


**Figure 73.** Three phenomena in particle-reinforced rubbers. (a) Percolation. (b) Mullins effect. (c) Payne effect.

volume, leading to a high adhesion toughness above 1000 J $m^{-2}$. The tough hydrogel adhesive has been developed for biological applications.[320−322]

The fatigue threshold of the alginate/PAAm hydrogel is ∼50 J $m^{-2}$.[323] It is conceivable to amplify the fatigue threshold by using a PAAm network of long strands. In principle, a PAAm network can be made into a tanglemer. The dense entanglements restrain swelling, and sparse cross-links amplify the toughness and fatigue threshold.

The strength of the ionic cross-links in the alginate network varies with the species of ions.[72] For example, $Na^+$ ions do not provide ionic cross-links, whereas $Ca^{2+}$ ions provide strong ionic cross-links. The mechanical properties can be greatly changed by ion exchange. As another example, $Fe^{2+}$ ions weakly cross-link the poly(acrylic acid) (PAAc) hydrogel, but $Fe^{3+}$ ions strongly cross-link the PAAc hydrogel. This fact has been used to design a photoresponsive hydrogel.[324] When a PAAc hydrogel cross-linked by $Fe^{3+}$ is exposed to ultraviolet light, $Fe^{3+}$ turns into $Fe^{2+}$ so that the hydrogel becomes brittle.

## 13. POLYMER NETWORKS REINFORCED BY HARD PARTICLES

A particle-reinforced rubber is a composite in which rigid particles are embedded within a polymer network. These particles enhance many properties, including the modulus, strength, and crack resistance. Particle-reinforced rubbers are widely used in high-volume applications, including tires, dampers, belts, and hoses.[77,78,325] The subject is broad, and attention here is focused on recent developments in the resistance of crack growth in particle-reinforced rubbers.

### 13.1. Hysteresis

In carbon black-reinforced rubber, carbon particles and polymer chains adhere primarily through noncovalent bonds. In a silica-reinforced rubber, the silica particles and polymer chains adhere primarily through covalent bonds. We first begin by reviewing some general phenomena in particle-reinforced rubbers, including percolation, the Mullins effect, and the Payne effect.

When particles have a spherical shape and the volume fraction of the particle is small (<20%), the modulus as a function of the particle volume fraction often follows the Guth−Gold model $E = E_0 (1 + 2.5\varphi + 14.1 \varphi^2)$, where $E$ is the modulus of the particle-reinforced rubber, $E_0$ is the modulus of the rubber matrix, and $\varphi$ is the volume fraction of the particles.[326] When the particle volume fraction exceeds a threshold (∼20 vol %), the particles percolate,[327] the modulus greatly increases as the particle volume fraction increases, and the trend deviates from the Guth−Gold model (Figure 73a). In applications requiring a high modulus, the particle volume fraction is higher than the percolation threshold.

In a particle-reinforced rubber, the particle−polymer interaction is commonly stronger than either the particle−particle interaction or the polymer−polymer interaction. Consequently, the particles do not contact one another directly but are separated by the polymer. When the particles percolate, a thin layer of rubber exists between two neighboring particles. The rigid particles constrain the deformation of the thin layer of rubber, which deforms much less than the composite. The composite is composed of two networks: a network of percolated particles and a network of cross-linked chains. The two networks are intertwined and adhere to each other. This architecture accounts for high modulus and low hysteresis when the stretch is small.[328]

When loaded to an intermediate stretch and then unloaded, the composite exhibits hysteresis. This hysteresis originates from the breaking of the noncovalent bonds between the polymers and the particles.[329,330] The noncovalent bonds can reform, but the reformation takes time. Consequently, during an immediate second loading, the stress−stretch curve nearly follows the first unloading curve until reaching the prior maximum stretch, beyond which the stress−stretch curve returns to the path of monotonic load (Figure 73b). This effect is called the "Mullins effect".[331] The Mullins effect in the particle-reinforced rubbers is not a sign of permanent damage but must be considered in applications involving repeated loading and unloading.

When a composite is subject to an oscillatory strain of small amplitude, the storage modulus decreases as the amplitude of strain increases, a phenomenon known as the "Payne effect" (Figure 73c).[332] At a small amplitude of strain, the noncovalent bonds between particles and polymers remain intact. As the amplitude of strain increases, the noncovalent bonds between particles and polymers begin to break, and the polymer matrix may slip relative to particles.

### 13.2. Carbon Black Reinforced Rubber

Carbon black-reinforced rubbers have been used in tires since 1912.[333] These materials have remained critical in rubber products: global carbon black production is on the order of several million tons per year, over 90 percent of which is used in rubber compounding.[334]

Carbon black is in the form of a powder, which consists of over 90% carbon. In a carbon black powder, many layers of graphene platelets stack into a primary spherical particles with diameters of ∼10−100 nm, several primary particles fuse into an aggregate with a size of 100−300 nm, and many aggregates


https://doi.org/10.1021/acs.chemrev.5c00663
Chem. Rev. XXXX, XXX, XXX−XXX

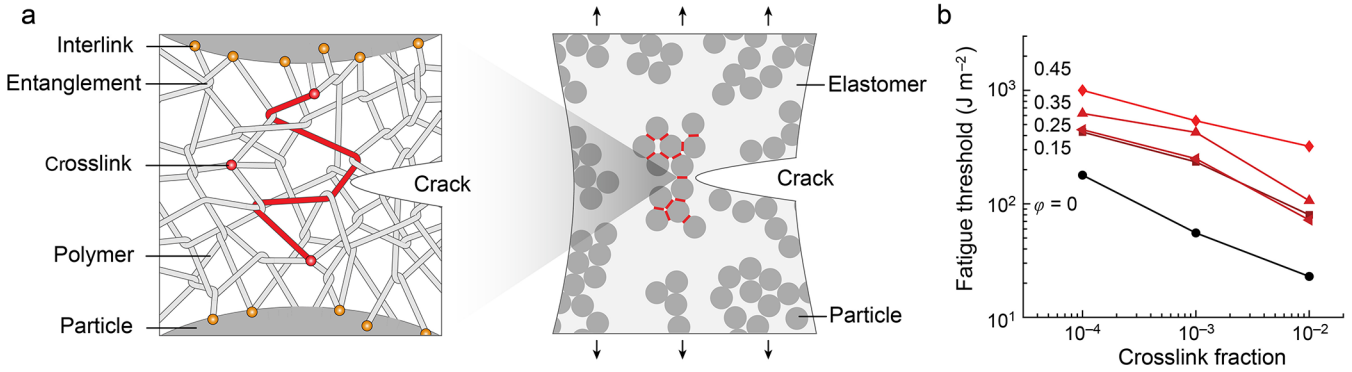


**Figure 74.** Multiscale stress deconcentration in a particle-reinforced rubber. (a) In the particle cluster, stress transmits to many rubbery gaps between particles. In the rubbery gap between two particles, stress transmits to a long polymer strand. (b) Fatigue threshold as a function of crosslink fraction for particle-reinforced rubbers with various particle volume fractions $\varphi$. Reproduced with permission from ref 99. Copyright 2023 Springer Nature.

join through van der Waals forces into an agglomerate with a size of up to a millimeter.[335]

The carbon black powder is mixed with rubber chains, along with other additives such as cross-linking agents and antioxidants. Mixing is commonly conducted using equipment such as internal mixers and roll mills. During such high-intensity mixing, the large agglomerate of carbon black breaks into small aggregates, and the long rubber chains are masticated into short chains. The aggregates are well dispersed in a continuous matrix of chains. The carbon−polymer mixture is called a compound. The compound is then cured at an elevated temperature, during which the chains cross-link into a network.

In the carbon black-reinforced rubber, the aggregate of carbon black particles is regarded as a working unit, and the individual carbon primary particles determine the specific surface area of the aggregates. Polymer chains adsorb on the surface of the aggregate by noncovalent bonds, forming so-called bound rubber.[336,337] The smaller the primary particles, the higher the bound rubber fraction and the stronger the reinforcement effect. Beside the extensive noncovalent adsorption, sparse covalent bonds may interlink rubber chains and carbon particles, as some radicals may be generated during the high-intensity mixing.[334]

Under cyclic load, the carbon black-reinforced rubber exhibits pronounced hysteresis, which is ascribed to the breaking of noncovalent bonds between the carbon particles and the polymer chains.[329,330] Some hysteresis remains over cycles due to the repeated breaking and reforming of the noncovalent bonds. The higher the volume fraction of the carbon particles, the higher the hysteresis. In tires, more hysteresis means higher rolling resistance and higher fuel consumption.

As the crack grows in a carbon black-reinforced rubber, toughness comes from the synergy of several processes. At the crack tip, the percolated carbon particles bridge the crack, and the high tension is deconcentrated among multiple gaps between carbon particles. This process is similar to that in a silica-reinforced rubber.[99] Around the crack tip, the noncovalent bonds between particles and polymers break, polymers may slip relative to particles, and cavitation may occur,[338−340] which dissipates an extensive amount of energy. For natural rubber, butyl rubber, strain-induced crystallization takes place. These processes lead to a high toughness of 10,000 to 100,000 J m$^{-2}$.

### 13.3. Silica-Reinforced Rubber

Silica is an inorganic nanoparticle of silicon dioxide. An untreated silica surface is covered with silanol (Si−OH) groups and is hydrophilic, which leads to poor compatibility when mixed with rubbers.[78] The unmodified silica tends to aggregate rather than disperse in rubber. The silica particles are always modified by a silane coupling agent. The silanol groups of the silane coupling agent react with silanol groups on the silica, leaving a hydrophobic end. This hydrophobic end can be a double bond or sulfur, which can form covalent interlinks with rubbers in subsequent processing. The covalent interlinks reduce energy dissipation during the cyclic load.[78] Silica-reinforced rubbers have been developed for "green tires", which have low rolling resistance and low fuel consumption.[341,342]

### 13.4. Long Polymer Strands Amplify the Fatigue Threshold of Particle-Reinforced Rubbers

Embedding particles in a rubber can greatly enhance the modulus and toughness. However, the fatigue threshold of particle-reinforced rubber has remained ∼100 J m$^{-2}$ for decades.[27,95,343] Compared to that of the pure rubbers, ∼50 J m$^{-2}$, the threshold is not greatly enhanced.

A particle-reinforced rubber with a greatly enhanced fatigue threshold is demonstrated in a model system of a particle-reinforced tanglemer (Figure 74).[99] When the volume fraction of particles exceeds ∼20 vol %, particles percolate.[344] The rubbery matrix has long polymer strands, and covalent bonds interlink particles and rubbery chains. The gap between the neighboring particles is thin, with a thickness much smaller than the diameter of a particle. Consequently, when a crack impinges on a particle cluster, the rubbery matrix in between the gaps undergoes triaxial stress, and strong particle−polymer interlinks transmit the stress. Because the particles are rigid, stress deconcentrates over many rubbery gaps between particles in the cluster. The rupture of a single gap dissipates energy stored in many gaps in the cluster. In each gap, the stress deconcentrates over a long polymer strand. The rupture of a single bond along the chain dissipates the energy stored in every bond along the strand (Figure 74a). Consequently, stress deconcentrates over two length scales: polymer strands and particle clusters. Long strands and clustered particles synergize across length scales to increase the threshold.

The design of a particle-reinforced tanglemer is demonstrated as follows. Silica particles are modified with carbon−


https://doi.org/10.1021/acs.chemrev.5c00663
Chem. Rev. XXXX, XXX, XXX−XXX

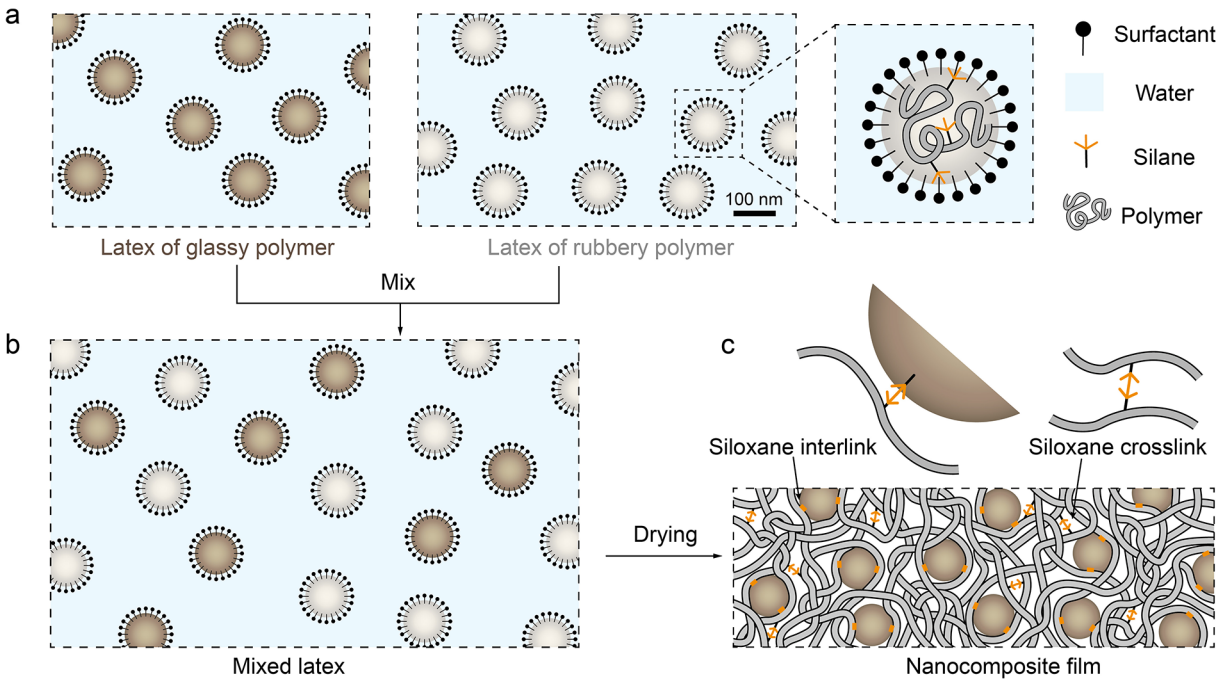


**Figure 75.** A particle-reinforced rubber of long strands prepared by mixing aqueous suspensions of dissimilar particles. (a) Each suspension is prepared separately, containing a single species of polymer chains copolymerized with a silane coupling agent. Each particle is covered with a surfactant. (b) Mix the two suspensions. (c) Upon drying, the glassy particles retain the shape, but the rubbery chains flow to form a continuous matrix. The silane coupling agents condensate into siloxane linkages, which cross-link the rubbery chains and interlink the rubbery chains to glassy particles. Reproduced with permission from ref 81. Copyright 2024 National Academy of Sciences under a CC BY-NC-ND 4.0 license.

carbon double bonds on surfaces. Suspend the silica particles in the liquid monomer ethyl acrylate (EA), along with small amounts of photoinitiator and cross-linker. Upon exposure to ultraviolet light, the monomers form a network of poly(ethyl acrylate) (PEA), and the silica particles are interlinked with PEA by covalent bonds. An unfilled PEA network of long strands, with a crosslinker-to-monomer molar ratio of $10^{-4}$, has a fatigue threshold of ~200 J $m^{-2}$ (Figure 74b). The network of long strands filled with silica particles at a particle fraction of 45 vol % achieves a threshold of ~1,000 J $m^{-2}$.

The low fatigue threshold of commercial particle-reinforced rubbers is caused by short polymer strands. Particle-reinforced rubbers are commonly prepared by mixing the particles and uncrosslinked polymer chains. This mixing is of high intensity, conducted in a machine such as an internal mixer, roll mill, and extruder. The high-intensity mixing masticates the polymer chains, lowering the chain length, which lowers the viscosity of the mixture and eases the mixing process. The short chains require a high cross-link density to form a proper network. In such a network of short strands, stress deconcentrates along a short strand.

In the silica-reinforced PEA, the particles are mixed with the precursor, and long polymer strands polymerize in situ, which avoids high-intensity mixing. Some rubbers, such as natural rubbers, are not available in monomeric form. Additionally, in situ polymerization presents challenges in heat removal, particularly when carried out in reactors at industrial scales. We have attempted to prepare particle-reinforced rubbers of long strands from pre-existing long polymers. To preserve the long polymers, we dissolve long rubber chains in an organic solvent and gently mix the polymer solution and filler particles by stirring, which avoids high-intensity mixing. The mixture is then dried, shaped, and sparsely cross-linked. The filler particles can be silica particles,[328] which form covalent interlinks with the rubber chains, or carbon black,[345] which form noncovalent bonds with the rubber chains. In both cases, the materials achieve a high modulus, high toughness, and a high fatigue threshold.

### 13.5. Particle-Reinforced Rubbers of Long Strands Prepared by Mixed Latexes

A latex of a synthetic polymer can be prepared by emulsion polymerization.[172] The polymer chains can be hydrophobic, long, and uncrosslinked. The latex particles can be suspended in water, stabilized by a surfactant. A particle-reinforced rubber of long strands can be prepared by mixing aqueous suspensions of dissimilar polymers, followed by drying, cross-linking, and interlinking.[81] In a model system, a latex of a rubbery polymer, PEA, and a latex of a glassy polymer, poly(methyl methacrylate) (PMMA), are separately prepared (Figure 75a). In each latex particle, polymer chains are copolymerized with a silane coupling agent. The polymer chains are long, uncrosslinked, and highly entangled. Each particle is covered with the same species of surfactant and is of similar diameter. The two latexes are readily mixed, and the mixed latex readily flows (Figure 75b). In the mixed latex, particles of dissimilar polymers are covered with the same surfactant and cannot distinguish each other. As water evaporates, latex particles form a close contact, at which the dissimilar polymers can distinguish each other but the viscosity becomes high, which prevents the two polymers from separating. The soft PEA chains flow to form a space-filling matrix, and the rigid PMMA particles maintain spherical shapes. The silane coupling agent slowly condensates to cross-link PEA chains and interlink PEA chains with the PMMA particles (Figure 75c). A composite with 40 vol % PMMA has a fatigue threshold of 1,100 J $m^{-2}$ and a toughness of 90,000 J $m^{-2}$. The method of mixed latexes


https://doi.org/10.1021/acs.chemrev.5c00663
Chem. Rev. XXXX, XXX, XXX−XXX

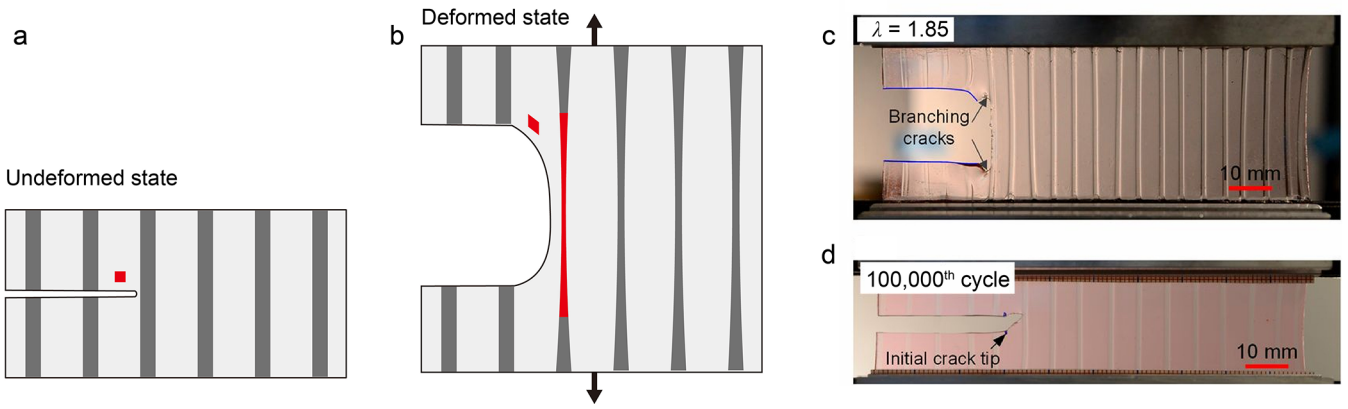


**Figure 76.** Crack growth in a stretchable fiber/matrix composite. (a) Unidirectional fibers of a soft and stretchable material are embedded in a matrix of much softer and much more stretchable material. A small piece of the matrix is marked by a red square. (b) When an applied force stretches the composite, the matrix shears greatly, deforms the red square into a parallelogram, blunts the crack, and deconcentrates the high tension over a long segment of the fiber. Strong fiber−matrix adhesion prevents sliding and separation. (c) Under monotonic load, the crack bifurcates in the PDMS/PDMS composite. (d) Under cyclic load, the crack arrests at a fiber without any further extension over 100,000 cycles. Reproduced with the permission from ref 73. Copyright 2019 National Academy of Sciences under a CC BY-NC-ND 4.0 license.

avoids high-intensity mixing, is free of organic volatiles, and is compatible with various open-air manufacturing processes, including coating, casting, spraying, printing, and brushing.

## 14. POLYMER NETWORKS REINFORCED BY FIBERS OR FABRICS

In a polymer network reinforced with fibers or a fabric, stress can deconcentrate over the length scale of the polymer mesh as well as that of fibers or fabric. The reinforcement can be stretchable fibers, crimped fibers, or knitted fabrics. Such composites are stretchable and will be reviewed. Polymer networks have also been reinforced with hard fibers and hard woven fabrics.[346−350] Such composites are not stretchable and will not be reviewed here.

### 14.1. Elastic and Tough Composite

A design of a stretchable composite has been demonstrated to simultaneously achieve low hysteresis and high toughness (Figure 76).[73,101] The composite has two constituents of a stretchable matrix and stretchable fibers (Figure 76a). The matrix is much softer than the fiber. The matrix and fiber form a strong adhesion.

At the crack tip, the large modulus contrast causes the soft matrix to shear greatly, which deconcentrates the high tension at the crack tip over a long segment of each fiber (Figure 76b). The strong adhesion prevents the fiber and matrix from slipping and separating. When the crack grows, the fiber ahead of the crack breaks, and the elastic energy stored in the long segment of fiber is dissipated. The rest regions of the composite deform elastically such that the toughness of the composite scales as

$$G_c \sim W_c L_{fiber} \tag{36}$$

where $W_c$ is the elastic energy density stored in the long segment of fiber before fracture, which is comparable to the work of fracture of the fiber, and $L_{fiber}$ is the length of the segment of fiber over which stress deconcentrates. The length scale of stress deconcentration can be as large as centimeters ($10^{-2}$ m). Taking the representative value of $W_c$ as $1 \times 10^6$ J m$^{-2}$, $G_c$ is on the order of 10,000 J m$^{-2}$.

The design is first demonstrated by using a PDMS/PDMS composite.[73] Stiff PDMS fiber (modulus ≈ 1.8 MPa) and soft PDMS (modulus ≈ 0.2 MPa) form a stretchable composite, where the fibers and matrix adhere by forming trapped entanglements, called topological adhesion.[351] The stiff PDMS, soft PDMS, and PDMS/PDMS composite all show small hysteresis. The toughness of both stiff PDMS and soft PDMS is around 300 J m$^{-2}$, whereas the toughness of the PDMS/PDMS composite is on the order of 10,000 J m$^{-2}$. When the precracked composite is under a monotonic load, the crack blunts and bifurcates near the interface between the matrix and fiber (Figure 76c). The stress deconcentration of the PDMS/PDMS composite also contributes to the fatigue threshold. When the composite is cyclically loaded by an amplitude of $G$ = 160 J m$^{-2}$, the crack arrests at the fiber/matrix interface without any further extension for 100,000 cycles (Figure 76d). Under similar loading conditions, the pure PDMS fractures after a few cycles.

The fatigue threshold of the elastic composite can be understood as

$$G_{th} \sim W_e L_{fiber} \tag{37}$$

where $W_e$ is the work of endurance of the fiber. $W_e$ is measured by the stress-cycle ($s$−$N$) curve, at which the sample survives a prescribed number of cycles of stretch. Taking the representative value of $W_e$ as $1 \times 10^5$ J m$^{-2}$, $G_{th}$ will be on the order of 1,000 J m$^{-2}$.

This high fatigue threshold is demonstrated by using a PDMS/PAAm composite,[101] where PDMS serves as fibers and a PAAm hydrogel serves as the matrix. The two materials have a 200-fold modulus contrast and a 5-fold stretchability contrast. The fiber and matrix are bonded by covalent links. The PDMS/PAAm composite achieves a fatigue threshold $G_{th}$ of about 1300 J m$^{-2}$ and a toughness $G_c$ of around 4200 J m$^{-2}$. This design also demonstrates high resistance to hydrolytic crack growth.[122]

The stretchable composite is compatible with various fabrication methods, such as 3D printing[157,352,353] and lithography.[354] These fabrication methods enable the elastic composite to be fabricated into three-dimensional complex shapes. The stretchable composites simultaneously achieve low hysteresis, high toughness, and a high fatigue threshold, which


https://doi.org/10.1021/acs.chemrev.5c00663
Chem. Rev. XXXX, XXX, XXX−XXX

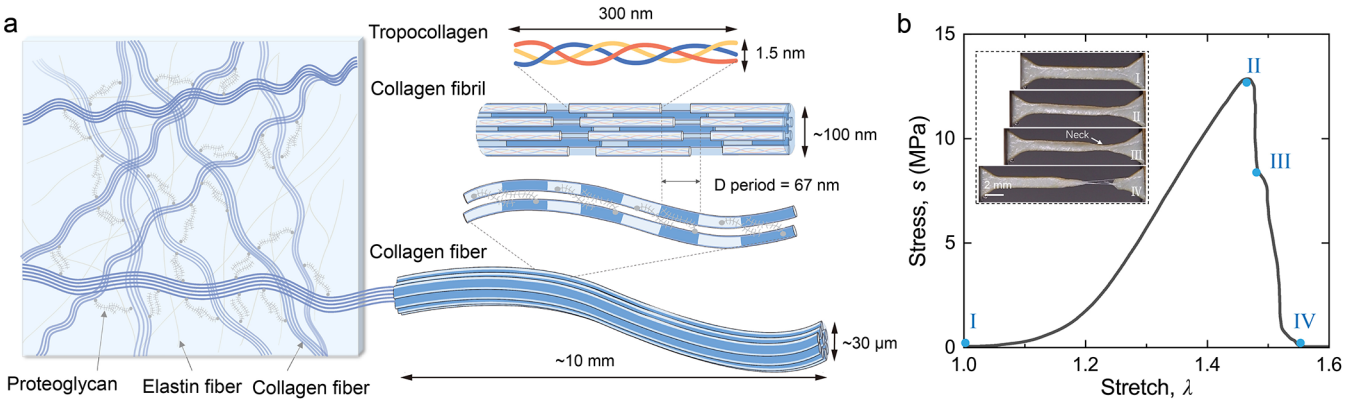


**Figure 77.** Structure and stress−stretch curve of bovine pericardium (BP). (a) Multiscale structure of BP. A network of collagen fibers embedded in a matrix of elastin and proteoglycan, in which collagen forms hierarchical structures: tropocollagen, fibril, and fiber. Reproduced with permission from ref 358. Copyright 2025 The American Association for the Advancement of Science under a Creative Commons CC-BY-NC license. (b) Stress−stretch curve of BP. Reproduced with permission from ref 75. Copyright 2023 The American Association for the Advancement of Science under a Creative Commons CC-BY-NC license.

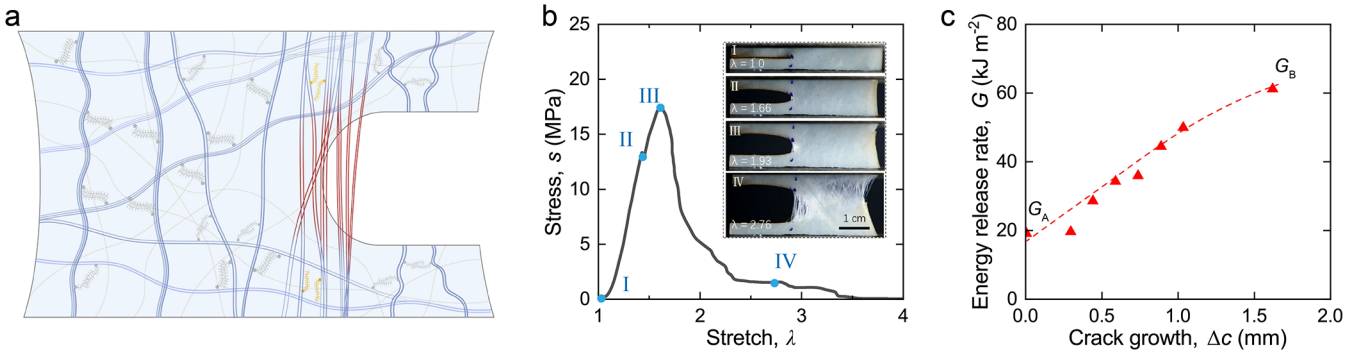


**Figure 78.** Toughness of BP. (a) Stress deconcentration in BP. When the crack grows in the soft matrix, the collagen fibers decrimp, reorient, and slip, bridging the crack. Reproduced with permission from ref 358. Copyright 2025 The American Association for the Advancement of Science under a Creative Commons CC-BY-NC license. (b) Stress−stretch curve of a precracked BP. (c) Crack-resistance curve. (b, c) Reproduced with permission from ref 75. Copyright 2023 The American Association for the Advancement of Science under a Creative Commons CC-BY-NC license.

hold promise in applications such as tissue engineering and biomedical devices.

## 14.2. Collagenous Tissue

Soft collagenous tissues, such as skins, tendons, ligaments, and heart valves, show extraordinary toughness and fatigue resistance.[75,355−360] In this section, we take the bovine pericardium (BP) membrane as an example to illustrate the origin of crack resistance of collagenous tissue.[75,358] The BP membrane is harvested from the bovine heart and has been used to replace heart valves of human patients.

In the BP membrane, the collagen fibers are crimped and form a network embedded in a soft matrix of elastin and proteoglycan (Figure 77a). The collagen forms a hierarchical structure of tropocollagen, collagen fibril, and collagen fiber.[355] Collagen fibers have a diameter of 10−50 $\mu$m and a length of ∼10 mm. The strength of a collagen fiber is 30−200 MPa.[361,362] In the soft matrix, the elastin fibers have a modulus of 300−600 kPa, and the elastin network has a low toughness of 20 J m$^{-2}$.[363] The crimped collagen fibers enable softness at small to moderate stretches, but high resistance to crack growth at large stretches. Elastin enables high elasticity of the collagen network at small deformation. The proteoglycan keeps the tissue hydrated and separates the fibrils to allow them to slip.

Stretch a dog-bone-shaped sample of BP until fracture (Figure 77b). At a small stretch, $1.0 < \lambda < 1.05$, the collagen fibers are crimped and the slope of the stress−stretch curve is small, ∼0.2 MPa, comparable to the modulus of the soft matrix. At a large stretch, $1.2 < \lambda < 1.4$, the collagen fibers are crimped and the slope of the stress−stretch curve is large, ∼100 MPa, comparable to the modulus of the collagen fiber. Before the stress reaches a peak (II), the sample deforms homogeneously. After the peak, the stress drops sharply, and the sample forms a localized neck (III). When the sample breaks at the neck, collagen fibers are pulled out (IV).

When a crack impinges upon a collagen fiber, the surrounding soft and weak matrix enables the fiber to decrimp, reorient, and slip. As the crack grows, the collagen fibers pull out from the matrix and bridge the crack surfaces (Figure 78a). The long collagen fiber deconcentrates stress. Once a long fiber breaks, the energy stored in the long segment of the fiber dissipates. The stress deconcentration by the long fiber leads to a high fatigue threshold of 4,300 J m$^{-2}$.[75]

The crack bridging by the long fiber at the crack tip allows for the dissipative process of fiber slip to happen in a large volume around the crack tip, which leads to a high toughness. Stretch a sample with a precut (Figure 78b), and BP exhibits a crack resistance curve (Figure 78c).[75] When $G < G_A$, the crack blunts, while the fibers reorient, decrimp, and the crack does


https://doi.org/10.1021/acs.chemrev.5c00663
Chem. Rev. XXXX, XXX, XXX−XXX

not grow. The crack starts to grow when $G = G_A \approx 15$ kJ m$^{-2}$. When $G_A < G < G_B$, the crack grows by increasing $G$, while the fibers pull out and bridge the crack. The longer the crack grows, the larger the bridging zone. After the crack propagates for 1.5 mm, the energy release rate increases to $G_B \approx 60$ kJ m$^{-2}$. When $G > G_B$, the whole sample grows multiple cracks.

We designate fracture toughness by the energy release rate at $G_c = G_A = 15$ kJ m$^{-2}$. The work of fracture is $W_c = 1.3 \times 10^6$ J m$^{-3}$. The fractocohesive length is $G_c/W_c \approx 1$ cm. When the crack propagates in a sample, a region around the crack tip dissipates energy, which resists crack growth. The fractocohesive length measures the flaw sensitivity of the material. BP is insensitive to the flaw up to centimeter size.

### 14.3. Polymer Network Reinforced by a Knitted Fabric

The fatigue-resistant collagenous tissues can be mimicked by a polymer network reinforced by a knitted fabric.[364] The polymer network serves as the soft matrix, and the knitted fabric behaves similarly to the crimped fibers. When the stretch is small to modest, the knitted fabric is stretchable so that the composite is soft. When the stretch is large, the knitted fabric becomes stiff so that the composite resists crack growth under cyclic stretch. The design is demonstrated by using a PVA hydrogel as the polymer network and knitted nylon as the fabric. The polymer network and fabric form strong adhesion by hydrogen bonds.[364]

Consider a crack growing in the wale direction of the knitted fabric (Figure 79a). During cyclic loading with an amplitude of

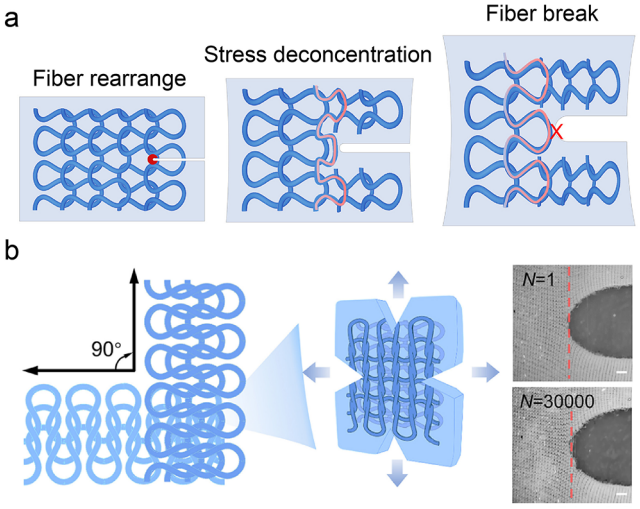


**Figure 79.** Polymer network reinforced by a knitted fabric. (a) Fatigue crack grows in the wale direction. (b) A composite hydrogel, in which a polymer network embedded two orthogonal layers of knitted fabrics, achieves a high fatigue threshold. Reproduced from ref 364.

energy release rate of ~5,000 J m$^{-2}$, the crack grows by ~1 mm and arrests. The fiber forms a bridging zone and does not break. The bridging fiber inhibits further crack growth. By embedding two orthogonally stacked layers of knitted fabric into the hydrogel matrix, the composite hydrogel is symmetric in both the vertical and horizontal directions and shows a high fatigue threshold of ~5,000 J m$^{-2}$ (Figure 79b).

## 15. CONCLUDING REMARKS AND OUTLOOK

This paper reviews the thermodynamic and molecular origins of crack resistance in polymer networks. Attention is focused on the idealization that the irreversible zone is small relative to the body (Section 1). We decompose the body into a zone of irreversible processes, two layers of scars, and a background of elasticity (Figure 4). The three regions are associated, respectively, with a reduction in free energy $G_{**}$, an excess in free energy $G_*$, and energy release rate $G$. The crack grows when $G = G_* + G_{**}$.

Sections 2−6 review the thermodynamics of crack growth. Under the idealization of localized irreversibility, the energy release rate is defined using an ideal body in which a crack is stationary and the body deforms by a reversible process of elasticity (Section 2). The energy release rate is then used to study the irreversible process of crack growth in a real body. The idealization of localized irreversibility divides the labor of studying crack growth into two tasks. First, in an ideal body, we relate the energy release rate to geometry and the load of the body through a boundary value problem of elasticity. Second, in a real body, we use the energy release rate to characterize crack resistance as a material property. This review treated the first task lightly, limited to a list of expressions for the energy release rate in commonly used experimental setups (Section 3). For a semi-infinite stationary crack in an infinite ideal body, a scaling analysis shows that the field of elastic energy density scales as $W(R, \Theta) = \frac{G}{R} f(\Theta)$ (Section 4). For a crack in a real body, this $1/R$ singular field is valid in an annulus, called the $G$-annulus, as long as the irreversible zone is much smaller than the body. This scaling relation leads to a definition of the length scale, called the fracticohesive length $G_c/W_c$, where $W_c$ is the work of fracture measured using a sample without a precut crack, and $G_c$ is the toughness measured by using a sample with a precut crack. The fractocohesive length is comparable to several material-specific lengths: the size of the irreversible zone around a crack tip, the size of flaws below which the strength is insensitive to the flaws, and the crack extension of the $R$-curve to the plateau. Materials can be designed to deconcentrate stress around crack tips (Section 5). A central question of fracture mechanics is, given a history of the energy release rate $G(t)$, what is the history of crack growth $c(t)$? In experiments, three histories of the energy release rate are applied (Section 6). A monotonically increasing energy release rate is used to measure the toughness and crack resistance curve. The cyclic energy release rate is used to study fatigue crack growth. The static energy release rate is used to study crack growth in materials undergoing viscoelasticity, hydrolysis, or poroelasticity.

Sections 7−14 illustrate the findings of the second task using representative polymer networks. The fundamental understanding of the mechanochemistry of crack growth gives rise to new opportunities to expand the property space yet poses challenges for processing. For example, crack resistance is greatly benefited by long polymers, yet the long polymers pose challenges in mixing and shaping. This leads to a performance−processing conflict. In the conventional dry-mixing process, it remains a challenge to mix long polymers with additives such as reinforcing particles while preserving the long chains. The performance−processing conflict may be resolved by developing and reimaging colloidal-based processes.[76,81] As another example, in radical polymerization-based 3D printing, the requirement of fast curing leads to short chains, and short chains degrade performance. This leads to a conflict between performance and printing speed. The conflict may be resolved


https://doi.org/10.1021/acs.chemrev.5c00663
Chem. Rev. XXXX, XXX, XXX−XXX

by developing coupling chemistries[365] or designing post-treatment processes.[157,268]

Abundant opportunities exist to take advantage of enhanced crack resistance in applications. Examples of recent work include tissue adhesives for wound dressing and surgery,[297,319−321] photoresponsible adhesives,[324] tissue-attached ultrasound,[366] replacement of tissues vulnerable to crack growth, such as heart valves,[364] cartilage,[367] and tendons,[368] flexible devices such as ionotronics,[369] soft electronics,[370] and soft robots.[371] The understanding of mechanochemistry also calls for the further development of computer simulations.[372,373]

This review focuses on crack growth in polymer networks. Similar ideas can be extended to thermoplastics. In a thermoplastic, noncovalent bonds between polymer chains are strong but are still much weaker than covalent bonds along the polymer chains. The concept of stress deconcentration still applies to thermoplastics.[97] While this principle is being established, opportunities are abundant to design thermoplastics to break the conflict between the yield strength and fatigue threshold. Besides, similar ideas also apply to mechanical metamaterials,[374,375] textiles,[376] composites,[377] and biological tissues.[20,75,356−358]

The idealization of localized irreversibility is powerful but also has its limitations. In particular, as noted before, the strength of a sample without a precut crack is orders of magnitude lower than the strength of covalent bonds. This large difference exists under monotonically creasing loads, cyclic loads, and static loads. When the flaws are below the fractocohesive length, this reduction in strength cannot be interpreted. The idealization of localized irreversibility is powerful but also has its limitations. For example, the strength of a sample without a precut crack is orders of magnitude lower than the strength of covalent bonds. This large difference exists under a monotonically increasing load, cyclic load, and static load. When the flaws are below the fractocohesive length, this reduction in strength cannot be interpreted in terms of crack resistance. Several studies have appeared recently,[57−59] but further studies are needed to understand how strengths can be amplified by design though the chemistry of bonds and the topology of networks. In many applications, crack growth is accompanied by a large-scale irreversible zone. The energy release rate is still commonly used, but the lack of elastic background makes the crack resistance measured in the experiment not a material property and specific to the shape of the body.

When a large part of a body undergoes irreversible processes, the idealization of localized irreversibility is invalid. Nonetheless, one can still consider two bodies: an ideal body in which deformation is described by a continuum field theory and a real body in which the crack grows by a process deviating from the continuum field theory. As long as the zone of deviation is small relative to the body, the ideal body can still be used to define the energy release rate, as has been done for an ideal body of plasticity,[378] viscoelasticity,[379] or poroelasticity.[380] A detailed treatment of this framework lies beyond the scope of the present review.

This review is limited to crack growth at low enough speeds that inertia is negligible and the material remains close to thermal equilibrium with the environment. At a high loading rate or a high crack growth speed, dynamic effects become significant, such as kinetic energy, elastic-wave radiation, and heat generation.[381,382] These contributions can alter both the driving force and toughness. High speed crack growth in polymers has been studied in recent decades.[383,384] The effect of chemistry and topology in material design on fast crack growth has been largely unexplored.

The molecular picture of crack resistance is well studied, but that of wear resistance is less clear. Wear of rubber tires has become an issue of polymer pollution.[385] Studies on the nature of wear and the development of wear-resistant polymeric materials will contribute to resolving rubber pollution.

Fracture mechanics has evolved a concept not commonly taught in thermodynamics—the localized irreversible process—which has led to the concept of the energy release rate. It is worthwhile to examine whether an analogous approach is applicable to other phenomena that feature localized irreversible processes. For example, the electrical breakdown in dielectrics has received some attention.[386−388]

This article reviews the recent development of the mechanochemistry of crack growth in polymer networks. The development has greatly benefited from collaborations between researchers with backgrounds in mechanics, chemistry, and polymer science. New opportunities have been identified to design the chemistry of bonds and the topology of networks to markedly amplify crack resistance. It is hoped that the fundamental understanding will soon be translated into polymer products as well as integrated into computational tools for designing materials.

## AUTHOR INFORMATION


### Corresponding Author

**Zhigang Suo** − *John A. Paulson School of Engineering and Applied Sciences, Harvard University, Cambridge, Massachusetts 02138, United States;* orcid.org/0000-0002-4068-4844; Email: suo@seas.harvard.edu

### Author

**Zheqi Chen** − *John A. Paulson School of Engineering and Applied Sciences, Harvard University, Cambridge, Massachusetts 02138, United States;* Present Address: Advanced Biomedical Instrumentation Centre, Hong Kong Science Park, HKSAR (Z.C.); orcid.org/0000-0001-7193-5426

Complete contact information is available at: https://pubs.acs.org/10.1021/acs.chemrev.5c00663


### Notes

The authors declare no competing financial interest.

### Biographies

Zheqi Chen is a postdoctoral fellow in the John A. Paulson School of Engineering and Applied Sciences at Harvard University. He received his Ph.D. degree in the College of Chemical and Biological Engineering at Zhejiang University in 2024. His research focuses on understanding the structure−property relation of soft materials and developing materials with extreme mechanical and functional properties.

Zhigang Suo is the Allen E. and Marilyn M. Puckett Professor of Mechanics and Materials at Harvard University. He earned a bachelor's degree at Xian Jiaotong University in 1985 and a Ph.D. at Harvard University in 1989. Suo joined the faculty of the University of California at Santa Barbara in 1989, Princeton University in 1997, and Harvard University in 2003. His research centers on the mechanical behavior of materials.



https://doi.org/10.1021/acs.chemrev.5c00663
Chem. Rev. XXXX, XXX, XXX−XXX

## ACKNOWLEDGMENTS

Z.S. acknowledges the support of the National Science Foundation under MRSEC (DMR-2011754) and of the Air Force Office of Scientific Research under FA9550-20-1-0397.

## REFERENCES

(1) Rowan, S. J.; Cantrill, S. J.; Cousins, G. R. L.; Sanders, J. K. M.; Stoddart, J. F. Dynamic Covalent Chemistry. *Angew. Chem., Int. Ed.* **2002**, *41*, 898−952.
(2) Zheng, N.; Xu, Y.; Zhao, Q.; Xie, T. Dynamic Covalent Polymer Networks: A Molecular Platform for Designing Functions beyond Chemical Recycling and Self-Healing. *Chem. Rev.* **2021**, *121*, 1716−1745.
(3) Müller-Dethlefs, K.; Hobza, P. Noncovalent Interactions: A Challenge for Experiment and Theory. *Chem. Rev.* **2000**, *100*, 143−168.
(4) Haynes, W. M. *CRC Handbook of Chemistry and Physics*; CRC Press, 2016.
(5) Israelachvili, J. N. *Intermolecular and Surface Forces*; Academic Press, 2011.
(6) Treloar, L. G. *The Physics of Rubber Elasticity*; Oxford University Press, 1975.
(7) Rubinstein, M.; Colby, R. H. *Polymer Physics*; Oxford University Press, 2003.
(8) Ferry, J. D. *Viscoelastic Properties of Polymers*; John Wiley & Sons, 1980.
(9) Thomas, A. G. The Development of Fracture Mechanics for Elastomers. *Rubber Chem. Technol.* **1994**, *67*, 50−67.
(10) Paris, P. C. Fracture Mechanics and Fatigue: A historical perspective. *Fatigue Fract. Eng. Mater. Struct.* **1998**, *21*, 535−540.
(11) Cotterell, B. *Fracture and Life*; World Scientific, 2010.
(12) Griffith, A. A. VI. The phenomena of rupture and flow in solids. *Philos. Trans. R. Soc. London A* **1921**, *221*, 163−198.
(13) Obreimoff, J. W. The splitting strength of mica. *Proc. R. Soc. A* **1930**, *127*, 290−297.
(14) Orowan, E. The Fatigue of Glass Under Stress. *Nature* **1944**, *154*, 341−343.
(15) Irwin, G. R. Fracture dynamics, fracture of metals. *American Society for Metals (ASM) Symposium*, 1947.
(16) Orowan, E. Fracture and strength of solids. *Rep. Prog. Phys.* **1949**, *12*, 185.
(17) Rivlin, R. S.; Thomas, A. G. Rupture of rubber. I. Characteristic energy for tearing. *J. Polym. Sci.* **1953**, *10*, 291−318.
(18) Benbow, J. J.; Roesler, F. C. Experiments on Controlled Fractures. *Proc. Phys. Soc. B* **1957**, *70*, 201.
(19) Evans, A. G. Perspective on the development of high-toughness ceramics. *J. Am. Ceram. Soc.* **1990**, *73*, 187−206.
(20) Launey, M. E.; Ritchie, R. O. On the Fracture Toughness of Advanced Materials. *Adv. Mater.* **2009**, *21*, 2103−2110.
(21) Thomas, A. G. Rupture of rubber. V. Cut growth in natural rubber vulcanizates. *J. Polym. Sci.* **1958**, *31*, 467−480.
(22) Paris, P. C. A rational analytic theory of fatigue. *Trends Eng.* **1961**, *13*, 9−14.
(23) Mullins, L. Rupture of Rubber, Part IX: Role of Hysteresis in the Tearing of Rubber. *Transactions, I. R. I.* **1985**, *35*, 213−222.
(24) Greensmith, H. W. Rupture of rubber. VIII. Comparisons of tear and tensile rupture measurements. *J. Appl. Polym. Sci.* **1960**, *3*, 183−193.
(25) Braden, M.; Gent, A. N. The attack of ozone on stretched rubber vulcanizates. I. The rate of cut growth. *J. Appl. Polym. Sci.* **1960**, *3*, 90−99.
(26) Wiederhorn, S. M. Influence of Water Vapor on Crack Propagation in Soda-Lime Glass. *J. Am. Ceram. Soc.* **1967**, *50*, 407−414.
(27) Lake, G. J.; Thomas, A. G. The strength of highly elastic materials. *Proc. R. Soc. A* **1967**, *300*, 108−119.
(28) Rice, J. R. Thermodynamics of the quasi-static growth of Griffith cracks. *J. Mech. Phys. Solids* **1978**, *26*, 61−78.
(29) Gong, J. P.; Katsuyama, Y.; Kurokawa, T.; Osada, Y. Double-Network Hydrogels with Extremely High Mechanical Strength. *Adv. Mater.* **2003**, *15*, 1155−1158.
(30) Gent, A. N. In *10 - Strength of Elastomers*; Mark, J. E., Erman, B., Eirich, F. R., Eds.; Academic Press: Burlington, 2005.
(31) Gong, J. P. Why are double network hydrogels so tough? *Soft Matter* **2010**, *6*, 2583−2590.
(32) Haque, M. A.; Kurokawa, T.; Gong, J. P. Super tough double network hydrogels and their application as biomaterials. *Polymer* **2012**, *53*, 1805−1822.
(33) Shibayama, M. Structure-mechanical property relationship of tough hydrogels. *Soft Matter* **2012**, *8*, 8030−8038.
(34) Zhao, X. Multi-scale multi-mechanism design of tough hydrogels: building dissipation into stretchy networks. *Soft Matter* **2014**, *10*, 672−687.
(35) Creton, C.; Ciccotti, M. Fracture and adhesion of soft materials: a review. *Rep. Prog. Phys.* **2016**, *79*, 046601.
(36) Long, R.; Hui, C. Fracture toughness of hydrogels: measurement and interpretation. *Soft Matter* **2016**, *12*, 8069−8086.
(37) Creton, C. 50th Anniversary Perspective: Networks and Gels: Soft but Dynamic and Tough. *Macromolecules* **2017**, *50*, 8297−8316.
(38) Zhao, X. Designing toughness and strength for soft materials. *Proc. Natl. Acad. Sci. U. S. A.* **2017**, *114*, 8138−8140.
(39) Bai, R.; Yang, J.; Suo, Z. Fatigue of hydrogels. *Eur. J. Mech. A/Solids* **2019**, *74*, 337−370.
(40) Yang, J.; Bai, R.; Chen, B.; Suo, Z. Hydrogel Adhesion: A Supramolecular Synergy of Chemistry, Topology, and Mechanics. *Adv. Funct. Mater.* **2020**, *30*, 1901693.
(41) Zhao, X.; Chen, X.; Yuk, H.; Lin, S.; Liu, X.; Parada, G. Soft Materials by Design: Unconventional Polymer Networks Give Extreme Properties. *Chem. Rev.* **2021**, *121*, 4309−4372.
(42) Long, R.; Hui, C.; Gong, J. P.; Bouchbinder, E. The Fracture of Highly Deformable Soft Materials: A Tale of Two Length Scales. *Annu. Rev. Condens. Matter Phys.* **2021**, *12*, 71−94.
(43) Kuang, X.; Arıcan, M. O.; Zhou, T.; Zhao, X.; Zhang, Y. S. Functional Tough Hydrogels: Design, Processing, and Biomedical Applications. *Accounts Mater. Res.* **2023**, *4*, 101−114.
(44) Mayumi, K.; Liu, C.; Yasuda, Y.; Ito, K. Softness, Elasticity, and Toughness of Polymer Networks with Slide-Ring Cross-Links. *Gels* **2021**, *7*, 91.
(45) Wang, M.; Hu, J.; Dickey, M. D. Tough Ionogels: Synthesis, Toughening Mechanisms, and Mechanical Properties—A Perspective. *JACS Au* **2022**, *2*, 2645−2657.
(46) Li, X.; Gong, J. P. Design principles for strong and tough hydrogels. *Nat. Rev. Mater.* **2024**, *9*, 380−398.
(47) Han, Z.; Lu, Y.; Qu, S. Design of Fatigue-Resistant Hydrogels. *Adv. Funct. Mater.* **2024**, *34*, 2313498.
(48) Xu, C.; Chen, Y.; Zhao, S.; Li, D.; Tang, X.; Zhang, H.; Huang, J.; Guo, Z.; Liu, W. Mechanical Regulation of Polymer Gels. *Chem. Rev.* **2024**, *124*, 10435−10508.
(49) Cho, Y. E.; Lee, S.; Ma, S. J.; Sun, J. Network design for soft materials: addressing elasticity and fracture resistance challenges. *Soft Matter* **2025**, *21*, 1603−1623.
(50) Steck, J.; Ahn, C. H.; Suo, Z. Polymers Resist Fatigue Crack Growth by Deconcentrating Stress. *Annu. Rev. Mater. Res.* **2025**, *55*, 333−358.
(51) Duan, S.; Hua, M.; Zhang, C. W.; Hong, W.; Yan, Y.; Jazzar, A.; Chen, C.; Shi, P.; Si, M.; Wu, D.; Lin, Z.; He, P.; Du, Y.; He, X. Noncovalent Aggregation for Diverse Properties in Hydrogels: A Comprehensive Review. *Chem. Rev.* **2025**, *125*, 7918−7964.
(52) Yang, C.; Suo, Z. Hydrogel ionotronics. *Nat. Rev. Mater.* **2018**, *3*, 125−142.
(53) Gibbs, J. W. On the equilibrium of heterogeneous substances. *Am. J. Sci.* **1878**, *s3-16*, 452−458.
(54) Smith, T. L. Strength of elastorners—a perspective. *Polym. Eng. Sci.* **1977**, *17*, 129−143.
(55) Bueche, F. Tensile strength of rubbers. *J. Polym. Sci.* **1957**, *24*, 189−200.


https://doi.org/10.1021/acs.chemrev.5c00663
*Chem. Rev.* XXXX, XXX, XXX−XXX

(56) Yang, C.; Yin, T.; Suo, Z. Polyacrylamide hydrogels. I. Network imperfection. *J. Mech. Phys. Solids* **2019**, *131*, 43−55.
(57) Tao, M.; Lavoie, S.; Suo, Z.; Cameron, M. K. The effect of scatter of polymer chain length on strength. *Extreme Mech. Lett.* **2023**, *61*, 102024.
(58) Mohanty, S.; Blanchet, J.; Suo, Z.; Cai, W. Why is the strength of a polymer network so low? *arXiv* 2025, DOI: 10.48550/arXiv.2502.11339.
(59) Yu, Z.; Jackson, N. E. Shortest Paths Govern Bond Rupture in Thermoset Networks. *Macromolecules* **2025**, *58*, 1728−1736.
(60) Tada, H.; Paris, P. C.; Irwin, G. R. *The Stress Analysis of Cracks Handbook*; ASME Press, 2000.
(61) Lindley, P. B. Energy for crack growth in model rubber components. *J. Strain Anal. Eng. Des.* **1972**, *7*, 132−140.
(62) Long, R.; Hui, C. Crack tip fields in soft elastic solids subjected to large quasi-static deformation — A review. *Extreme Mech. Lett.* **2015**, *4*, 131−155.
(63) Chen, C.; Wang, Z.; Suo, Z. Flaw sensitivity of highly stretchable materials. *Extreme Mech. Lett.* **2017**, *10*, 50−57.
(64) Sun, J.; Zhao, X.; Illeperuma, W. R.; Chaudhuri, O.; Oh, K. H.; Mooney, D. J.; Vlassak, J. J.; Suo, Z. Highly stretchable and tough hydrogels. *Nature* **2012**, *489*, 133−136.
(65) Drury, J. L.; Dennis, R. G.; Mooney, D. J. The tensile properties of alginate hydrogels. *Biomaterials* **2004**, *25*, 3187−3199.
(66) Baumberger, T.; Ronsin, O. From thermally activated to viscosity controlled fracture of biopolymer hydrogels. *J. Chem. Phys.* **2009**, *130*, 061102.
(67) Akagi, Y.; Sakurai, H.; Gong, J. P.; Chung, U.; Sakai, T. Fracture energy of polymer gels with controlled network structures. *J. Chem. Phys.* **2013**, *139*, 144905.
(68) Nian, G.; Kim, J.; Bao, X.; Suo, Z. Making Highly Elastic and Tough Hydrogels from Doughs. *Adv. Mater.* **2022**, *34*, 2206577.
(69) Kim, J.; Zhang, G.; Shi, M.; Suo, Z. Fracture, fatigue, and friction of polymers in which entanglements greatly outnumber cross-links. *Science* **2021**, *374*, 212−216.
(70) Wang, Y.; Nian, G.; Kim, J.; Suo, Z. Polyacrylamide hydrogels. VI. Synthesis-property relation. *J. Mech. Phys. Solids* **2023**, *170*, 105099.
(71) Fleck, N. A.; Kang, K. J.; Ashby, M. F. Overview no. 112: The cyclic properties of engineering materials. *Acta Metall. Mater.* **1994**, *42*, 365−381.
(72) Yang, C. H.; Wang, M. X.; Haider, H.; Yang, J. H.; Sun, J.; Chen, Y. M.; Zhou, J.; Suo, Z. Strengthening Alginate/Polyacrylamide Hydrogels Using Various Multivalent Cations. *ACS Appl. Mater. Interfaces* **2013**, *5*, 10418−10422.
(73) Wang, Z.; Xiang, C.; Yao, X.; Le Floch, P.; Mendez, J.; Suo, Z. Stretchable materials of high toughness and low hysteresis. *Proc. Natl. Acad. Sci. U. S. A.* **2019**, *116*, 5967−5972.
(74) Launey, M. E.; Buehler, M. J.; Ritchie, R. O. On the Mechanistic Origins of Toughness in Bone. *Annu. Rev. Mater. Res.* **2010**, *40*, 25−53.
(75) Zeng, L.; Liu, F.; Yu, Q.; Jin, C.; Yang, J.; Suo, Z.; Tang, J. Flaw-insensitive fatigue resistance of chemically fixed collagenous soft tissues. *Sci. Adv.* **2023**, *9*, No. eade7375.
(76) Nian, G.; Chen, Z.; Bao, X.; Tan, M. W. M.; Kutsovsky, Y.; Suo, Z. Natural rubber with high resistance to crack growth. *Nat. Sustain.* **2025**, *8*, 692−701.
(77) Gent, A. N. *Engineering with Rubber: How to Design Rubber Components*; Carl Hanser Verlag GmbH Co KG, 2012.
(78) Wang, M. Effect of Polymer-Filler and Filler-Filler Interactions on Dynamic Properties of Filled Vulcanizates. *Rubber Chem. Technol.* **1998**, *71*, 520−589.
(79) Chan, M. K. V.; Williams, J. G. Plane strain fracture toughness testing of high density polyethylene. *Polym. Eng. Sci.* **1981**, *21*, 1019−1026.
(80) Lamri, A.; Shirinbayan, M.; Pereira, M.; Truffault, L.; Fitoussi, J.; Lamouri, S.; Bakir, F.; Tcharkhtchi, A. Effects of strain rate and temperature on the mechanical behavior of high-density polyethylene. *J. Appl. Polym. Sci.* **2020**, *137*, 48778.
(81) Chen, Z.; Zhang, G.; Luo, Y.; Suo, Z. Rubber-glass nanocomposites fabricated using mixed emulsions. *Proc. Natl. Acad. Sci. U. S. A.* **2024**, *121*, No. e2322684121.
(82) Scetta, G.; Euchler, E.; Ju, J.; Selles, N.; Heuillet, P.; Ciccotti, M.; Creton, C. Self-Organization at the Crack Tip of Fatigue-Resistant Thermoplastic Polyurethane Elastomers. *Macromolecules* **2021**, *54*, 8726−8737.
(83) Hua, M.; Wu, S.; Ma, Y.; Zhao, Y.; Chen, Z.; Frenkel, I.; Strzalka, J.; Zhou, H.; Zhu, X.; He, X. Strong tough hydrogels via the synergy of freeze-casting and salting out. *Nature* **2021**, *590*, 594−599.
(84) Bao, G.; Suo, Z. Remarks on Crack-Bridging Concepts. *Appl. Mech. Rev.* **1992**, *45*, 355−366.
(85) Dugdale, D. S. Yielding of steel sheets containing slits. *J. Mech. Phys. Solids* **1960**, *8*, 100−104.
(86) Zhou, Y.; Hu, J.; Zhao, P.; Zhang, W.; Suo, Z.; Lu, T. Flaw-sensitivity of a tough hydrogel under monotonic and cyclic loads. *J. Mech. Phys. Solids* **2021**, *153*, 104483.
(87) Flory, P. J. *Principles of Polymer Chemistry*; Cornell University Press, 1953.
(88) Mark, J. E.; Mark, J. E. *Physical Properties of Polymers Handbook*; Springer, 2007.
(89) Zhang, W.; Gao, Y.; Yang, H.; Suo, Z.; Lu, T. Fatigue-resistant adhesion I. Long-chain polymers as elastic dissipaters. *Extreme Mech. Lett.* **2020**, *39*, 100813.
(90) Wang, S.; Hartquist, C.; Zhao, X.; Deng, B. Nonlocal Intrinsic Fracture Energy of Polymerlike Networks. *Phys. Rev. Lett.* **2023**, *131*, 228102.
(91) Wang, S.; Cui, Q.; Matusik, W.; Deng, B.; Zhao, X.; Hartquist, C. Scaling Law for Intrinsic Fracture Energy of Diverse Stretchable Networks. *Phys. Rev. X.* **2025**, *15*, 011002.
(92) Yu, Q. M.; Tanaka, Y.; Furukawa, H.; Kurokawa, T.; Gong, J. P. Direct Observation of Damage Zone around Crack Tips in Double-Network Gels. *Macromolecules* **2009**, *42*, 3852−3855.
(93) Ducrot, E.; Chen, Y.; Bulters, M.; Sijbesma, R. P.; Creton, C. Toughening Elastomers with Sacrificial Bonds and Watching Them Break. *Science* **2014**, *344*, 186−189.
(94) Ahagon, A.; Gent, A. N. Threshold fracture energies for elastomers. *J. Polym. Sci. Polym. Phys. Ed.* **1975**, *13*, 1903−1911.
(95) Robertson, C. G.; Stoček, R.; Mars, W. V. In *The Fatigue Threshold of Rubber and Its Characterization Using the Cutting Method*; Heinrich, G., Kipscholl, R., Stoček, R., Eds.; Springer International Publishing: Cham, 2021.
(96) Hassan, S.; Kim, J.; Suo, Z. Polyacrylamide hydrogels. IV. Near-perfect elasticity and rate-dependent toughness. *J. Mech. Phys. Solids* **2022**, *158*, 104675.
(97) Ahn, C. H.; Chen, Z.; Bao, X.; Suo, Z. How does a polymer glass resist fatigue crack growth? *Soft Matter* **2025**, *21*, 3040−3046.
(98) Bhowmick, A. K. Threshold Fracture of Elastomers. *Journal of Macromolecular Science, Part C* **1988**, *28*, 339−370.
(99) Steck, J.; Kim, J.; Kutsovsky, Y.; Suo, Z. Multiscale stress deconcentration amplifies fatigue resistance of rubber. *Nature* **2023**, *624*, 303−308.
(100) Guo, X.; Dong, X.; Zou, G.; Zhang, H.; Zeng, K.; Gao, H.; Zhai, W. Multiscale toughening mechanisms in biomimetic tendon-like hydrogels. *Proc. Natl. Acad. Sci. U. S. A.* **2025**, *122*, No. e2424124122.
(101) Xiang, C.; Wang, Z.; Yang, C.; Yao, X.; Wang, Y.; Suo, Z. Stretchable and fatigue-resistant materials. *Mater. Today* **2020**, *34*, 7−16.
(102) Tvergaard, V.; Hutchinson, J. W. The relation between crack growth resistance and fracture process parameters in elastic-plastic solids. *J. Mech. Phys. Solids* **1992**, *40*, 1377−1397.
(103) Rühle, M.; Evans, A. G. High toughness ceramics and ceramic composites. *Prog. Mater. Sci.* **1989**, *33*, 85−167.
(104) Zhang, T.; Lin, S.; Yuk, H.; Zhao, X. Predicting fracture energies and crack-tip fields of soft tough materials. *Extreme Mech. Lett.* **2015**, *4*, 1−8.
(105) Catalanotti, G.; Camanho, P. P.; Xavier, J.; Dávila, C. G.; Marques, A. T. Measurement of resistance curves in the longitudinal


https://doi.org/10.1021/acs.chemrev.5c00663
Chem. Rev. XXXX, XXX, XXX−XXX

failure of composites using digital image correlation. *Compos. Sci. Technol.* **2010**, *70*, 1986−1993.
(106) Brandes, E. A.; Brook, G. B. *Smithells Metals Reference Book*; Elsevier, 2013.
(107) Hutchinson, J. W.; Suo, Z. In *Mixed Mode Cracking in Layered Materials*; Hutchinson, J. W., Wu, T. Y., Eds.; Elsevier, 1991; Vol. *29*.
(108) Nalla, R. K.; Kruzic, J. J.; Kinney, J. H.; Ritchie, R. O. Mechanistic aspects of fracture and R-curve behavior in human cortical bone. *Biomaterials* **2005**, *26*, 217−231.
(109) Yang, Q. D.; Thouless, M. D. Mixed-mode fracture analyses of plastically-deforming adhesive joints. *Int. J. Fract.* **2001**, *110*, 175−187.
(110) Gent, A. N. Adhesion and Strength of Viscoelastic Solids. Is There a Relationship between Adhesion and Bulk Properties? *Langmuir* **1996**, *12*, 4492−4496.
(111) Gent, A. N.; Petrich, R. P.; Tabor, D. Adhesion of viscoelastic materials to rigid substrates. *Proc. R. Soc. A* **1969**, *310*, 433−448.
(112) de Gennes, P. G. Soft Adhesives. *Langmuir* **1996**, *12*, 4497−4500.
(113) Knauss, W. G. A review of fracture in viscoelastic materials. *Int. J. Fract.* **2015**, *196*, 99−146.
(114) Brener, E. A.; Persson, B. N. J. Crack propagation in viscoelastic solids. *Phys. Rev. E* **2005**, *71*, 036123.
(115) Bai, R.; Chen, B.; Yang, J.; Suo, Z. Tearing a hydrogel of complex rheology. *J. Mech. Phys. Solids* **2019**, *125*, 749−761.
(116) Yang, X.; Yang, J.; Chen, L.; Suo, Z. Hydrolytic crack in a rubbery network. *Extreme Mech. Lett.* **2019**, *31*, 100531.
(117) Stengl, R.; Tan, T.; Gösele, U. A Model for the Silicon Wafer Bonding Process. *Jpn. J. Appl. Phys.* **1989**, *28*, 1735.
(118) Ciccotti, M. Stress-corrosion mechanisms in silicate glasses. *J. Phys. D: Appl. Phys.* **2009**, *42*, 214006.
(119) Shi, M.; Jiao, Q.; Yin, T.; Vlassak, J. J.; Suo, Z. Hydrolysis embrittles poly(lactic acid). *MRS Bull.* **2023**, *48*, 45−55.
(120) Kadoma, A.; Jiao, Q.; Vlassak, J. J.; Suo, Z. Hydrolytic crack growth and embrittlement in poly(ethylene terephthalate). *J. Mech. Phys. Solids* **2023**, *176*, 105303.
(121) Shi, M.; Steck, J.; Yang, X.; Zhang, G.; Yin, J.; Suo, Z. Cracks outrun erosion in degradable polymers. *Extreme Mech. Lett.* **2020**, *40*, 100978.
(122) Jiao, Q.; Shi, M.; Yin, T.; Suo, Z.; Vlassak, J. J. Composites retard hydrolytic crack growth. *Extreme Mech. Lett.* **2021**, *48*, 101433.
(123) Gent, A. N. Some chemical effects in fatigue cracking of vulcanized rubbers. *J. Appl. Polym. Sci.* **1962**, *6*, 497−502.
(124) Colin, X.; Mavel, A.; Marais, C.; Verdu, J. Interaction between Cracking and Oxidation in Organic Matrix Composites. *J. Compos. Mater.* **2005**, *39*, 1371−1389.
(125) Hong, W.; Zhao, X.; Zhou, J.; Suo, Z. A theory of coupled diffusion and large deformation in polymeric gels. *J. Mech. Phys. Solids* **2008**, *56*, 1779−1793.
(126) Yu, Y.; Landis, C. M.; Huang, R. Steady-state crack growth in polymer gels: A linear poroelastic analysis. *J. Mech. Phys. Solids* **2018**, *118*, 15−39.
(127) Rice, J. R.; Cleary, M. P. Some basic stress diffusion solutions for fluid-saturated elastic porous media with compressible constituents. *Rev. Geophys.* **1976**, *14*, 227−241.
(128) Noselli, G.; Lucantonio, A.; McMeeking, R. M.; DeSimone, A. Poroelastic toughening in polymer gels: A theoretical and numerical study. *J. Mech. Phys. Solids* **2016**, *94*, 33−46.
(129) Naassaoui, I.; Ronsin, O.; Baumberger, T. A poroelastic signature of the dry/wet state of a crack tip propagating steadily in a physical hydrogel. *Extreme Mech. Lett.* **2018**, *22*, 8−12.
(130) Baumberger, T.; Ronsin, O. Environmental control of crack propagation in polymer hydrogels. *Mech. Soft Mater.* **2020**, *2*, 14.
(131) Yang, Y.; Guo, H.; Du, Z.; Hong, W.; Lu, T.; Wang, T. Rate-dependent fracture of hydrogels due to water migration. *J. Mech. Phys. Solids* **2022**, *167*, 105007.
(132) Caulfield, M. J.; Qiao, G. G.; Solomon, D. H. Some Aspects of the Properties and Degradation of Polyacrylamides. *Chem. Rev.* **2002**, *102*, 3067−3084.
(133) Kulicke, W. M.; Kniewske, R.; Klein, J. Preparation, characterization, solution properties and rheological behaviour of polyacrylamide. *Prog. Polym. Sci.* **1982**, *8*, 373−468.
(134) Gupta, M. K.; Bansil, R. Laser Raman spectroscopy of polyacrylamide. *J. Polym. Sci. Polym. Phys. Ed.* **1981**, *19*, 353−360.
(135) Sekine, Y.; Takagi, H.; Sudo, S.; Kajiwara, Y.; Fukazawa, H.; Ikeda-Fukazawa, T. Dependence of structure of polymer side chain on water structure in hydrogels. *Polymer* **2014**, *55*, 6320−6324.
(136) Hatakeyema, T.; Yamauchi, A.; Hatakeyema, H. Studies on bound water in poly(vinyl alcohol). Hydrogel by DSC and FT-NMR. *Eur. Polym. J.* **1984**, *20*, 61−64.
(137) Yan, C.; Kramer, P. L.; Yuan, R.; Fayer, M. D. Water Dynamics in Polyacrylamide Hydrogels. *J. Am. Chem. Soc.* **2018**, *140*, 9466−9477.
(138) Tanaka, N.; Ito, K.; Kitano, H. Raman spectroscopic study of hydrogen bonding of polyacrylamide in heavy water. *Macromolecules* **1994**, *27*, 540−544.
(139) Zhang, E.; Bai, R.; Morelle, X. P.; Suo, Z. Fatigue fracture of nearly elastic hydrogels. *Soft Matter* **2018**, *14*, 3563−3571.
(140) Zhong, D.; Wang, Z.; Xu, J.; Liu, J.; Xiao, R.; Qu, S.; Yang, W. A strategy for tough and fatigue-resistant hydrogels via loose cross-linking and dense dehydration-induced entanglements. *Nat. Commun.* **2024**, *15*, 5896.
(141) Sato, K.; Nakajima, T.; Hisamatsu, T.; Nonoyama, T.; Kurokawa, T.; Gong, J. P. Phase-Separation-Induced Anomalous Stiffening, Toughening, and Self-Healing of Polyacrylamide Gels. *Adv. Mater.* **2015**, *27*, 6990−6998.
(142) Takeo Masuike, T. M.; Seiji Taki, S. T.; Kazuhiro Hara, K. H.; Shoichi Kai, S. K. Change of Temperature and Elastic Stiffness during Dehydration Process of Polyacrylamide Gel. *Jpn. J. Appl. Phys.* **1995**, *34*, 4997.
(143) Wang, M.; Xiao, X.; Siddika, S.; Shamsi, M.; Frey, E.; Qian, W.; Bai, W.; O Connor, B. T.; Dickey, M. D. Glassy gels toughened by solvent. *Nature* **2024**, *631*, 313−318.
(144) Zheng, D.; Lin, S.; Ni, J.; Zhao, X. Fracture and fatigue of entangled and unentangled polymer networks. *Extreme Mech. Lett.* **2022**, *51*, 101608.
(145) Waltz, V.; Yeh, C. J.; Baumann, C.; Göstl, R.; Comtet, J.; Creton, C.; Slootman, J. Quantifying Rate- and Temperature-Dependent Molecular Damage in Elastomer Fracture. *Phys. Rev. X.* **2020**, *10*, 041045.
(146) Wang, S.; Panyukov, S.; Rubinstein, M.; Craig, S. L. Quantitative Adjustment to the Molecular Energy Parameter in the Lake-Thomas Theory of Polymer Fracture Energy. *Macromolecules* **2019**, *52*, 2772−2777.
(147) Saitta, A. M.; Klein, M. L. Polyethylene under tensil load: Strain energy storage and breaking of linear and knotted alkanes probed by first-principles molecular dynamics calculations. *J. Chem. Phys.* **1999**, *111*, 9434−9440.
(148) Du, C.; Hill, R. J. Complementary-DNA-Strand Cross-Linked Polyacrylamide Hydrogels. *Macromolecules* **2019**, *52*, 6683−6697.
(149) Zheng, Y.; Kiyama, R.; Matsuda, T.; Cui, K.; Li, X.; Cui, W.; Guo, Y.; Nakajima, T.; Kurokawa, T.; Gong, J. P. Nanophase Separation in Immiscible Double Network Elastomers Induces Synergetic Strengthening, Toughening, and Fatigue Resistance. *Chem. Mater.* **2021**, *33*, 3321−3334.
(150) Zhang, G.; Kim, J.; Hassan, S.; Suo, Z. Self-assembled nanocomposites of high water content and load-bearing capacity. *Proc. Natl. Acad. Sci. U. S. A.* **2022**, *119*, No. e2203962119.
(151) de Gennes, P. G. Reptation of a Polymer Chain in the Presence of Fixed Obstacles. *J. Chem. Phys.* **1971**, *55*, 572−579.
(152) Doi, M.; Edwards, S. F. Dynamics of concentrated polymer systems. Part 1.—Brownian motion in the equilibrium state. *J. Chem. Soc., Faraday Trans. 2* **1978**, *74*, 1789−1801.
(153) Rubinstein, M. Discretized model of entangled-polymer dynamics. *Phys. Rev. Lett.* **1987**, *59*, 1946−1949.
(154) Rubinstein, M.; Panyukov, S. Elasticity of Polymer Networks. *Macromolecules* **2002**, *35*, 6670−6686.


https://doi.org/10.1021/acs.chemrev.5c00663
*Chem. Rev.* XXXX, XXX, XXX−XXX

(155) Norioka, C.; Inamoto, Y.; Hajime, C.; Kawamura, A.; Miyata, T. A universal method to easily design tough and stretchable hydrogels. *NPG Asia Mater.* **2021**, *13*, 34.
(156) Bao, X.; Nian, G.; Kutsovsky, Y.; Kim, J.; Jiao, Q.; Suo, Z. Low-intensity mixing process of high molecular weight polymer chains leads to elastomers of long network strands and high fatigue threshold. *Soft Matter* **2023**, *19*, 5956−5966.
(157) Dhand, A. P.; Davidson, M. D.; Zlotnick, H. M.; Kolibaba, T. J.; Killgore, J. P.; Burdick, J. A. Additive manufacturing of highly entangled polymer networks. *Science* **2024**, *385*, 566−572.
(158) Fu, L.; Li, L.; Bian, Q.; Xue, B.; Jin, J.; Li, J.; Cao, Y.; Jiang, Q.; Li, H. Cartilage-like protein hydrogels engineered via entanglement. *Nature* **2023**, *618*, 740−747.
(159) Wang, F.; Kosovsky, L. M.; Krist, E. C.; Kruse, B. J.; Zhukhovitskiy, A. V. Trapped entanglements in polymer networks: formation and characterization. *Trends in Chemistry* **2024**, *6*, 447−458.
(160) Graessley, W. W. *The Entanglement Concept in Polymer Rheology*; Springer: Berlin, 1974.
(161) Kavassalis, T. A.; Noolandi, J. Entanglement scaling in polymer melts and solutions. *Macromolecules* **1989**, *22*, 2709−2720.
(162) Zhang, G.; Steck, J.; Kim, J.; Ahn, C. H.; Suo, Z. Hydrogels of arrested phase separation simultaneously achieve high strength and low hysteresis. *Sci. Adv.* **2023**, *9*, No. eadh7742.
(163) Bao, X.; Chen, Z.; Nian, G.; Tan, M. W. M.; Ahn, C. H.; Kutsovsky, Y.; Suo, Z. Unusually long polymers crosslinked by domains of physical bonds. *Nat. Commun.* **2025**, *16*, 4749.
(164) Zhu, R.; Zhu, D.; Zheng, Z.; Wang, X. Tough double network hydrogels with rapid self-reinforcement and low hysteresis based on highly entangled networks. *Nat. Commun.* **2024**, *15*, 1344.
(165) Liang, C.; Dudko, V.; Khoruzhenko, O.; Hong, X.; Lv, Z.; Tunn, I.; Umer, M.; Timonen, J. V. I.; Linder, M. B.; Breu, J.; Ikkala, O.; Zhang, H. Stiff and self-healing hydrogels by polymer entanglements in co-planar nanoconfinement. *Nat. Mater.* **2025**, *24*, 599−606.
(166) Wang, F.; Kruse, B. J.; Dickenson, J. C.; Zhukhovitskiy, A. V. Supramolecular Templation of Entanglements and Their Spectroscopic Detection in Polymer Elastomers. *Macromolecules* **2024**, *57*, 4016−4023.
(167) Pike, M.; Watson, W. F. Mastication of rubber, I. Mechanism of plasticizing by cold mastication. *J. Polym. Sci.* **1952**, *9*, 229−251.
(168) Ceresa, R. J.; Watson, W. F. Mastication of rubber. VII. Mechanical degradation of polymers during mastication. *J. Appl. Polym. Sci.* **1959**, *1*, 101−106.
(169) Colby, R. H.; Fetters, L. J.; Graessley, W. W. The melt viscosity-molecular weight relationship for linear polymers. *Macromolecules* **1987**, *20*, 2226−2237.
(170) Aguirre, M.; Ballard, N.; Gonzalez, E.; Hamzehlou, S.; Sardon, H.; Calderon, M.; Paulis, M.; Tomovska, R.; Dupin, D.; Bean, R. H.; Long, T. E.; Leiza, J. R.; Asua, J. M. Polymer Colloids: Current Challenges, Emerging Applications, and New Developments. *Macromolecules* **2023**, *56*, 2579−2607.
(171) van Beilen, J. B.; Poirier, Y. Establishment of new crops for the production of natural rubber. *Trends. Biotechnol.* **2007**, *25*, 522−529.
(172) Lovell, P. A.; Schork, F. J. Fundamentals of Emulsion Polymerization. *Biomacromolecules* **2020**, *21*, 4396−4441.
(173) Winnik, M. A. Latex film formation. *Curr. Opin. Colloid Interface Sci.* **1997**, *2*, 192−199.
(174) Taylor, J. W.; Winnik, M. A. Functional latex and thermoset latex films. *JCT Research* **2004**, *1*, 163−190.
(175) Dillon, R. E.; Matheson, L. A.; Bradford, E. B. Sintering of synthetic latex particles. *Journal of Colloid Science* **1951**, *6*, 108−117.
(176) Routh, A. F.; Russel, W. B. A Process Model for Latex Film Formation: Limiting Regimes for Individual Driving Forces. *Langmuir* **1999**, *15*, 7762−7773.
(177) Hahn, K.; Ley, G.; Schuller, H.; Oberthür, R. On particle coalescence in latex films. *Colloid Polym. Sci.* **1986**, *264*, 1092−1096.
(178) Takamura, K.; Urban, D. *Polymer Dispersions and Their Industrial Applications*; Wiley Online Library, 2003.
(179) Fetters, L. J.; Lohse, D. J.; Richter, D.; Witten, T. A.; Zirkel, A. Connection between Polymer Molecular Weight, Density, Chain Dimensions, and Melt Viscoelastic Properties. *Macromolecules* **1994**, *27*, 4639−4647.
(180) Tanaka, Y.; Tarachiwin, L. Recent Advances in Structural Characterization of Natural Rubber. *Rubber Chem. Technol.* **2009**, *82*, 283−314.
(181) Tanaka, Y. Structural Characterization of Natural Polyisoprenes: Solve the Mystery of Natural Rubber Based on Structural Study. *Rubber Chem. Technol.* **2001**, *74*, 355−375.
(182) Tarkanian, M. J.; Hosler, D. America's First Polymer Scientists: Rubber Processing, Use and Transport in Mesoamerica. *Lat. Am. Antiq.* **2011**, *22*, 469−486.
(183) Morawetz, H. History of Rubber Research. *Rubber Chem. Technol.* **2000**, *73*, 405−426.
(184) Hancock, T. *Personal Narrative of the Origin and Progress of the Caoutchouc or India-Rubber Manufacture in England*; Longman, Brown, Green, Longmans, & Roberts: London, 1857.
(185) Calzonetti, J. A.; Laursen, C. J. Patents of Charles Goodyear: His International Contributions to the Rubber Industry. *Rubber Chem. Technol.* **2010**, *83*, 303−321.
(186) Staudinger, H. In *On Polymerization*; Leicester, H. M., Ed.; Harvard University Press: Cambridge, MA, 1968.
(187) Katz, J. R. Röntgenspektrographische Untersuchungen am gedehnten Kautschuk und ihre mögliche Bedeutung für das Problem der Dehnungseigenschaften dieser Substanz. *Naturwissenschaften.* **1925**, *13*, 410−416.
(188) Yip, E.; Cacioli, P. The manufacture of gloves from natural rubber latex. *J. Allergy. Clin. Immunol.* **2002**, *110*, S3−S14.
(189) Medalia, A. I.; Townsend, H. B.; Grover, H. N. Measuring Wet Gel Strength of Coagulant-Dipped Films. *Anal. Chem.* **1954**, *26*, 697−703.
(190) Blackley, D. C. *Polymer Latices: Science and Technology*; Springer Science & Business Media, 2012; Vol. 3.
(191) Fries, H.; Pandit, R. R. Mastication of Rubber. *Rubber Chem. Technol.* **1982**, *55*, 309−327.
(192) Busse, W. F. Mastication of Rubber An Oxidation Process. *Industrial & Engineering Chemistry* **1932**, *24*, 140−146.
(193) Angier, D. J.; Chambers, W. T.; Watson, W. F. Mastication of rubber. VI. Viscosity and molecular weight relationships for natural rubber after cold mastication. *J. Polym. Sci.* **1957**, *25*, 129−138.
(194) Harmon, D. J.; Jacobs, H. L. Degradation of natural rubber during mill mastication. *J. Appl. Polym. Sci.* **1966**, *10*, 253−257.
(195) Miyamoto, Y.; Yamao, H.; Sekimoto, K. Crystallization and Melting of Polyisoprene Rubber under Uniaxial Deformation. *Macromolecules* **2003**, *36*, 6462−6471.
(196) Toki, S.; Fujimaki, T.; Okuyama, M. Strain-induced crystallization of natural rubber as detected real-time by wide-angle X-ray diffraction technique. *Polymer* **2000**, *41*, 5423−5429.
(197) Toki, S.; Sics, I.; Ran, S.; Liu, L.; Hsiao, B. S. Molecular orientation and structural development in vulcanized polyisoprene rubbers during uniaxial deformation by in situ synchrotron X-ray diffraction. *Polymer* **2003**, *44*, 6003−6011.
(198) Trabelsi, S.; Albouy, P. A.; Rault, J. Crystallization and Melting Processes in Vulcanized Stretched Natural Rubber. *Macromolecules* **2003**, *36*, 7624−7639.
(199) Albouy, P.; Vieyres, A.; Pérez-Aparicio, R.; Sanséau, O.; Sotta, P. The impact of strain-induced crystallization on strain during mechanical cycling of cross-linked natural rubber. *Polymer* **2014**, *55*, 4022−4031.
(200) Le Cam, J. B. Energy storage due to strain-induced crystallization in natural rubber: The physical origin of the mechanical hysteresis. *Polymer* **2017**, *127*, 166−173.
(201) Albouy, P.; Sotta, P. In *Strain-Induced Crystallization in Natural Rubber*; Auriemma, F., Alfonso, G. C., de Rosa, C., Eds.; Springer International Publishing: Cham, 2017.
(202) Candau, N.; Laghmach, R.; Chazeau, L.; Chenal, J.; Gauthier, C.; Biben, T.; Munch, E. Strain-Induced Crystallization of Natural


https://doi.org/10.1021/acs.chemrev.5c00663
*Chem. Rev.* XXXX, XXX, XXX−XXX

Rubber and Cross-Link Densities Heterogeneities. *Macromolecules* **2014**, *47*, 5815−5824.
(203) Trabelsi, S.; Albouy, P. A.; Rault, J. Stress-Induced Crystallization around a Crack Tip in Natural Rubber. *Macromolecules* **2002**, *35*, 10054−10061.
(204) Huneau, B. Strain-induced crystallization of natural rubber: A review of X-Ray Diffraction Investigations. *Rubber Chem. Technol.* **2011**, *84*, 425−452.
(205) Toki, S. *5 - The Effect of Strain-Induced Crystallization (SIC) on the Physical Properties of Natural Rubber (NR)*; Kohjiya, S., Ikeda, Y., Eds.; Woodhead Publishing, 2014.
(206) McMeeking, R. M.; Evans, A. G. Mechanics of Transformation-Toughening in Brittle Materials. *J. Am. Ceram. Soc.* **1982**, *65*, 242−246.
(207) Lindley, P. B. Relation between hysteresis and the dynamic crack growth resistance of natural rubber. *Int. J. Fract.* **1973**, *9*, 449−462.
(208) Chenal, J.; Chazeau, L.; Guy, L.; Bomal, Y.; Gauthier, C. Molecular weight between physical entanglements in natural rubber: A critical parameter during strain-induced crystallization. *Polymer* **2007**, *48*, 1042−1046.
(209) Zhu, J. Bioactive modification of poly(ethylene glycol) hydrogels for tissue engineering. *Biomaterials* **2010**, *31*, 4639−4656.
(210) Peppas, N. A.; Stauffer, S. R. Reinforced uncrosslinked poly (vinyl alcohol) gels produced by cyclic freezing-thawing processes: a short review. *J. Controlled Release* **1991**, *16*, 305−310.
(211) Wang, Z.; Wei, H.; Huang, Y.; Wei, Y.; Chen, J. Naturally sourced hydrogels: emerging fundamental materials for next-generation healthcare sensing. *Chem. Soc. Rev.* **2023**, *52*, 2992−3034.
(212) Vrandečić, N. S.; Erceg, M.; Jakić, M.; Klarić, I. Kinetic analysis of thermal degradation of poly(ethylene glycol) and poly(ethylene oxide)s of different molecular weight. *Thermochim. Acta* **2010**, *498*, 71−80.
(213) Lin, C.; Anseth, K. S. PEG Hydrogels for the Controlled Release of Biomolecules in Regenerative Medicine. *Pharm. Res.* **2009**, *26*, 631−643.
(214) Hoffman, A. S. Hydrogels for biomedical applications. *Adv. Drug Delivery Rev.* **2012**, *64*, 18−23.
(215) Quartarone, E.; Mustarelli, P.; Magistris, A. PEO-based composite polymer electrolytes. *Solid State Ion.* **1998**, *110*, 1−14.
(216) Vashahi, F.; Martinez, M. R.; Dashtimoghadam, E.; Fahimipour, F.; Keith, A. N.; Bersenev, E. A.; Ivanov, D. A.; Zhulina, E. B.; Popryadukhin, P.; Matyjaszewski, K.; Vatankhah-Varnosfaderani, M.; Sheiko, S. S. Injectable bottlebrush hydrogels with tissue-mimetic mechanical properties. *Sci. Adv.* **2022**, *8*, No. eabm2469.
(217) Durst, C. A.; Cuchiara, M. P.; Mansfield, E. G.; West, J. L.; Grande-Allen, K. J. Flexural characterization of cell encapsulated PEGDA hydrogels with applications for tissue engineered heart valves. *Acta Biomater.* **2011**, *7*, 2467−2476.
(218) Cuchiara, M. P.; Allen, A. C. B.; Chen, T. M.; Miller, J. S.; West, J. L. Multilayer microfluidic PEGDA hydrogels. *Biomaterials* **2010**, *31*, 5491−5497.
(219) Warr, C.; Valdoz, J. C.; Bickham, B. P.; Knight, C. J.; Franks, N. A.; Chartrand, N.; Van Ry, P. M.; Christensen, K. A.; Nordin, G. P.; Cook, A. D. Biocompatible PEGDA Resin for 3D Printing. *ACS Appl. Bio Mater.* **2020**, *3*, 2239−2244.
(220) Sakai, T.; Matsunaga, T.; Yamamoto, Y.; Ito, C.; Yoshida, R.; Suzuki, S.; Sasaki, N.; Shibayama, M.; Chung, U. Design and Fabrication of a High-Strength Hydrogel with Ideally Homogeneous Network Structure from Tetrahedron-like Macromonomers. *Macromolecules* **2008**, *41*, 5379−5384.
(221) Sakai, T.; Akagi, Y.; Matsunaga, T.; Kurakazu, M.; Chung, U.; Shibayama, M. Highly Elastic and Deformable Hydrogel Formed from Tetra-arm Polymers. *Macromol. Rapid Commun.* **2010**, *31*, 1954−1959.
(222) Matsunaga, T.; Sakai, T.; Akagi, Y.; Chung, U.; Shibayama, M. Structure Characterization of Tetra-PEG Gel by Small-Angle Neutron Scattering. *Macromolecules* **2009**, *42*, 1344−1351.
(223) Hiroi, T.; Ohl, M.; Sakai, T.; Shibayama, M. Multiscale Dynamics of Inhomogeneity-Free Polymer Gels. *Macromolecules* **2014**, *47*, 763−770.
(224) Akagi, Y.; Matsunaga, T.; Shibayama, M.; Chung, U.; Sakai, T. Evaluation of Topological Defects in Tetra-PEG Gels. *Macromolecules* **2010**, *43*, 488−493.
(225) Lin, T.; Wang, R.; Johnson, J. A.; Olsen, B. D. Topological Structure of Networks Formed from Symmetric Four-Arm Precursors. *Macromolecules* **2018**, *51*, 1224−1231.
(226) Lin, S.; Ni, J.; Zheng, D.; Zhao, X. Fracture and fatigue of ideal polymer networks. *Extreme Mech. Lett.* **2021**, *48*, 101399.
(227) Zhong, M.; Wang, R.; Kawamoto, K.; Olsen, B. D.; Johnson, J. A. Quantifying the impact of molecular defects on polymer network elasticity. *Science* **2016**, *353*, 1264−1268.
(228) Kienberger, F.; Pastushenko, V. P.; Kada, G.; Gruber, H. J.; Riener, C.; Schindler, H.; Hinterdorfer, P. Static and Dynamical Properties of Single Poly(Ethylene Glycol) Molecules Investigated by Force Spectroscopy. *Single Mol.* **2000**, *1*, 123−128.
(229) Okumura, Y.; Ito, K. The Polyrotaxane Gel: A Topological Gel by Figure-of-Eight Cross-links. *Adv. Mater.* **2001**, *13*, 485−487.
(230) Liu, C.; Kadono, H.; Mayumi, K.; Kato, K.; Yokoyama, H.; Ito, K. Unusual Fracture Behavior of Slide-Ring Gels with Movable Cross-Links. *ACS Macro Lett.* **2017**, *6*, 1409−1413.
(231) Jiang, L.; Liu, C.; Mayumi, K.; Kato, K.; Yokoyama, H.; Ito, K. Highly Stretchable and Instantly Recoverable Slide-Ring Gels Consisting of Enzymatically Synthesized Polyrotaxane with Low Host Coverage. *Chem. Mater.* **2018**, *30*, 5013−5019.
(232) Hu, P.; Madsen, J.; Huang, Q.; Skov, A. L. Elastomers without Covalent Cross-Linking: Concatenated Rings Giving Rise to Elasticity. *ACS Macro Lett.* **2020**, *9*, 1458−1463.
(233) Li, W.; Wang, X.; Liu, Z.; Zou, X.; Shen, Z.; Liu, D.; Li, L.; Guo, Y.; Yan, F. Nanoconfined polymerization limits crack propagation in hysteresis-free gels. *Nat. Mater.* **2024**, *23*, 131−138.
(234) Liu, C.; Morimoto, N.; Jiang, L.; Kawahara, S.; Noritomi, T.; Yokoyama, H.; Mayumi, K.; Ito, K. Tough hydrogels with rapid self-reinforcement. *Science* **2021**, *372*, 1078−1081.
(235) Mayumi, K. Tough polymer gels reinforced by strain-induced crystallization. *Polym. J.* **2025**, *57*, 449−453.
(236) Hashimoto, K.; Enoki, T.; Liu, C.; Li, X.; Sakai, T.; Mayumi, K. Strain-Induced Crystallization in Tetra-Branched Poly(ethylene glycol) Hydrogels with a Common Network Structure. *Macromolecules* **2024**, *57*, 1461−1468.
(237) Hartquist, C. M.; Lin, S.; Zhang, J. H.; Wang, S.; Rubinstein, M.; Zhao, X. An elastomer with ultrahigh strain-induced crystallization. *Sci. Adv.* **2023**, *9*, No. eadj0411.
(238) Hashimoto, K.; Shiwaku, T.; Aoki, H.; Yokoyama, H.; Mayumi, K.; Ito, K. Strain-induced crystallization and phase separation used for fabricating a tough and stiff slide-ring solid polymer electrolyte. *Sci. Adv.* **2023**, *9*, No. eadi8505.
(239) Lee, K. Y.; Mooney, D. J. Alginate: Properties and biomedical applications. *Prog. Polym. Sci.* **2012**, *37*, 106−126.
(240) Zhao, X.; Huebsch, N.; Mooney, D. J.; Suo, Z. Stress-relaxation behavior in gels with ionic and covalent crosslinks. *J. Appl. Phys.* **2010**, *107*, 063509.
(241) Baumberger, T.; Caroli, C.; Martina, D. Solvent control of crack dynamics in a reversible hydrogel. *Nat. Mater.* **2006**, *5*, 552−555.
(242) Drobny, J. G. *Handbook of Thermoplastic Elastomers*; Elsevier, 2014.
(243) Bates, C. M.; Bates, F. S. 50th Anniversary Perspective: Block Polymers—Pure Potential. *Macromolecules* **2017**, *50*, 3−22.
(244) Shi, W.; Lynd, N. A.; Montarnal, D.; Luo, Y.; Fredrickson, G. H.; Kramer, E. J.; Ntaras, C.; Avgeropoulos, A.; Hexemer, A. Toward Strong Thermoplastic Elastomers with Asymmetric Miktoarm Block Copolymer Architectures. *Macromolecules* **2014**, *47*, 2037−2043.
(245) Lodge, T. P. Block Copolymers: Past Successes and Future Challenges. *Macromol. Chem. Phys.* **2003**, *204*, 265−273.


https://doi.org/10.1021/acs.chemrev.5c00663
*Chem. Rev.* XXXX, XXX, XXX−XXX

(246) Steube, M.; Johann, T.; Barent, R. D.; Müller, A. H. E.; Frey, H. Rational design of tapered multiblock copolymers for thermoplastic elastomers. *Prog. Polym. Sci.* **2022**, *124*, 101488.
(247) Bates, F. S.; Fredrickson, G. H. Block Copolymer Thermodynamics: Theory and Experiment. *Annu. Rev. Phys. Chem.* **1990**, *41*, 525−557.
(248) Gent, A. N.; Hamed, G. R. Adhesion of Elastomers, with Special Reference to Triblock Copolymers. *Rubber Chem. Technol.* **1978**, *51*, 354−364.
(249) Liang, H.; Wang, Z.; Dobrynin, A. V. Strain-Adaptive Self-Assembled Networks of Linear-Bottlebrush-Linear Copolymers. *Macromolecules* **2019**, *52*, 8617−8624.
(250) Wang, C. Tear Strength of Styrene-Butadiene-Styrene Block Copolymers. *Macromolecules* **2001**, *34*, 9006−9014.
(251) Koo, C. M.; Hillmyer, M. A.; Bates, F. S. Structure and Properties of Semicrystalline-Rubbery Multiblock Copolymers. *Macromolecules* **2006**, *39*, 667−677.
(252) Barent, R. D.; Perevyazko, I.; Mikusheva, N.; Floudas, G.; Frey, H. Linear (IS)nI Multiblock Copolymers: Tailoring the Softness of Thermoplastic Elastomers by Flexible Polyisoprene End Blocks. *Macromolecules* **2023**, *56*, 5792−5802.
(253) Spontak, R. J.; Smith, S. D. Perfectly-alternating linear (AB)n multiblock copolymers: Effect of molecular design on morphology and properties. *J. Polym. Sci., Part B: Polym. Phys.* **2001**, *39*, 947−955.
(254) Fang, J.; Gao, X.; Luo, Y. Synthesis of (hard-soft-hard)x multiblock copolymers via RAFT emulsion polymerization and mechanical enhancement via block architectures. *Polymer* **2020**, *201*, 122602.
(255) Miao, X.; Han, R.; Tian, J.; Ma, Y.; Müller, A. J.; Li, Z. Building Ultrastrong, Tough and Biodegradable Thermoplastic Elastomers from Multiblock Copolyesters Via a "Reserve-Release" Crystallization Strategy. *Angew. Chem., Int. Ed.* **2025**, *64*, No. e202417627.
(256) Petrović, Z. S.; Ferguson, J. Polyurethane elastomers. *Prog. Polym. Sci.* **1991**, *16*, 695−836.
(257) Yilgör, I.; Yilgör, E.; Wilkes, G. L. Critical parameters in designing segmented polyurethanes and their effect on morphology and properties: A comprehensive review. *Polymer* **2015**, *58*, A1−A36.
(258) Koerner, H.; Kelley, J. J.; Vaia, R. A. Transient Microstructure of Low Hard Segment Thermoplastic Polyurethane under Uniaxial Deformation. *Macromolecules* **2008**, *41*, 4709−4716.
(259) Kojio, K.; Matsuo, K.; Motokucho, S.; Yoshinaga, K.; Shimodaira, Y.; Kimura, K. Simultaneous small-angle X-ray scattering/wide-angle X-ray diffraction study of the microdomain structure of polyurethane elastomers during mechanical deformation. *Polym. J.* **2011**, *43*, 692−699.
(260) Rahmawati, R.; Masuda, S.; Cheng, C.; Nagano, C.; Nozaki, S.; Kamitani, K.; Kojio, K.; Takahara, A.; Shinohara, N.; Mita, K.; Uchida, K.; Yamasaki, S. Investigation of Deformation Behavior of Thiourethane Elastomers Using In Situ X-ray Scattering, Diffraction, and Absorption Methods. *Macromolecules* **2019**, *52*, 6825−6833.
(261) Ng, H. N.; Allegrezza, A. E.; Seymour, R. W.; Cooper, S. L. Effect of segment size and polydispersity on the properties of polyurethane block polymers. *Polymer* **1973**, *14*, 255−261.
(262) Eceiza, A.; Martin, M. D.; de la Caba, K.; Kortaberria, G.; Gabilondo, N.; Corcuera, M. A.; Mondragon, I. Thermoplastic polyurethane elastomers based on polycarbonate diols with different soft segment molecular weight and chemical structure: Mechanical and thermal properties. *Polym. Eng. Sci.* **2008**, *48*, 297−306.
(263) Kojio, K.; Furukawa, M.; Motokucho, S.; Shimada, M.; Sakai, M. Structure-Mechanical Property Relationships for Poly(carbonate urethane) Elastomers with Novel Soft Segments. *Macromolecules* **2009**, *42*, 8322−8327.
(264) Buckley, C. P.; Prisacariu, C.; Martin, C. Elasticity and inelasticity of thermoplastic polyurethane elastomers: Sensitivity to chemical and physical structure. *Polymer* **2010**, *51*, 3213−3224.
(265) Datta, J.; Kasprzyk, P. Thermoplastic polyurethanes derived from petrochemical or renewable resources: A comprehensive review. *Polym. Eng. Sci.* **2018**, *58*, E14−E35.
(266) Wang, X.; Zhan, S.; Lu, Z.; Li, J.; Yang, X.; Qiao, Y.; Men, Y.; Sun, J. Healable, Recyclable, and Mechanically Tough Polyurethane Elastomers with Exceptional Damage Tolerance. *Adv. Mater.* **2020**, *32*, 2005759.
(267) Li, Z.; Zhu, Y.; Niu, W.; Yang, X.; Jiang, Z.; Lu, Z.; Liu, X.; Sun, J. Healable and Recyclable Elastomers with Record-High Mechanical Robustness, Unprecedented Crack Tolerance, and Superhigh Elastic Restorability. *Adv. Mater.* **2021**, *33*, 2101498.
(268) Fang, Z.; Mu, H.; Sun, Z.; Zhang, K.; Zhang, A.; Chen, J.; Zheng, N.; Zhao, Q.; Yang, X.; Liu, F.; Wu, J.; Xie, T. 3D printable elastomers with exceptional strength and toughness. *Nature* **2024**, *631*, 783−788.
(269) Scetta, G.; Selles, N.; Heuillet, P.; Ciccotti, M.; Creton, C. Cyclic fatigue failure of TPU using a crack propagation approach. *Polym. Test.* **2021**, *97*, 107140.
(270) Yeh, F.; Hsiao, B. S.; Sauer, B. B.; Michel, S.; Siesler, H. W. In-Situ Studies of Structure Development during Deformation of a Segmented Poly(urethane-urea) Elastomer. *Macromolecules* **2003**, *36*, 1940−1954.
(271) Scetta, G.; Ju, J.; Selles, N.; Heuillet, P.; Ciccotti, M.; Creton, C. Strain induced strengthening of soft thermoplastic polyurethanes under cyclic deformation. *J. Polym. Sci.* **2021**, *59*, 685−696.
(272) Stauffer, S. R.; Peppast, N. A. Poly(vinyl alcohol) hydrogels prepared by freezing-thawing cyclic processing. *Polymer* **1992**, *33*, 3932−3936.
(273) Peppas, N. A. Turbidimetric studies of aqueous poly(vinyl alcohol) solutions. *Makromol. Chem.* **1975**, *176*, 3433−3440.
(274) Hassan, C. M.; Peppas, N. A. Structure and Morphology of Freeze/Thawed PVA Hydrogels. *Macromolecules* **2000**, *33*, 2472−2479.
(275) Hassan, C. M.; Peppas, N. A. Cellular PVA hydrogels produced by freeze/thawing. *J. Appl. Polym. Sci.* **2000**, *76*, 2075−2079.
(276) Adelnia, H.; Ensandoost, R.; Shebbrin Moonshi, S.; Gavgani, J. N.; Vasafi, E. I.; Ta, H. T. Freeze/thawed polyvinyl alcohol hydrogels: Present, past and future. *Eur. Polym. J.* **2022**, *164*, 110974.
(277) Lin, S.; Liu, X.; Liu, J.; Yuk, H.; Loh, H.; Parada, G. A.; Settens, C.; Song, J.; Masic, A.; McKinley, G. H.; Zhao, X. Anti-fatigue-fracture hydrogels. *Sci. Adv.* **2019**, *5*, No. eaau8528.
(278) Lin, S.; Liu, J.; Liu, X.; Zhao, X. Muscle-like fatigue-resistant hydrogels by mechanical training. *Proc. Natl. Acad. Sci. U. S. A.* **2019**, *116*, 10244−10249.
(279) Liang, X.; Chen, G.; Lin, S.; Zhang, J.; Wang, L.; Zhang, P.; Wang, Z.; Wang, Z.; Lan, Y.; Ge, Q.; Liu, J. Anisotropically Fatigue-Resistant Hydrogels. *Adv. Mater.* **2021**, *33*, 2102011.
(280) Liu, J.; Lin, S.; Liu, X.; Qin, Z.; Yang, Y.; Zang, J.; Zhao, X. Fatigue-resistant adhesion of hydrogels. *Nat. Commun.* **2020**, *11*, 1071.
(281) Wu, S.; Hua, M.; Alsaid, Y.; Du, Y.; Ma, Y.; Zhao, Y.; Lo, C.; Wang, C.; Wu, D.; Yao, B.; Strzalka, J.; Zhou, H.; Zhu, X.; He, X. Poly(vinyl alcohol) Hydrogels with Broad-Range Tunable Mechanical Properties via the Hofmeister Effect. *Adv. Mater.* **2021**, *33*, 2007829.
(282) Guo, X.; Dong, X.; Zou, G.; Gao, H.; Zhai, W. Strong and tough fibrous hydrogels reinforced by multiscale hierarchical structures with multimechanisms. *Sci. Adv.* **2023**, *9*, No. eadf7075.
(283) Sun, T. L.; Kurokawa, T.; Kuroda, S.; Ihsan, A. B.; Akasaki, T.; Sato, K.; Haque, M. A.; Nakajima, T.; Gong, J. P. Physical hydrogels composed of polyampholytes demonstrate high toughness and viscoelasticity. *Nat. Mater.* **2013**, *12*, 932−937.
(284) Luo, F.; Sun, T. L.; Nakajima, T.; Kurokawa, T.; Zhao, Y.; Sato, K.; Ihsan, A. B.; Li, X.; Guo, H.; Gong, J. P. Oppositely Charged Polyelectrolytes Form Tough, Self-Healing, and Rebuildable Hydrogels. *Adv. Mater.* **2015**, *27*, 2722−2727.
(285) Ihsan, A. B.; Sun, T. L.; Kurokawa, T.; Karobi, S. N.; Nakajima, T.; Nonoyama, T.; Roy, C. K.; Luo, F.; Gong, J. P. Self-Healing Behaviors of Tough Polyampholyte Hydrogels. *Macromolecules* **2016**, *49*, 4245−4252.
(286) Luo, F.; Sun, T. L.; Nakajima, T.; King, D. R.; Kurokawa, T.; Zhao, Y.; Ihsan, A. B.; Li, X.; Guo, H.; Gong, J. P. Strong and Tough


https://doi.org/10.1021/acs.chemrev.5c00663
*Chem. Rev.* XXXX, XXX, XXX−XXX

Polyion-Complex Hydrogels from Oppositely Charged Polyelectrolytes: A Comparative Study with Polyampholyte Hydrogels. *Macromolecules* **2016**, *49*, 2750−2760.
(287) Cui, K.; Sun, T. L.; Liang, X.; Nakajima, K.; Ye, Y. N.; Chen, L.; Kurokawa, T.; Gong, J. P. Multiscale Energy Dissipation Mechanism in Tough and Self-Healing Hydrogels. *Phys. Rev. Lett.* **2018**, *121*, 185501.
(288) Cui, K.; Ye, Y. N.; Sun, T. L.; Yu, C.; Li, X.; Kurokawa, T.; Gong, J. P. Phase Separation Behavior in Tough and Self-Healing Polyampholyte Hydrogels. *Macromolecules* **2020**, *53*, 5116−5126.
(289) Li, X.; Cui, K.; Kurokawa, T.; Ye, Y. N.; Sun, T. L.; Yu, C.; Creton, C.; Gong, J. P. Effect of mesoscale phase contrast on fatigue-delaying behavior of self-healing hydrogels. *Sci. Adv.* **2021**, *7*, No. eabe8210.
(290) Hołyst, R. Some features of soft matter systems. *Soft Matter* **2005**, *1*, 329−333.
(291) Li, X.; Gong, J. P. Role of dynamic bonds on fatigue threshold of tough hydrogels. *Proc. Natl. Acad. Sci. U. S. A.* **2022**, *119*, No. e2200678119.
(292) Li, X.; Cui, K.; Sun, T. L.; Meng, L.; Yu, C.; Li, L.; Creton, C.; Kurokawa, T.; Gong, J. P. Mesoscale bicontinuous networks in self-healing hydrogels delay fatigue fracture. *Proc. Natl. Acad. Sci. U. S. A.* **2020**, *117*, 7606−7612.
(293) Hu, X.; Vatankhah-Varnoosfaderani, M.; Zhou, J.; Li, Q.; Sheiko, S. S. Weak Hydrogen Bonding Enables Hard, Strong, Tough, and Elastic Hydrogels. *Adv. Mater.* **2015**, *27*, 6899−6905.
(294) Wang, Y. J.; Zhang, X. N.; Song, Y.; Zhao, Y.; Chen, L.; Su, F.; Li, L.; Wu, Z. L.; Zheng, Q. Ultrastiff and Tough Supramolecular Hydrogels with a Dense and Robust Hydrogen Bond Network. *Chem. Mater.* **2019**, *31*, 1430−1440.
(295) Du, C.; Zhang, X. N.; Sun, T. L.; Du, M.; Zheng, Q.; Wu, Z. L. Hydrogen-Bond Association-Mediated Dynamics and Viscoelastic Properties of Tough Supramolecular Hydrogels. *Macromolecules* **2021**, *54*, 4313−4325.
(296) Wang, Y.; Jia, K.; Xiang, C.; Yang, J.; Yao, X.; Suo, Z. Instant, Tough, Noncovalent Adhesion. *ACS Appl. Mater. Interfaces* **2019**, *11*, 40749−40757.
(297) Yuk, H.; Varela, C. E.; Nabzdyk, C. S.; Mao, X.; Padera, R. F.; Roche, E. T.; Zhao, X. Dry double-sided tape for adhesion of wet tissues and devices. *Nature* **2019**, *575*, 169−174.
(298) Wang, S.; Hu, Y.; Kouznetsova, T. B.; Sapir, L.; Chen, D.; Herzog-Arbeitman, A.; Johnson, J. A.; Rubinstein, M.; Craig, S. L. Facile mechanochemical cycloreversion of polymer cross-linkers enhances tear resistance. *Science* **2023**, *380*, 1248−1252.
(299) Sperling, L. H. *Interpenetrating Polymer Networks: An Overview*; American Chemical Society, 1994; Vol. *239*.
(300) Na, Y.; Tanaka, Y.; Kawauchi, Y.; Furukawa, H.; Sumiyoshi, T.; Gong, J. P.; Osada, Y. Necking Phenomenon of Double-Network Gels. *Macromolecules* **2006**, *39*, 4641−4645.
(301) Webber, R. E.; Creton, C.; Brown, H. R.; Gong, J. P. Large Strain Hysteresis and Mullins Effect of Tough Double-Network Hydrogels. *Macromolecules* **2007**, *40*, 2919−2927.
(302) Zheng, Y.; Wang, Y.; Tian, F.; Nakajima, T.; Hui, C.; Gong, J. P. Unique stick-slip crack dynamics of double-network hydrogels under pure-shear loading. *Proc. Natl. Acad. Sci. U. S. A.* **2024**, *121*, No. e2322437121.
(303) Nakajima, T.; Furukawa, H.; Tanaka, Y.; Kurokawa, T.; Osada, Y.; Gong, J. P. True Chemical Structure of Double Network Hydrogels. *Macromolecules* **2009**, *42*, 2184−2189.
(304) Zhou, Y.; Zhang, W.; Hu, J.; Tang, J.; Jin, C.; Suo, Z.; Lu, T. The Stiffness-Threshold Conflict in Polymer Networks and a Resolution. *J. Appl. Mech.* **2020**, *87*, 031002.
(305) Nakayama, A.; Kakugo, A.; Gong, J. P.; Osada, Y.; Takai, M.; Erata, T.; Kawano, S. High Mechanical Strength Double-Network Hydrogel with Bacterial Cellulose. *Adv. Funct. Mater.* **2004**, *14*, 1124−1128.
(306) Nakajima, T.; Sato, H.; Zhao, Y.; Kawahara, S.; Kurokawa, T.; Sugahara, K.; Gong, J. P. A Universal Molecular Stent Method to Toughen any Hydrogels Based on Double Network Concept. *Adv. Funct. Mater.* **2012**, *22*, 4426−4432.
(307) Zhang, H. J.; Sun, T. L.; Zhang, A. K.; Ikura, Y.; Nakajima, T.; Nonoyama, T.; Kurokawa, T.; Ito, O.; Ishitobi, H.; Gong, J. P. Tough Physical Double-Network Hydrogels Based on Amphiphilic Triblock Copolymers. *Adv. Mater.* **2016**, *28*, 4884−4890.
(308) Ye, Y. N.; Cui, K.; Hong, W.; Li, X.; Yu, C.; Hourdet, D.; Nakajima, T.; Kurokawa, T.; Gong, J. P. Molecular mechanism of abnormally large nonsoftening deformation in a tough hydrogel. *Proc. Natl. Acad. Sci. U. S. A.* **2021**, *118*, No. e2014694118.
(309) Nonoyama, T.; Gong, J. P. Tough Double Network Hydrogel and Its Biomedical Applications. *Annu. Rev. Chem. Biomol. Eng.* **2021**, *12*, 393−410.
(310) Sohma, J. Mechanochemistry of polymers. *Prog. Polym. Sci.* **1989**, *14*, 451−596.
(311) Matsuda, T.; Kawakami, R.; Namba, R.; Nakajima, T.; Gong, J. P. Mechanoresponsive self-growing hydrogels inspired by muscle training. *Science* **2019**, *363*, 504−508.
(312) Wang, Z. J.; Jiang, J.; Mu, Q.; Maeda, S.; Nakajima, T.; Gong, J. P. Azo-Crosslinked Double-Network Hydrogels Enabling Highly Efficient Mechanoradical Generation. *J. Am. Chem. Soc.* **2022**, *144*, 3154−3161.
(313) Mu, Q.; Cui, K.; Wang, Z. J.; Matsuda, T.; Cui, W.; Kato, H.; Namiki, S.; Yamazaki, T.; Frauenlob, M.; Nonoyama, T.; Tsuda, M.; Tanaka, S.; Nakajima, T.; Gong, J. P. Force-triggered rapid microstructure growth on hydrogel surface for on-demand functions. *Nat. Commun.* **2022**, *13*, 6213.
(314) Wang, Z. J.; Li, W.; Li, X.; Nakajima, T.; Rubinstein, M.; Gong, J. P. Rapid self-strengthening in double-network hydrogels triggered by bond scission. *Nat. Mater.* **2025**, *24*, 607−614.
(315) Ju, J.; Sanoja, G. E.; Cipelletti, L.; Ciccotti, M.; Zhu, B.; Narita, T.; Yuen Hui, C.; Creton, C. Role of molecular damage in crack initiation mechanisms of tough elastomers. *Proc. Natl. Acad. Sci. U. S. A.* **2024**, *121*, No. e2410515121.
(316) Slootman, J.; Yeh, C. J.; Millereau, P.; Comtet, J.; Creton, C. A molecular interpretation of the toughness of multiple network elastomers at high temperature. *Proc. Natl. Acad. Sci. U. S. A.* **2022**, *119*, No. e2116127119.
(317) Rose, S.; Prevoteau, A.; Elzière, P.; Hourdet, D.; Marcellan, A.; Leibler, L. Nanoparticle solutions as adhesives for gels and biological tissues. *Nature* **2014**, *505*, 382−385.
(318) Yuk, H.; Zhang, T.; Lin, S.; Parada, G. A.; Zhao, X. Tough bonding of hydrogels to diverse non-porous surfaces. *Nat. Mater.* **2016**, *15*, 190−196.
(319) Li, J.; Celiz, A. D.; Yang, J.; Yang, Q.; Wamala, I.; Whyte, W.; Seo, B. R.; Vasilyev, N. V.; Vlassak, J. J.; Suo, Z.; Mooney, D. J. Tough adhesives for diverse wet surfaces. *Science* **2017**, *357*, 378−381.
(320) Ma, Z.; Bourquard, C.; Gao, Q.; Jiang, S.; De Iure-Grimmel, T.; Huo, R.; Li, X.; He, Z.; Yang, Z.; Yang, G.; Wang, Y.; Lam, E.; Gao, Z.; Supponen, O.; Li, J. Controlled tough bioadhesion mediated by ultrasound. *Science* **2022**, *377*, 751−755.
(321) Freedman, B. R.; Kuttler, A.; Beckmann, N.; Nam, S.; Kent, D.; Schuleit, M.; Ramazani, F.; Accart, N.; Rock, A.; Li, J.; Kurz, M.; Fisch, A.; Ullrich, T.; Hast, M. W.; Tinguely, Y.; Weber, E.; Mooney, D. J. Enhanced tendon healing by a tough hydrogel with an adhesive side and high drug-loading capacity. *Nat. Biomed. Eng.* **2022**, *6*, 1167−1179.
(322) Wu, K. C.; Freedman, B. R.; Kwon, P. S.; Torre, M.; Kent, D. O.; Bi, W. L.; Mooney, D. J. A tough bioadhesive hydrogel supports sutureless sealing of the dural membrane in porcine and ex vivo human tissue. *Sci. Transl. Med.* **2024**, *16*, No. eadj0616.
(323) Bai, R.; Yang, Q.; Tang, J.; Morelle, X. P.; Vlassak, J.; Suo, Z. Fatigue fracture of tough hydrogels. *Extreme Mech. Lett.* **2017**, *15*, 91−96.
(324) Gao, Y.; Wu, K.; Suo, Z. Photodetachable Adhesion. *Adv. Mater.* **2019**, *31*, 1806948.
(325) Hamed, G. R. Reinforcement of Rubber. *Rubber Chem. Technol.* **2000**, *73*, 524−533.


https://doi.org/10.1021/acs.chemrev.5c00663
*Chem. Rev.* XXXX, XXX, XXX−XXX

(326) Guth, E. Theory of Filler Reinforcement. *J. Appl. Phys.* **1945**, *16*, 20−25.
(327) Powell, M. J. Site percolation in randomly packed spheres. *Phys. Rev. B* **1979**, *20*, 4194−4198.
(328) Tan, M. W. M.; Nian, G.; Chen, Z.; Bao, X.; Kutsovsky, Y.; Suo, Z. Amplifying toughness in silica reinforced natural rubber by preserving long chains. 2025, submitted for publication.
(329) Bueche, F. Molecular basis for the mullins effect. *J. Appl. Polym. Sci.* **1960**, *4*, 107−114.
(330) Bueche, F. Mullins effect and rubber-filler interaction. *J. Appl. Polym. Sci.* **1961**, *5*, 271−281.
(331) Mullins, L. Softening of Rubber by Deformation. *Rubber Chem. Technol.* **1969**, *42*, 339−362.
(332) Payne, A. R. The dynamic properties of carbon black-loaded natural rubber vulcanizates. Part I. *J. Appl. Polym. Sci.* **1962**, *6*, 57−63.
(333) Stickney, P. B.; Falb, R. D. Carbon Black-Rubber Interactions and Bound Rubber. *Rubber Chem. Technol.* **1964**, *37*, 1299−1340.
(334) Robertson, C. G.; Hardman, N. J. Nature of Carbon Black Reinforcement of Rubber: Perspective on the Original Polymer Nanocomposite. *Polymers* **2021**, *13*, 538.
(335) Donnet, J. *Carbon Black: Science and Technology*; CRC Press, 1993.
(336) Dannenberg, E. M. Bound Rubber and Carbon Black Reinforcement. *Rubber Chem. Technol.* **1986**, *59*, 512−524.
(337) Wolff, S.; Wang, M.; Tan, E. Filler-Elastomer Interactions. Part VII. Study on Bound Rubber. *Rubber Chem. Technol.* **1993**, *66*, 163−177.
(338) Gent, A. N.; Park, B. Failure processes in elastomers at or near a rigid spherical inclusion. *J. Mater. Sci.* **1984**, *19*, 1947−1956.
(339) Fond, C. Cavitation criterion for rubber materials: A review of void-growth models. *J. Polym. Sci., Part B: Polym. Phys.* **2001**, *39*, 2081−2096.
(340) Zhang, H.; Scholz, A. K.; Merckel, Y.; Brieu, M.; Berghezan, D.; Kramer, E. J.; Creton, C. Strain induced nanocavitation and crystallization in natural rubber probed by real time small and wide angle X-ray scattering. *J. Polym. Sci., Part B: Polym. Phys.* **2013**, *51*, 1125−1138.
(341) Sarkawi, S. S.; Kaewsakul, W.; Sahakaro, K.; Dierkes, W. K.; Noordermeer, J. W. A review on reinforcement of natural rubber by silica fillers for use in low-rolling resistance tires. *J. Rubber Res.* **2015**, *18*, 203−233.
(342) Rattanasom, N.; Saowapark, T.; Deeprasertkul, C. Reinforcement of natural rubber with silica/carbon black hybrid filler. *Polym. Test.* **2007**, *26*, 369−377.
(343) Gent, A. N.; Lai, S.; Nah, C.; Wang, C. Viscoelastic Effects in Cutting and Tearing Rubber. *Rubber Chem. Technol.* **1994**, *67*, 610−618.
(344) Heinrich, G.; Klüppel, M. *Recent Advances in the Theory of Filler Networking in Elastomers*; Springer: Berlin, 2002.
(345) Li, C.; Tan, M. W. M.; Bao, X.; Nian, G.; Kutsovsky, Y.; Suo, Z. Resolving Toughness-Modulus Conflict in Carbon Black Reinforced Natural Rubber by Preserving Long Chains. 2025, submitted for publication.
(346) King, D. R.; Sun, T. L.; Huang, Y.; Kurokawa, T.; Nonoyama, T.; Crosby, A. J.; Gong, J. P. Extremely tough composites from fabric reinforced polyampholyte hydrogels. *Mater. Horiz.* **2015**, *2*, 584−591.
(347) Cui, W.; King, D. R.; Huang, Y.; Chen, L.; Sun, T. L.; Guo, Y.; Saruwatari, Y.; Hui, C.; Kurokawa, T.; Gong, J. P. Fiber-Reinforced Viscoelastomers Show Extraordinary Crack Resistance That Exceeds Metals. *Adv. Mater.* **2020**, *32*, 1907180.
(348) Cui, W.; Huang, Y.; Chen, L.; Zheng, Y.; Saruwatari, Y.; Hui, C.; Kurokawa, T.; King, D. R.; Gong, J. P. Tiny yet tough: Maximizing the toughness of fiber-reinforced soft composites in the absence of a fiber-fracture mechanism. *Matter* **2021**, *4*, 3646−3661.
(349) Gao, Y.; Han, X.; Chen, J.; Pan, Y.; Yang, M.; Lu, L.; Yang, J.; Suo, Z.; Lu, T. Hydrogel-mesh composite for wound closure. *Proc. Natl. Acad. Sci. U. S. A.* **2021**, *118*, No. e2103457118.
(350) Tang, J.; Liu, F.; Chen, X.; Suo, Z.; Tang, J. Cyclic tearing of a woven fabric embedded in a soft matrix. *Int. J. Fract.* **2025**, *249*, 4.
(351) Yang, J.; Bai, R.; Suo, Z. Topological Adhesion of Wet Materials. *Adv. Mater.* **2018**, *30*, 1800671.
(352) Yang, H.; Ji, M.; Yang, M.; Shi, M.; Pan, Y.; Zhou, Y.; Qi, H. J.; Suo, Z.; Tang, J. Fabricating hydrogels to mimic biological tissues of complex shapes and high fatigue resistance. *Matter* **2021**, *4*, 1935−1946.
(353) Li, C.; Yang, H.; Suo, Z.; Tang, J. Fatigue-Resistant elastomers. *J. Mech. Phys. Solids* **2020**, *134*, 103751.
(354) Liu, X.; Wu, J.; Qiao, K.; Liu, G.; Wang, Z.; Lu, T.; Suo, Z.; Hu, J. Topoarchitected polymer networks expand the space of material properties. *Nat. Commun.* **2022**, *13*, 1622.
(355) Gautieri, A.; Vesentini, S.; Redaelli, A.; Buehler, M. J. Hierarchical Structure and Nanomechanics of Collagen Microfibrils from the Atomistic Scale Up. *Nano Lett.* **2011**, *11*, 757−766.
(356) Yang, W.; Sherman, V. R.; Gludovatz, B.; Schaible, E.; Stewart, P.; Ritchie, R. O.; Meyers, M. A. On the tear resistance of skin. *Nat. Commun.* **2015**, *6*, 6649.
(357) Bircher, K.; Zündel, M.; Pensalfini, M.; Ehret, A. E.; Mazza, E. Tear resistance of soft collagenous tissues. *Nat. Commun.* **2019**, *10*, 792.
(358) Tang, J.; Chen, X.; Liu, F.; Zeng, L.; Suo, Z.; Tang, J. Why are soft collagenous tissues so tough? *Sci. Adv.* **2025**, *11*, No. eadw0808.
(359) Huang, W.; Restrepo, D.; Jung, J.; Su, F. Y.; Liu, Z.; Ritchie, R. O.; McKittrick, J.; Zavattieri, P.; Kisailus, D. Multiscale Toughening Mechanisms in Biological Materials and Bioinspired Designs. *Adv. Mater.* **2019**, *31*, 1901561.
(360) Buehler, M. J. Nature designs tough collagen: Explaining the nanostructure of collagen fibrils. *Proc. Natl. Acad. Sci. U. S. A.* **2006**, *103*, 12285−12290.
(361) Gentleman, E.; Lay, A. N.; Dickerson, D. A.; Nauman, E. A.; Livesay, G. A.; Dee, K. C. Mechanical characterization of collagen fibers and scaffolds for tissue engineering. *Biomaterials* **2003**, *24*, 3805−3813.
(362) Meyers, M. A.; Chen, P.; Lin, A. Y.; Seki, Y. Biological materials: Structure and mechanical properties. *Prog. Mater. Sci.* **2008**, *53*, 1−206.
(363) Yu, X.; Suki, B.; Zhang, Y. Avalanches and power law behavior in aortic dissection propagation. *Sci. Adv.* **2020**, *6*, No. eaaz1173.
(364) Chen, X.; Liu, F.; Yu, Q.; Yang, M.; Suo, Z.; Tang, J. A soft and fatigue-resistant material that mimics heart valves. *Matter* **2025**, *8*, 101926.
(365) Bao, B.; Zeng, Q.; Li, K.; Wen, J.; Zhang, Y.; Zheng, Y.; Zhou, R.; Shi, C.; Chen, T.; Xiao, C.; Chen, B.; Wang, T.; Yu, K.; Sun, Y.; Lin, Q.; He, Y.; Tu, S.; Zhu, L. Rapid fabrication of physically robust hydrogels. *Nat. Mater.* **2023**, *22*, 1253−1260.
(366) Wang, C.; Chen, X.; Wang, L.; Makihata, M.; Liu, H.; Zhou, T.; Zhao, X. Bioadhesive ultrasound for long-term continuous imaging of diverse organs. *Science* **2022**, *377*, 517−523.
(367) Yang, F.; Zhao, J.; Koshut, W. J.; Watt, J.; Riboh, J. C.; Gall, K.; Wiley, B. J. A Synthetic Hydrogel Composite with the Mechanical Behavior and Durability of Cartilage. *Adv. Funct. Mater.* **2020**, *30*, 2003451.
(368) Sun, M.; Li, H.; Hou, Y.; Huang, N.; Xia, X.; Zhu, H.; Xu, Q.; Lin, Y.; Xu, L. Multifunctional tendon-mimetic hydrogels. *Sci. Adv.* **2023**, *9*, No. eade6973.
(369) Wang, Y.; Jia, K.; Suo, Z. Non-faradaic junction sensing. *Nat. Rev. Mater.* **2025**, *10*, 176−190.
(370) Yuk, H.; Lu, B.; Zhao, X. Hydrogel bioelectronics. *Chem. Soc. Rev.* **2019**, *48*, 1642−1667.
(371) Liu, X.; Liu, J.; Lin, S.; Zhao, X. Hydrogel machines. *Mater. Today* **2020**, *36*, 102−124.
(372) Ge, T.; Grest, G. S.; Robbins, M. O. Tensile Fracture of Welded Polymer Interfaces: Miscibility, Entanglements, and Crazing. *Macromolecules* **2014**, *47*, 6982−6989.
(373) Barney, C. W.; Ye, Z.; Sacligil, I.; McLeod, K. R.; Zhang, H.; Tew, G. N.; Riggleman, R. A.; Crosby, A. J. Fracture of model end-linked networks. *Proc. Natl. Acad. Sci. U. S. A.* **2022**, *119*, No. e2112389119.


https://doi.org/10.1021/acs.chemrev.5c00663
*Chem. Rev.* XXXX, XXX, XXX−XXX

(374) Surjadi, J. U.; Aymon, B. F. G.; Carton, M.; Portela, C. M. Double-network-inspired mechanical metamaterials. *Nat. Mater.* **2025**, *24*, 945−954.
(375) Shaikeea, A. J. D.; Cui, H.; O'Masta, M.; Zheng, X. R.; Deshpande, V. S. The toughness of mechanical metamaterials. *Nat. Mater.* **2022**, *21*, 297−304.
(376) Liu, F.; Suo, Z.; Tang, J. How does a glass fabric tear under cyclic force? *J. Mech. Phys. Solids* **2022**, *158*, 104659.
(377) Lavoie, S. R.; Hassan, S.; Kim, J.; Yin, T.; Suo, Z. Toughness of a composite in which sliding between fibers and matrix is rate-sensitive. *Extreme Mech. Lett.* **2021**, *46*, 101317.
(378) Hutchinson, J. W. Fundamentals of the phenomenological theory of nonlinear fracture mechanics. *Trans. ASME, J. Appl. Mech.* **1983**, *50*, 1042.
(379) Schapery, R. A. A theory of crack initiation and growth in viscoelastic media. *Int. J. Fract.* **1975**, *11*, 141−159.
(380) Bouklas, N.; Landis, C. M.; Huang, R. Effect of Solvent Diffusion on Crack-Tip Fields and Driving Force for Fracture of Hydrogels. *J. Appl. Mech.* **2015**, *82*, 081007.
(381) Freund, L. B.; Freud, L. B. *Dynamic Fracture Mechanics*; Cambridge University Press, 1998.
(382) Fineberg, J.; Bouchbinder, E. Recent developments in dynamic fracture: some perspectives. *Int. J. Fract.* **2015**, *196*, 33−57.
(383) Bouchbinder, E.; Goldman, T.; Fineberg, J. The dynamics of rapid fracture: instabilities, nonlinearities and length scales. *Rep. Prog. Phys.* **2014**, *77*, 046501.
(384) Marder, M. Simple models of rapid fracture. *Physica D* **1993**, *66*, 125−134.
(385) Wik, A.; Dave, G. Occurrence and effects of tire wear particles in the environment - A critical review and an initial risk assessment. *Environ. Pollut.* **2009**, *157*, 1−11.
(386) McMeeking, R. M. On mechanical stresses at cracks in dielectrics with application to dielectric breakdown. *J. Appl. Phys.* **1987**, *62*, 3116−3122.
(387) Suo, Z. Models for breakdown-resistant dielectric and ferroelectric ceramics. *J. Mech. Phys. Solids* **1993**, *41*, 1155−1176.
(388) Neusel, C.; Schneider, G. A. Size-dependence of the dielectric breakdown strength from nano- to millimeter scale. *J. Mech. Phys. Solids* **2014**, *63*, 201−213.


https://doi.org/10.1021/acs.chemrev.5c00663
*Chem. Rev.* XXXX, XXX, XXX−XXX